Revista Română de Inginerie Civilă

Indexată în bazele de date internationale (BDI)

ProQuest, IET INSPEC, EBSCO, GOOGLE SCHOLAR, CROSSREF, TDNET, DIMENSIONS, DRJI, J-GATE, INDEX COPERNICUS, ULRICH'S, JOURNALSEEK, RESEARCH GATE, SEMANTIC SCHOLAR

Volumul 15 (2024), Numărul 3

MATRIX ROM
3 Politehnicii Street, Bucharest, Romania
Tel. +4021.4113617, +40733882137
e-mail: office@matrixrom.ro
www.matrixrom.ro

EDITORIAL BOARD

Romanian Journal of Civil Engineering is founded, published and funded by publishing house MATRIX ROM
Executive Director: mat. Iancu ILIE

Online edition ISSN 2559-7485
Print edition ISSN 2068-3987; ISSN-L 2068-3987

Numerical Fire Simulation: Key Tools in Fire Safety for Modern Engineering

Simulare numerică a incendiului: instrumente cheie în securitatea la incendiu pentru ingineria modernă

Emanuil-Petru Ovadiuc[1], Ilinca Năstase[1], Răzvan Calotă[1]

[1] Technical University of Civil Engineering of Bucharest, Romania
Lacul Tei Blvd, No 124

E-mail: academicovadiuc@gmail.com, ilinca.nastase@cambi.ro, razvan.calota@utcb.ro

DOI: 10.37789/rjce.2024.15.3.1

Abstract. Fire simulation is a crucial tool in modern engineering for improving fire safety in constructions, especially in complex compartmental designs. It provides practical insights into structural fire behavior, the impact of combustible materials, and fire development, aiding in the formulation of effective fire safety measures. PyroSim, a graphical interface based on the Fire Dynamics Simulator (FDS), simplifies the creation and management of complex fire models. It supports file imports from AutoCAD DXF and DWG formats, offers background options from GIF, JPG, or PNG drawings, and includes tools for creating and validating multiple meshes. These simulations are essential for obtaining comprehensive data on various fire-related properties, such as temperatures, gas concentrations, smoke volume, pressures, and more, to ensure alignment with real-world conditions.

Key words: Fire simulation, Modern engineering, 3D modeling, PyroSim, Combustible materials.

1. Introduction

Fire simulation stands is indispensable within modern engineering, playing a very important role in ensuring the safety of buildings in the face of potential fire hazards [1]. In a multitude of contexts, especially when dealing with structural designs, fire simulation is a pragmatic tool necessary to gain insights into fire dynamics. It facilitates the comprehension of how flames interact with various structural components, the influence of combustible materials within confined spaces, and the progression of a fire event [2].

Linked with this indispensable field lies PyroSim, a globally used tool for making well-informed decisions regarding fire safety in building design [3]. Developed as a graphical interface built upon the Fire Dynamics Simulator (FDS) framework, PyroSim stands as a must in managing intricate fire models [4]. AutoCAD

DXF and DWG files can be imported, where 3D objects are meticulously recognized as obstacles.

Furthermore, PyroSim empowers users with the ability to import images in GIF, JPG, or PNG formats, which is important giving the possibility for very fast model tracing directly over these imported images [5]. Beyond these capabilities, PyroSim integrates tools designed to facilitate the creation and validation of multiple meshes, offering multiple advantages: parallel processing to enhance model resolution, fine-tuning of mesh geometries to reduce cell counts and resolution time, and the ability to adjust resolution levels across distinct areas of interest [6].

The path to a successful fire simulation, however, lies in the fidelity of the obtained results [7]. To this end, fire simulation programs provide comprehensive statistical insights into the behavior of various combustible materials and substances in fire scenarios [8,9]. This tool is used with dexterity by fire safety specialists, endowing them with mathematically data encompassing a variety of fire-related parameters, including temperatures (both air and surfaces), concentrations (of oxygen, combustion gases, and smoke), visibility (intricately tied to smoke levels), pressures within distinct spaces, and the interplay of temperature and pressure fields [10,11].

2. Building Design

To transform the building plans into a three-dimensional model, the SketchUp program was employed. Consequently, a three-dimensional model was successively created for each level of the building (basement, ground floor, 1st floor, 2nd floor, 3rd floor, 4th floor).

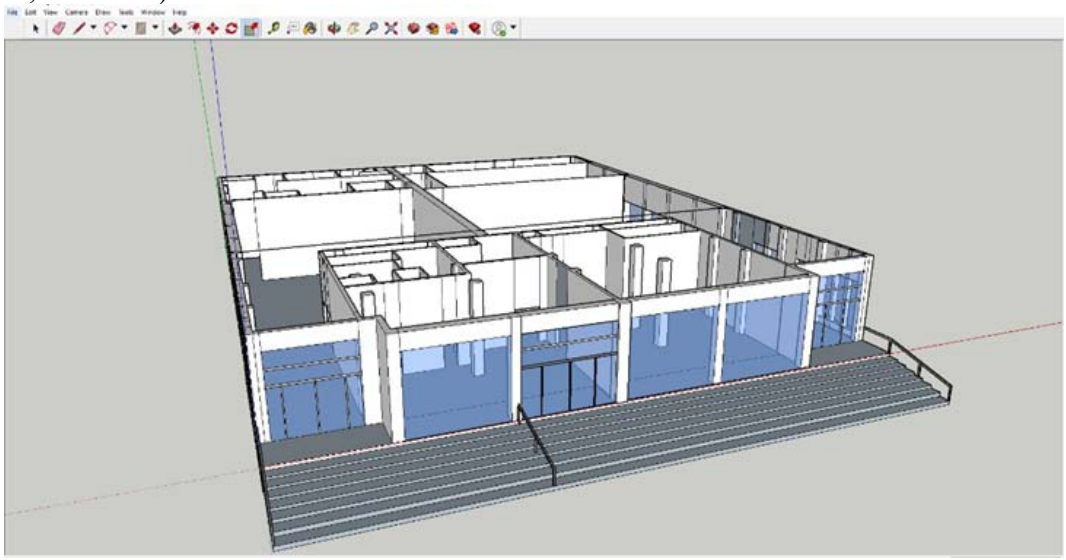

Figure 1 - 3D Ground Floor

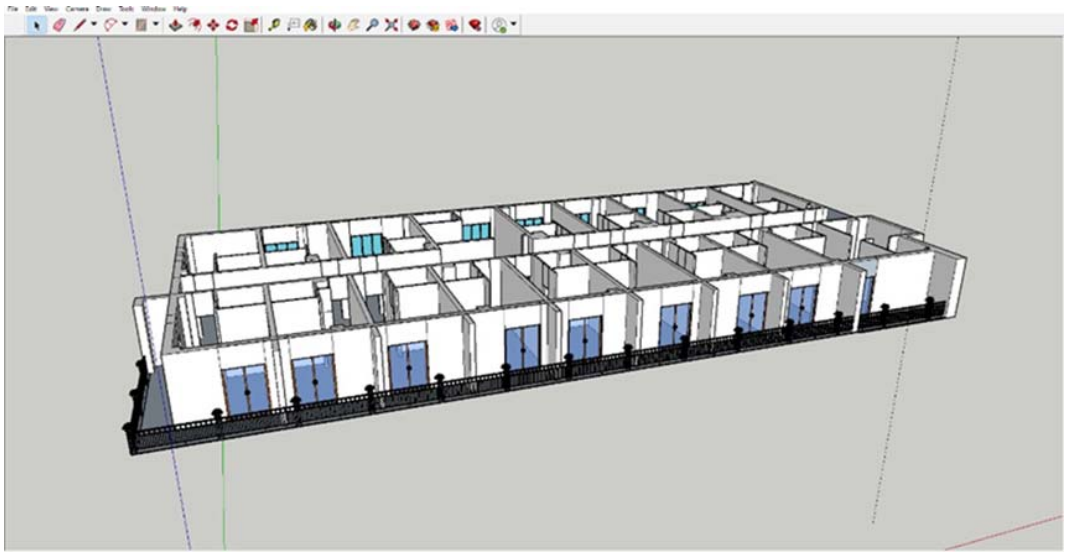

Figure 2 - 3D Current Floor

Figure 3 - 3D Hotel

In the end, by superimposing these models, the overall shape of the entire building was obtained, which was then introduced into the PyroSim program to perform the fire simulation. Introducing the building's shape into PyroSim enabled the creation of a detailed virtual environment for simulating fire behavior inside it.

3. Fire Simulation in a Room on the Hotel's Top Floor

The fire simulation was conducted on the upper floor of the hotel, situated on a concrete floor, with the hotel's structure composed of 25 cm thick BCA masonry exterior walls and 10 cm thick BCA masonry interior walls.

Space dimensions:
Length – 39.55 m
Width – 16.80 m
Height – 3.00 m
Usable area – 664.44 m^2
Volume – 1993.32 m^3

The top floor of the hotel comprises 18 accommodation rooms and a main hallway. Each accommodation room on this floor exhibits the following characteristics, as per Table 1:

Table 1

Accommodation Room Characteristics

Space	Usable Area (sqm)	Combustible Material	Mi(kg)	Qi(Mj/kg)	Sq(Mj)	Qi(Mj/sqm)
Accommodation Room	19.38	Wood	200.00	18.40	3680.00	349.03
	Textiles	50.00	16.75	837.50		
	PVC	80.00	21.80	1744.00		
	Other materials	30.00	16.75	502.50		

3.1. Fire Initiation

The ignition source originates at the bed level, 0.4 m above the floor, with minimal smoke production initially. This situation can be explained by the limited amount of combustible material consumed, and the flame initially dominates due to the presence of a substantial amount of oxygen in the room. The source of fire initiation is attributed to open flame work execution without adhering to fire prevention and extinguishing rules and measures.

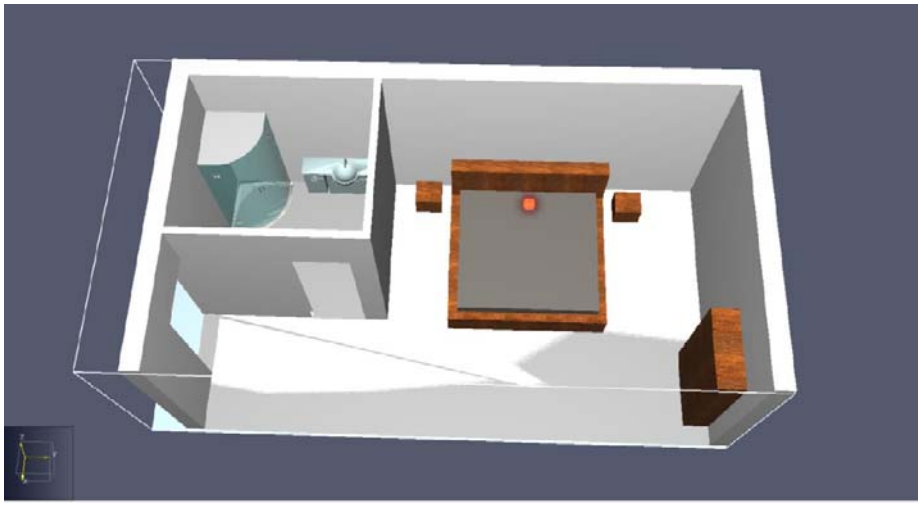

Figure 4 - Fire Initiation

3.2. Fire Development

The flames predominantly spread horizontally rather than vertically because there are no combustible materials above the initial flames to sustain upward combustion. This slowing of fire propagation upwards occurs as there is no available fuel at the upper part of the room. As the fire develops, the smoke becomes denser than in the initial stage. Smoke naturally accumulates at the room's upper part, rising due to heat and density differences. The hot gases and smoke accumulating beneath the ceiling form a hot layer at the room's upper part. This hot layer gradually thickens as the fire progresses. It thermally affects and influences the materials at its level through radiant and convective heat transfer. The elevated temperatures in the hot layer can lead to material deterioration and increase the fire's spread risk.

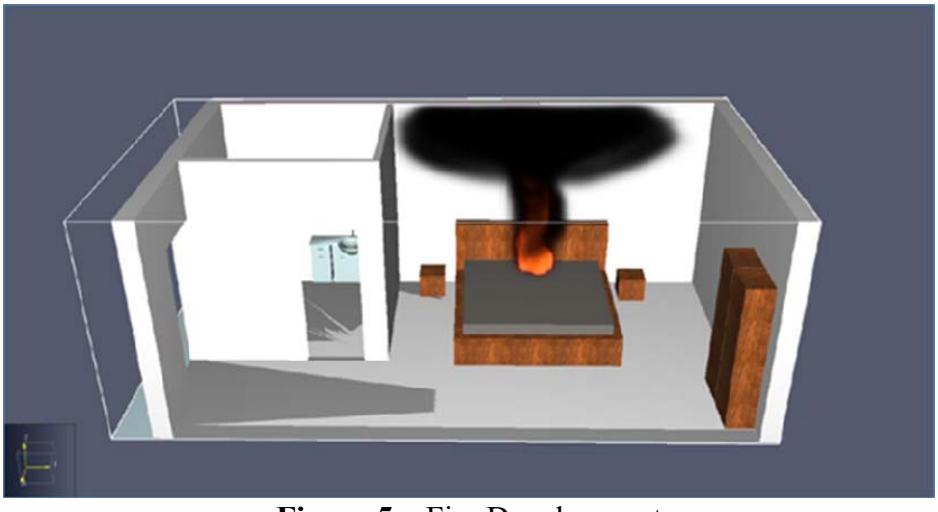

Figure 5 – Fire Development

3.3. Smoke Generation

Materials such as plastics, textiles, and wood used in furniture manufacturing can release a substantial amount of dense smoke in the event of a fire. As the fire progresses, the smoke can spread throughout the room, a phenomenon called "flooding" (see Figure 6). Smoke and toxic gases generated during material combustion tend to rise towards the upper part of the room. As the fire continues to burn, the smoke becomes extremely dense, and if not vented out of the room, it can occupy a significant portion of the room's volume. Smoke release from the burning area significantly reduces visibility inside the space. This diminished visibility impacts the safe evacuation of people inside and delays emergency service intervention actions. Firefighters responding to such fires aim to establish access routes to the fire and extinguish it from the interior. However, smoke becomes an obstacle to achieving this objective. In such a situation, when there is an external oxygen supply, the danger of a phenomenon called "backdraft" arises.

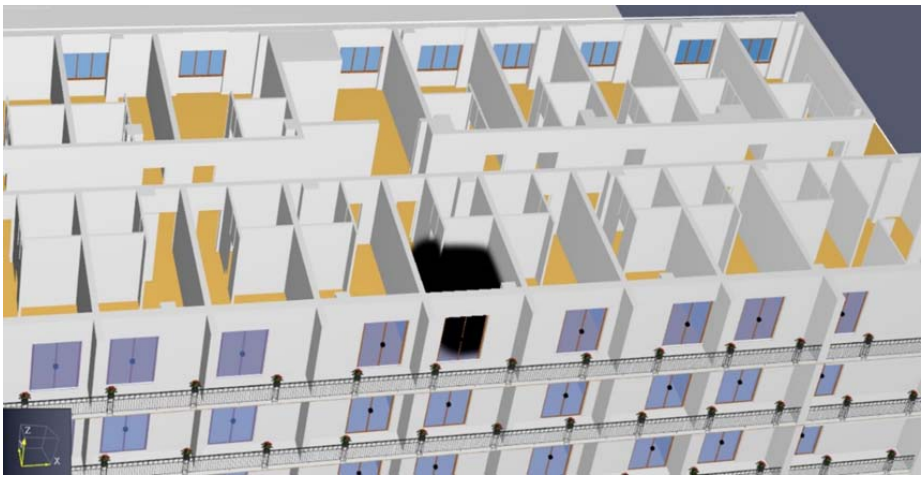

Figure 6 - Initial Smoke Release

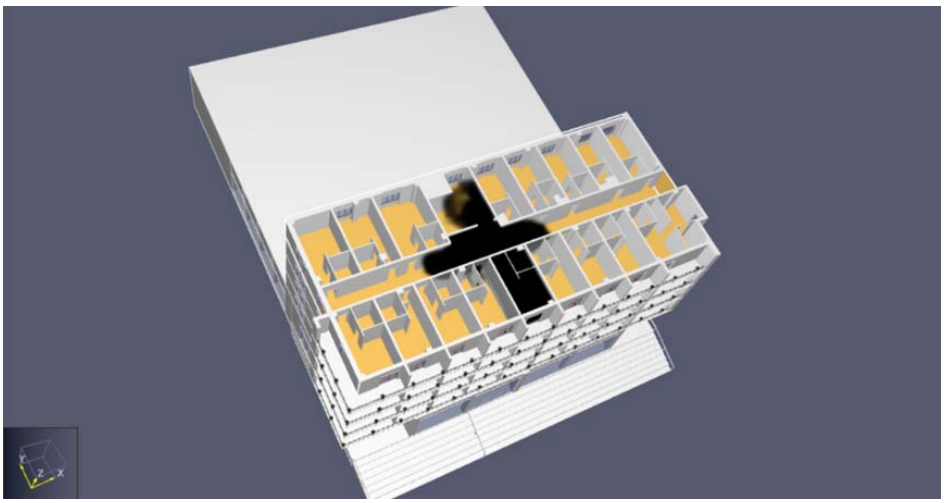

Figure 7 - Smoke Release in the Hallway and Adjacent Rooms

By running the simulation, it becomes apparent that after 50 seconds, smoke spreads and covers the entire floor area (see Figure 8). Observing the simulation, one can see how smoke gradually rises and spreads throughout the room before uniformly spreading over all areas of the floor.

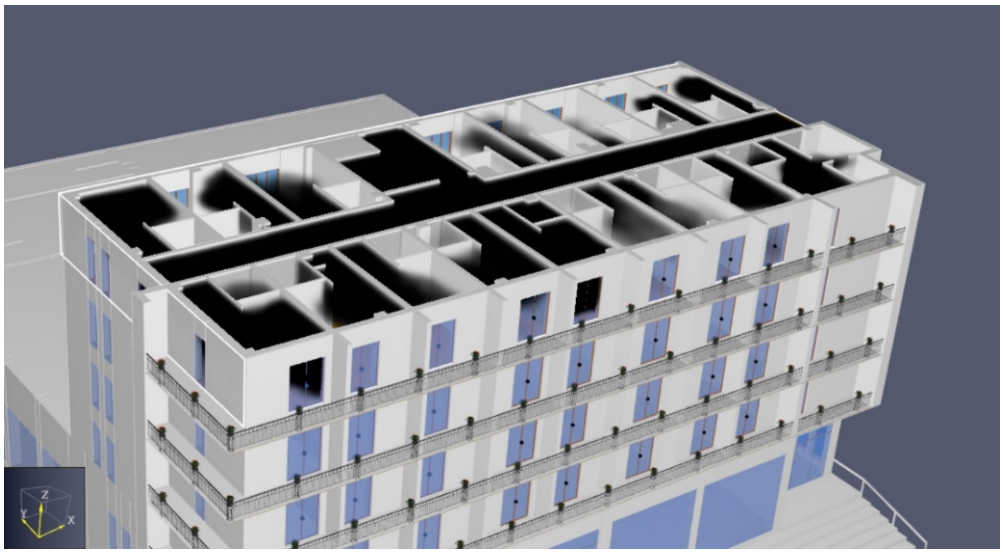

Figure 8 - Smoke Release Across the Entire Floor

3.4. Temperature Distribution

To monitor temperature distribution during a fire, both 3D section visualization and 2D section visualization were employed. These methods allow for observing and understanding how temperature propagates within the room, evolves over time, and is influenced by specific fire factors.

3.4.1. 3D Section Visualization

In the 3D section visualization, temperature is represented on a three-dimensional model of the room. This provides a three-dimensional perspective of how heat and elevated temperatures spread in space. High-temperature zones can be identified, and the way they move and expand during the fire's progress can be tracked. The three-dimensional visualization offers a more complete and detailed picture of temperature distribution inside the fire.

During the fire, temperatures recorded inside the space are very high. In the focal area, measurements show that temperatures can reach up to 720 °C (as per Figure 9).

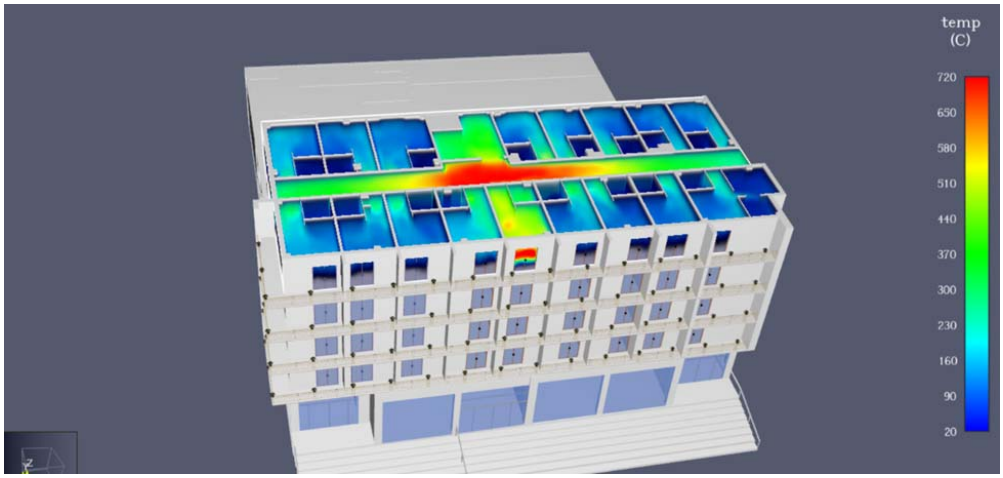

Figure 9 - Vertical Temperature Distribution

With the help of the three-dimensional visualization, it's possible to see temperature values at all points along the floor. It's observed that high temperatures ranging from 20°C to 720°C are recorded, even up to the ceiling level (as measured on the vertical plane). In the hallway, the highest temperatures are recorded, ranging from 240-720 °C. These elevated temperatures indicate an intense fire in the hallway, resulting from the strong combustion of combustible materials and the presence of a substantial amount of oxygen, facilitating temperature increase in this space.

3.4.2. 2D Section Visualization

On the other hand, in the 2D section visualization, temperature is represented in a two-dimensional plane. This plane can be either a horizontal or vertical section of the room. By obtaining these sections, high-temperature areas and how they propagate in a specific direction can be more clearly highlighted. The 2D section visualization can provide a more detailed view of temperature variations in different parts of the room, aiding in identifying areas with the greatest fire propagation risk.

A horizontal section can be useful for observing how heat propagates through different layers of the room. This can reveal temperature variations between different levels and assist in evaluating the risk of fire spreading upwards or downwards. For example, high-temperature areas can be identified at the top of the room, indicating that smoke and heat accumulate there.

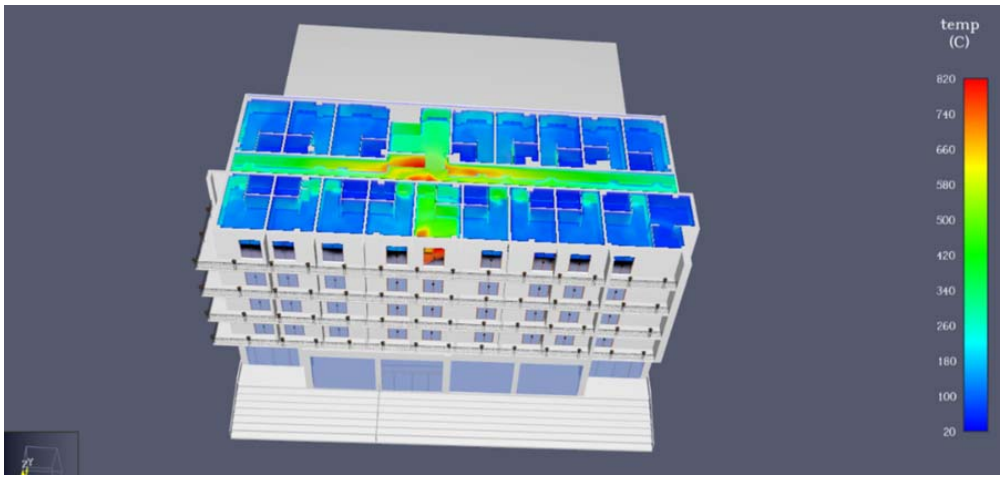

Figure 10 - Horizontal Temperature Distribution

The horizontal section is located at the top level and serves to monitor the distribution of heat released at the ceiling level. This allows for an approximation of the fire resistance time of the ceiling. At a height of 3 meters, high temperatures ranging from 500 ºC to 820 ºC are recorded (see Figure 10). The temperature from the focal area rapidly spreads horizontally at the ceiling level. This phenomenon results from the accumulation of hot gases and smoke from the combustible materials in the hotel room. Smoke and particles generated during combustion initially spread horizontally, gradually occupying the entire ceiling area.

Both three-dimensional and two-dimensional visualizations are valuable tools for monitoring and understanding temperature behavior during a fire.

3.5. Visibility on the Floor Level

Visibility represents an observer's ability to identify an object against the background at a certain distance. In the context of occupant safety, visibility is often used as an essential requirement.

Reduced visibility due to dense smoke can create significant difficulties in safely evacuating people from a building or in locating and fighting the fire by firefighters. Figure 11 illustrates the visibility capacity of occupants across the entire top floor of the hotel. It shows how smoke can spread and affect visibility in various areas of the floor during a fire.

As smoke spreads horizontally, it can be observed that areas closer to the focal point exhibit reduced visibility. In these areas, dense smoke and particles resulting from the combustion of combustible materials can limit visibility to a few meters ahead (between 0 and 9 m). As one moves away from the focal point and approaches lateral and opposite areas, visibility may improve.

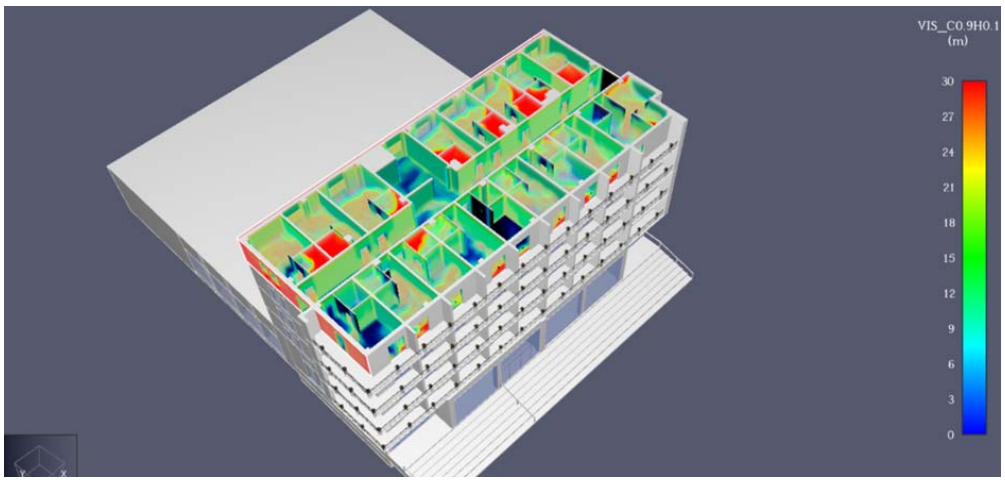

Figure 11 - Visibility on the Floor Level

In light of the identified visibility deficiencies in Figure 11, the following measures are necessary to ensure safe evacuation:

Verification and reevaluation of the lighting system: It is essential to check the proper functioning of emergency lighting and general lighting in critical areas and on evacuation routes. If deficiencies are found or if the light is not sufficiently intense, adjustments or replacements should be made to ensure optimal visibility during a fire.

Proper placement of evacuation signage: Evacuation signs must be placed in visible locations at an appropriate height and in sufficient numbers to guide guests and staff to emergency exits. Existing signage visibility should be checked, and additional signs should be added where necessary.

Obstacle removal: Careful inspection of every area of the hotel is required to identify and eliminate any obstacles that could hinder visibility or access to evacuation routes. This may include furniture, equipment, or any other objects that could block sightlines or pathways to exits.

Review of the evacuation plan: The hotel's evacuation plan needs to be reviewed and updated following the fire simulation and the identification of visibility-related issues. Ensure that the plan is clear, easy to understand, and includes precise instructions regarding evacuation routes and assembly points.

Implementing these measures will contribute to improving visibility in the hotel in the event of a fire and will enhance the effectiveness of evacuation.

4. Conclusions

In conclusion, fire simulation represents an indispensable tool in modern engineering and the fire safety of buildings [12]. Through simulations, a deeper understanding of the fire behavior of load-bearing structures, combustible materials, and the destructive effect of fire is obtained, providing guidance for the implementation of the most suitable fire safety measures [13].

The use of the SketchUp program to transform building plans into three-dimensional models allows for a detailed representation of each level of the building, facilitating fire simulation and evaluation of its behavior inside the structure [14]. Superimposing the obtained shapes for each level and introducing them into the PyroSim program enables precise fire simulation in a virtual environment [15].

The fire simulation conducted on the upper floor of the hotel, with the initiation source being open flame work execution without adhering to fire prevention and extinguishing rules and measures, highlighted the danger posed by plastics, textiles, and wood in generating dense smoke and its propagation throughout the room [16].

For monitoring temperature distribution during a fire, multiple measurement plans were used, both horizontal, allowing visualization of temperature distribution in space, and vertical, crossing the focal point and providing temperature information in that area [17].

Visibility is an essential requirement in ensuring occupant safety in the event of a fire. Reduced visibility due to dense smoke can create significant difficulties in safely evacuating people and in firefighters' intervention in locating and extinguishing the fire [18].

In conclusion, fire simulation and visibility assessment are crucial tools in ensuring the fire safety of buildings, providing essential information for the development and implementation of effective fire prevention and protection measures [19].

5. References

[1] Anderson, J. R., & Smith, P. Q. (2019). Fire Simulation and Safety in Modern Engineering. Fire Engineering, 42(3), 58-63.

[2] Brown, A. R., & Smith, L. M. (2020). PyroSim and Fire Dynamics: A Comprehensive Overview. International Journal of Fire Safety, 15(2), 87-99.

[3] Chen, W., et al. (2017). Integrating PyroSim and AutoCAD for Enhanced Fire Modeling. Journal of Computational Engineering, 8(4), 213-225.

[4] Davis, R. S., & Wilson, E. D. (2019). Fire Simulation: Bridging Theory and Practice. Fire Safety Journal, 64, 32-41.

[5] García, M. A., & Martinez, J. L. (2018). Advancements in Fire Simulation: The PyroSim Perspective. Journal of Fire Science, 20(1), 45-56.

[6] Johnson, D. R., & Brown, T. A. (2019). Exploring Fire Simulation for Complex Compartmental Designs. Structural Safety, 35(2), 187-199.

[7] Lee, H. S., & Kim, S. J. (2021). Fire Modeling in Modern Engineering: The Role of PyroSim. Fire Technology, 54(3), 225-239.

[8] Roberts, M. J., & Johnson, P. D. (2021). PyroSim: A Tool for Advancing Fire Safety in Building Design. Fire and Materials, 44(1), 12-26.

[9] Smith, K. R., et al. (2020). Fire Dynamics Simulation and Its Impact on Building Safety. Journal of Architectural Engineering, 26(3), 128-138.

[10] Thomas, A. B., et al. (2018). PyroSim in Fire Safety Engineering: Current Trends and Future Prospects. Journal of Fire Protection Engineering, 22(5), 189-204.
[11] Wang, L., et al. (2018). Advancing Fire Simulation: The Promise of PyroSim. Fire Safety Science, 10(2), 85-97.
[12] Anderson, J. R., & Smith, P. Q. (2019). Fire Simulation and Safety in Modern Engineering. Fire Engineering, 42(3), 58-63.
[13] Brown, A. R., & Smith, L. M. (2020). PyroSim and Fire Dynamics: A Comprehensive Overview. International Journal of Fire Safety, 15(2), 87-99.
[14] Chen, W., et al. (2017). Integrating PyroSim and AutoCAD for Enhanced Fire Modeling. Journal of Computational Engineering, 8(4), 213-225.
[15] Davis, R. S., & Wilson, E. D. (2019). Fire Simulation: Bridging Theory and Practice. Fire Safety Journal, 64, 32-41.
[16] García, M. A., & Martinez, J. L. (2018). Advancements in Fire Simulation: The PyroSim Perspective. Journal of Fire Science, 20(1), 45-56.
[17] Johnson, D. R., & Brown, T. A. (2019). Exploring Fire Simulation for Complex Compartmental Designs. Structural Safety, 35(2), 187-199.
[18] Lee, H. S., & Kim, S. J. (2021). Fire Modeling in Modern Engineering: The Role of PyroSim. Fire Technology, 54(3), 225-239.
[19] Roberts, M. J., & Johnson, P. D. (2021). PyroSim: A Tool for Advancing Fire Safety in Building Design. Fire and Materials, 44(1), 12-26.

The impact of Public Law Restrictions in the field of constructions

Impactul Restricțiilor de Drept Public în domeniul construcțiilor

Alexandra-Paula Frenț[1], Ana-Cornelia Badea[1], Petre Iuliu Dragomir[1], Gheorghe Badea[1]

[1]Technical University of Civil Engineering Bucharest
Lacul Tei Blvd, No 124, Bucharest, Romania

Email: alexandra-paula.frent@phd.utcb.ro, ana.badea@utcb.ro, petre.dragomir@utcb.ro, gheorghe.badea@utcb.ro

DOI: 10.37789/rjce.2024.15.3.2

Abstract. Increasing population density in urban areas in recent decades has led to the need to develop the building environment in an accelerated way, being necessary for the construction of buildings and their vertical development for a higher percentage of occupancy of the population on a small area of land. Urban expansion has determined the need to impose restrictions on public law through laws and regulations, to reduce the negative impact on the environment and to increase the quality of life of the population. Integrating restrictions, rights and responsibilities into cadastral systems would be an important step in developing integrated real estate management systems. This article aims to monitor the impact of public law restrictions on buildings in the urban area and to present urban regulations and legislation in Romania with applicability in the field of construction through the study of case in which a 3D model of representation and visualization of the restrictions of public law of the buildings is developed.

Key words: Public Law-Restriction, 3D Cadastre, legislative framework, RRRs

1. Introduction

Most of Europe's major cities have been undergoing urban expansion in recent decades. Population growth in urban and metropolitan areas has led to the need to develop the built environment in these areas. This has led to the vertical development of buildings [1], necessitating the imposition of restrictions, rights and responsibilities (RRRs) in accordance with applicable technical regulations and specific legislation in force.

Public law restrictions in the field of construction are conditions set by authorities [2] through laws, regulations and standards, in order to limit the rights of land owners, for the protection of public interests [2]. For a better understanding of these restrictions it

would be necessary to visualize them in the form of 3D models [1], which leads to the need for the development of 3D cadastral systems [2].

Even if public law restrictions in the field of construction as well as in related fields, such as archaeology, environmental protection, mining, aviation, etc. can only be applied in 3D space [3], the current legislative framework in Romania only offers applicability in 2D space of these restrictions, rights and responsibilities.

The need to implement restrictions, rights and responsibilities on real estate owned by owners in an informational system is found internationally, being a current topic in scientific research [4], [5], [6], [7], [8].

So far there are several countries that have tried to develop information systems for the registration, management and 3D visualisation of public law restrictions, but in most of these systems public law restrictions could only be partially implemented [5]. Among these countries are Switzerland, Sweden, Norway, the Australian states of Victoria and Queensland, Austria, Canada etc [5].

As for the Cadastre of Public Law Restrictions in Switzerland, it has been implemented since 2012 and became operational in 2016, being considered a successful project [8]. This project aimed to develop 26 geoportals, one for each canton in Switzerland, in which there was information from the urban planning regulations for each canton [8]. At the moment of starting the project to implement the cadastre of public law restrictions there were 2D cadastral systems in almost all cantons, which included the following elements: measured cadastral data, roads, natural hazards, data related to spatial planning [8].

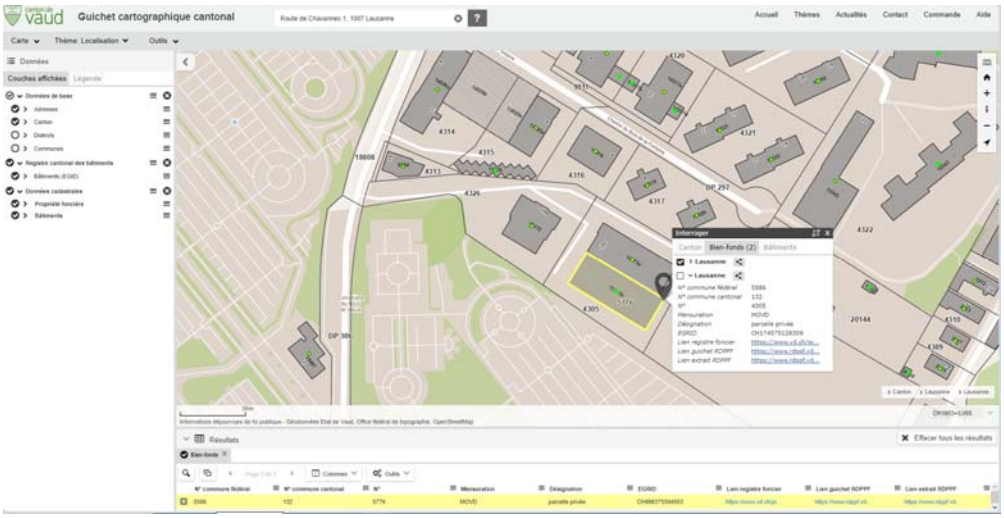

Fig. 1. Cadastral records system, Vaud, Switzerland [9]

Within the development project of the public law restrictions cadastre information system, data from the existing cadastral system was used, supplemented with the restrictions applied to each building according to the zoning regulations and the legislation in force [8]. For each building, a digital report can be generated from the

public law restrictions cadastre, in which all restrictions applicable to that building are highlighted, including the legal basis of these restrictions [8].

Fig. 2. Cadastral system of public law restrictions Vaud, Switzerland [10]

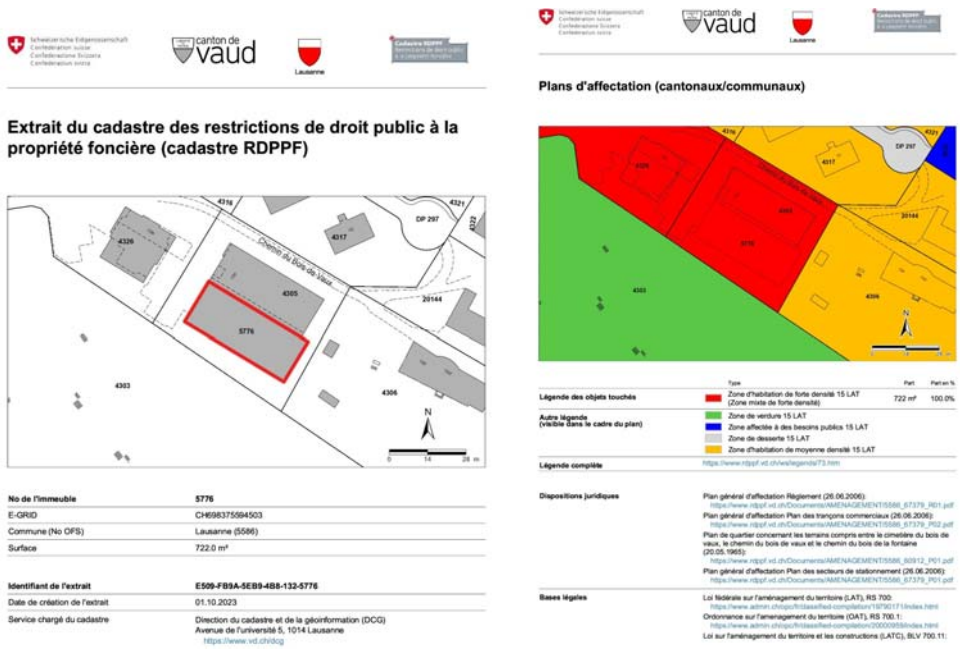

Fig. 3. Digital report of the cadastral system of public law restrictions Vaud, Switzerland [10]

Through this article we aim to create a 3D model for the visualization of public law restrictions in the field of construction in the studied area. The restrictions, rights and responsibilities presented in the paper are found in the national legislation through the laws issued by the Romanian Government and the regulations adopted by the local administrations.

The public law restrictions are initiated by the Romanian legislative apparatus and transposed to the European Union directives. This article aims to support the need for

the development of an information system for the registration, management and visualisation of public law restrictions applied to the built environment.

2. Materials and methods

This section presents the existing public law restrictions in the urban planning and building regulations that apply in Romania, highlighting the need to develop the 3D cadastre by integrating restrictions, rights and responsibilities in the field of construction. These restrictions will be visualized in the case study on the extension of a condominium building on the horizontal and vertical. ArcGIS Pro software, version 2.5, was used to create the 3D model. Through the 3D model of the studied area it will be possible to observe the public law restrictions that apply in the field of construction and the need to modify the current legislation in order to implement and visualize the restrictions in a 3D space.

2.1. Regulations in construction domain

The aim of building regulations is to establish a high level of quality in the design and execution of construction works, leading to the protection of human life, society and the environment [11], [12].

The law that underpins building regulations in Romania is Law 10 of 18 January 1995 on quality in construction, issued by the Romanian Parliament.

In order to obtain quality buildings, it is mandatory to maintain the following requirements throughout the life of the construction: mechanical strength and stability, fire safety, hygiene, health and environment, safety and accessibility in operation, noise protection, energy saving and thermal insulation, sustainable use of natural resources [12]. All these fundamental requirements are applied according to the category of importance of the building through regulations and technical building standards [12].

2.2. Urban planning regulations

Urban planning regulations impose 3D restrictions on real estate. Public law restrictions resulting from urban planning activities impact on land use, infrastructure and implementation of special economic policies, transportation, education, energy consumption, public investment, environmental conservation and traditional architecture [7].

The law that regulates urban planning provisions in Romania is Law 350 of 6 July 2021 on spatial and urban planning, issued by the Romanian Parliament. The main objectives of urban planning regulations are balanced spatial development in which the expansion of built-up areas is controlled, the protection of natural and built heritage and the improvement of the quality of life in urban and rural areas [13] [14].

Also, in spatial planning activity, the request for public participation in the decision-making process is mandatory in all phases of the elaboration or update of the urban and spatial planning process[13].

Restrictions, rights and responsibilities in urban planning are outlined in the urban planning certificate, which is issued by the county or local public administration authority [13]. This informative act establishes the legal, technical and economic regime according to the specific regulations of each area of interest [13].

The urban planning regulations in the field of construction lead to public law restrictions on the minimum and maximum height of the building depending on the surface of the land on which a certain percentage of occupation and use is imposed according to the destination and location of the building.

By applying the public law restrictions imposed in urban planning regulations, the main physical dimensions of a building are determined: surface area and volume. In the integrated cadastre and land registration system in Romania, buildings are represented in a 2D space, being known only their surface area.

Even if most of the restrictions, rights and responsibilities have applicability in 3D space being characterized by three-dimensional data, such as the volume of a building, the legislation in force does not allow the implementation and visualization of these restrictions in a 3D cadastre information system.

2.3. How to register in the integrated cadastre and land registration system in Romania

At present, the registration in the integrated cadastre and land registration system of real estate is carried out in accordance with the Law no.7 of 13 March 1996, on cadastre and real estate registration issued by the Romanian Parliament and based on the Regulation of reception and registration in the cadastre and land registration records approved by Order 600 of 8 February 2023 issued by the National Agency for Cadastre and Real Estate Registration.

The integrated cadastre and land registration system includes the technical, economic and legal records of the real estate in the same administrative-territorial unit: commune, town and municipality [15], [16]. The cadastre information system through which ANCPI manages the cadastre and land registration of Romania is called "e-Terra".

The registration of data on real estate in Romania is carried out by natural or legal persons authorized by National Agency for Cadastre and Land Registration of Romania (ANCPI). Thus, access to the integrated cadastre and land registration system is only through a user account provided by ANCPI.

Fig.4. Interface of the integrated cadastre and land registration system in Romania [17]

For the registration of the buildings in the existing cadastral system, the creation of a new documentation and the selection of the type of technical documentation according to the specifics of each building is initiated.

The cadastral information system requires the selection of the county and the administrative-territorial unit in which the building is located for which the spatial and non-spatial data are to be registered in order to load the map of the studied area.

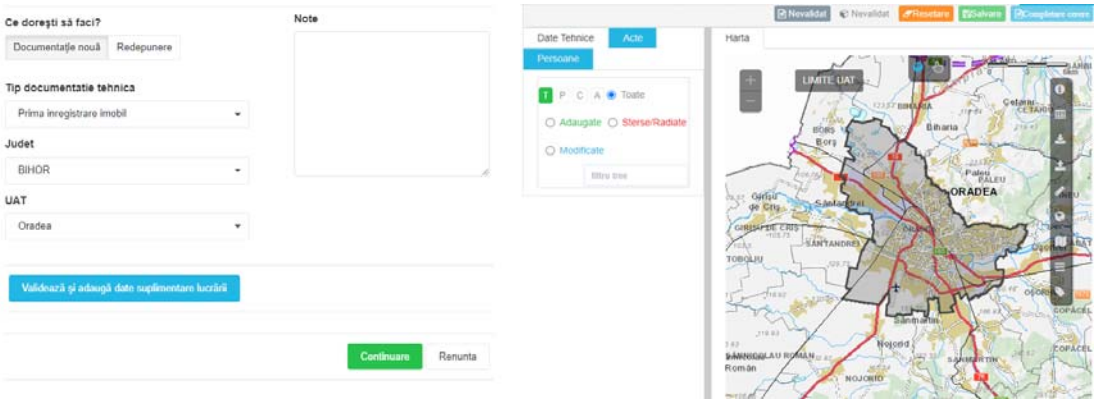

a) b)

Fig. 5. a) Initiation of new documentation for the registration of buildings in the integrated cadastre and land registration system [17]; b) Map generated following the registration of new documentation in the integrated cadastre and land registration system

Within the cadastral information system, 2D vector spatial data of the closed polygon type are recorded with associated textual data.

Fig. 6. Date spatiale vectoriale de tip poligon inchis din zona studiata in cadrul acestui articol Closed polygon spatial vector data from the area studied [17]

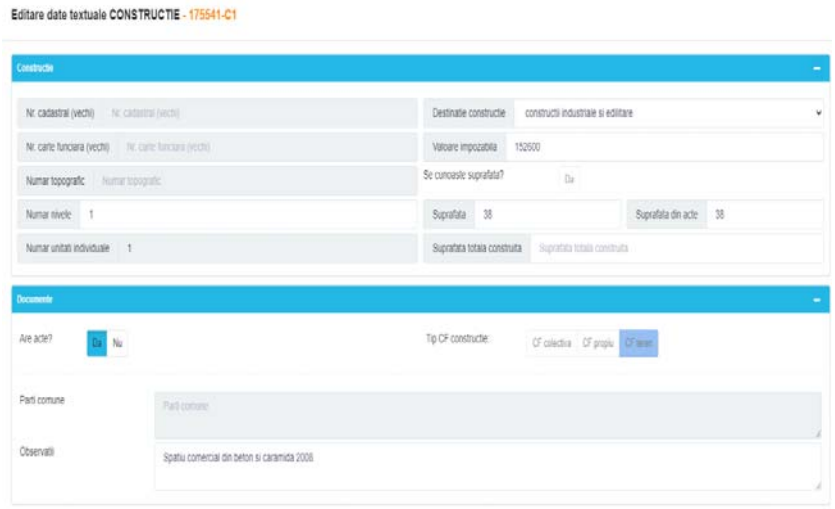

Fig. 7. Textual data associated with the construction studied [17]

After completing the registration of the property data and saving the documentation, the application starts working, being checked and solved by the ANCPI specialized staff. Thus, following the solution of the application, the property is associated with a unique cadastral number and is registered in the land register.

Individuals and legal entities authorized by ANCPI can view and download land registers from all over Romania, only for information purposes and not for use in the civil circuit.

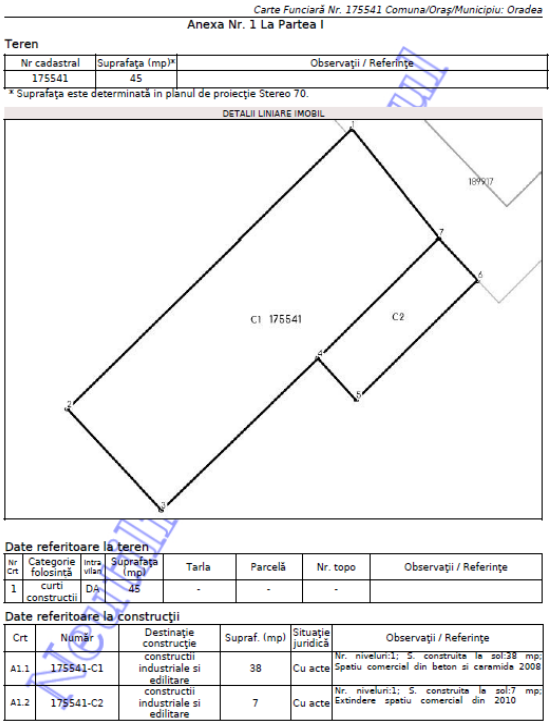

Carte Funciară Nr. 175541 Comuna/Oraș/Municipiu: Oradea

Anexa Nr. 1 La Partea I

Teren

Nr cadastral	Suprafața (mp)*	Observații / Referințe
175541	45	

* Suprafața este determinată în planul de proiecție Stereo 70.

DETALII LINIARE IMOBIL

Date referitoare la teren

Nr Crt	Categorie folosință	Intra vilan	Suprafața (mp)	Tarla	Parcelă	Nr. topo	Observații / Referințe
1	curti constructii	DA	45	-	-	-	

Date referitoare la construcții

Crt	Număr	Destinație construcție	Supraf. (mp)	Situație juridică	Observații / Referințe
A1.1	175541-C1	construcții industriale si edilitare	38	Cu acte	Nr. niveluri:1; S. construita la sol:38 mp; Spatiu comercial din beton si caramida 2008
A1.2	175541-C2	construcții industriale si edilitare	7	Cu acte	Nr. niveluri:1; S. construita la sol:7 mp; Extindere spatiu comercial din 2010

Fig. 8. Land register extract from the integrated cadastre and land registration system for the studied property, Romania [17]

Regarding the development of a cadastral information system to record and manage restrictions, rights and responsibilities on real estate in Romania, the cadastre of public law restrictions developed in Switzerland can be a best practice model that can be applied in Romania.

Even if we cannot talk about a 3D cadastre in terms of the public law restrictions cadastre developed in Switzerland, where spatial data are still represented and visualized in a 2D space, 3D public law restrictions can be successfully applied to 2D spatial data.

2.4. Case study

In this article we have chosen as a case study for highlighting the need to implement public law restrictions in the field of construction in a 3D cadastre, a condominium building in Oradea, Bihor county, over which partially overlaps vertically a body of the adjacent building.

a) b)

Fig. 9. a) Building in the study area, main facade [18]; b) Building in the study area, top view [18]

In this article, I have presented the general legal framework for the application of the provisions in the field of urban and spatial planning, for the building studied I will present the restrictions, rights and responsibilities according to the local urban planning regulation of the municipality of Oradea related to the general urban plan of the municipality of Oradea.

In order to find out the public law restrictions applied to the studied area, the general urban plan (PUG) was studied with the regulations of the territorial unit of reference, information that is published on the local public administration website. According to the general urban plan, the studied building is subject to restrictions in the area of public institutions and services constituted in independent assemblies.

According to the local urban planning regulations, the merging of land with neighbouring buildings for the purpose of building extension is allowed, with a setback from the alignment of 10m [19].

Also, the maximum permitted height of buildings must not exceed 18m [19] and the height of the existing buildings in the alignment must be taken into account when

constructing or extending a building. The volumetric configuration of the buildings will be established in exceptional conditions by the detailed urban plan (PUD) or by the zoning urban plan (PUZ) [19].

The maximum percentage of land occupation for the studied area must not exceed 60% and the maximum land use coefficient must not exceed 2.8 [16]. For these restrictions presented, derogations from the local urban planning regulations may be applied by PUD or PUZ depending on the urban context [19].

3. Results

In order to apply the public law restrictions on the building, it was necessary to carry out measurements and to draw up a more detailed topographical study to determine the maximum height of the building and the horizontal extension, compared to the topographical study currently required for registration in the national integrated cadastre and land registration system.

Fig. 10. Integration of geospatial data into a database of the studied area using ArcGIS Pro software

The symbolism used in figure 5, represents the studied building in purple colour, the red colour highlights the extension of the studied building, the green colour represents the volume of the neighbouring building which partially overlaps the studied building and imposes restrictions on the studied building and its extension and the blue colour represents the neighbouring buildings in the study area.

A 3D model was generated to visualize and manage the public law restrictions applied to the studied building.

Public law restrictions are textual data that cannot be materialised on the ground, but which impose certain restrictions, rights and responsibilities in the field of construction. The representation of these restrictions in a 3D space by means of specialised software makes it possible to understand the need to apply these public law restrictions on buildings.

In the case study, the public law restrictions affect the maximum height of the studied building, and a maximum height of 2.75 m is imposed to which the extension of the studied building can be realized. This restriction is imposed by the building body which is superimposed above the studied building at a height of 3.10 m and by the existing interior installations in the area to be extended which are located at a height of 2.75 m. Following the application of these restrictions the footprint of the extended building and its volume are imposed.

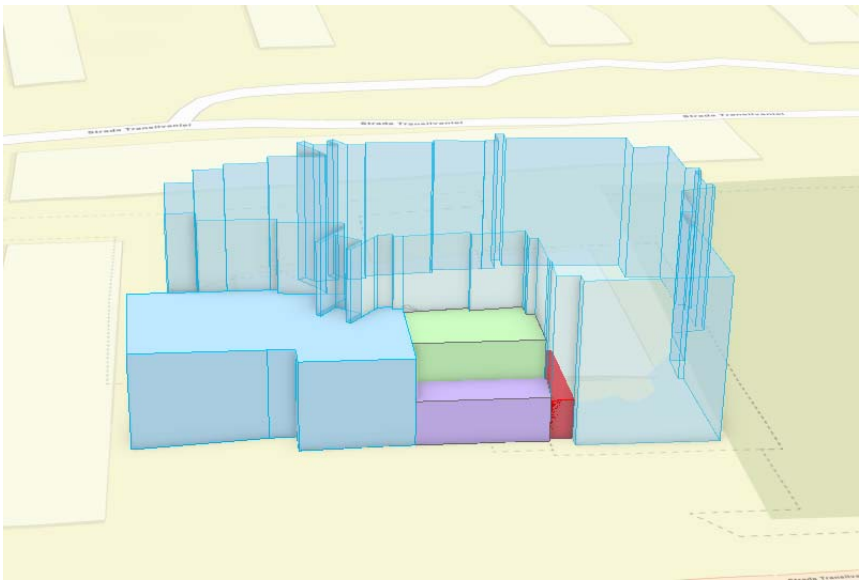

Fig. 11. 3D Public law restrictions in the study area highlighted using ArcGIS Pro software

These restrictions, rights and responsibilities have a legal but also a technical impact on the field of construction, as certain building limits are imposed. They cannot be visualized and managed at the moment in the national cadastral system, because the integrated cadastre and land registration system in Romania only provides the representation of plots and buildings in 2D space together with the property rights applicable in 2D space, without any reference to the imposed urban planning restrictions.

The current Romanian legislation does not offer the possibility of integrating 3D public law restrictions into the national cadastre system, as parcels and buildings located on the Romanian territory are represented as 2D entities.

The realization of the 3D model of the public law restrictions applied to the studied buildings required the study of several legal documents with different sources, this can lead to the hindrance of the development of the cadastre of the public law restrictions, by the significant changes of the legislative documents and the need to trace them in several sources.

The implementation of 3D models of public law restrictions allows detailed representation of the legal space in which the restrictions apply, contributing to the accurate presentation of the rights over real estate [7].

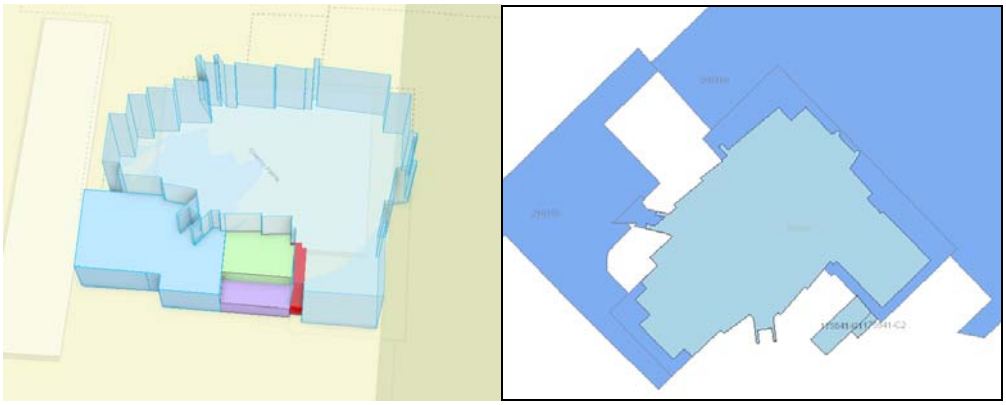

a) b)

Fig. 12. a) 3D model of public law restrictions in the study area using ArcGIS Pro software;
b) The studied area registered in the integrated cadastre and land registration system in Romania [19]

The 3D model generated in the case study shows major differences from the national cadastral system in the delimitation of each building through its representation in 3D space, being generated the volume occupied by each building and the height regime according to the regulations imposed in the national legislation.

4. Conclusion

In this paper the public law restrictions in the field of construction, through urban planning regulations according to the legislation in force and their importance in the development of the built environment have been highlighted.

Even if these public law restrictions applied in the field of construction exist and are regulated in national legislation, they are not integrated in the integrated cadastre and land registration system in Romania.

Real estate represented by parcels and buildings are currently registered in the integrated cadastre and land registration system in a 2D space by means of closed polygon vector spatial data and non-spatial, textual data. Through these closed polygons only the total ground area of each building is determined, not the total built-up area or the volume of the building, because the national cadastral system allows the registration, management and visualisation of the data in a 2D space and for the determination of the volume of the building and the representation of its built-up area a 3D cadastral system needs to be developed. Thus, at the moment the public law restrictions applied in the field of buildings cannot be managed by 2D cadastral systems because the lack of legislation supporting the stratification of buildings in a 3D space allows partial application of 3D restrictions, rights and responsibilities.

The development of the cadastre of public law restrictions requires the registration and management of 3D geospatial data together with the restrictions applied to each real estate property, thus achieving a fully operational system for the management of public law restrictions on the built environment.

References

[1]. D. Kitsakis, E. Dimopoulou, 2016 "Possibilities of Integrating Public Law Restrictions to 3D Cadastres", 5th International FIG 3D Cadastre Workshop 18-20 October 2016, Athens, Greece;

[2]. A. C. Badea, G. Badea, 2020 "Analysing the Opportunity of Implementing an Integrated 3D Public-Law Restrictions System in the Romanian Context", Modern Technologies for the 3rd Millennium, 23 October 2020, Oradea, ISSN, România;

[3]. D. Kitsakis, I. Papageorgaki, 2017 "Towards 3D modelling of public law restrictions in water bodies", European Water, vol. 60, pp. 395 – 401;

[4]. E. Dimopoulou, E. Elia, 2012 "Legal Aspects of 3D Property Rights, Restrictions and Responsibilities in Greece and Cyprus", 3rd International Workshop on 3D Cadastres: Developments and Practices, 25-26 October 2012, Shenzhen, China;

[5]. D. Kitsakis, J. M. Paasch, J. Paulsson, G. Navratil, N. Vučić, M. Karabin, M. El-Mekawy, M. Koeva, K. Janečka, D. Erba, R. Alberdi, M. Kalantari, Z. Yang, J. Pouliot, F. Roy, M. Montero, A. Alvarado, S. Karki, 2018 "Best Practices 3d Cadastres - Chapter 1. Legal foundations", published by The International Federation of Surveyors (FIG), March 2018, Copenhagen, Denmark;

[6]. J. M. Paasch, J. Paulsson, G. Navratil, N. Vučić, D.Kitsakis, M. Karabin, M. El-Mekawy, 2016 "Building a modern cadastre: Legal issues in describing real property in 3D", Geodetski Vestnik, vol. 60, no.2, pp.256-268;

[7]. D., Kitsakis, E. Dimopoulou, 2017 "Addressing Public Law Restrictions within a 3D Cadastral Context". ISPRS International Journal of Geo-Information, volume 6, issue 7, pp. 182;

[8]. M. Besse, 2021 "The Cadastre of Public-law Restrictions on landownership (PLR Cadastre)in Switzerland", FIG e-Working Week 2021, Smart Surveyors for Land and Water Management - Challenges in a New Reality, 21–25 June 2021, Netherlands;

[9]. www.geo.vd.ch (accessed October, 2023);

[10]. www.rdppf.vd.ch (accessed October, 2023);

[11]. Legea 50 din 29 iulie 1991, privind autorizarea executării lucrărilor de construcții a fost adoptata de Parlamentul Romaniei, publicata in Monitorul Oficial nr. 933 din 13 octombrie 2004;

[12]. Legea 10 din 18 ianuarie 1995 privind calitatea în construcții a fost adoptata de Parlamentul Romaniei, publicata in Monitorul Oficial nr. 765 din 30 septembrie 2016;

[13]. Legea 350 din 6 iunie 2001, privind amenajarea teritoriului și urbanismul, a fost adoptată de Parlamentul României, publicată în Monitorul Oficial nr. 373 din 10 iunie 2001;

[14]. Norme metodologice din 26 februarie 2016 de aplicare a Legii nr. 350/2001 privind amenajarea teritoriului și urbanismul și de elaborare și actualizare a documentațiilor de urbanism, emisa de Ministerul Dezvoltării Regionale si Administrației Publice, publicata in Monitorul Oficial nr. 199 din 17 martie 2016;

[15]. Legea 7 din 13 martie 1996, cadastrului si a publicitatii imobiliare emisa de Parlamentul Romaniei, publicata in Monitorul Oficial nr. 201 din 3 martie 2006;

[16]. Regulament din 8 februarie 2023 de receptive si inscriere in evidentele de cadastru si carte funciara, emis de Agentia Nationala de Cadastru si Carte Funciara, publicat in Monitorul Oficial nr. 125bis din 14 februarie 2023;

[17]. www.eterra.ancpi.ro (accessed October, 2023);

[18]. www.google.com/maps (accessed October, 2023);

[19]. www.oradea.ro (accessed October, 2023);

Acknowledgements

This study id developed using Esri software licenses provided by the Doctoral School of the Technical University of Civil Engineering Bucharest.

This study was conducted within the Geodetic Engineering Measurements and Spatial Data Infrastructures Research Centre, Faculty of Geodesy, Technical University of Civil Engineering Bucharest.

The influence of ventilation with heat recovery, and solar energy in the sizing of soil collectors

Influența ventilației cu recuperarea căldurii și a energiei solare în dimensionarea captatorilor de sol

Florin Vladimir Mihailov [1], Sebastian Parfene[1], Grațiela Țârlea [1]

[1]Universitatea Tehnică de Construcții București.
Bd.lacul Tei nr. 122-124, cod 02396, Sector 2, București, Romania
E-mail: florin-vladimir.mihailov@phd.utcb.ro

DOI: 10.37789/rjce.2024.15.3.3

Abstract. *The European Green Pact aims to make Europe neutral in terms of climate and CO2 emissions by 2050. The residential sector contributes to the emission of greenhouse gases in a proportion of over 39%, of which 28% represent emissions generated by energy consumption to ensure climatic conditions (heating, cooling), 11% are emissions resulting from technological manufacturing processes of construction materials, and an undefined percentage represents energy consumption for the thermal preparation of food. Actions aimed at reducing greenhouse gas emissions go in the direction of replacing building materials with a high CO2 footprint with traditional materials and with a low degree of processing, and replacing large greenhouse gas-generating heating and cooling sources with alternative, renewable sources without reducing or compromising comfort. The use of heat pumps, and especially those that use geothermal resources, for heating and domestic hot water preparation is becoming an attractive and decisive solution in the effort to reduce greenhouse gas emissions. In order to set a budget for the investment and to make a decision, it is necessary to dimension the equipment and implicitly the soil collectors (the length and quantity of boreholes needed for operation).*

Key words: heat pump, renewable resources, geothermal resource, energy efficiency, traditional solutions

Rezumat. *Prin pactul verde European se are în vedere ca până în anul 2050 Europa să devina neutră din punct de vedere climatic și al emisiilor de CO_2. Sectorul rezidențial contribuie la emiterea gazelor cu efect de seră în proporție de peste 39%, dintre acestea 28% reprezintă emisiile generate de consumul de energie pentru asigurarea condițiilor climatice (încălzire, răcire), iar 11% sunt emisii rezultate în urma proceselor tehnologice de fabricare a materialelor pentru construcții, un procent nedefinit îl reprezintă consumul de energie pentru prepararea termică a hranei. Acțiuni menite să reducă emisiile gazelor cu efect de seră se duc în direcția înlocuirii materialelor de construcții cu amprentă ridicată de CO_2 cu materiale tradiționale și cu un grad scăzut de procesare, înlocuirea surselor de încălzire și răcire mari generatoare de gaze cu efect de seră cu surse alternative, regenerabile, fără reducerea sau compromiterea confortului. Utilizarea pompelor de căldură, și în special a celor ce folosesc resursa geotermală, pentru încălzire și preparare apă caldă menajeră devine o soluție atractivă și determinantă în efortul de reducere a emisiilor gazelor cu efect de seră. Dimensionarea echipamentelor și implicit a captatorilor de sol, (lungimea și numărul de foraje necesar*

funcționării) este o etapă preliminară stabilirii unui buget pentru realizarea investiției și tot o dată un factor decisiv în luarea unei decizii.

Cuvinte cheie: pompă de căldură, resurse regenerabile,resursă geotermală, eficiență energetică, soluții tradiționale

1. Introduction

In light of the current energy crisis and Europe's goal to become the first continent with net CO2 emissions neutrality by 2050, [5] solutions are being sought to reduce the consumption of fossil fuels and to find new solutions and technologies that are environmentally friendly and do not produce greenhouse gases..

A sector with a consistent contribution of greenhouse gas emissions is the residential sector, which produces more than 39% of greenhouse gas emissions, of which 28% are emissions resulting from energy consumption to ensure comfort thermal (heating/cooling) and 11% are generated by the building materials manufacturing industry.

The use of renewable energy sources represents a viable solution for reducing greenhouse gas emissions resulting from the burning of fossil fuels. The seasonal nature of solar energy (1) makes the heat pump a concrete alternative for replacing equipment that uses fossil fuels.

Depending on the environment from which the heat is extracted, heat pumps are classified into air-water, water-water, soil-water heat pumps. If for air-to-water heat pumps they have the evaporator predefined by the manufacturer and subject to limiting conditions the minimum outside air temperature for heat extraction and variable COP, with temperature, known; instead for heat pumps, water-water and soil-water, additional works are required consisting of drilling for water or geothermal, works that impose additional costs, mostly unknown at the time of system design.

2. Presentation of the work

In this paper, an analysis is made of the dimensioning of the soil collector for soil-water heat pumps, as well as the influences of the energy balance and the energy performance of the building equipped with such a pump in the dimensioning of the soil collectors.

The subject of the analysis is a building, Fig. 1, to be built, predominantly made of ecological materials (wood, reeds, and straw bales), using traditional constructive solutions subject to modern technological updates.

The building, with a footprint of 70 sq m, is to be used as an agro-tourism accommodation unit and has on the ground floor a living room of 26 sq m, a technical space/kitchen of 13 sq m, two bathrooms of 4 sq m each, the staircase and access hall, and in the attic there are 4 bedrooms of 12 sq m each (Fig.2).

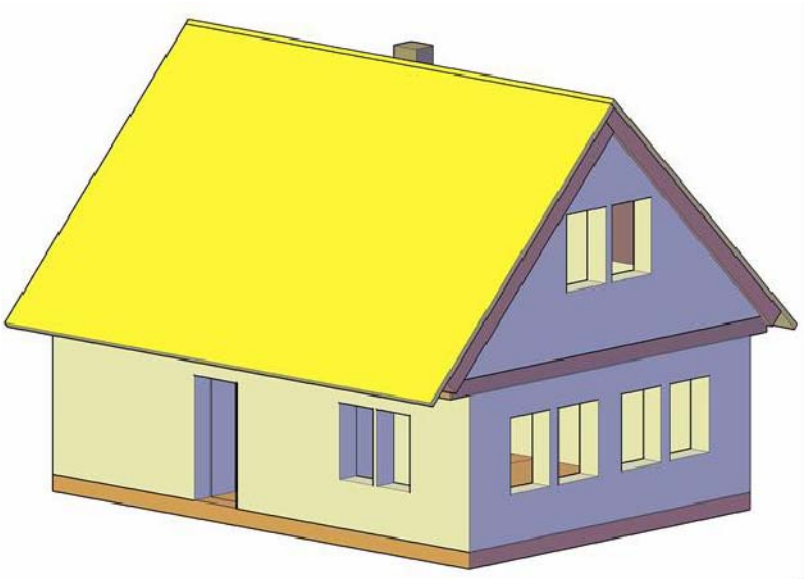

Figure.1 Ecological construction will be built according to the building regulations in the Danube Delta.

The energy analysis will follow the determination of the calculation heat requirement determined according to SR 1907-1 and the establishment of the annual energy requirement for heating according to C107. The calculation will be made for the minimum standardized resistances according to MC 001 and for the resistances determined by the chosen constructive solution.

The obtained results will be analyzed from the perspective of the parameters necessary for the operation of soil-water heat pumps in optimal conditions and the requirements for geothermal drilling.

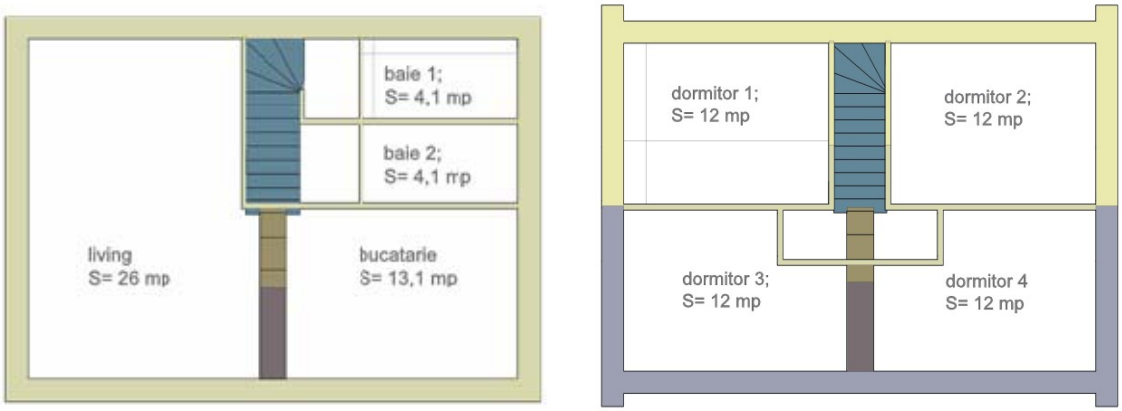

(a) (b)

Figure. 2. Ground floor plan (a), Attic plan (b)

3. Technical parameters

The composition of the tire and the thermotechnical characteristics [4] of the

constructive elements are presented in Table (1), compared to the solution of the resistances of the tire components according to the constructive solution, Table (2), an increase in the average corrected resistance of the tire, Table (3).

Table 1

Thermotechnical characteristics of tire elements - minimum requirements						
Nr.crt	The Construction Element	A	R'm	τ	(A·τ)/R'm	percentage of the building envelope
		m^2	m^2K/W	--	W/K	%
0	1	2	3	4	5	6
1	Flooring	57.33	5.00	1	11.47	23.25
2	Exterior walls	109.17	4.00	1	27.29	44.26
3	Exterior carpentry	17.55	1.11	1	15.80	7.12
4	Sarpannta	57.33	6.67	1	8.60	23.25
5	Outer door	5.25	0.77	1	6.82	2.13
T O T A L	Suprafață anvelopă	246.63	**3.525**	--	69.97	
VOLUM	m³	303.85				

Table 2

Thermotechnical characteristics of tire elements - constructive solution						
Nr.crt	The Construction Element	A	R'm	τ	(A·τ)/R'm	percentage of the building envelope
		m^2	m^2K/W	--	W/K	%
0	1	2	3	4	5	6
1	Flooring	57.33	5.69	1	10.08	23.25
2	Exterior walls	109.17	5.58	1	19.57	44.26
3	Exterior carpentry	17.55	1.77	1	9.93	7.12
4	Sarpannta	57.33	6.97	1	8.22	23.25
5	Outer door	5.25	0.77	1	6.82	2.13
T O T A L		246.63	**4.516**	--	54.62	
VOLUME	m³	303.85				

Table 3

		S1	S2	GROWTH
		R'm	R'm	
		m^2K/W	m^2K/W	%
		3	3	
Flooring		5.00	5.69	13.76
Exterior walls		4.00	5.58	39.47
Exterior carpentry		1.11	1.77	59.05
Sarpannta		6.67	6.97	4.57
Outer door		0.77	0.77	0.00
Medium resistance		3.52	4.52	28.10

3.1 Determination of the calculation heat requirement SR1907-1

The calculation of heat requirement Q0 expressed in watts, determined by formula (1) represents the parameter that establishes the technical characteristics of the heating equipment: radiators, heat generators, radiant surfaces, etc. It depends on the degree of insulation, respectively, on the thermal resistance of the tire elements and on the supply of fresh air for ventilation.

$$Q^{NEC}_{tot} = Q^{NEC}_{tra} + Q^{NEC}_{aer} \quad (W) \quad (1)$$

- Q^{NEC}_{tot} = total heat flow (W)
- Q^{NEC}_{tra} = the heat flow lost through transmission; formula (2) (W)
- Q^{NEC}_{aer} = thermal flow for heating fresh air; formula (3) (W)

$$Q^{NEC}_{tra} = c_m * \sum \frac{A_j}{R_j} * \left(\theta_i - \theta_{e_j}\right) + Q_S \quad (W) \quad (2)$$

$$Q^{NEC}_{Aer} = 0{,}334 * n_a * C_m * V_i * (\theta_i - \theta_e) + Q_u \quad (W) \quad (3)$$

The calculation was performed in 3 (three) scenarios;

- Scenario 1: The tire elements have the minimum standardized resistances; the number of air exchanges is 0.5; without ventilation with heat recovery, the calculation of the external temperature is -15°C.
- Scenario 2: The tire elements have the resistances determined in the laboratory for the constructive solution; the number of air exchanges is 0.5 [h^{-1}] without ventilation with heat recovery.
- Scenario 3: The tire elements have the resistances determined in the laboratory for the constructive solution; the number of air exchanges is 0.053 []. calculated for a requirement of 25 m^3h for one user, the

calculated outdoor temperature was corrected to 17.8°C, ventilation with recovery heat, and the recovery efficiency was 92% [2].

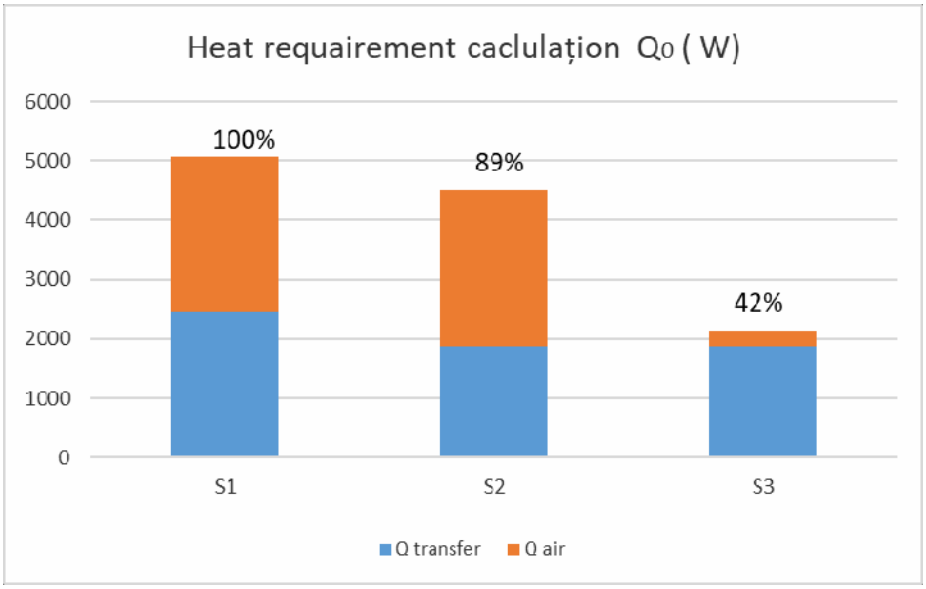

Figure. 3 Calculation of heat requirement

To compensate for heat losses, equipment with a minimum thermal power of 6 kW in scenario 1, 5.5 kW in scenario 2, and 2.6 kW in scenario 3 is required.

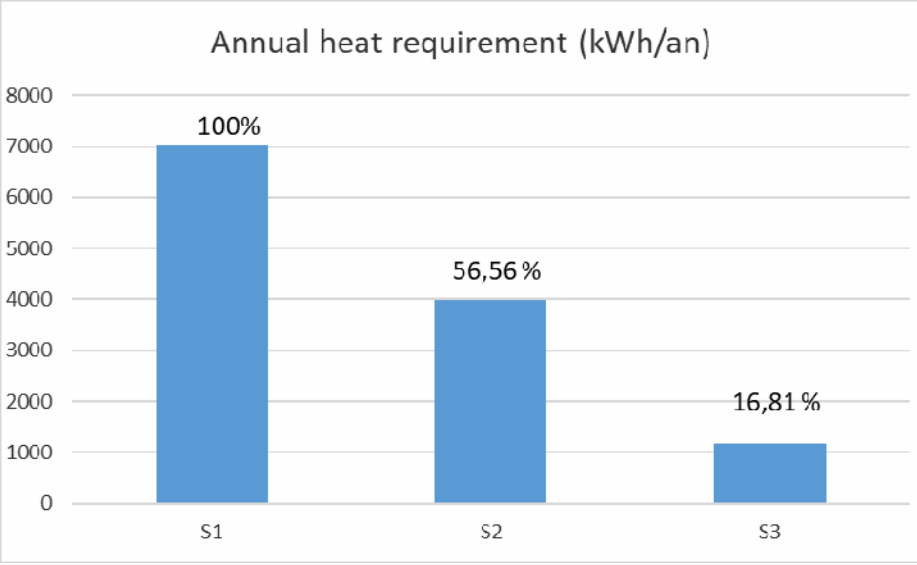

Figure. 4 The annual heat requirement

1. Increasing the corrected average resistance by 28% generates a reduction in the calculation heat requirement by 11% and a reduction in the annual heat requirement by 43.44%.

2. Increasing the corrected average resistance by 28% and using ventilation with heat recovery with an efficiency of 92% generates a reduction in the calculation heat requirement by 58% and a reduction in the annual heat requirement by 83.19%.

3.2 Establishing the annual energy requirement for domestic hot water preparation

According to I9/2022, Annex 1.2, the specific water requirement, V _(s,day) and the specific hot water requirement, V _(s,day,ac) for buildings (except residential buildings) for accommodation units of 2 stars, without laundry, is 190 liters/person.day cold water and 76 liters/person.day. The volume of daily hot water consumption is calculated with formula (4).

$$V_{ac,zi} = V_{s,zi,ac} * N_p \quad (4)$$

Table 4 shows the calculation of the hot water and thermal energy requirements to bring the cold water from 10 °C to a temperature of 60 °C, including the annual energy requirement.

Table 4

necesarul maxim anual de energie pentru preparare apă caldă												
	ian	feb	mar	apr	mai	iun	iul	aug	sep	oct	nov	dec
nr persoane	8	8	8	8	8	8	8	8	8	8	8	8
litri/pers,zi	76	76	76	76	76	76	76	76	76	76	76	76
litri/zi	608	608	608	608	608	608	608	608	608	608	608	608
kwh/zi	34.7	34.7	34.7	34.7	34.7	34.7	34.7	34.7	34.7	34.7	34.7	34.7
nr zile, lună	31	28	31	30	31	30	31	31	30	31	30	31
litri/lună	18848	17024	18848	18240	18848	18240	18848	18848	18240	18848	18240	18848
kwh/lună	1075.63	971.54	1075.63	1040.94	1075.63	1040.94	1075.63	1075.63	1040.94	1075.63	1040.94	1075.63
kwh/an	12664.71											

3.3 The annual energy requirement for domestic hot water preparation and heating

The cumulative annual energy requirement for the production of domestic hot water and heat was determined for the three calculation scenarios represented in Fig. 5.

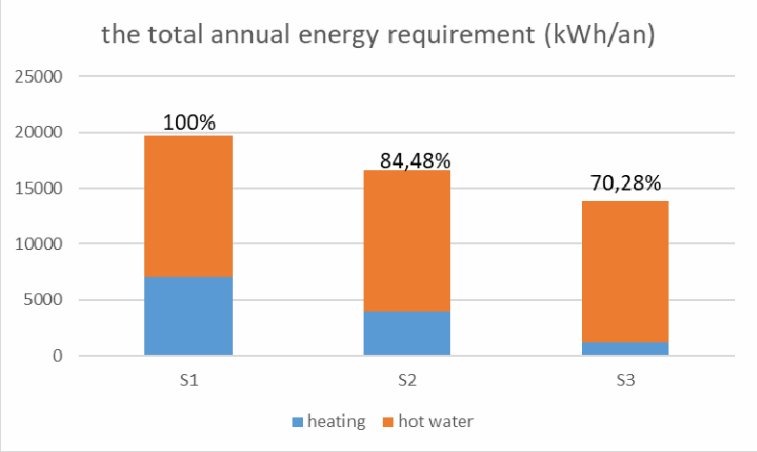

Figure. 5 Total annual heat requirement: hot water + heating

4. Solar thermal energy available

Solar energy has a seasonal character [3], in which the available energy is influenced by the calendar period of the year [7], by the latitude at which the equipment is installed, by the mounting angle of the solar energy capture elements, and the efficiency of the equipment to capture solar energy. Fig. 6 shows the average monthly energy available in the place. Zimnicea per square meter in the case of installation angles of 0°, 45°, and 90°.

For the analyzed building, it was decided to mount a solar system with vacuumed thermal tubes in a closed loop, which has 60 tubes. The net capture area is 7.8 m^2. Hot water is stored in two boilers connected in series, with a total capacity of 620 liters (120 liters + 500 liters).

The solar thermal system dimensioned in this way fully covers the hot water requirement for the months of March–October [6] and has input for preparing hot water in the months of November–February. Fig 7.

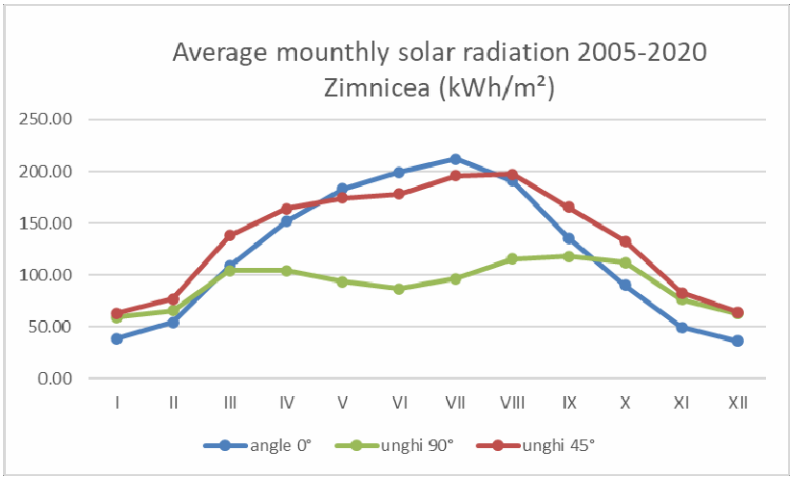

Figure. 6, Average monthly radiation for the period 2005–2020 for different montaj angles

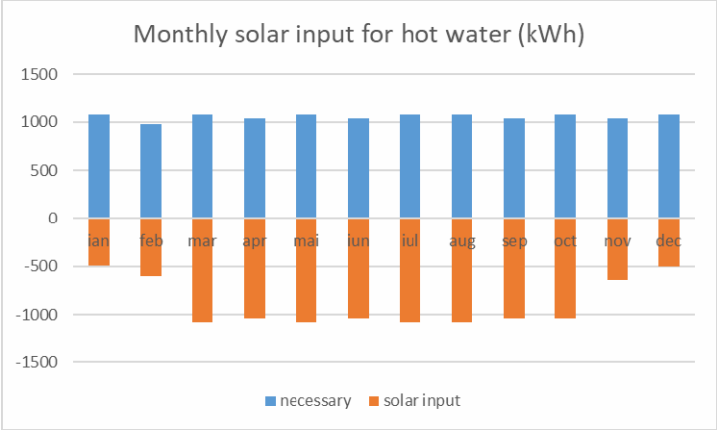

Figure. 7. Solar input for hot water preparation.

The introduction of solar energy into the energy balance reduces the annual energy requirement in scenario 1 by 54.3%, in scenario 2 by 64.29% and in scenario 3 by 77.28%.Fig. 8

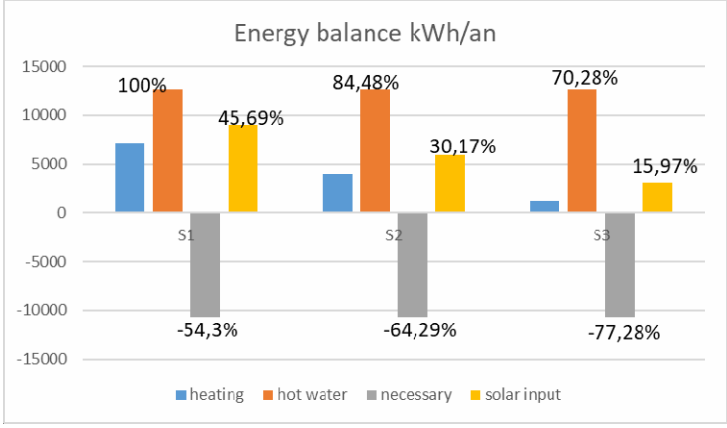

Figure. 8. Bilanțul energetic.

4. Results analysis

For the building under analysis, in the three working scenarios, the thermal powers were determined (Table 5), based on which possible options for choosing the heat pump were identified.

Table 5

scenario	**Q nec**	Qheat	Qhw	**Qtotal1**	Qsolar	**Qtotal2**
	W	kWh/an	kWh/an	**kWh/an**	kWh/an	**kWh/an**
S1	**5067**	7039	12664,71	**19703,71**	-10701	**9002,66**
S2	**4498**	3981	12664,71	**16645,71**	-10701	**5944,66**
S3	**2143**	1183	12664,71	**13847,71**	-10701	**3146,66**

Following the market study, the following equipment was identified as being able to satisfy the comfort requirement: Table 6

Table 6

technical specifications	Flow	Qheat	Δt
tip pompă căldură	m³/h	kWh	°C
TMC 22 hyper-jet	1.20	8	3
NIBE S1155	1.08	8	3
ecoGEO B/C 1-9	1.32	9	3

Heat transfer in the soil collector is of the conductive convective type in the stationary regime in the cylindrical wall.

Convective components, respectively, the hydraulic component of the soil collectors, must be sized in such a way as to ensure the minimum temperature difference to ensure vaporization of the refrigerant at the nominal flow indicated by the heat pump manufacturer.

Figure 9 shows the principle diagram of heat exchange in an environment with a constant temperature (soil temperature).

In this case

- t_1'=t_1"=t_{sol}
- t_2"= t_1"-2°C
- t_2'= t_2"- Δt minimum required

The minimum required Δt represents the minimum required temperature difference in the evaporator.

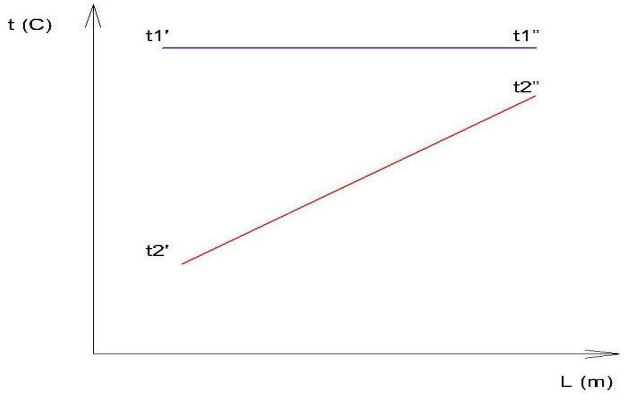

Figure. 9. Diagram of heat transfer in a medium with a constant temperature

The analysis of soil collectors will be carried out on two levels;

1. Hydraulic (convective) analysis of the solution adopted for the realization of soil collectors; pipe diameter, material conductivity, heat exchange surface, economic speeds.

2. Analysis of the environment (conductive transfer through the cylindrical wall) from which heat is extracted; specific heat of the soil (unit/average); density; initial temperature (at the entrance to the heating season); final temperature (at the exit from the heating season); regeneration capacity so that the soil temperature escapes to the initial temperature upon entering the heating season.

Hydraulic analysis of the soil collector, determination of the heat exchange surface, maintaining a minimum temperature difference Δt in the vaporizer, determining the length and number of boreholes.

The LMTD method for a two-fluid heat exchanger uses relations (5), (6), and (7)

$$Q_1 = \dot{m}_1 * c_1 * (t_1' - t_1'') = \dot{C}_1 * (t_1' - t_1'') \quad (5)$$

$$Q_2 = \dot{m}_2 * c_2 * (t_2'' - t_2') = \dot{C}_2 * (t_2'' - t_2') \quad (6)$$

$$Q_{tr} = K * A * \Delta t_m \quad (7)$$

Considering that the heat transfer from the hot source is exclusively conductive in a cylindrical wall, then formula (5) turns into formula (5').

$$Q_1 = \frac{2\pi\lambda l}{ln\frac{r_2}{r_1}} * (t_1 - t_2) = \frac{\pi l}{\frac{1}{2\lambda} ln\frac{d_2}{d_1}} (t_1 - t_2) \quad (5')$$

In which case

- t_1= soil temperature
- $t_2 = \frac{t_2' + t_2''}{2}$ (8)

Q1=Q2=Qtr

Calculation parameters:

- The density of the working fluid, ρ=kg/m³
- The specific heat of the working fluid c=J/kgxK
- The diameter of the soil trap d=m
- Flow section A=m²
- Primary circuit fluid flow Q=m/s, m³/h

5. Conclusions

The use of ventilation with heat recovery and solar energy generates significant reductions in the realization of soil traps of up to 87%.

The thermal requirement for heating of 25% of the thermal capacity of the equipment has the effect of a reduced operating time and, implicitly, a reduction in wear and savings on energy consumption.

The reduction of investment costs generated by the realization of geothermal wells adapted to the corrected energy requirement makes the solution of using geothermal heat pumps attractive..

It is important once again to continue the study by analyzing the heat transfer in the soil between the thermal agent that circulates through the pipes of the collector and the energy stored in the soil, determining the amount of heat extracted, and evaluating the resilience time between two seasons.

A solution to encourage the adoption of solutions with geothermal heat pumps is subsidizing, with up to 100% of the drilling.

For the purchase of heating equipment with zero CO2 emissions, access to loans with subsidized interest up to 0% must be ensured.

6. Bibliografie

[1] https://atreashop.ro/wp-content/uploads/2022/08/Atrea-Catalog-Tehnic-Duplex_EC5_RO.pdf accesat la data de 30.09.2023 , ora 22.36

[2] The potential of solar radiation to reduce dependence on fossil fuels, energy analysis Phd Florin Mihailov, 23nd International Scientifc Multidisciplinary Conference on Earth and Planetary Sciences SGEM 2023, 01-10.07.2323

[3] The potential of solar radiation to reduce dependence on fossil fuels, energy analysis, Phd Florin Mihailov,
23nd International Scientifc Multidisciplinary Conference on Earth and Planetary Sciences SGEM 2023, 01-10.07.2323

[4] Metodologie de calcul al performanței energetice a clădirilor, indicativ Mc 001-2022

[5] https://commission.europa.eu/strategy-and-policy/priorities-2019-2024/european-green-deal_ro

[6] https://joint-research-centre.ec.europa.eu/pvgis-online-tool_en

[7] A. E. Gürel , Ü. Agbulut , H. Bakır , A. Ergün, G. Yıldız. 2023. *A state of art review on estimation of solar radiation with various models*. Heliyon, Volume 9, Issue 2, February 2023, e13167[5]

Reduction of sodium valproate compounds concentrations in water intended for human consumption by activated carbon

Reducerea concentrației de compuși de valproat de sodiu în apa destinată consumului uman prin cărbune activ

Khemis Oussama[1], Prof. Dr. Ing. Gabriel Racoviteanu[2]

[1]Department environnement, Technical University Construction Bucharest.
Bulevardul Lacul Tei 124, București 020396, Roumanie.
E-mail:khemis.oussama21000@gmail.com

[2]Department environnement, Technical University Construction Bucharest.
Bulevardul Lacul Tei 124, București 020396, Roumanie.
E-mail: racoviteanu.gabriel@gmail.com

DOI: 10.37789/rjce.2024.15.3.4

Abstract. In our research project with the objective of reducing the pharmaceutical substance valproate sodium, it is aimed to reduce the concentrations of this pharmaceutical compound. Their water retention is carried out by several treatments and among these unconventional treatment methods such as: advanced oxidation, biological product with biomass, adsorption and catalytic oxidation suitable for this type of hulls.
Due to the fact that part of the drugs are dispensed in pharmacies without a prescription, they are used and would be part of it, but also their metabolites end up in insurface water. Similarly, the intensive use of antibiotics and growth hormones in animal husbandry and the resulting insufficient treatment of surfacewaters by these elements.
Pharmaceuticals are generally synthetic organic layers that are used for the purpose of improving animal and human health. Overuse of torah needles leads to their elimination andthe elimination of their metabolites through the urine. Similarly, dispensing without a prescription leads to the rare expiration of these substances which, when expired, mostly endup in the landfill.
Internationally, there are studies of the risk posed by pharmaceuticals, their metabolites fromwater often intended for human consumption, and research into various means of reducing their concentration in water intended for human consumption.
For the realization of the research project, studies will be reintegrated on laboratory facilities and pilot facilities of the water treatment laboratory of the Colentine laboratory complex, Faculty of Hydrotechnics. In this experimental research at colentina laboratory (romania) we 'to study the pharmaceutical substance valproate sodium with the treatment of adsorption by activated carbon at different concentrations (0.4, 0.8 and 1.6 mg/l) at two different flow rates (1.25 l/minand 2.5 l/min).

Key words: pharmaceutical substance, valproate sodium, pollution of surface, adsorption.

1. Introduce

Our research aims to reduce pharmaceutical concentrations in water intended for human consumption.

In this work, we used the pharmaceutical substance metoclopramide as a pollutant with different and low concentrations that can be found in the ecosystem (1.6, 0.8 and 0.4 mg/l).

Among all the adsorption processes that do not give chemical toxicity compared to other processes that pose a danger to the ecosystem when it does not comply with the exact treatment measures used.

In our experimental research, we use a granular activated carbon adsorption process, and this process is also cheaper compared to other processes with a very high adsorption percentage.

1. Working method used

Among all the adsorption processes that do not give chemical toxicity compared to other processes that cause danger to the ecosystem when it does not respect the exact treatment measures used.

In our experimental research we use a process of adsorption by granulated active

carbon which does not give human or animal toxicity and also this process is cheaper compared to other processes with a very high percentage of adsorption.

There are three steps to follow as follows:

• The first step is to wash the granulated activated carbon with tap water for 48 hours ina 1000-liter capacity water tank to release all the pollutants it contains.

• the second step takes three samples at 15min intervals (15min, 30min, 45min) of thesubstance sodium valproate.

Each solution is directly analyzed by TOC measurement.

1.1. Analyzer TOC

TOC is used to measure organic micropollutants in water (wastewater and hazardous waste in the aquatic environment) and gives the total amount of oxygen by chemical oxidation of organic matter in the sample under high heat condition (148C°). The advantage of COT can analyze several samples at the same time (more than 60 samples) is each result remains almost 10min compared to other products which need a few days (eg the BOD remains five days to see the result).

In our research project the products used as presented in Figure 1

It must be placed in a place with a temperature between 15C° and 20C° in order to preserve its chemical properties.

Figure 1 TOC Analyzer.

1.2. Treatment pilot

The O_3/CA pilot consists of two cylindrical reactors (R1=200mm, R2=100mm):

• the R1 reactor includes an ozone mixer which allows the injection of ozone into the waterto be treated

• the R2 reactor includes granulated activated carbon (GAC) and a water level regulator inorder to obtain the solution to the treated water.

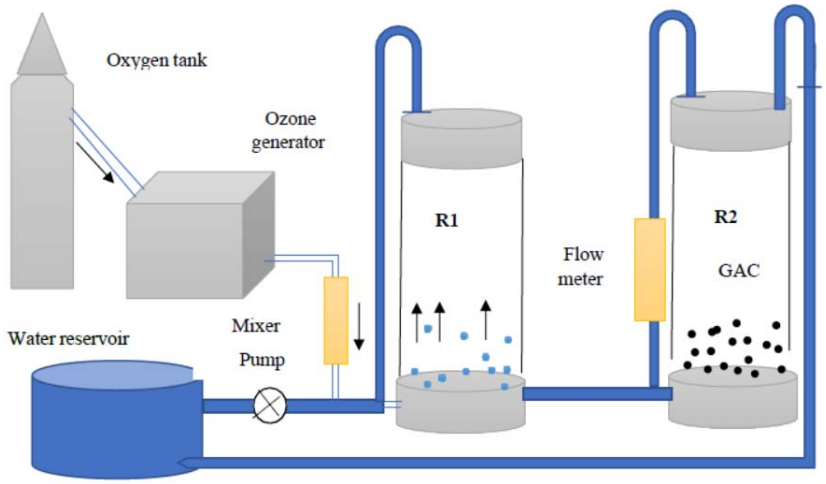

Figure 2 Diagram of the processing driver.

2. Main results obtained

2.1. Degradation of sodium valproate at a concentration of 1.6 mg/l

Figure 3 shows the percentage elimination with the active carbon adsorption process at a concentration of 1.6 mg/l.

We can see in this figure for the concentration 1.6 mg/l of sodium valproate in the flow rate (1.25 l/min) the elimination rates are very sufficient in the time 45min which gives percentages that exceed the half with values of 55.25%.

In the 30min contact time the flow rate of 1.25 l/min gives an elimination rate of 53.75 ٪ however in the 2.5 l/min flow rate it gives a low rate with a value of 41.5 ٪ but in the 15min time and in the flow rate 1.25 l/min the elimination rate is insufficient (49.62٪) compared tothe other flow rate which is low with a value of 33.5٪

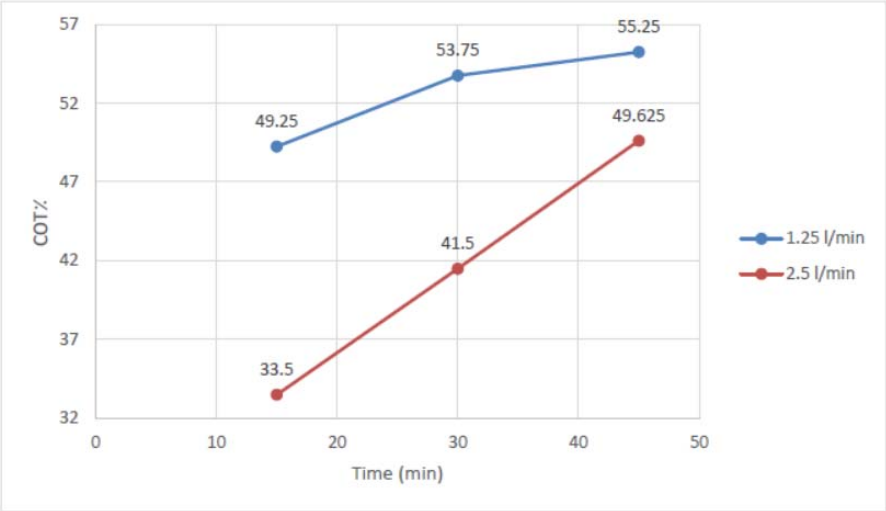

Figure 3 Percentage of adsorption by CA alone at a concentration of 1.6 mg/l.

2.2. Degradation of sodium valproate at a concentration of 0.8 mg/l

Figure 4 shows the percentage of elimination with the active carbon adsorption process at aconcentration of 0.8 mg/l.

We can see in this figure for the concentration 0.8 mg/l of sodium valproate with a flow rateof 1.25 l/min the elimination by the process of adsorption by active carbon is sufficient and the rate of elimination exceeds 50٪ at all contact times, on the other hand in the flow rate of 2.5 l/min it is not sufficient for other flow rates and its elimination rate does not exceed 50٪ inthe times of 15 and 30min with a percentage of 46.88 and 49.63٪, but in the time 45min it gives an interesting rate with a value of 50.31٪.

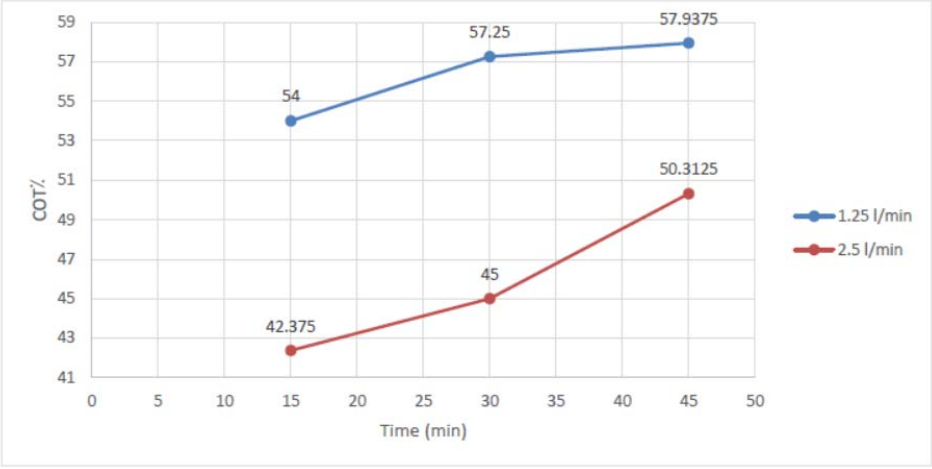

Figure 4 Percentage of adsorption by CA alone at a concentration of 0.8 mg/l.

2.3. Degradation of sodium valproate at a concentration of 0.4 mg/l

Figure 5 shows the percentage elimination with the active carbon adsorption process at a concentration of 0.4 mg/l.

We can see in this figure for the concentration 0.4 mg/l of sodium valproate with a flow rate of 1.25 l/min the elimination by the process of adsorption by active carbon is very sufficient because we obtain a rate of elimination with a value of 61 ٪ in the contact time 45min, on theother hand in the flow 2.5 l/min and at the same time it gives a percentage of elimination 51.5٪and the difference between the two flows varies 10٪

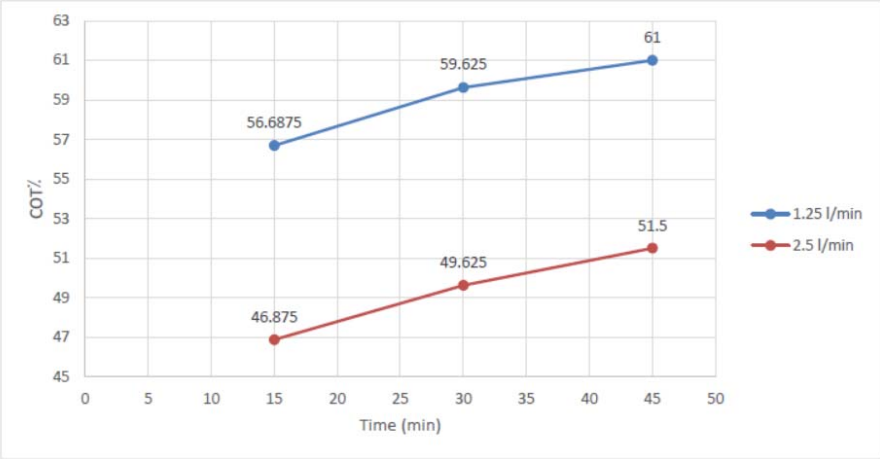

Figure 5 Percentage of adsorption by CA alone at a concentration of 0.4 mg/l.

5. Conclusion

The adsorption process using granular activated carbon which is applied to the valproate sodium substance gives interesting results with elimination percentages up to 61٪ at a concentration of 0.4 mg/l at a flow rate of 1.25 l/min and 51.5٪ at the same concentration at a flow rate of 2.5 l/min and this percentage increases with decreasing concentrations and also decreasing flow rates.

We conclude that the activated carbon adsorption process is particularly effective in yielding more hydroxyl radicals that attack these pharmaceutical pollutants.

References

[1] A. Bhatnagar, W. Hogland, M. Marques, M. Sillanpää, An overview of the modification methods of activated carbon for its water treatment applications, Chem. Eng. J. 219 (2013) 499–511, https://doi.org/10.1016/j.cej.2012.12.038.

[2] Kim, I., Tanaka, H., 2010. Use of ozone-based processes for the removal of pharmaceuticals detected in a wastewater treatment plant.Water Environ. Res. 82, 294e301.

[3] Carbajo, M., Rivas, F.J., Beltrán, F., Alvarez, P., Medina, F., 2006. Effects of different catalysts on the ozonation of pyruvic acid in water. Ozone-Sci. Eng. 28, 229e235.
[4] Fent, K., Weston, A.A., Caminada, D., 2006. Ecotoxicology of human pharmaceuticals. Aquat. Toxicol. 76, 122–159.
[5] Geissen, V., Mol, H., Klumpp, E., Umlauf, G., Nadal, M., van der Ploeg, M., van de Zee, S.E.A.T.M., Ritsema, C.J., 2015. Emerging pollutants in the environment: a challenge for water resource management. Int. Soil Water Conserv. Res. 3, 57–65.

The influence of the analyzed data lengths variability on the behavior of the GEV and Pearson III distributions

Influența variabilității lungimilor datelor analizate asupra comportamentului distribuțiilor GEV și Pearson III

Cristian Gabriel Anghel[1], Cosmin Craciun[2], Constantin Albert Titus[3], Cornel Ilinca[4]

[1,2,4]Technical University of Civil Engineering Bucharest
Lacul Tei Boulevard Nr. 124, Bucharest 020396, Romania
[3]Politehnica University Timisoara, Romania
Piata Victoriei Nr. 2, Timisoara, Romania

[1]*E-mail: cristian.anghel@utcb.ro*
[2]*E-mail: cosmin.craciun@phd.utcb.ro*
[3]*E-mail: albert.constantin@upt.ro*
[4]*E-mail: cornel.ilinca@utcb.ro*

DOI: 10.37789/rjce.2024.15.3.5

Abstract. This manuscript presents the influence of the variability of the recorded data series on the behavior and generation of quantile values for two of the most used statistical distributions in the frequency analysis of extreme events in hydrology, namely the generalized extreme value (GEV) distribution and the Pearson III distribution. The methods for estimating the analyzed parameters are the method of ordinary moments and the method of linear moments, which represent two of the most used methods for estimating the parameters of statistical distributions. According to the results obtained, the L-moments method represents a more stable and robust method characterized by much smaller biases than the ordinary moments method, for quantile values in the field of rare and very rare events (low and very low annual exceedance probabilities).

Key words: estimation parameters; method of ordinary moments; method of linear moments; Pearson III; GEV.

1. Introduction

The variability of the lengths of recorded data has an important role in determining the maximum extreme values in hydrology, especially in the frequency analysis of maximum flows and precipitation.

In general, the direct determination of these maximum values corresponding to the annual exceedance probabilities of interest in hydrology is done through frequency analysis [1].

This implies the use of certain statistical distributions, respectively certain parameter estimation methods [2-4].

Regarding the probability distributions, two of the most used distributions are the generalized extreme value (GEV) distribution and the Pearson III distribution [2-5]. In recent materials [4,6-12], important contributions have been made to these distributions as well as to a significantly large number of other distributions and families of distributions.

As parameter estimation methods, the method of ordinary moments (MOM) and L- moments methods are two of the most analyzed methods, having the advantage of being based on statistical indicators that can be determined regionally [5]. Otherwise, the L-moments method is the most used method in the processes of regionalization of extreme events.

Regarding these two distributions and parameter estimation methods, important contributions were made by Anghel and Ilinca [4,6-12] who made contributions regarding the approximate estimation of the parameters; relations and variation diagrams of higher order indicators for the L-moment method; expression of the inverse function using predefined functions in Excell and Mathcad; the expression of the inverse function with the frequency factor estimated with the L-moments method, as well as the approximation relations of these frequency factors (depending on τ_3) for the most common annual exceedance probabilities in the FFA.

Considering that in the frequency analysis it is desirable to obtain results characterized by a low degree of uncertainty, a determining role is played by the influence of the variability of the analyzed data lengths, knowing that small and medium data lengths can be characterized by relative errors that increase with the decrease of the annual probability of exceeding. The rarer the event, the greater the relative errors (bias). They also depend on the intrinsic characteristics of the analyzed distribution as well as on the parameter estimation method.

2. Methods and Materials

The analyzed estimation methods are MOM and L-moments. The analysis consists in highlighting the deviations due to the influence of the sizes of the analyzed data sets. Considering that the values of rare and very rare quantiles are of interest in the FFA, the analysis presents the maximum flow with the probability of exceeding equal to 0.01%, the determination of this value being mandatory for the verification of Dams type retention works of importance class 1 [13].

In general, this stage of highlighting the deviations from the theoretical curve is a subsequent stage of establishing the best distribution, thus we have the certainty that the data set analyzed comes from the respective distribution.

In the case of MOM, these deviations are presented for usual values of the coefficient of variation encountered in the analysis of extreme events in hydrology. The skewness coefficient is established by choosing the 3 multiplication coefficients depending on the genesis of the maximum flows according to Romanian practice [14].

In the case of the L-moments method, the biases are presented for the entire matrix of the theoretical values of the τ_2 and τ_3 indicators (τ_3 being considered positive). The coefficient of L-variation (τ_2) always takes positive values between 0 and 1. The limits of L-skewness vary between $2 \cdot \tau_2 - 1 \leq \tau_3 < 1$, and those of L-kurtosis between $\frac{1}{4} \cdot (5 \cdot {\tau_3}^2 - 1) \leq \tau_4 < 1$ [5].

In general, L-skewness is considered positive, the same approach being present in this manuscript.

The method of determining the biases consists in choosing the theoretical values of the indicators specific to the methods, estimating the parameters of the distributions, and recalculating all these values through sampling. For simplicity, the arithmetic mean (expected value) is chosen as 1.

The Table 1 presents the most important relationships that characterize these two statistical distributions necessary for their use in FFA, such as the density function, the cumulative function, the inverse function (quantile function) [1-5].

Table 1

The analyzed distributions

Distri.	Density function $f(x)$	Complementary cumulative distribution function, $F(x)$	Quantile function $x(p)$
PE3	$\frac{(x-\gamma)^{\alpha-1}}{\beta^{\alpha} \cdot \Gamma(\alpha)} \cdot exp\left(-\frac{x-\gamma}{\beta}\right) = \frac{1}{\beta} \cdot dgamma\left(\frac{x-\gamma}{\beta}, \alpha\right)$	$1 - \frac{1}{\beta \cdot \Gamma(\alpha)} \cdot \int_{\gamma}^{x} \left(\frac{x-\gamma}{\beta}\right)^{\alpha-1} \cdot exp\left(-\frac{x-\gamma}{\beta}\right) dx = \frac{\Gamma\left(\alpha, \frac{x-\gamma}{\beta}\right)}{\Gamma(\alpha)}$	$\gamma + \beta \cdot qgamma(1-p, \alpha)$
GEV	$\frac{1}{\Gamma(\alpha)} \cdot \left\|\frac{\beta}{\theta}\right\| \cdot \left(\frac{x-\gamma}{\theta}\right)^{\alpha \cdot \beta - 1} \cdot exp\left(-\left(\frac{x-\gamma}{\theta}\right)^{\beta}\right)$	$1 - exp\left(-\left(1 - \frac{\alpha}{\beta} \cdot (x-\gamma)\right)^{\frac{1}{\alpha}}\right)$	$\gamma + \frac{\beta}{\alpha} \cdot (1 - (-ln(1-p))^{\alpha})$

The exact and approximate parameter estimation relationships, respectively the **τ3-τ4** variation relationships are presented in [2,5,6,8]. The predefined functions in Mathcad are also equivalent in Excel, as was presented in other materials [8].

3. Results and Disscutions

The analysis is presented for the most common values of the higher order statistical indicators found in the FFA.

In the sampling process (after determining the parameters and implicitly the theoretical values of the inverse function of the distribution) the Hazen empirical probability is used, because it has been observed that it is claimed for these two

distributions and parameter estimation methods, on the grounds that in the sampling process the values on the three levels of bias (indicators, parameters and quantiles) should be characterized by the smallest deviations from the theoretical values. Deviations are expressed in percentages. A positive bias means that the calculated values (for the sample) are lower than the theoretical values (population) and require an increase with the resulting percentage. In the opposite case, for a negative bias, the values need to be reduced by the resulting percentage.

Thus, Table 2 shows the results obtained by applying the most used empirical probabilities in FFA, for the least interested events, namely the maximum value with the annual probability of exceeding 0.01%, 0.1%, 0.5% and 1%.

Table 2

Empirical probability choice. Results for 25 values. Pearson III distribution.

n=25 values; Cv=1; Cs=3*Cv								
Bias	**Weibull**	**Hazen**	**Blom**	**Cunnane**	**Adamowski**	**Cegodaev**	**Hirsh**	**Landwehr/ APL**
$Q_{0.01\%}$	39.1%	21.3%	27.3%	26.2%	32.0%	30.2%	49.0%	28.5%
$Q_{0.1\%}$	35.4%	18.4%	24.1%	23.0%	28.5%	26.9%	45.3%	25.3%
$Q_{0.5\%}$	31.2%	15.2%	20.4%	19.5%	24.7%	23.1%	41.0%	21.6%
$Q_{1\%}$	28.6%	13.2%	18.2%	17.3%	22.3%	20.8%	38.4%	19.4%

Thus, after identifying the corresponding empirical probability, sampling is done (n=80, 50 and 25 values) recalculating each time the statistical indicators of the series, the distribution parameters and the quantile values.

For example, tables 3 and 4 show these biases on the 3 levels, for the usual values of C_V and τ_2, for the Pearson III distribution.

Table 3

The biases for Pearson III distribution: MOM.

C_V=0.5; C_S=3*Cv				C_V=0.5; C_S=4*Cv		
Indicator	**Record length**			**Record length**		
	80	**50**	**25**	**80**	**50**	**25**
Cv	1.00%	1.40%	1.10%	1.60%	2.20%	1.90%
Cs	10.7%	14.1%	20.5%	12.2%	15.7%	22.2%
μ	0.20%	0.30%	0.60%	0.20%	0.30%	0.70%
a	-25.4%	-35.4%	-58.0%	-29.5%	-40.6%	-65%
b	11.7%	15.5%	22.7%	13.8%	17.8%	25.6%
γ	-28.1%	-42.3%	-85.0%	-13.9%	-19.3%	-31.9%
$Q_{0.01\%}$	4.88%	6.53%	2.55%	6.70%	8.83%	3.53%

Indicator	C_V=0.5; C_S=3*Cv			C_V=0.5; C_S=4*Cv		
	Record length			Record length		
	80	50	25	80	50	25
$Q_{0.1\%}$	3.93%	5.28%	3.45%	5.44%	7.21%	4.74%
$Q_{0.5\%}$	3.05%	4.09%	3.45%	4.19%	5.59%	4.74%
$Q_{1\%}$	2.55%	3.45%	5.33%	3.53%	4.74%	7.21%

Table 4

The biases for Pearson III distribution: L-moments.

Indicator	τ_2=0.182; τ_3=0.1; τ_4=0.126			τ_2=0.67; τ_3=0.5; τ_4=0.25		
	Record length			Record length		
	80	50	25	80	50	25
τ_2	4.95%	4.40%	0.60%	-0.75%	-1.19%	-1.70%
τ_3	-0.09%	-0.14%	-0.27%	-1.05%	-1.65%	-3.22%
τ_4	-2.38%	-3.97%	-6.35%	-1.60%	-2.80%	-5.20%
a	0.19%	0.28%	0.56%	2.84%	2.84%	7.58%
b	-1.06%	-1.06%	-3.19%	-1.60%	-2.53%	-5.01%
γ	43.8%	55.0%	70.0%	50.0%	50.0%	75.0%
$Q_{0.01\%}$	-0.43%	-0.70%	-1.33%	-0.99%	-1.58%	-3.10%
$Q_{0.1\%}$	-0.40%	-0.63%	-1.21%	-0.81%	-1.30%	-2.55%
$Q_{0.5\%}$	-0.36%	-0.56%	-1.02%	-0.62%	-0.97%	-1.90%
$Q_{1\%}$	-0.32%	-0.49%	-0.92%	-0.48%	-0.77%	-1.50%

Taking into account that in practice we can meet various regimes, with different variability, Tables 5 and 6 show the biases of the Pearson III distribution for MOM, respectively for the L-moments method for the entire matrix of statistical indicators (for the rare event $Q_{0.01\%}$). It can be seen that in the case of MOM, for medium and large data variabilities and skewness, the biases are significant. In the case of the L-moments method, the biases are very small. In table 6, the highlighted areas represent the usual range of values recorded in the frequency analysis of extreme events in hydrology.

Table 5

The biases for Pearson III distribution: MOM. Extended fields of statistical indicators.

0.01% annual exceedance probability										
ξ	C_v									
	0.1	**0.3**	**0.5**	**0.7**	**0.9**	**1.1**	**1.3**	**1.5**	**1.7**	**2**
Records, n=80										
2	0.33	1.67	3.22	4.87	6.56	8.31	10.1	11.9	13.71	16.4
3	0.42	2.5	4.88	7.48	10.2	12.9	15.6	18.3	20.9	24.8
4	0.62	3.35	6.7	10.3	13.9	17.6	21.1	24.5	27.8	32.5
Records, n=50										
2	0.46	2.31	4.37	6.51	8.69	11.0	13.2	15.4	17.7	21.0
3	0.63	3.42	6.53	9.84	13.3	16.7	20.0	23.3	26.5	31.1
4	0.89	4.51	8.83	13.4	17.9	22.4	26.7	30.8	34.7	40.3
Records, n=25										
2	0.71	3.58	6.69	9.76	12.8	15.85	18.98	21.97	24.98	29.38
3	1.04	5.22	9.74	14.4	19.1	23.6	28.1	32.4	36.6	42.4
4	1.37	6.84	12.9	19.17	25.3	31.2	36.8	42.0	47.0	53.8

Table 6

The biases for Pearson III distribution: L-moments. Extended fields of statistical indicators.

0.01% annual exceedance probability									
τ_3	τ_2								
	0.1	**0.2**	**0.3**	**0.4**	**0.5**	**0.6**	**0.7**	**0.8**	**0.9**
Records, n=80									
0	-0.35	-0.49	-0.53	-0.58	-0.61	-0.62	-0.63	-0.64	-0.65
0.1	-0.352	-0.5	-0.54	-0.56	-0.61	-0.63	-0.64	-0.65	-0.66
0.2	-0.41	-0.53	-0.59	-0.62	-0.63	-0.66	-0.67	-0.67	-0.69
0.3	-0.5	-0.62	-0.68	-0.72	-0.72	-0.74	-0.76	-0.77	-0.77
0.4	-0.61	-0.75	-0.8	-0.82	-0.85	-0.86	-0.87	-0.88	-0.88
0.5	-0.75	-0.87	-0.93	-0.96	-0.97	-0.99	-1.0	-1.01	-1.01
0.6	-0.92	-1.05	-1.1	-1.13	-1.15	-1.16	-1.17		
0.7	-1.2	-1.33	-1.38	-1.4	-1.42	-1.42	-1.43	-1.44	-1.45
0.8	-1.72	-1.85	-1.89	-1.92	-1.94	-1.95	-1.96	-1.96	-1.96
0.9	-3.28	-3.42	-3.46	-3.49	-3.5	-3.52	-3.52	-3.53	-3.53
Records, n=50									
0	-0.55	-0.74	-0.85	-0.9	-0.94	-0.96	-0.98	-1.0	-1.01
0.1	-0.55	-0.74	-0.83	-0.91	-0.96	-0.98	-0.99	-1.01	-1.02
0.2	-0.64	-0.83	-0.92	-0.97	-0.99	-1.03	-1.05	-1.05	-1.07
0.3	-0.77	-0.97	-1.06	-1.12	-1.13	-1.16	-1.18	-1.19	-1.2
0.4	-1.0	-1.16	-1.26	-1.29	-1.33	-1.35	-1.37	-1.37	-1.39
0.5	-1.2	-1.39	-1.48	-1.52	-1.55	-1.57	-1.58	-1.6	-1.61

0.01% annual exceedance probability									
τ_3	τ_2								
	0.1	**0.2**	**0.3**	**0.4**	**0.5**	**0.6**	**0.7**	**0.8**	**0.9**
0.6	-1.5	-1.68	-1.77	-1.82	-1.85	-1.86	-1.88	-1.89	-1.9
0.7	-1.96	-2.17	-2.25	-2.28	-2.31	-2.33	-2.34	-2.35	-2.36
0.8	-2.86	-3.08	-3.16	-3.2	-3.22	-3.24	-3.25	-3.26	-3.27
0.9	-5.66	-5.89	-5.98	-6.02	-6.05	-6.07	-6.08	-6.09	-6.09
Records, n=25									
0	-1.05	-1.41	-1.59	-1.7	-1.78	-1.84	-1.88	-1.91	-1.94
0.1	-1.04	-1.42	-1.61	-1.71	-1.8	-1.85	-1.89	-1.92	-1.95
0.2	-1.2	-1.56	1.72	-1.82	-1.88	-1.94	-1.97	-1.99	-2.02
0.3	-1.46	-1.83	-2.0	-2.09	-2.14	-2.18	-2.22	-2.24	-2.26
0.4	-1.84	-2.22	-2.4	-2.48	-2.55	-2.58	-2.61	-2.63	-2.66
0.5	-2.33	-2.74	-2.89	-2.98	-3.04	-3.08	-3.11	-3.13	-3.15
0.6	-2.99	-3.4	-3.57	-3.65	-3.71	-3.75	-3.78	-3.8	-3.82
0.7	-4.05	-4.48	-4.65	-7.73	-4.79	-4.82	-4.85	-4.87	-4.88
0.8	-6.18	-6.65	-6.82	-6.91	-6.96	-7.0	-7.03	-7.05	-7.06
0.9	-13.4	-13.9	-14.1	-14.2	-14.3	-14.3	-14.4	-14.4	-14.4

Tables 7 and 8 show the results obtained with the GEV distribution. It can be seen that the influence of the variability of the recorded data is much more pronounced than in the case of the Pearson III distribution, due to the fact that this is a heavy tail distribution. Even in this case, the L-moments method gives better results, the biases being much smaller than MOM.

Table 7

The biases for GEV distribution: MOM. Extended fields of statistical indicators.

0.01% annual exceedance probability										
ξ	C_V									
	0.1	**0.3**	**0.5**	**0.7**	**0.9**	**1.1**	**1.3**	**1.5**	**1.7**	**2**
Records, n=80										
2	-0.012	1.74	5.71	10.9	16.2	21.0	25	28.4	31.1	34.4
3	0.15	4	11.5	19.0	25.2	29.9	33.4	36.0	38.1	40.5
4	0.36	7	17.1	25.4	31.1	35.1	38	40.1	41.8	43.6
Records, n=50										
2	0.02	2.5	7.7	13.9	20.0	25.3	29.6	33.2	36.1	39.4
3	0.3	5.4	14.5	23.1	29.7	34.6	38.3	41.0	43.2	45.6
4	0.6	9.0	20.9	29.9	35.9	40.1	43.0	45.1	46.8	48.6
Records, n=25										
2	0.1	4.1	11.4	19.4	26.7	32.6	37.3	41.1	44.1	47.5
3	0.5	8.3	20.0	30.0	37.3	42.5	46.2	49.0	51.2	53.6
4	1.0	13.0	27.3	37.3	43.7	47.9	50.9	53.0	54.7	56.5

Table 8

The biases for GEV distribution: L-moments. Extended fields of statistical indicators.

0.01% annual exceedance probability									
t3	**t2**								
	0.1	**0.2**	**0.3**	**0.4**	**0.5**	**0.6**	**0.7**	**0.8**	**0.9**
Records, n=80									
0	-0.44	-0.66	-0.79	-0.87	-0.94	-0.98	-1.02	-1.05	-1.07
0.1	-0.57	-0.78	-0.89	-1.01	-1.01	-1.04	-1.07	-1.09	-1.1
0.2	0.09	0.11	0.12	0.12	0.13	0.13	0.13	0.13	0.14
0.3	3.02	3.48	3.66	3.76	3.82	3.86	3.89	3.91	3.93
0.4	9.62	10.41	10.7	10.85	10.95	11.01	11.05	11.09	11.12
0.5	19.97	20.85	21.17	21.33	21.43	21.49	21.5	21.57	21.6
0.6	32.9	33.72	34	34.15	34.23	34.3	34.33	34.36	34.39
0.7	46.7	47.4	47.6	47.8	47.8	47.9	47.9	47.9	48.0
0.8	59.6	60.3	60.5	60.6	60.6	60.7	60.7	60.7	60.8
0.9	70.4	71.1	71.4	71.5	71.6	71.6	71.7	71.7	71.7
Records, n=50									
0	-0.68	-1.01	-1.21	-1.35	-1.44	-1.51	-1.57	-1.6	-1.64
0.1	-0.86	-1.18	-1.35	-1.45	-1.52	-1.57	-1.61	-1.64	-1.66
0.2	0.05	0.07	0.07	0.08	0.08	0.08	0.08	0.08	0.08
0.3	3.87	4.48	4.7	4.83	4.91	4.96	5.0	5.03	5.05
0.4	12.0	12.97	13.34	13.53	13.64	13.72	13.78	13.82	13.85
0.5	23.9	24.96	25.34	25.53	25.64	25.72	25.78	25.82	25.85
0.6	37.85	38.79	39.12	39.28	39.38	39.44	39.49	39.53	39.56
0.7	51.8	52.6	52.9	53.0	53.1	53.2	53.2	53.2	53.2
0.8	64.3	65.0	65.2	65.3	65.4	65.4	65.5	65.5	65.5
0.9	74.2	75.0	75.2	75.4	75.4	75.5	75.5	75.6	75.6
Records, n=25									
0	-1.27	-1.89	-2.26	-2.51	-2.69	-2.82	-2.92	-3	-3.07
0.1	-1.54	-2.12	-2.42	-2.61	-2.73	-2.82	-2.89	-2.95	-2.99
0.2	-0.09	-0.12	-0.13	-0.13	-0.14	-0.14	-0.14	-0.14	-0.15
0.3	5.45	6.27	6.6	6.77	6.88	6.95	7.01	7.05	7.08
0.4	16.14	17.45	17.9	18.2	18.35	18.46	18.54	18.59	18.64
0.5	30.4	31.75	32.22	32.46	32.61	32.71	32.78	32.84	32.88
0.6	45.58	46.72	47.11	47.31	47.43	47.51	47.56	47.61	47.64
0.7	59.5	60.4	60.7	60.9	61.0	61.0	61.1	61.1	61.1
0.8	71.0	71.8	72.0	72.2	72.2	72.3	72.3	72.3	72.4
0.9	79.6	80.4	80.6	80.8	80.9	80.9	81.0	81.0	81.0

For usual values of the coefficient of variation, skewness, coefficient of L-variation and L-skewness, Figure 1 shows the curves of the inverse functions, at different sampling values (n=25,50,80) compared to the theoretical values (n>1000),

for both distributions and both parameter estimation methods.

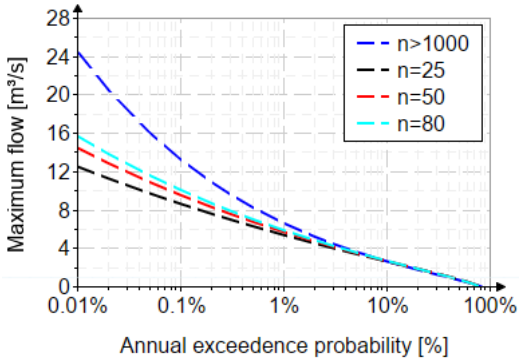

(a) GEV, MOM (μ=1; C_v=1.5; C_s=3)

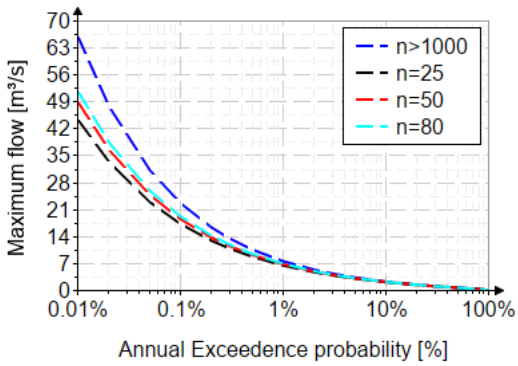

(b) GEV, L-moments (L_1=1; τ_2=0.6; τ_3=0.5)

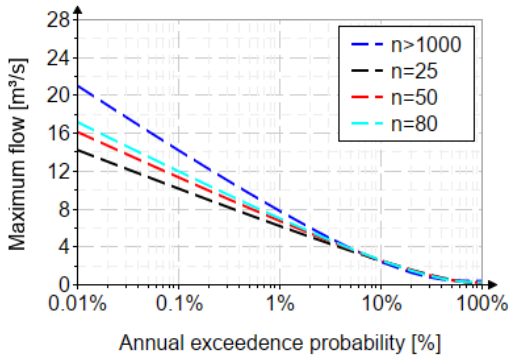

(c) PE3, MOM (μ=1; C_v=1.5; C_s=3)

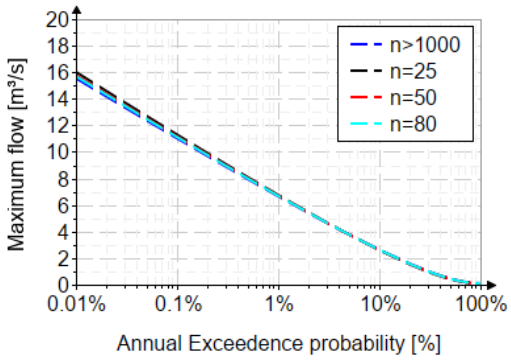

(d) PE3, L-moments (L_1=1; τ_2=0.6; τ_3=0.5)

Fig. 1. Evaluations of the quantile function.

4. Conclusions

The frequency analysis has an important role in the direct determination of the maximum flows, corresponding to the low annual probabilities of exceeding.

Considering that in many cases a small number of records are available, the probability distributions are, depending on the parameter estimation method, more or less influenced by this variability of the recorded data lengths.

Considering that the Pearson III and generalized extreme value (GEV) distributions are two of the most used statistical distributions in FFA, the main objective of the manuscript was to highlight the behavior of these distributions and the biases of the inverse function at different river regimes, highlighted by the theoretical values of the higher order statistical indicators.

According to the obtained results, of the two parameter estimation methods (for the two distributions), the least affected by this variability is the L-moments method, the resulting biases on the entire theoretical definition matrix of the statistical indicators being much smaller than in the case of the method of ordinary moments.

Of the two analyzed distributions, the GEV distribution is more affected, due to its intrinsic characteristic of being a heavy-tail distribution.

Thus, taking into account this deviation from the theoretical values, it is very important that the confidence interval of the distribution chosen as the best model is presented in the FFA. An accessible solution is the representation of the confidence interval using Chow's approximate relationship [6,15], an advantage being also represented by the fact that in recent materials it has also been adapted to the L-moments method [7-12]. It is thus desired to avoid the use of non-technical concepts such as the uncertainty interval [16].

References

[1] Bulletin 17B Guidelines for determining Flood Flow Frequency; Hydrology Subcommittee, Interagency Advisory Committee on Water Data, U.S. Department of the Interior, U.S. Geological Survey, office of Water Data Coordination, Reston, Virginia: 1981.
[2] Rao, A.R.; Hamed, K.H. Flood Frequency Analysis; CRC Press LLC: Boca Raton, FL, USA, 2000.
[3] Gubareva, T.S.; Gartsman, B.I. Estimating Distribution Parameters of Extreme Hydrometeorological Characteristics by L-Moment Method. Water Resour. 2010, 37, 437–445.
[4] Anghel, C.G.; Ilinca, C. Parameter Estimation for Some Probability Distributions Used in Hydrology. Appl. Sci. 2022, 12, 12588. https://doi.org/10.3390/app122412588.
[5] Hosking, J.R.M and Wallis, J.R. (1997) Regional Frequency Analysis: An Approach Based on L−moments. Cambridge University Press, UK, http://dx.doi.org/10.1017/cbo9780511529443.
[6] Ilinca, C.; Anghel, C.G. Flood-Frequency Analysis for Dams in Romania. Water 2022, 14, 2884. https://doi.org/10.3390/w14182884.
[7] Anghel, C.G.; Stanca, S.C.; Ilinca, C. Two-Parameter Probability Distributions: Methods, Techniques and Comparative Analysis. Water 2023, 15, 3435. https://doi.org/10.3390/w15193435.
[8] Ilinca, C.; Anghel, C.G. Flood Frequency Analysis Using the Gamma Family Probability Distributions. Water 2023, 15, 1389. doi: 10.3390/w15071389.
[9] Ilinca, C.; Anghel, C.G. Frequency Analysis of Extreme Events Using the Univariate Beta Family Probability Distributions. Appl. Sci. 2023, 13, 4640. doi: 10.3390/app13074640.
[10] Anghel, C.G.; Ilinca, C. Evaluation of Various Generalized Pareto Probability Distributions for Flood Frequency Analysis. Water 2023, 15, 1557. doi: 10.3390/w15081557.
[11] Anghel, C.G.; Ilinca, C. Predicting Flood Frequency with the LH-Moments Method: A Case Study of Prigor River, Romania. Water 2023, 15, 2077. doi: 10.3390/w15112077.
[12] Anghel, C.G.; Stanca, S.C.; Ilinca, C. Extreme Events Analysis Using LH-Moments Method and Quantile Function Family. Hydrology 2023, 10, 159. doi: 10.3390/hydrology10080159.
[13] STAS 4068/2-87*;* Annual probabilities of maximum flows and volumes under normal and special operating conditions. The Romanian Standardization Institute: Bucharest, Romania, 1987.
[14] STAS 4068/1962; Maximum Water Discharges and Volumes, Determination of maximum Water Discharges and Volumes of Watercourses, the Romanian standardization institute, Bucharest, Romania.
[15] V.T.Chow, D.R.Maidment, L.W.Mays Applied Hydrology, 1988, MCGraw-Hill, Inc., ISBN 007-010810-2.
[16] Drobot, R.; Draghia, A.F.; Chendes, V.; Sirbu, N.; Dinu, C. Consideratii privind viiturile sintetice pe Dunare. Hidrotehnica 2023, 68. (In Romanian).

Exploring the Applicability and Insights of the Pearson Type III Distribution in Flood Frequency Analysis

Explorarea aplicabilității și perspectivelor distribuției Pearson de tip III în analiza frecvenței inundațiilor

Cristian Anghel[1], Stefan Ciprian Stanca[2] , Cornel Ilinca[3]

[1,2,3]Technical University of Civil Engineering Bucharest
Lacul Tei Boulevard Nr. 124, Bucharest 020396, Romania
[1]*E-mail: cristian.anghel@utcb.ro*
[2]*E-mail: stefan-ciprian.stanca@phd.utcb.ro*
[4]*E-mail: cornel.ilinca@utcb.ro*

DOI: 10.37789/rjce.2024.15.3.6

Abstract. *Being the parent distribution in Romania, the Pearson III distribution (PE3) is one of the statistical distributions that is most frequently used in flood frequency analysis (FFA). All the components required for the simple implementation of PE3 distribution in FFA are presented in this manuscript. The estimated methods and exact and approximate relationships for estimating the parameters and frequency factors particular to the distribution are described. All of these factors are used to identify maximum flows with various annual exceedance probabilities, using data collected at the 6 rivers with different morphometric characteristics and different lengths of data series. Five parameter estimation techniques are used in this comparative analysis, i.e. the method of ordinary moments (MOM), the method of linear moments (L-moments), the high-order linear moments method (LH-moments), the method of maximum likelihood (MLE) and the method of least squares (LSM). Given the results, it can be assumed that the L-moments approach is more reliable, stable, robust and less sensitive to variations in recorded data lengths, as well as to the presence of outliers.*

Key words: approximate form; confidence interval; estimation parameters; frequency factors; method of ordinary moments; method of linear moments; Pearson III.

1. Introduction

The flood frequency analysis (FFA) enables the computation of values with a certain likelihood of occurrence, which is crucial in the management of water resources and the design of hydrotechnical projects.

The Pearson III (PE3) distribution is one of the distributions that is most frequently employed in the statistical analysis of extreme data, along with the Log-Normal, GEV, and Log-Pearson distributions [1-7]. The PE3 distribution was applied,

using different parameter estimation methods, for the frequency analysis of floods in [5, 8–10], the frequency analysis of maximum precipitation in [11–13], and the low flow frequency analysis in [4, 14]. In the investigation of flood frequency in Romania, PE3 serves as the parent distribution [7, 10].

The distribution is a special case of the four-parameter gamma distribution and a generalized version of the two-parameter gamma distribution. It is a member of the family of gamma distributions. In Romania, the PE3 distribution is used exclusively using the method of ordinary moments using the Foster-Ribkin table and linear interpolation, an approach that represents a legacy of the Soviet influence, inferior compared to modern methods of analysis.

Without closed forms, the cumulative complementary function (CDF) and the inverse function (quantile) of the PE3 distribution are represented in this article using predefined Mathcad functions that are comparable to other functions from other specialized programs (Excell).

For the method of ordinary moments (MOM), L-moments method and LH-moments, the quantile function can also be represented with the frequency factor, which is a real help considering the inverse function is defined by the gamma function.

In general, the PE3 distribution is applied using the MOM and L-moments parameter estimation methods, which are two of the most used parameter estimation methods in FFA [1, 4, 5, 10]. In comparison to other parameter estimate approaches, the L-moments method is renowned for being far more stable and less subject to bias [5,8,14,15]. The higher order linear moments (LH-moments) approach can be used to generate the "separation effect" [16]. Without explicit sample censoring, Wang proposed this method in 1997 [17], and it quickly rose to become one of the FFA's most used techniques. Only when FFA is employing the Annual Maximum Series (AMS) is its use advised. This approach lessens the impact of small maximum values in the frequency analysis by generalizing the approach of linear moments. As a result, high maximum values—always reflecting floods—are given more significance.

Regarding parameter estimation with MOM, it is generally preferred because the estimation relationships are simple and easy to use. However, it presents the disadvantage of the fact that higher-order statistical indicators (skewness and kurtosis) require correction. A solution to correct the skewness coefficient is represented by the approach of Bobee and Robitaille [1,2,5]. In Romania, this impediment was partially solved by choosing the skewness depending on the genesis of the maximum flows. Thus, according to Romanian regulations [18], a coefficient of 2 is chosen if the maximum flows come exclusively from snow melt, a coefficient of 3 if the origin is mixed (snow melt and rain), respectively a coefficient of 4 if the maximum flows come exclusively from rains. Unfortunately, this approach is often used incorrectly and excessively, because it is only valid for hydrographic basins with a surface of less than 100 km^2, because it uses an approximation considering the coefficient of variation having the value 1 and the maximum flows having the genesis exclusively from rains.

To estimate the parameters with L-moments (and also for MLE and LSM), it is necessary to solve a system of nonlinear equations, which leads to some difficulties. Thus, for the ease use of it, parameters approximation relations (for L-moments) are

presented, using polynomial, exponential or rational functions. An important contribution, was made by Hosking [8] who for the first time presented relations for the estimation of the shape parameter within the complete domain of L-skewness, relations improved by Anghel and Ilinca [7].

For the LH-moments method, important contributions were made by [32-41], in which a significant number of distributions were analyzed, among which the most important are Wakeby, Lambda, Pearson V, the CHI, the inverse CHI, the Wilson–Hilferty, the Pseudo-Weibull, the Log-normal, the generalized Pareto Type I and the Fréchet distributions.

Regarding the least squares method, the manuscript presents a comparative analysis that identifies the best empirical probability that fits the PE3 distribution, so that by sampling the errors on the three levels (statistical indicators, estimation of parameters and quantities) to be as small as possible.

For the maximum likelihood method, the parameters of the PE3 distribution have a valid solution only if the skewness coefficient is lower than 2, an aspect noted both in the present analysis and in the observations of other researchers [5].

Given that uncertainties are a part of all statistical analyses, the relationships for calculating the confidence interval for the Pearson III distribution—which is required to quantify uncertainties—are described using both the Chow [19] (for MOM, L- and LH-moments) and Kite approximations (for MOM) [5]. The Chow's relation, for a 95% confidence level, is based on a Gaussian assumption, being a simplified approach. In general, all the quantiles that exceed the probabilities of the recorded values are characterized by a significant degree of uncertainty since the observed data is relatively short in duration. There are three levels of uncertainty due to the bias introduced by the fluctuation in the length of the recorded data, which must be considered when estimating the statistical indicators unique to the used method as well as when determining the values of the parameters and quantiles. These levels of uncertainty, which are distinctive to the Pearson III distribution, along with the estimate techniques and the range of data lengths, are presented in the text.

Thus, in order to highlight all these particular aspects of the PE3 distribution using these 5 parameter estimation methods, a comparative analysis is presented on 6 case studies, with different morphometric and statistical characteristics.

2. Methods

2.1. Probability Density Function and Cumulative Distribution Function

The probability density function, $f(x)$ and the complementary cumulative distribution function $F(x)$, for PE3 are [5,7,20]:

$$f(x) = \frac{(x-\gamma)^{\alpha-1}}{\beta^{\alpha} \cdot \Gamma(\alpha)} \cdot exp\left(-\frac{x-\gamma}{\beta}\right) = \frac{1}{\beta} \cdot dgamma\left(\frac{x-\gamma}{\beta}, \alpha\right) \quad 1)$$

$$F(x) = 1 - \frac{1}{\beta \cdot \Gamma(\alpha)} \cdot \int_{\gamma}^{x} \left(\frac{x-\gamma}{\beta}\right)^{\alpha-1} \cdot exp\left(-\frac{x-\gamma}{\beta}\right) dx = \frac{\Gamma\left(\alpha, \frac{x-\gamma}{\beta}\right)}{\Gamma(\alpha)} \quad 2)$$

where α, β, γ are the shape, the scale and the position parameters and x can take any values of range $\gamma < x < \infty$ if $\beta > 0$ or $-\infty < x < \gamma$ if $\beta < 0$ and $\alpha > 0$.

2.2. Quantile function

The PE3 distribution does not have a closed form for the inverse function $x(p)$. This can be expressed using predefined functions from dedicated programs, such as: $qgamma$ function (Mathcad), $gamma.inv$ function (Excell), etc. In this article, the relationships are defined using predefined functions in Mathcad.

The quantile of the PE3 distribution has the following expression:

$$x(p) = x\big(F(x)\big) = F(x)^{-1} = \gamma + \beta \cdot qgamma(1-p, \alpha) \quad 3)$$

where p is the probability of exceedance. If $\beta < 0$ (negative skewness) then the first argument of the inverse of the distribution function Gamma, $\Gamma^{-1}(1-p;\alpha)$ becomes $\Gamma^{-1}(p;\alpha)$.

The built-in function from Mathcad $qgamma(1-p,\alpha) = \gamma^{-1}\big((1-p)\cdot \Gamma(\alpha), \alpha\big)$, returns the inverse cumulative probability distribution for probability p, for the Gamma distribution, where γ^{-1} is the inverse of the lower incomplete gamma function.

Based on the frequency factor, the inverse functions for MOM, L-moments, and LH-moments can be written as follows:

$$x(p) = \mu + \sigma \cdot K_{MOM}(p, \alpha) \quad (4)$$

$$x(p) = L_1 + L_2 \cdot K_L(p, \alpha) \quad (5)$$

$$x(p) = L_{H1} + L_{H2} \cdot K_{LH}(p, \alpha) \quad (6)$$

where μ is the expectation and σ $^{\sigma}$ is the standard deviation; L_1 and L_2 are the first two L-moments; L_{H1} and L_{H2} are the first two LH-moments; $K_{MOM}(p,\alpha), K_L(p,\alpha)$ and $K_{LH}(p,\alpha)$ represent the frequency factors for estimating the parameters with MOM L-moments and LH-moments.

The exact relationships for frequency factors, are:

$$K_{MOM}(p,\alpha) = \frac{qgamma(1-p,\alpha) - \alpha}{\sqrt{\alpha}} \quad (7)$$

$$K_L(p,\alpha) = \frac{\sqrt{\pi} \cdot \Gamma(\alpha)(qgamma(1-p,\alpha) - \alpha)}{\Gamma(\alpha + 0.5)} \quad (8)$$

$$K_{LH}(p,\alpha) = \frac{\frac{2}{3}\cdot(qgamma(1-p,\alpha) - 2\cdot z_2)}{z_1} \quad (9)$$

where the expressions for z_1 and z_2 can be found in section 2.3.

Numerous approximation relations of the frequency factor are published in the literature [5] for MOM estimation, the most significant being the Kite approximation, for $|C_s| < 2$, the Cornish-Fisher approximation, for $|C_s| < 2$, the Wilson-Hilferty approximation, for $|C_s| < 2$, the modified Wilson-Hilferty approximation, for $0.25 \leq C_s \leq 9.75$.

The frequency factor with MOM can also be approximated using a polynomial development in skewness (C_s):

$$K_{MOM}(p,C_s) = a + b\cdot C_s + c\cdot C_s^2 + d\cdot C_s^3 + e\cdot C_s^4 + f\cdot C_s^5 + g\cdot C_s^6 + h\cdot C_s^7 \quad (10)$$

Table 1 lists the polynomial function coefficients for the annual exceedance probability that are utilized the most in technical hydrology.

Table 1

Coefficients of the approximation function with MOM

P [%]	a	b	c	d	e	f	g	h
0.01	3.71828	2.1462	0.15579	-0.0769315	0.0150378	-0.0017271	0.0001106	-0.00000303
0.1	3.09014	1.42629	0.049631	-0.0421189	0.00794983	-0.00083309	0.00004794	-0.00000118
0.5	2.57601	0.937811	-0.00485114	-0.024367	0.00459158	-0.0004292	0.00002047	-0.00000038
1	2.32661	0.733146	-0.0218707	-0.0185502	0.00358677	-0.00031539	0.00001302	-0.00000017
2	2.05408	0.533496	-0.034201	-0.0138703	0.00286305	-0.00023957	0.00000831	-0.000000042
3	1.88115	0.419782	-0.0389303	-0.0116643	0.00257668	-0.00021375	0.00000687	-0.000000006
5	1.64524	0.280836	-0.0418754	-0.0094549	0.00237315	-0.00020267	0.00000657	0.0000000005
10	1.28196	0.103328	-0.0395043	-0.0074825	0.00241382	-0.00023132	0.00000899	-0.00000008
20	0.842052	-0.052671	-0.027535	-0.0068667	0.002969	-0.00033372	0.00001445	-0.00000016
40	0.254237	-0.164334	0.0070463	-0.015678	0.0078439	-0.0013773	0.00010621	-0.00000308
50	0.0006921	-0.174131	0.019451	-0.018001	0.010156	-0.002096	0.00018921	-0.00000639
80	-0.845883	-0.010892	-0.041893	0.064938	-0.022096	0.0033839	-0.0002494	0.0000072

Given that the frequency factor is stated using the Gamma function, which can be challenging to calculate, an approximation relation based on the L-skewness and annual exceedance probability is presented. The approximation is the following polynomial relation:

$$K_{TL}(p, \tau_3) = a + b \cdot \tau_3 + c \cdot \tau_3^2 + d \cdot \tau_3^3 \quad (11)$$

In Table 2, the coefficients of the polynomial function for the most popular annual exceedance probabilities are shown.

Table 2

Coefficients of the approximation function with L-moments

P [%]	a	b	c	d
0.01	6.590	23.38	17.214	-3.7117
0.1	5.4765	15.559	8.986	0.47591
0.5	4.5651	10.245	4.4167	1.5525
1	4.1231	8.0174	2.8187	1.5366
2	3.6401	5.8441	1.4754	1.2797
3	3.3336	4.6063	0.81958	1.042
5	2.9154	3.094	0.14699	0.66702
10	2.2715	1.1625	-0.45319	0.08242
20	1.4918	-0.53214	-0.63128	-0.39305
40	0.44907	-1.699	-0.25238	-0.49031
50	0.0000044	-1.814	0.00423	-0.28014
80	-1.4918	-0.52533	0.62038	0.92798
90	-2.2715	1.1681	0.44733	1.14

The three parameters' values vary depending on the estimating technique employed. The relationships for estimating the parameters of the PE3 distribution described in the section that follows.

2.3. Parameter estimation

The parameter estimation is presented for MOM, L-moments and LH-moments, common methods in flood frequency analysis. The advantage of these methods is that they are characterized by statistical indicators (expected value, coefficient of variation, skewness, L-skewness, and LH-kurtosis) that can be determined regionally. Regarding the LH-moments method, only the relationships for the 1st order level are analyzed, because an alternative to the analysis using the Annual Exceedance Series (AES) is desired.

The distribution parameters' expressions for MOM estimation can be found in [5, 10]. Regarding the parameter estimation with L-moments, using the quantile function, the exact parameter estimate for the L-moment technique is carried out numerically (definite integrals). Using the Gaussian Quadrature method, the integrals are numerically determined. But, an approximate form of parameter estimation can be adopted, because the third L-moments (L_3) and L-skewness ($\tau_3 = L_3/L_2$), depends only on the shape coefficient [7,8].

Like the L-moments method, exact equations for estimation with LH-moments are obtained from solving a system of nonlinear equations using defined integrals. For this method, LH-skewness is also characterized only by the shape parameter. Thus, it

was possible to obtain approximate relations for estimating this parameter, giving values for LH-skewness. Thus, for the LH−moments method, α can be approximate with the next relation:

If $0.12 < |\tau_{H3}| \leq 0.34$:

$$\alpha = exp\begin{pmatrix} 7757.0921831+40914.6033757 \cdot ln(|\tau_{H3}|) + \\ 93713.9484593 \cdot ln(|\tau_{H3}|)^2 + 121792.0331514 \cdot ln(|\tau_{H3}|)^3 + \\ 98255.1222272 \cdot ln(|\tau_{H3}|)^4 + 50397.8680523 \cdot ln(|\tau_{H3}|)^5 + \\ 16054.8135102 \cdot ln(|\tau_{H3}|)^6 + 2904.9945626 \cdot ln(|\tau_{H3}|)^7 + \\ 228.664592 \cdot ln(|\tau_{H3}|)^8 \end{pmatrix} \quad (12)$$

If $0.34 < |\tau_{H3}| \leq 0.85$:

$$\alpha = exp\begin{pmatrix} -13.4247904 - 121.5293664 \cdot ln(|\tau_{H3}|) - \\ 649.9763722 \cdot ln(|\tau_{H3}|)^2 - 2075.3170378 \cdot ln(|\tau_{H3}|)^3 - \\ 4110.4652507 \cdot ln(|\tau_{H3}|)^4 - 5114.9286399 \cdot ln(|\tau_{H3}|)^5 - \\ 3890.8525714 \cdot ln(|\tau_{H3}|)^6 - 1653.2523283 \cdot ln(|\tau_{H3}|)^7 - \\ 300.612615 \cdot ln(|\tau_{H3}|)^8 \end{pmatrix} \quad (13)$$

$$\beta = \frac{2 \cdot L_{H2}}{3 \cdot z_1} \quad (14)$$

$$\gamma = L_{H1} - 2 \cdot \beta \cdot z_2 \quad (15)$$

where, $z_1 = \int_0^1 qgamma(p, \alpha) \cdot (3 \cdot p^2 - 2 \cdot p) \cdot dp$, which can be approximated with the following equation:

$$z_1 = \frac{-0.00315255+0.87292281 \cdot \alpha + 0.18314623 \cdot \alpha^2}{\begin{pmatrix} 1 + 2.01526823 \cdot \alpha + 0.07089912 \cdot \alpha^2 - \\ 0.00034641 \cdot \alpha^3 + 0.00000094 \cdot \alpha^4 \end{pmatrix}} \quad (16)$$

and, $z_2 = \int_0^1 qgamma(p, \alpha) \cdot p \cdot dp$, which can be approximated with the following equation:

$$z_2 = \frac{\begin{pmatrix} 0.01180195 + 0.87724953 \cdot \alpha + 0.46798927 \cdot \alpha^2 + \\ 0.01808637 \cdot \alpha^3 + 0.00004649 \cdot \alpha^4 \end{pmatrix}}{1 + 0.80457526 \cdot \alpha + 0.03470298 \cdot \alpha^2 + 0.0000921 \cdot \alpha^3} \quad (17)$$

The MLE method is an easy method for estimating the parameters of a theoretical distribution, which consists in the logarithm and the derivation of the objective function, the latter being the product of the probability density function. By deriving the logarithmic objective function depending on the parameters of the theoretical distribution and minimizing them, the following system of a nonlinear equation results that leads to the determination of the position parameter [5,20].

The least squares method is a less used method because the estimation of the parameters is not robust, it can be used for an initial estimation of the parameters used as kernels for methods using the gradient method. It is a method that uses the cumulative function of the theoretical distribution [5,10,20].

3. Case Studies

As case studies, the frequency analysis of the maximum flows on 6 rivers (Ialomita, Siret, Bahna, Jijia, Nicolina and Viseu) with different morphometric and statistical characteristics is carried out.

Figure 1 shows the locations of the six monitoring stations, for the six studied rivers.

The analysis period varies, each monitoring station being characterized by a length of measurements greater than 20 years.

In the case of the analysis using the method of ordinary moments, the skewness coefficient is chosen according to the genesis of the flows, by multiplying the coefficient of variation of the analyzed data by a coefficientt (ξ), in order to reflect this genesis. The mathematical meaning of statistical indicators can be found in reference materials such as [7,10].

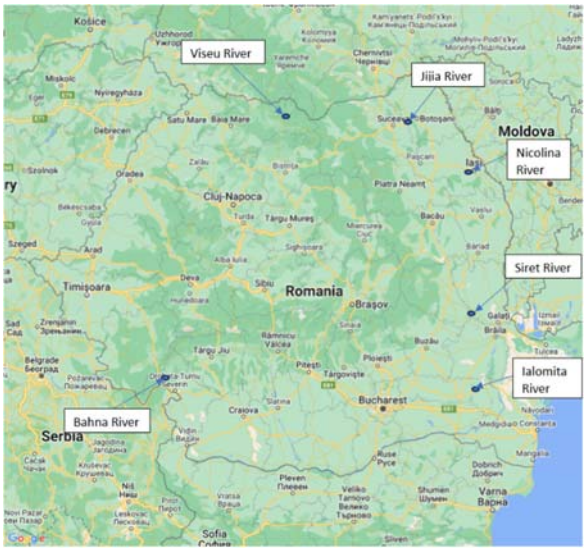

Fig. 1. Location of the six analyzed rivers.

The most important morphometric information regarding the rivers analyzed are highlighted in Table 3 [21].

Table 3

The morphometric elements for the analyzed rivers.

River	Length [km]	Average Stream Slope [‰]	Sinuosity Coefficient [−]	Average Altitude, [m]	Catchments Area, [km^2]
Ialomita	417	1.5	1.88	327	10350
Siret	559	1.7	1.86	515	42890
Jijia	275	1.0	1.45	152	5757
Bahna	35	28	1.45	559	137
Nicolina	20	16	1.37	138	177
Viseu	82	15	1.31	1011	1581

Tables 4 and 5 list the statistical indicator values for the examined data sets.

Table 4

The statistical indicators for the analyzed rivers: MOM

River	Number of records (n)	Hydrometric Station	MOM			
			ξ	μ	C_v	C_s
			[−]	[m^3/s]	[−]	[−]
Ialomita	33	Tandarei	2	224	0.527	0.33
Siret	39	Lungoci	2	1443	0.634	1.41
Jijia	35	Vladeni	3	56.1	0.824	1.85
Bahna	30	Bahna	3	13.3	1.519	3.11
Nicolina	39	Iasi	3	14.1	1.193	2.80
Viseu	20	Bistra	3	392	0.694	2.66

Table 5

The statistical indicators for the analyzed rivers: L-and LH-moments method

River	L-moments method							LH-moments method						
	L_1	L_2	L_3	L_4	τ_2	τ_3	τ_4	L_{H1}	L_{H2}	L_{H3}	L_{H4}	τ_{H2}	τ_{H3}	τ_{H4}
	[m^3/s]	[m^3/s]	[m^3/s]	[m^3/s]	[−]	[−]	[−]	[m^3/s]	[m^3/s]	[m^3/s]	[m^3/s]	[−]	[−]	[−]
Ialomita	224	68.6	6.13	1.69	0.306	0.089	0.025	293	56.1	5.22	2.30	0.191	0.093	0.041
Siret	1443	490	112	90.6	0.339	0.228	0.185	1932	451	135	89.9	0.233	0.299	0.199
Jijia	56.1	23.2	7.86	6.01	0.414	0.338	0.259	79.4	23.3	9.25	6.13	0.294	0.396	0.263
Bahna	13.3	8.10	4.91	3.52	0.608	0.608	0.436	21.3	9.73	5.62	3.68	0.456	0.577	0.378
Nicolina	14.1	7.55	3.60	2.22	0.536	0.477	0.294	21.6	8.36	3.88	2.34	0.386	0.464	0.280
Viseu	392	121	63.5	49.3	0.309	0.525	0.407	513	138	75.2	53.0	0.270	0.543	0.383

Results and Discussions

The analysis's goal is to assess how well the methods provided here perform in order to forecast the values of the quantiles corresponding to rare and very rare events.

Considering that the quantile values are the ones of interest, the presented results will be based on this aspect. Figure 2 shows the results obtained on the 6 case studies, using the 5 analyzed estimation methods, as well as the confidence interval for the L-moments method. For plotting positions, the Hazen formula was used ($P = \frac{(i-0.5)}{n}$) [19].

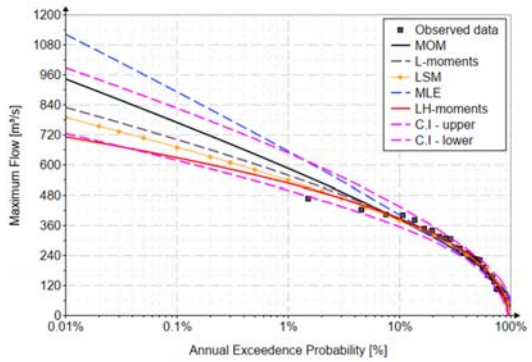

(a) Ialomita

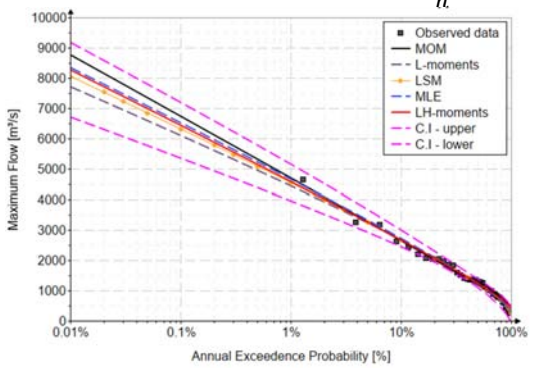

(b) Siret

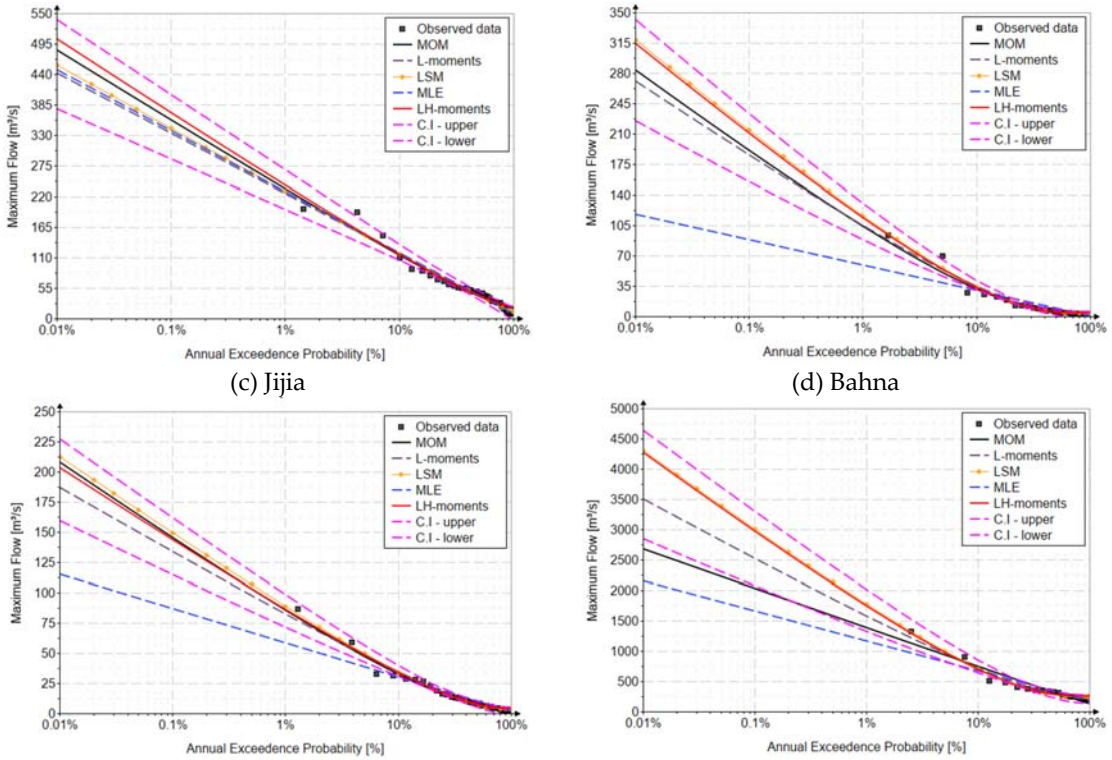

(c) Jijia (d) Bahna

(e) Nicolina (f) Viseu

Fig. 2. Evaluations of the quantile function for the five methods of parameter estimation.

The confidence interval is built for L-moments, based on Chow's approximation [1, 5, 10] defined for a statistical distribution for 90% confidence level (10% significance level). This assumes that the confidence interval is a variable function of the probability and standard error specific to each statistical distribution [5, 19].

Analyzing the obtained results, it can be observed that for the data series with skewness greater than 2 (Nicolina, Viseu and Bahna), the maximum likelihood method has no solution, the generated quantile values being characterized by very large errors, the errors increasing togheter with the increase of the skewness value.

In the case of the method of ordinary moments, the resulting values are significantly influenced by the small length of the data series, an aspect that can also be observed in the case of the Viseu river (n=20 values). This aspect is due to the particularities of the method, the errors being directly proportional to the increase in the degree of the statistical indicators that need to be calibrated (variance and skewness). Also, the establishment of skewness based on the genesis of the flows (without a complex analysis regarding this genesis), implies a subjective nature of the analysis which is a disadvantage. These errors are accentuated when, for basins larger than 100 km^2, the simplified approach is usually used, considering the variation coefficient as 1 and the multiplication coefficient as 4. For comparison, the graph of the curves corresponding to the three values of the multiplication coefficient for the Siret river is presented. This subjective character also appears in the case of the least squares method, many researchers choosing the Weibull probability as the predefined empirical

probability, which otherwise leads to significant deviations. The empirical probability must be established depending on the estimation method and the nature of the distribution used. Important contributions regarding this aspect have been made in recent materials [22], the Hazen empirical probability being the one that generates the smallest deviations from the theoretical values of the Pearson III distribution.

In the graphs of Figure 3, these particular aspects of the method of ordinary moments and the least square method are presented.

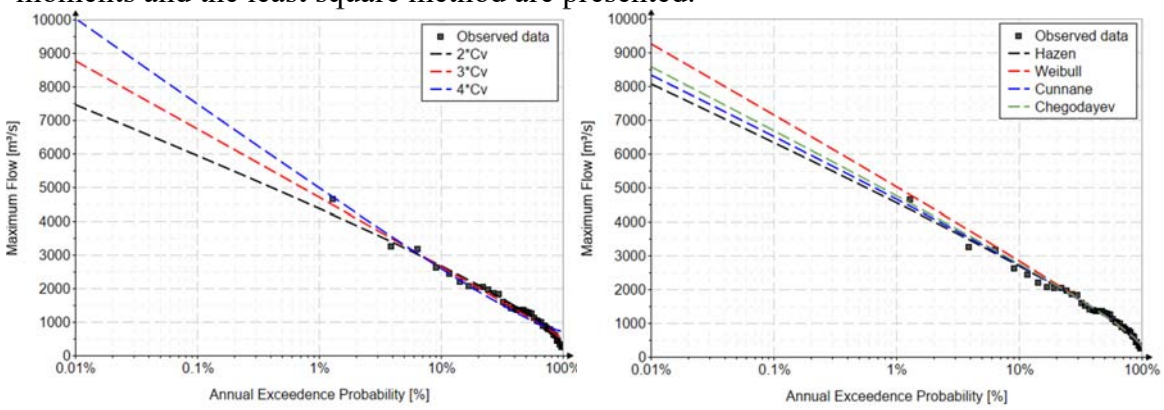

(a) MOM (b) LSM

Fig. 3. Comparative analysis for the Siret river.

Among the five analyzed methods, the L-moments method is the recommended one, being more stable and robust for short data lengths. It also represents, along with the LH-moments method, the only parameter estimation methods that present clear selection criteria, namely the calibration of higher-order linear moments, with approximate relationships and graphs of variation of these two indicators. The LH-moments method is also a method that, although it uses the series of maximum annual flows, it can be used as an alternative to the frequency analysis with partial series, fulfilling the same role, namely assigning a smaller weight to the lower extreme values (these are not always flood flows, but only maximum values corresponding to each year of analysis, representing the main disadvantage of using the block maximum/annual maximum method).

4. Conclusions

The Pearson III distribution is frequently used in hydrology, in Romania it is the parent distribution in flood frequency analysis.

In Romania, in most cases, the Pearson III distribution is used using tabular calculation developed only for MOM, with inadequate linear interpolation. Moreover, it is used inappropriately (for basins larger than 100 km^2). In recent materials [7,10,23], important contributions were made regarding the applicability of the Pearson III distribution, using the MOM and L-moments estimation methods.

Considering the results obtained on the 6 case studies, the following conclusions can be drawn:

- the method of linear moments is a much more stable, robust method and less sensitive to the variability of recorded data lengths, as well as to the presence of outliers. It is the only method that has clear criteria for selecting the best distribution, namely the calibration of higher order indicators, thus being able to make a pre-selection of the necessary distributions taking into account the values of the two indicators specific to the analyzed set. The same observations are also valid for the LH-moments method, which also has the advantage of the fact that it partially fulfills the so-called "separation effect" of the maximum flows from the annual series of maximum flows (comparable to the analysis of partial series);

- the Pearson III distribution cannot be applied, for skewness values greater than 2, using the maximum likelihood method of parameter estimation.

- the method of ordinary moments is recommended to be used only in the case of large data series (n>100 values), so that the correction of the skewness of the analyzed data set is minimal. The simplified approach of choosing skewness as 4 cannot be used for watershed larger than 100 km^2;

- the application of the Pearson III distribution using the least squares method is recommended to be performed only using the Hazen empirical probability, because after the comparative analysis it was observed that the biases compared to the theoretical values (population) are the smallest for this empirical probability.

These elements presented in the article are part of a wider research carried out in the Faculty of Hydrotechnics, in the elaboration of some proposals for the implementation of the L-moments method, in the future regulations regarding the analysis of extreme events in Romania and abandoning the old Soviet practices of use of the Pearson III distribution and some non-tehnical concepts without a mathematical basis such as the uncertainty interval [24].

References

[1] Bulletin 17B Guidelines for determining Flood Flow Frequency; Hydrology Subcommittee, Interagency Advisory Committee on Water Data, U.S. Department of the Interior, U.S. Geological Survey, office of Water Data Coordination, Reston, Virginia: 1981.

[2] Bulletin 17C Guidelines for determining Flood Flow Frequency; U.S. Department of the Interior, U.S. Geological Survey, Reston, Virginia: 2017.

[3] World Meteorological Organization. (WMO-No.100) 2018 Guide to Climatological Practices; WMO: Geneva, Switzerland, 2018.

[4] EM 1110-2-1415 Hydrologic Frequency Analysis, Engineering and Design; Department of the Army U.S. Army Corps of Engineers: 1993.

[5] Rao, A.R.; Hamed, K.H. Flood Frequency Analysis; CRC Press LLC: Boca Raton, FL, USA, 2000.

[6] Gubareva, T.S.; Gartsman, B.I. Estimating Distribution Parameters of Extreme Hydrometeorological Characteristics by L-Moment Method. Water Resour. 2010, 37, 437–445.

[7] Anghel, C.G.; Ilinca, C. Parameter Estimation for Some Probability Distributions Used in Hydrology. Appl. Sci. 2022, 12, 12588. https://doi.org/10.3390/app122412588.

[8] Hosking, J.R.M and Wallis, J.R. (1997) Regional Frequency Analysis: An Approach Based on L−moments. Cambridge University Press, UK, http://dx.doi.org/10.1017/cbo9780511529443.

[9] Hosking, J.R.M. L-moments: Analysis and Estimation of Distributions using Linear, Combinations of Order Statistics. J. R. Statist. Soc. 1990, 52, 105–124.

[10] Ilinca, C.; Anghel, C.G. Flood-Frequency Analysis for Dams in Romania. Water 2022, 14, 2884. https://doi.org/10.3390/w14182884
[11] Ciupak, M.; Ozga-Zieliński, B.; Tokarczyk, T.; Adamowski, J. A Probabilistic Model for Maximum Rainfall Frequency Analysis. Water 2021, 13, 2688. https://doi.org/10.3390/w13192688.
[12] Nwaogazie IL, Sam MG. Probability and non-probability rainfall intensity-duration-frequency modeling for port-harcourt metropolis, Nigeria. Int J Hydro. 2019;3(1):66-75. DOI: 10.15406/ijh.2019.03.00164.
[13] Ye, L., Hanson, L. S., Ding, P., Wang, D., and Vogel, R. M.: The probability distribution of daily precipitation at the point and catchment scales in the United States, Hydrol. Earth Syst. Sci., 22, 6519–6531, https://doi.org/10.5194/hess-22-6519-2018, 2018.
[14] Matalas N.C. Probability Distribution of Low Flows. Statistical Studies in Hydrology. Geological Survey, United States Covernment Printing Office, USA, Washington:1963.
[15] Greenwood, J.A.; Landwehr, J.M.; Matalas, N.C.; Wallis, J.R. Probability Weighted Moments: Definition and Relation to Parameters of Several Distributions Expressable in Inverse Form. Water Resour. Res. 1979, 15, 1049–1054, https://doi.org/10.1029/wr015i005p01049.
[16] Houghton, J.C. Birth of a parent: The Wakeby distribution for modeling flood flows. Water Resour. Res. 1978, 14, 1105–1109.
[17] Wang, Q.J. LH moments for statistical analysis of extreme events. Water Resour. Res. 1997, 33, 2841–2848.
[18] STAS 4068/1962; Maximum Water Discharges and Volumes, Determination of maximum Water Discharges and Volumes of Watercourses, the Romanian standardization institute, Bucharest, Romania.
[19] V.T.Chow, D.R.Maidment, L.W.Mays Applied Hydrology, 1988, MCGraw-Hill, Inc., ISBN 007-010810-2.
[20] Singh, V.P. Entropy-Based Parameter Estimation in Hydrology; Springer Science + Business Media: Dordrecht, The Netherlands.
[21] The Romanian Water Classification Atlas, Part I—Morpho−Hydrographic Data on the Surface Hydrographic Network; Ministry of the Environment: Bucharest, Romania, 1992.
[22] Anghel, C.G.; Stanca, S.C.; Ilinca, C. Two-Parameter Probability Distributions: Methods, Techniques and Comparative Analysis. Water 2023, 15, 3435. https://doi.org/10.3390/w15193435.
[23] Ilinca, C.; Anghel, C.G. Flood Frequency Analysis Using the Gamma Family Probability Distributions. Water 2023, 15, 1389. doi: 10.3390/w15071389.
[24] Drobot, R.; Draghia, A.F.; Chendes, V.; Sirbu, N.; Dinu, C. Consideratii privind viiturile sintetice pe Dunare. Hidrotehnica 2023, 68. (In Romanian).

Assessment of the levels of service for roads in the Central Business District (CBD) of Akure, Nigeria

Evaluarea nivelurilor serviciului pentru drumuri din districtul central de afaceri (CBD) Akure, Nigeria

Adelakun Salami [1], Olufikayo Aderinlewo [1], Moses Tanimola [1]

[1] Civil and Environmental Engineering Department
Federal University of Technology, P.M.B. 704, Akure, Nigeria
E-mail: ooaderinlewo@futa.edu.ng

DOI: 10.37789/rjce.2024.15.3.7

Abstract. *Traffic metering parameters in the CBD of Akure such as traffic composition and volume-capacity ratio were collected and evaluated to determine the levels of service of the selected major roads namely Oba Adesida road (directions A and B): direction A from Cathedral junction to 'A' Division and Direction B from 'A' Division to Cathedral junction and Arakale road (directions C and D): direction C from Isikan roundabout to NEPA roundabout and direction D from NEPA roundabout to Isikan Roundabout. The traffic composition analysis revealed the passenger car/taxi as the predominant mode while poor parking system, trading activities along the carriageway, bad roads, construction activities were identified as factors affecting the levels of service.*
Key words: *Traffic metering; Levels of Service; traffic composition; volume-capacity ratio, junction.*

1. Introduction

Efficient transport systems provide economic, social opportunities and benefits that result in positive multiplier effects such as accessibility to markets, employment and safety. However, inefficient transport systems have economic costs such as reduced or missed opportunity, lower quality of life and adverse effects on people's lives [1].

Traffic congestion means there are more vehicles trying to use a given road facility than it can handle- without exceeding acceptable levels of delay or inconvenience. In major cities, this occurs mostly during certain times of the day called peak periods or rush hours. There are two clear parameters within a single equation that causes congestion, which is the balance between the demand and the supply of road space [2].

Level of Service (LOS) can be defined as a designated term used to qualitatively describe the operating conditions of a roadway based on parameters such as volume/capacity ratio, speed, travel time, maneuverability, delay and safety [3]. It

designates six levels of service for each type of facility, from A to F, with Los "A" representing the best conditions and LOS "F" the worst.

The operating conditions for these six levels of service identified are as follows [4]:

- Level of service "A": Free flow with low volume and high speed, traffic density is low, with speed controlled by drivers desired speed limits and physical roadway conditions individual users are virtually unaffected by others in the traffic stream : volume-capacity ratios (v/c) vary from 0.00 to 0.60.
- Level of service "B": represents the range of stable flow but the presence of other users in the traffic stream begins to be noticeable. Freedom to select desired speed is relatively unaffected but there is a slight decline in the freedom to maneuver within the traffic stream from LOS A: v/c vary from 0.61 to 0.70
- Level of service "C" represents the range of stable flow but the selection of speed is affected by the presence of others. Maneuvering within the traffic stream requires substantial vigilance on the part of the user, v/c vary from 0.71 to 0.80.this is the target LOS for some urban and most rural highways.
- Level of service "D": Approaches flow, with tolerable operation speed being maintained through considerably affected changes in operating conditions. Fluctuations in volume and temporary restrictions to flow may cause substantial drops in operation speeds. Drivers have little freedom to maneuver; comfort and convenience are low, but conditions can be tolerated for short periods of time. Minor incidents are expected to create delays, v/c vary from 0.81 to 0.90
- Level of service "E": unstable flow, operating at capacity, cannot be described by speed alone but represent operations at even lower operating speeds than in level D with volumes at or near the capacity of highway. At capacity, speeds are typical but not always in the neighborhood of 50km/h. Flow is unstable and there may be stoppage of momentary duration. Drivers' level of comfort becomes poor. Freedom to maneuver within the traffic stream is extremely difficult, v/c vary from 0.91 to 1.00
- Level of service "F". Forced flow operations at low speeds, where volumes are above capacity. Conditions result from queues of vehicles backing up from a restriction downstream. Speeds are reduced substantially and stoppage may occur for long or short period of time, because of downstream congestion.travel time cannot be predicted, with generally more demand than capacity. A road in a constant traffic jam is at this LOS. In extreme conditions, both speed and volume can drop to zero, v/c is greater than 1.00

There is a need for Passenger Car Equivalence (PCE) to be defined by the traffic engineer both in the design of traffic facilities and also in the management of vehicles operations [5]. Each vehicular type such as tricycles, car, buses, truck/lorry in the traffic stream cannot be considered as equivalent to each other as there is significant difference in the vehicular and flow characteristics of each vehicle class. Therefore a Passenger Car Equivalent is majorly the impact that a mode of transport has on traffic variables (such as headway, speed, density) compared to a single car [6]. Table 1 shows the Passenger Car Equivalents used to convert the traffic volume to passenger car unit per hour (PCU/h).

The traffic volume in Akure Central Business District was analyzed so as to reveal the cause of parking problems [7]. Increased volume of traffic ribbon development/street trading and improper structural layout/land use pattern within the Central Business District (CBD) were factors responsible for these problems. Oyemekun and Arakale roads are the major arterials in Akure metropolis. The aim of the research is to determine the nature of traffic in terms of volume/capacity ratio as well as determine the future level of service of these routes (Direction A and B). The result of this research will help transportation agencies and government in proffering adequate measures for reduction of traffic congestion on major roads in Akure and similar capital cities in Nigeria.

Table 1

Passenger Car Equivalents

Vehicle Type	Equivalent Passenger Car Units
Pedal Cycle, Tricycles and Motor Cycles	0.5
Motor-car, Station Wagon, Taxi, Kit-Car	1
Pick-up, Jeep, Land Rover, Light Delivery Van, Minibus Trailer attached to above	2
2-Axle Truck Class, Lorry including Timber	2
Lorry, Truck, Mammy Wagon, Petrol Tanker Trailer attached to above	3
3 to 5 Axle Combination, Tractor Trailer including Low Loader, Petrol Tanker, Bus (Excluding Municipal)	3
Municipal Bus, More than 5 Axle Combination	4

Source: FMW&H Nigeria Highway Manual (2013)

2. Materials and Methods

Akure is the administrative capital of Ondo State. Akure became the state capital of Ondo State in 1976. The town is located on latitude $70^0$15′North of the Equator and Longitude $50^0$05′East of the Greenwich Meridian. The climate is hot and humid with two distinct seasons, the rainy and dry seasons. The rainy season lasts for seven months (April – October) and the dry season for five months (November–March). The rainfall is about 1524 mm per year and the atmospheric temperature ranges between 28˚C and 31˚C with a relative humidity of 80 percent [3]. The most noticeable of the physical expansion of the city is its population growth and urban landmass. The population rose from 123,000 in 1985 to 239,124 in 1991. The national population projection for the year 1996 and 2000 put the city population at 269,207 and 298,712 respectively. However, a sharp increase was recorded in the 2006 census, which put Akure South at 353,211 [8]. The projection for the year 2020 put the city population at 571,740 with a growth rate of about 3.5 percent per annum [9]. Figures 1 shows Akure Street Map highlighting the Central Business District.

Fig. 1. Akure Street Map Highlighting the Central Business District. Source: Google Map, (2019)

The research covers two selected major roads:

a. Oba Adesida road: Direction A which is from Catheral Junction to A Division and Direction B which is from A division to Catheral junction.

b. Arakale road: Direction C which is from Isinkan Roundabout to NEPA roundabout and Direction D which is from NEPA roundabout to Isinkan Rounabout as shown in Table 2.

The following are some of the materials used in carrying out this research: Stop watch, Traffic Jackets, Cine Camera and recording sheets. A reconnaissance visit was made to the study area for on-the-spot evaluation of some selected traffic congestion points. Traffic data collected were on the field, using camera to capture three dimensional situations of traffic jam and traffic counts.

Table 2

Selected routes segmentation

Routes 1	Direction A	Direction B
Oba Adesida	Cathedral Junction to A" Division	"A" Division to Cathedral Junction
Routes 2	Direction C	Direction D
Arakale	Isinkan Roundabout to NEPA Roundabout	NEPA Roundabout to Isinkan Roundabout

These two routes were selected as they were the major feeders of other arterial routes critical to traffic flow in the study area. Traffic parameters were metered using cine cameras which were placed on the pedestrian bridge in front of the Akure central Mosque on Oba – Adesida Road (OAR) and Globec Plaza Opposite Adedeji Park on Arakale Road (ARR). These two points served as vantage points from the road section to take inventory of the morning, afternoon and evening peak periods. These peak

periods were established to be between 7:00-9:00am, 12:00-2:00pm and 4:00-6:00pm for morning, afternoon and evening respectively on weekdays (Monday to Friday); 9:00-11:00am, 12:00-2:00pm and 4:00-6:00pm on Saturdays; 7:30-9:30am, 12:00-2:00pm and 4:00-6:00pm on Sundays [10].

Data on traffic composition and volume were collected by recording the types of vehicles namely motorcycles, cars, vans or buses and trucks captured by the video footage in a sheet [11]. These were arranged on the sheet in ascending order of their vehicular capacities. The sheet was marked as vehicles passed the reference point on the road as shown in the video footage. The traffic volume was converted to passenger car unit per hour (pcu/h) by multiplying each vehicle with their respective passenger car unit equivalents in order to get the approximate number of vehicles that ply the selected roads during the chosen peak periods in terms of passenger car [12].

The capacity for two – lane road is 2800pcu/h, therefore the level of service was determined by the analysis of volume – capacity ratio (v/c) traffic projection for 10 years.

$$Q_n = Q_0(1+r)^n \quad (1)$$

where:

Q_n - Projected traffic volume (pcu/h)

r -Traffic growth rate

n - Number of years for which projection is made

Q_0 - Observed maximum traffic volume

Assuming a traffic growth rate of 3% [13] for developing countries, a projection period not greater than 20 years is recommended [14].

3. Results and Discussion

Tables 3 and 4 show the traffic composition of vehicles that ply Oba Adesida and Arakale roads for the week. The tables revealed that the most predominant mode of transport along the two roads are passenger cars/taxi which constitute approximately 84.57% and 64.39% respectively, followed by motorcycles which constitute 13.26% and 32.48 respectively while tricycles, mini buses /vans, buses and trucks/lorries constitute the rest of the percentages

Table 3

Traffic Composition for Oba - Adesida Road during Peak Periods for the week

Vehicle Class	Morning Peak	Afternoon Peak	Evening Peak	Total	Percentage (%)
Bicycle	51	11	32	94	0.07
Motorcycle	4,502	5,716	6,942	17,160	13.26
Tricycle	33	37	44	114	0.09
Passenger Car	35,132	33,172	41,112	109,416	84.57
Mini van	42	56	53	151	0.12
Buses	515	498	646	1659	1.28
Trucks/Lorries	151	342	294	787	0.61
	40,426	39,832	49,123	129,381	100

Table 4

Traffic Composition for Arakale Road during Peak Periods for the week

Vehicle Class	Morning peak	Afternoon peak	Evening peak	Total	Percentage (%)
Bicycle	34	13	43	90	0.08
Motorcycle	11,549	11,385	12,103	35,037	32.48
Tricycle	61	85	106	252	0.23
Passenger Car	23,042	20,567	25,859	69,468	64.39
Mini van	47	65	77	189	0.18
Buses	472	679	684	1,835	1.70
Trucks/Lorries	215	406	389	1,010	0.94
	35,420	33,200	39,261	107,881	100

Traffic Flow

Tables 5 and 6 present the maximum hourly volume (MHV) for Oba–Adesida and Arakale roads for the week. The MHV recorded for Oba –Adesida road for both directions is 2369.5 pcu/h and 1860pcu/h while that of Arakale road is 1987.5 pcu/h and 1876.5pcu/h. The implications of these values as obtained for the maximum volume on both routes depict the high level of commercial activities going on in the CBD. As more people commute towards and along these routes for their daily activities, this often times result in traffic hold-ups and jams. Such result is expected around the CBD because of the commercial activities constantly occurring there [15].

Table 5

Maximum and minimum flow and passenger car unit for Oba Adesida road

	DIRECTION A				DIRECTION B			
Week	Veh/h		PCU/h		Veh/h		PCU/h	
	Max	Min	Max	Min	Max	Min	Max	Min
Monday	2171	1626	1815.5	1369	1992	1440	1613.5	1272
Tuesday	2257	1550	1866	1291	1932	1539	1631	1314.50
Wednesday	2856	1835	2369.5	1498.5	1919	1585	1680	1421
Thursday	2261	1528	1927.5	1427	1915	1457	1703	1260.50
Friday	2555	1867	2122.5	1459	1936	1702	1502.5	1355
Saturday	2837	2074	2259.5	1683	2110	1719	1720.50	1401.50
Sunday	2191	2025	1831	1604.50	2272	1828	1860	1505

Table 6

Maximum and minimum flow and passenger car unit for Arakale road

	DIRECTION C				DIRECTION D			
Week	Veh/h		PCU/h		Veh/h		PCU/h	
	Max	Min	Max	Min	Max	Min	Max	Min
Monday	2298	1592	1805	1281.5	1968	1488	1557	1215.5
Tuesday	2317	1772	1776	1413.5	2008	1702	1684.5	1352
Wednesday	2515	1483	1987.5	1282	2274	1833	1796.5	1463.5
Thursday	2101	1699	1609.5	1265	2465	1807	1876.5	1459
Friday	2089	1895	1644	1423.5	2051	1752	1557.5	1343.5
Saturday	2167	1709	1697.5	1412.5	2060	1856	1630	1482.5
Sunday	1912	1490	1474.5	1170.5	2020	1789	1569.5	1482.5

Volume- Capacity Ratio

Table 7 presents the results for the future level of service of both Oba – Adesida and Arakale roads.

Table 7

Analysis of Volume to Capacity Ratio and Levels of Service for peak period on both routes.

Routes	MHV week (vph)	Volume to Capacity Ratio (V/C)	Level of Service (LOS)	Remark	Maximum Projected Traffic (10yrs)	Future Volume to Capacity Ratio (V/C)	Level of Service (LOS)	Remark
Oyemekun to Oba-Adesida	2856	1.09	F	Unfavourable	3848	1.47	F	Unfavourable
Oba-Adesida to Oyemekun	2272	0.87	D	Unfavourable	3053	1.17	F	Unfavourable
Isikan to Arakale	2515	0.97	E	Unfavourable	3580	1.37	F	Unfavourable
Arakale to Isikan	2465	0.95	E	Unfavourable	3313	1.27	F	Unfavourable

The implication and the causes of level of service on each direction has been highlighted in Table 7. Furthermore, the future Level of Service for all the routes (directions) is “F” which indicates severe congestion by the year 2029. However, the highest volume was recorded for Oba Adesida direction A which as a result of the presence of commercial activities around the surrounding areas such as car street, Akure town hall, post office, Erekesan market and Olukayode building with no parking system along the stretch unlike direction B. Table 8 shows the summary results of causes, effects and measures taken for the levels of service obtained along both directions.

Table 8

Summary result showing effects, causes and measures of level of service along the routes

Route	LOS	PAG standard	Causes	Effect of the level of service	Measures
Cathedral Junction to A" Division {Oba Adesida direction A)	F	Heavy congestion	Increased volume of traffic which is predominated by passenger car/taxi, poor parking system, increase socio economic activities	Unstable flow, drivers level of comfort is poor	Restriction of illegal activities. Increase the capacity. Replacement of existing transport modes
"A" Division to Cathedral Junction{Oba Adesida direction B)	D	Heavy congestion	Approaches unstable, high density, poor levels of comfort and convenience.	Unstable flow, drivers level of comfort is poor	Restriction of illegal activities. Increase the capacity. Replacement of existing transport modes
Isinkan Roundabout to NEPA Roundabout(Arakale direction C)	E	Heavy congestion	Long vehicles park to off load, poor maintenance of alternative roads. Poor parking	Unstable flow, operating at capacity	Maintenance of alternative roads. Making frequent use the available parking space
NEPA Roundabout to Isinkan Roundabout(Arakale direction D)	E	Heavy congestion	Long vehicles park to off load, poor maintenance of alternative roads .poor parking\	Unstable flow, operating at capacity	Maintenance of alternative roads. Marking frequent use the available parking space

4. Conclusions

The level of traffic and corresponding levels of service on Oba Adesida road, direction A and B and Arakale road, directions C and D were determined through metering parameters such as traffic composition and volume/capacity ratio. The corresponding present level of service is F, D, E, and E respectively. The effect is that for all the routes, unstable flow, high density and poor comfort and convenience subsist. Assuming a projection of 10 years for developing countries, the levels of service for all the routes was obtained as "F" which would imply severe congestion by 2029. Therefore to sustain, develop and maintain transportation infrastructure in Akure and Nigeria at large, design measures such as expansion of roads leading to the CBD,

abolition of illegal parking/trading, and provision of adequate parking facilities should be implemented.

Conflicts of Interest: The authors declare no conflicts of interest.

References

[1] Z. Riha, I. Dockalikova, J. Tichy, D. Kostial, „Solving transportation externalities, economic approaches and their risks, Open Engineering, vol. 12, no. 1, 2022, pp. 1-10.
[2] A. S. Kumarage, „Urban traffic congestion: The problem and solutions, Economic Review, 2004, pp. 1-9.
[3] S. A. Ajayi, A. O. Owolabi, A. A. Busari, „Measures that enhance favorable levels of service and their modes of sustainability on major roads in Akure, South-Western Nigeria. Proceedings of the 3rd International Conference on African Development Issues, Ota-Ogun State, Nigeria, August 2016, pp. 329-336.
[4] L. R. Kadiyali, „Traffic engineering and transport planning; Khanna Publishers: Delhi, India, 2011
[5] S. Anand, S. V. C. Sekhar, M. R. Karim, „Development of passenger car unit (PCU) values for Malaysia, Journal of the Eastern Asia Society for Transportation Studies 1999, vol. 3, no. 3.
[6] U. Salisu, O. O. Oyesiku, „Traffic survey analysis: Implications for road transport planning in Nigeria, Scientific Journal on Transport and Logistics, vol. 11, no. 2, 2020, pp. 12-22.
[7] A. O. Owolabi, O. O. Ojuri, „An analysis of traffic volume and parking in the central area of Akure, International journal of transport studies, vol. 1, no. 2, 2004, pp. 40-47.
[8] N.P.C., „Census 2006 National Summary. National Population Commission 2007.
[9] E. E. Okoko, „A predictive modeling of spatial interaction pattern in the transport system in Akure. Unpublished PhD Thesis, Federal University of Technology, Akure 2002.
[10] A. O. Owolabi, O. J. Oyedepo, E. E. Okoko, „Predictive modeling of entry flow at rotary intersections in Akure, a developing city and capital of Ondo state, Nigeria, Journal of Transport Literature, vol. 9, no. 2, 2016, pp. 10-14.
[11] M. M. Rahman, J. Jahan, Y. Zhou, „Alleviating traffic congestion by the strategy of modal shift from private cars to public transports: A case of Dhaka City, Bangladesh. In Carmichael T.; Yang Z. (eds). Springer Proceedings in Complexity, Springer, 2020, pp. 101-115.
[12] S. Srikanth, A. Mehar, „A modified approach for estimation of passenger car units on intercity divided multilane highways, Archives of transport, vol. 42, no. 2, pp. 65-74.
[13] Transport and Road Research Laboratory, „Road Note 31 - A guide to the structural design of bitumen-surfaced roads in tropical and sub-tropical countries, 3rd ed., Her Majesty's stationery Office, Crowthorne, 1997.
[14] FMW&H, „Federal Republic of Nigeria Highway Design Manual. Federal Ministry of Works and Housing, Nigeria, 2013.
[15] E. F. Ogunbodede, „Assessment of traffic congestions in Akure (Nigeria) using GIS approach: Lessons and challenges for urban sustenance, American Journal of Engineering Research, vol. 2, no. 2, 2003, pp. 15-21.

Lightweight gypsum composite with plastic waste incorporation for building construction applications

Compozit ușor din ghips cu încorporarea deșeului de plastic pentru aplicații în construcția clădirilor

Bogdan Valentin Paunescu[1], Enikö Volceanov[2,3], Marius Florin Dragoescu[4], Lucian Paunescu[5]

[1] Consitrans SA
56 Polona street, sector 1, Bucharest 010504, Romania
E-mail: pnscbogdan@yahoo.com

[2] University "Politehnica" of Bucharest, Faculty of Science and Materials Engineering
313 Independence Splai, sector 6, Bucharest 060042, Romania
E-mail: evolceanov@yahoo.com

[3] Metallurgical Research Institute SA
39 Mehadia street, sector 6, Bucharest 060543, Romania
E-mail: evolceanov@yahoo.com

[4] University "Politehnica" of Bucharest, Faculty of Applied Chemistry and Material Science
1-7 Gh. Polizu street, sector 1, Bucharest 011061, Romania
E-mail: mar_dmf@gmail.com

[5] Cosfel Actual SRL
95-97 Calea Grivitei, sector 1, Bucharest 010705, Romania
E-mail: lucianpaunescu16@gmail.com

DOI: 10.37789/rjce.2024.15.3.8

Abstract. *Aiming at making lightweight gypsum-based composite whose mechanical strength to be acceptably high, the current work tested the combined use of some recycled plastic waste (polyethylene terephthalate-PET, polypropylene, and expanded polystyrene) as well as silica fume, a very fine powder as by-product in metallurgical industry, having the ability to improve the composite mechanical properties. The optimal combination of fillers included PET (1 wt. %) and polypropylene (1 wt. %) whose fibrous structure influenced the decrease of bulk density up to 540 kg·m^{-3} as well as especially the increase of flexural strength up to 4 MPa.*

Key words: *lightweight gypsum composite, plastic waste, aluminum powder, fiber, polymer.*

Rezumat. *Vizând fabricarea compozitului ușor pe bază de ghips a cărui rezistență mecanică să fie acceptabil de înaltă, lucrarea curentă a testat utilizarea combinată a*

unor deșeuri reciclate de plastic polietilenă tereftalata-PET, polipropilenă și polistiren expandat), precum și nanosilica, o foarte fină pulbere ca produs secundar al industriei metalurgice, având capacitatea de a îmbunătăți proprietățile mecanice ale compozitului. Combinația optimă a materialelor de umplutură a inclus PET (1 wt. %) și polipropilenă (1 wt. %) a căror structură fibroasă a influențat reducerea densității în vrac până la 540 kg·m^{-3}, precum și, în mod special, creșterea rezistenței la încovoiere până la 4 MPa.

Cuvinte cheie: compozit ușor din ghips, deșeu de plastic, pulbere de aluminiu, fibră, polimer.

1. Introduction

Calcined gypsum plaster known also as ”plaster of Paris” is a building sulfate material mainly used for protective or decorative coating of walls and ceilings. Gypsum is a water-containing calcium silicate. After calcination processes the water of crystallization is partially removed, resulting in calcined gypsum ($CaSO_4 \cdot 0.5H_2O$) [1]. Gypsum plaster is a replacement for sand cement plaster more expensive. The main properties of gypsum plaster are: light weight, less water-curing, insulation for temperature control, and eliminates shrinkage cracks. According to [2], perlite and vermiculite are lightweight minerals, being suitable for their application in making gypsum composites. They have excellent properties that improve gypsum plaster characteristics. Perlite, that is a volcanic glass, is one of the most effective natural minerals. Water is absorbed into the raw perlite matrix developing its ability to expand when heated. The properties of perlite are: light weight, insulating properties, without organic contaminants, non-flammable, and pest-proof. Vermiculite is a hydrated magnesium aluminum silicate mineral. Vermiculite is a hydrated magnesium aluminum silicate mineral. Subjected to heat, vermiculite expands forming particles. Its main properties are: light weight, fireproof, compressible, strongly absorbent, non-reactive, and increases its volume in water up to three times.

A method of reducing the weight of gypsum-based materials is the use of light inorganic or organic fillers. The inorganic fillers most often used are perlite and wollastonite. According to [3], a mixture of fly ash-lime-gypsum including 5-10 % perlite and very low microsilica addition allowed to obtain a composite with the bulk density of 730 kg·m^{-3} and compression strength of 2.3 MPa. Another combination of materials that led to acceptable results was the use of vermiculite (20 wt. %) together with polypropylene fibers [4]. The bulk density was reduced by about 10 % and simultaneously the thermal conductivity by 30 %. However, the decrease in the mechanical strength by up to 30 % at the same time was the negative aspect of the test.

Two variants of making composites based on lightweight gypsum were tested [5], containing foamed gypsum matrices with low density using aggregates with higher density as well as matrices with higher density using aggregates with low density. The method with higher density matrix and lightweight aggregates was the optimal option. Using 5 wt. % expanded perlite the test led to a bulk density of 547 kg·m^{-3}, heat conductivity of 0.12 W·m^{-1}·K^{-1} and compression strength of 2 MPa. On the other

hand, composites with low density of the foamed matrix and higher density of aggregates had good thermal properties, but too low compression strength.

Authors of the current paper have performed experiments on making lightweight gypsum-based materials using calcined gypsum, $Ca(OH)_2$, fly ash, perlite, silica fume, carboxy-methyl cellulose, and aluminum powder [6]. Bulk density had relatively low values (530-600 $kg \cdot m^{-3}$), heat conductivity was between 0.129-0.184 $W \cdot m^{-1} \cdot K^{-1}$, compression strength within the limits of 1.2-2.2 MPa, and water-absorption up to 3.9 vol. %.

In terms of energy, the use of perlite and vermiculite as aggregates for lightweight gypsum has a negative influence on the environment due to the relatively high energy consumption during processing. The incorporation of polystyrene wastes (both extruded and expanded polystyrene) substituting perlite and vermiculite is a viable solution]7]. Expanded polystyrene is used in constructions to insulate walls and floors, while extruded polystyrene is used to insulate the roof.

The addition of cork waste and other fillers such as cellular glass, expanded polystyrene, extruder polystyrene or polyurethane wastes showed a reduction in bulk density. However, the mechanical strength was affected, being also reduced [8]. As a conclusion of this work, polystyrene wastes can be used as alternative aggregates in the gypsum mass, replacing perlite and vermiculite.

Other experiments reported in the literature [9] used polystyrene beads (2 wt. %) and polypropylene fiber (2 wt. %), obtaining a reduction of about 50 % of bulk density, while the tensile strength increased by 23 %.

The attempt of some researchers to extremely reduce the bulk density (up to 200 $kg \cdot m^{-3}$) led to the serious damage of mechanical strength.

According to the paper [10], the physical and mechanical properties of gypsum-based composites can be favourably influenced by recycled non-degradable materials (e.g. wet wipes). The experimental results showed that more effective materials can be manufactured with a small decrease in density compared to ordinary gypsum. The improvement of mechanical properties is worth noting. In the case of starting mixtures with 2.5 wt. % recycled fibers, flexural strength value increased by 19 %. One of the most widely used polyethylene plastics is polyethylene terephthalate (PET). Plastic foam waste such as extruded polystyrene, expanded polystyrene and polyurethane foam were used as lightweight aggregates in gypsum-based composites with better thermal properties.

Polypropylene fiber as textile waste with a very high annual generation rate worldwide has led to the increase of plastic waste reserves. Recently, recycling this waste for construction applications has become a viable solution. The paper [11] presents different fiber contents (between 0.25-0.55 wt. %) and water/powder ratios (between 0.6-0.9 %) in the gypsum-based composite experimentally manufactured. Different thicknesses of flexural plates (9-18 mm) incorporating recycled fibers, reinforced with different mesh types were produced. The results showed that the density of the composite decreased by up to 26 % as the fiber content increased. Compression and flexural strength decreased with the increase of the fiber content and

the water/powder ratio, still remaining within the acceptable limits of 1 and 2 MPa, respectively.

A study on the effect of including plastic fiber waste on mechanical and durability characteristics of foamed gypsum was carried out in the work [12]. The fibers were introduced in proportions within the limits of 0.25-1 wt. %. The experimental results showed that by this addition, the workability of gypsum foam decreased. However, the samples with up to 0.75 % plastic fibers reached the highest flexural and compression strength values. The water-absorbing of these samples increased with the increase in the proportion of added fibers.

The influence of the content of polypropylene fibers and their length on physico-mechanical characteristics of gypsum particleboard were analyzed in [13]. The effect of the quantity and length of fibers is felt by values of internal bond resistance and modulus of rupture of the composite. The highest value levels of fiber content (9 %) and fiber length (9 mm) were experimentally determined. A high content of polypropylene fiber reduces the internal bond strength, modulus of rupture and modulus of elasticity.

In the work [14] hemp and sheep wool fibers were used for the reinforcement of gypsum composite. The aim of the research was to evaluate the ability of these bio-materials to enhance the fracture toughness of gypsum matrix. The results showed that wool fibers improved the mechanical performance more effectively compared to hemp fibers due to the high adhesion at the interface of the fiber and the gypsum matrix.

To reduce the open structure of expanded polystyrene particles, a modern technique was tested in [15]. Their heat treatment at low temperature (120-130 °C) improved the performance of polystyrene by reducing the volume and increasing its density. Expanded polystyrene with bulk density between 40-100 $kg \cdot m^{-3}$ was incorporated as filler material for making the gypsum composite. According to the measurement results, the compression strength had very low values (between 15-136 kPa) and the material density was also reduced (between 48-194 $kg \cdot m^{-3}$). The noise reduction coefficient had values between 600-800 Hz and the sound absorption coefficient reached 0.88.

The present work started from the need to increase the mechanical strength of gypsum foam composites. Different fiber types incorporated in the mixture of materials as fillers can represent the viable technical solution considering the previous results of their application as reinforcement of other material types (e.g. concrete, cement). Using usual components of the gypsum foam making process (calcined gypsum, fly ash, hydrated lime, aluminum powder as a foaming agent), polyethylene terephthalate fiber, polypropylene fiber, expanded polystyrene, and silica fume (as an ultrafine powder) were incorporated. These materials were grouped into three combinations, each representing an experimental version as follows: polyethylene terephthalate-silica fume, polypropylene fiber-polyethylene terephthalate, and expanded polystyrene-silica fume. The use of experimental association of two types of materials each with reinforcing role constitutes the originality of this work.

2. Materials and methods

Calcined gypsum ($CaSO_4 \cdot 0.5H_2O$) is available on the market in granulated state below 1mm. For its use in experiment, the material was ground in a ball mill, being selected after sieving the grain size under 100 μm.

Fly ash was provided by Paroseni-Thermal power plant (Romania) being captured from electrofilters of the plant's energy boiler. Under the conditions of using lignite as a solid fuel, the fly ash composition included 46.5 % SiO_2, 23.7 % Al_2O_3, 10.1 % ($Na_2O + K_2O$), 8.6 % Fe_2O_3, 3.2 % MgO, and 7.9 % CaO. The initial grain size of the ash was under 250 μm, and it was necessary to grind it to reduce the dimensions under 80 μm. By using fly ash, the weight proportion of gypsum as a binder could be slightly reduced.

Polyethylene terephthalate was recycled from post-consumer PET packaging waste, cut and ground in the form of particles below 2 mm. Due to its fibrous structure, this waste has a major role in reinforcing the final product to increase the mechanical strength to an acceptable level.

Polypropylene fiber and expanded polystyrene fiber were recycled from plastic waste existing among the residual materials of a building site. Wastes were cut, ground, and selected after sieving at the grain size below 1.5 mm.

The chosen foaming agent was the fine aluminum powder (below 10 μm) previously produced through own nitrogen jet atomization technique of recycled aluminum waste melted by microwave irradiation [6].

Hydrated lime ($Ca(OH)_2$), known also as slaked lime, was adopted for developing the corrosion reaction of aluminum in aqueous solution.

Silica fume with SiO_2 content more than 93 % is a by-product of metallurgy industry. It is a highly pozzolanic material being usually used to increase mechanical and durability properties of concrete. Silica fume is an ultrafine material with spherical particles less than 1 μm diameter. It is available on the market, the main supplier being China.

Three compositional variants were adopted for the experiment including calcined gypsum, fly ash, hydrated lime, and aluminum powder maintained in constant weight proportion as well as polyethylene terephthalate + silica fume (version 1), polypropylene fiber + polyethylene terephthalate (version 2), and expanded polystyrene + silica fume (version 3). The composition of the three experimental versions is presented in Table 1.

Table 1

Composition of experimental versions

Composition	Version 1 ($kg \cdot m^{-3}$)	Version 2 ($kg \cdot m^{-3}$)	Version 3 ($kg \cdot m^{-3}$)
Calcined gypsum	79.0	79.0	79.0
Fly ash	6.0	6.0	6.0
Hydrated lime	10.0	10.0	10.0
Aluminum powder	3.0	3.0	3.0
Polyethylene terephthalate	1.2	1.0	-

Composition	Version 1 ($kg \cdot m^{-3}$)	Version 2 ($kg \cdot m^{-3}$)	Version 3 ($kg \cdot m^{-3}$)
Silica fume	0.8	-	0.9
Polypropylene	-	1.0	-
Expanded polystyrene	-	-	1.1
Water addition	30.0	30.0	30.0

The method adopted for obtaining gypsum foam is based on the use of gaseous hydrogen as a foaming gas resulting from the corrosion process of fine aluminum particles in aqueous solution of $Ca(OH)_2$. The process takes place at room temperature, being efficient in terms of energy, unlike the foaming techniques of silicate materials using an expanding agent that releases the necessary gas at high temperatures (800-1100 °C).

The basic chemical reaction of foaming with fine aluminum powder forming katoite ($Ca_3Al_2(OH)_{12}$) that enters the gypsum mass and hydrogen is the following:

$$2Al + 3Ca(OH)_2 + 6H_2 = Ca_3Al_2(OH)_{12} + 3H_2 \quad (1)$$

It was experimentally applied by authors of the current paper [16] in the cold foaming process of glass waste for producing glass foam.

According to [17], the reaction mechanism is complex including several stages (2-5) that occur at the aluminum particle/aqueous solution interface.

$$Al_2O_3 + H_2O = 2AlOOH \quad (2)$$

$$AlOOH + H_2O = Al(OH)_3 \quad (3)$$

$$Al(OH)_3 + OH^- = Al(OH)_4 \quad (4)$$

$$3Ca^{2+} + 2Al(OH)_4 + 3H_2O = Ca_3Al_2(OH)_{12} + 6H_2 \quad (5)$$

The paste was prepared into a cylindrical metal mold by stirring with a rate of 800 rpm up to it began the expansion process.

Usual methods were used to characterize the gypsum foam samples. The determination of bulk density and porosity was carried out by applying the water intrusion method (Archimedes' method), according to ASTM D792-20 standard. Heat conductivity was measured by heat-flow method-ASTM E1225-04 [18]. Compression strength was determined with TA.XTplus Texture analyzer and flexural strength was investigated by conducting the three-point bend test on the specimen (ASTM D790) [19]. Using the usual technique of immersing the specimen under water (ASTM D570) the water-absorbing capacity was determined. Microstructural particularities of samples were observed with ASONA 100X Zoom Smartphone Microscope.

3. Results and discussion

The amount of wet starting mix of 300 g was used in all versions tested. The making process with an average duration of around 10 min was carried out at room temperature (24 °C).

The three experimental versions were made with calcined gypsum, fly ash, hydrated lime, aluminum powder, and water addition in weight proportions shown in Table 1 kept constant, to which different combinations of plastic waste and silica fume were added in order to improve the mechanical strength of gypsum foam.

The three gypsum foam specimens (shown in Fig. 1) were subjected to investigations to determine the physico-mechanical and thermal characteristics. The results are presented in Table 2.

a b c

Fig. 1. Appearance images of gypsum-based composite
a – version 1; b – version 2; c – version 3.

Table 2

Physico-mechanical and thermal characteristics

Characteristic	Version 1	Version 2	Version 3
Bulk density ($kg \cdot m^{-3}$)	570	540	590
Porosity (%)	72.7	74.0	71.6
Heat conductivity ($W \cdot m^{-1} \cdot K^{-1}$)	0.178	0.169	0.180
Compression strength (MPa)	2.4	1.9	2.5
Flexural strength (MPa)	3.2	4.0	3.1
Water-absorbing (vol. %)	3.6	3.3	3.5
Pore size (mm)	0.3-0.6	0.4-0.9	0.1-0.3

The data in Table 2 show modifications of physical, mechanical, and thermal characteristics influenced by the additions of fibrous plastic waste as well as silica fume as a by-product of the metallurgical industry. Two important effects of using fibers are the decrease of bulk density (540-590 $kg \cdot m^{-3}$) that determines also decreasing the heat conductivity (0.169-0.180 $W \cdot m^{-1} \cdot K^{-1}$) and increasing the porosity (71.6-74.0 %), i.e. improving insulation properties as well as the increase of mechanical strength of composite, especially of flexural strength (3.1-4.0 MPa). These effects have already been previously observed by researchers in the field and numerous works have published these conclusions [20-22].

The most effective combination of fibers in gypsum foam was polyethylene terephthalate (PET)-polypropylene (version 2), because the insulation properties were the best (bulk density of 540 $kg \cdot m^{-3}$, heat conductivity of 0.169 $W \cdot m^{-1} \cdot K^{-1}$, and porosity of 74.0 %), while the flexural strength clearly had the highest value of 4.0 MPa. The combinations that included silica fume together with plastic wastes (versions 1 and 3) were less porous, the flexural strength was lower compared to version 2 and only the compression strength was slightly higher (2.4-2.5 MPa) compared to the optimal version.

The microstructural appearance of composite foam specimens is shown in Fig. 2.

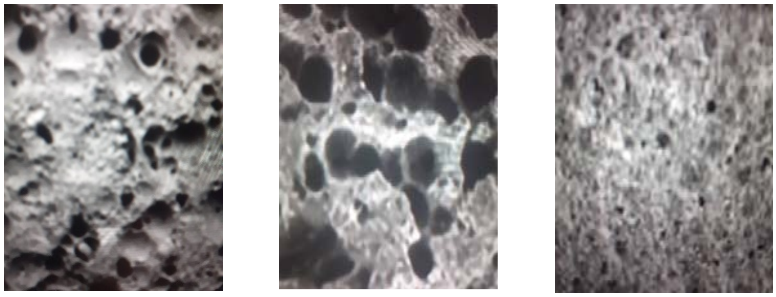

Fig. 2. Microstructural appearance of composite samples
a – version 1; b – version 2; c – version 3.

The pore size range in the optimal version (no. 2) had the highest values (0.4-0.9 mm) among the three tested versions. The gypsum foam specimen corresponding to version 3 had the lowest pore size values (0.1-0.3 mm), thus explaining the highest bulk density value.

The research presented in this paper aimed at improving the mechanical properties of gypsum foam, characterized mainly by its porous and lightweight structure. The use of fibrous material additions is a method recently applied in several types of dense composites to increase their strength and durability to very high limits. In the case of lightweight composites, low-density fillers are necessary and the most well-known light inorganic materials are perlite and vermiculite, but their large-scale application raises problems with ecological impact. Therefore, the search for optimal solutions of preparing lightweight composites (including gypsum foam) was oriented towards plastic waste containing fibers.

Nanomaterials of the silica fume type are also known due to their ability to improve the mechanical properties of any type of composite. For this reason, silica fume was included among the materials used in this experiment.

The most favourable corelation between thermal insulation properties and mechanical strength of the gypsum composite was obtained in the case of using the combination of polyethylene terephthalate (PET) fiber with polypropylene fiber (in equal weight proportions of 1 % of the total amount of dry gypsum composite). Bulk

density was minimal (540 kg·m^{-3}) and flexural strength reached the highest value (4 MPa).

4. Conclusions

The work aimed at the production of a lightweight gypsum-based composite whose mechanical strength should be acceptably high despite its porous structure. Except for calcined gypsum, fly ash, and hydrated lime, the specific ingredients of the material mixture as well as aluminum powder as an expanding agent, combinations of plastic waste (polystyrene terephthalate, polypropylene, and expanded polystyrene) and a micromaterial (silica fume) were used alternatively in the three experimental versions. The results showed the tendency to decrease the bulk density (540-590 kg·m^{-3}) by comparison with gypsum foam without the addition of fibers and to increase the flexural strength (especially), but also the compression strength. Flexural strength had values within the limits of 3.1-4.0 MPa and compression strength in the range of 1.9-2.5 MPa. The pore size of specimen microstructure was influenced by the nature of plastic wastes in combination with silica fume, however, the dimensions had low values from 0.1 to 0.9 mm. Water-absorbing of samples was influenced to a small extent, the values being maintained in the limited range of 3.3-3.6 vol. %. The work originality was the simultaneous combination of two fiber-supplier fillers into the material mixture. The optimal version was chosen that of combination polyethylene terephthalate and polypropylene, which led to obtaining bulk density of 540 kg·m-3 and flexural strength of 4.0 MPa. The ecological and economic product based on gypsum is suitable for applications mainly in the building construction. Lucrarea se va încheia cu un paragraf de concluzii în care vor fi menţionate rezultatele originale obţinute şi eventualele posibilităţi de aplicare ale acestora.

References

[1] C. Klein, C.S. Huribut Jr., „Manual of Mineralogy", 20th edition, John Wiley, 1985, pp. 352-353, ISBN 978-0-471-80580-9.

[2]*** „Perlite and Vermiculite: Lightweight Aggregates in Gypsum", Dicalite Management Group, 2017. https://www.dicalite.com/2017/11/perlite-vermiculite-lightweight-aggregates-gypsum/

[3] I. Demir, M. Serhat Baspinar, „Effect of silica fume and expanded perlite addition on the technical properties of the fly ash-lime-gypsum mixture", Construction and Building Materials, vol. 22, no. 6, 2008, pp. 1299-1304.

[4] O. Gencel, J.J. del Coz Diaz, M. Sütcü, „Properties of gypsum composite containing vermiculite and polypropylene fibers: Numerical and environmental results", Energy and Buildings, vol. 70, 2014, pp. 135-144.

[5] Alena Vimmrova, M. Kappert, L. Svoboda, R. Černy, „Lightweight gypsum composite: Design strategies for multi-functionality", Cement and Concrete Composites, Elsevier, vol. 33, no. 1, 2011, pp. 84-89.

[6] L. Paunescu, S.M. Axinte, B.V. Paunescu, „Light weight gypsum-based material manufactured by expanding process with aluminum powder", Revista Romana de Inginerie Civila, vol. 13, no. 2, 2022, pp. 138-148, ISSN 2068-3987.

[7] M. del Rio Merino, P.V. Saez, I. Longobardi, J. Santa Cruz Astorqui, C. Porras-Amores, „Redesignin lightweight gypsum with mixes of polystyrene waste from construction and demolition waste", Journal of Cleaner Production, Elsevier, vol. 220, 2019, pp. 144-151.
[8] A. San Antonio Gonzalez, M. Del Rio Merino, C. Viñas Arrebola, P. Villoria-Saez, „Lightweight material made with gypsum and extruded polystyrene waste with enhanced thermal behavior", Construction and Building Materials, Elsevier, vol. 93, 2015, pp. 57-63.
]9] B. Sayil, E. Gurdal„The physical properties of polystyrene aggregated gypsum blocks", Proceedings of the 8th International Conference on Durability Materials and Composites, vol. 1-4, pp. 496-504, Vancouver, Canada, May 30-June 3, 1999.
[10] M.I. Romero-Gomez, M.A. Pedreño-Rojas, F. Perez-Galvez, P. Rubio de Hita, „Characterization of gypsum composites with polypropylene fibers from non-degradable wet wipes", Journal of Building Engineering, Elsevier, vol. 34, 2021. https://doi.org/10.1016/j.jobe.2020.101874
[11] R. Alyousef, W. Abbass, F. Aslam, M. Imran Shah, (2023) „Potential of waste woven polypropylene fiber and textile mesh for production of gypsum-based composite", Case Studies in Construction Materials, Elsevier, vol. 18, 2023. https://doi.org/10.1016/j.cscm.2023.e02099
[12] S.A. Yildizel, Y. Dikiciasik, „Waste plastic fiber reinforced foamed gypsum", in Gypsum: Sources, Uses and Properties, (Ippolito, M.N. ed.), Nova Science Publisher, ISBN 978-1-68507-932-1, 2022.
[13] Y.H. Deng, T. Furuno, „Properties of gypsum particleboard reinforced with polypropylene fibers", Journal of Wood Science, vol. 47, 2001, pp. 445-450.
[14] A.P. Fantilli, D. Jozwiak-Niedzwiedzka, P. Denis, „Bio-fibres as a reinforcement of gypsum composites", Materials (Basel), Koenders, E. (ed.), vol. 14, no. 17, 2021. https://doi.org/10.3390/ma14174830
[15] P.P. Argalis, G. Bumanis, D. Bajare, „Gypsum composites with modified waste expanded polystyrene", Journal of Composites Science, vol. 7, no. 5, 2023. https://doi.org/10.3390/jcs7050203
[16] L. Paunescu, S.M. Axinte, B.V. Paunescu, „New manufacturing method of glass foam by cold expansion of glass waste", Journal La Multiapp, vol. 2, no. 3, 2021, pp. 1-9.
[17] S. Kaneshira, S. Kanamori, K. Nagashima, T. Saeki, H. Visbal, T. Fukui, K. Hirao, „Controllable hydrogen release via aluminium powder corrosion in calcium hydroxide solution", Asian Ceramic Societies, vol. 1, no. 3, 2013, pp. 296-303.
[18] N. Yűksel, „The review of some commonly used methods and techniques to measure the thermal conductivity of insulation materials", in Insulation Materials in Context of Sustainability, Almusaed, A., Almssad, A. (eds.), ISBN 978-953-51-2625-6, 2016. https://doi.org/10.5772/64157
[19] G. Rathnakar, H.K. Shivanan, „Experimental evaluation of strength and stiffness of fibre reinforced composites under flexural loading", International Journal of Engineering and Innovative Technology, vol. 2, no. 7, ISSN 2277-3754, 2013.
[20] G. Kalaprasad, J. Kuruvilla, T. Sabu, „Influence of short glass fiber addition on the mechanical properties of sisal reinforced low density polyethylene composites", Journal of Composite Materials, vol. 31, no. 5, 1997.
[21] F. Yao, Q. Wu, Y. Lei, Y. Xu, „Rice straw fiber-reinforced high-density polyethylene composite: Effect of fiber type and loading", Industrial Crops and Products, Elsevier, vol. 28, no. 1, 2008, pp. 63-72.
[22] S. Grzesiak, M. Pahn, M. Schultz-Cornelius, S. Harenberg, C. Hahn, „Influence of fiber addition on the properties of high-performance concrete", Materials (Basel), Fantilli, A.P. (ed.), vol. 14, no. 13, 2021. https://doi,org/10.3390/ma14133736

Study of the durability of stabilized earth based on recycled sediment

Studiul durabilității pământului stabilizat pe baza de sedimente reciclate

Nezha Gueffaf[*,1], Bahia Rabehi [2], Noureddine Mesboua[1,3], Khaled Boumchedda[4]

[1]Research Unit Materials, Processes and Environment (UR-MPE), University M'Hamed Bougara Boumerdes, Avenue of Independence, Boumerdes, 35000, Algeria.
n.gueffaf@univ-boumerdes.dz
[2]Department of Civil Engineering, Research Unit Materials, Processes and Environment (UR-MPE), University M'Hamed Bougara Boumerdes, Avenue of Independence, Boumerdes, 35000, Algeria
b.rabehi@univ-boumerdes.dz
[3]Department Technology of chemical engineering, Institut of Technology, University of Bouira, Algeria
n.mesboua@univ-bouira.dz
[4]Department of Civil Engineering, Research Unit Materials, Processes and Environment (UR-MPE), University M'Hamed Bougara Boumerdes, Avenue of Independence, Boumerdes, 35000, Algeria
k.boumchedda@univ-boumerdes.dz

DOI: 10.37789/rjce.2024.15.3.9

Abstract. *The durability of blocks made by earth can be improved considerably by the addition of different stabilizers. In this work, two stabilizers have been used: cement. The elaborated specimens are evaluated by various laboratory tests, and durability is evaluated by examination of walls exposed to real climatic conditions. It has been noted that all treated walls showed no signs of deterioration after 2 years exposure in real climatic conditions even though the laboratory test conditions are more severe compared to the natural climatic conditions of the region of Algiers where this present work has been carried out. The blocs stabilized by cement showed the best durability behavior.*
Key words: *Recycled Sediment; Stabilizers; durability tests; Climatic conditions exposure.*

Corresponding author. E-mail address: n.mesboua@univ-bouira.dz

1 Introduction

To limit the vulnerability of raw earth construction to the adverse effects of the environment, the solution is to stabilize the granular material. Earthen construction is sensitive to water, which causes rapid deterioration of the material under severe weather conditions. Speeded up tests are used to compare the performances of stabilized earthen blocks used under laboratory exposure conditions for block making. However, it is not possible to test the complex series of conditions such as rain, sun, temperature, humidity, and wind in the laboratory. It is noted that little work has been carried out relating the performance of the blocks under almost the same conditions to that of real walls.

Some research works on the stabilization by mechanical way of the compressed earth blocks on the effect of type of compaction (dynamic, static and vibro-static) on the mechanical performance and the durability of the stabilized earth blocks, resulting from the region of Algiers East, were led by Bahar and al [1]. It was found that the three different compaction methods used did not significantly affect the dry density of the soil. Mechanical stabilization by dynamic compaction seems to give better results compared to static or vibro-static compaction. For dry blocks, dynamic compaction was found to provide the highest compressive strength at all levels of cement stabilization (0% to 20%). Undoubtedly, earth was the first building material used by man.

Bahar and Benazzoug[2] has studied the effect of chemical stabilizers and their combinations on the durability of a clay or sand was investigated ; The results showed that the improvement of the durability of the earth material can be done by a treatment based on cement and lime, which allows to obtain interesting properties on sands and clays. The durability is considerably improved by the mixed treatment.

A study of the adhesion of compressed earth masonry elements was carried out by Walker and al. [3]. The blocks were made of reconstituted earth stabilised with cement. The blocks were compacted using a manual press. Two mortar formulations were used: cement/lime/sand and earth/cement. The results revealed the formation of etringite in the interface in the presence of water, which influences the mechanical behaviour of the masonry. The higher the clay content, the higher the water content of the blocks needed to achieve higher bond strength. The results showed a low bond strength of the earth mortars, while increasing the clay content caused the bond strength to drop considerably. For the tests carried out by Walker [4], Cement does not play a major role in consistency measurements either. As far as workability is concerned, a mortar with cement is more workable, but the clay content of the soil must be taken into account. If the clay contains less than 12% colloids, workability is guaranteed.

Within the framework of this work, a certain number of tests related to durability (drying wetting tests, erosion, natural aging). These tests would offer the possibility to

appreciate the resistance of the blocks towards water and help to optimize the choice for a better quality of blocks.

Materials and Methods

1.1 Materials

1.1.1 Sediments

The material used as raw material for the elaboration of the blocks is the sediments of the Koudiat- Acerdoune dam in the Bouira region (fig. 1).

Figure 1: dam of Koudiat-Acerdoune.

The chemical analysis of sediments FRX represent 57.91% SiO_2, 8.81% Al_2O_3, 11.91% CaO,0.52% TiO_2, 4.40% Fe_2O_3, 0.88% MgO, 0.51% Na_2O and 0.86% K_2O.
The particle size distribution (the relative content of clay, sand and gravel) of the sediment (fig.2) was obtained according to the standards NF P94-057[5] and NF P94-056[6] .
It is mainly composed of sand (37%) particles, with 13.63% of fine particles, which reveal that the sediment corresponds to a sandy lime soil.

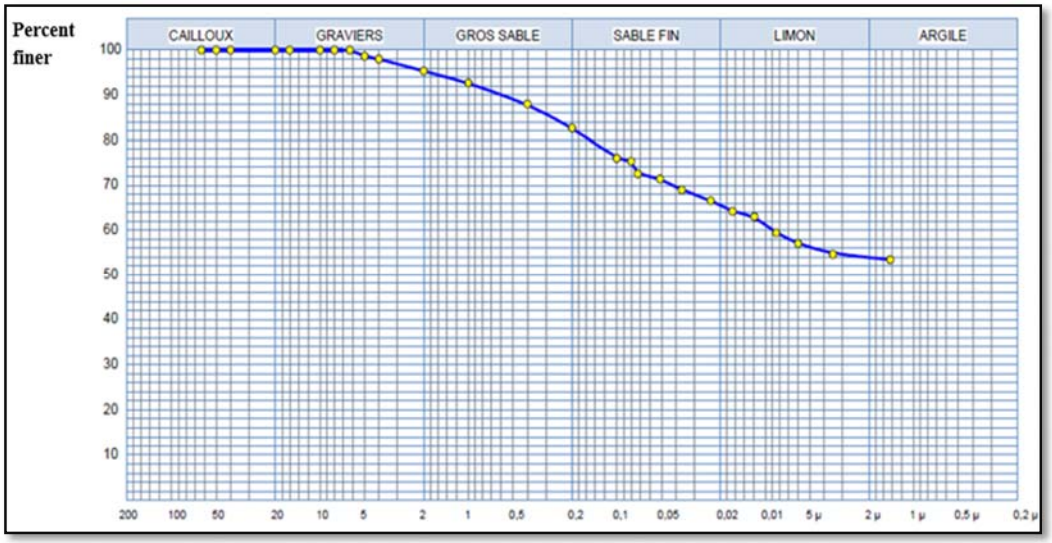

Figure 2: Grain size distribution of the tested sediment.

The Atterberg limit determined according to NF P94-051[7], the sediment represents 36.49% of liquid limit, plastic limit of 23.58% and plasticity index of 12.42 %.

According to the classification according to GTR 1992 [8], we can classify the sediments in the soil type A_2.

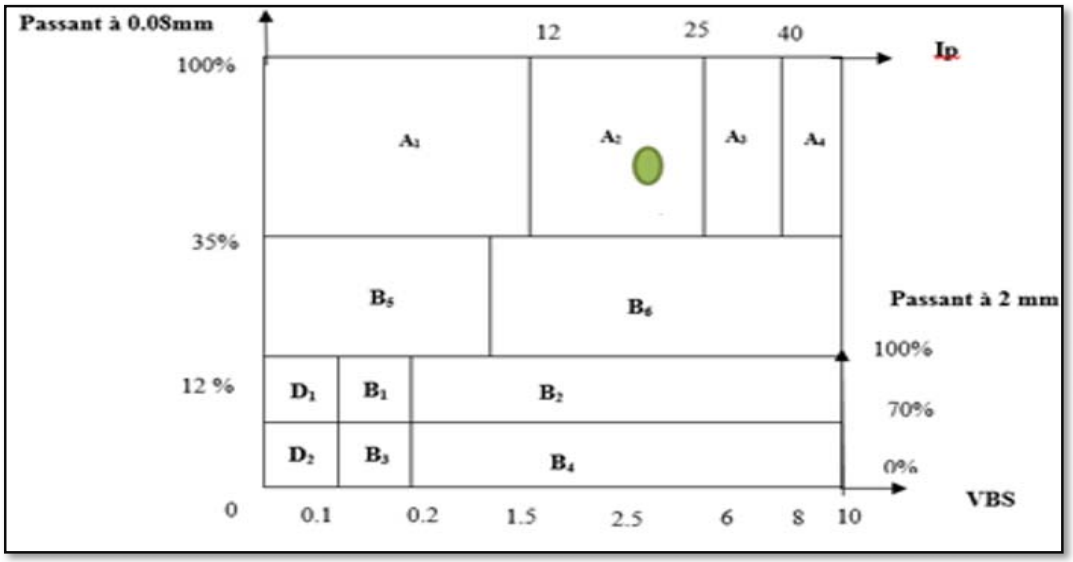

Figure 3: Sediment classification according to GTR 1992.

1.1.2 Cement and lime

In this work, we used a compound Portland cement. The type of cement is a CEM II of strength class 42.5 R according to EN 197-1 (2001).

Figure 4 represents the particle size curve by laser of cement used. The curve shows that the volume of particles with a diameter of less than 10 µm is the range of 50 %, the volume of particles is a little larger for cement, and the large diameters have a dimension more than 50µm.

The type of lime is to be used in principle; the preference is never the less given to the air lime of Ghardaia, figure 5 represents the granulometric curve by laser of the lime used.

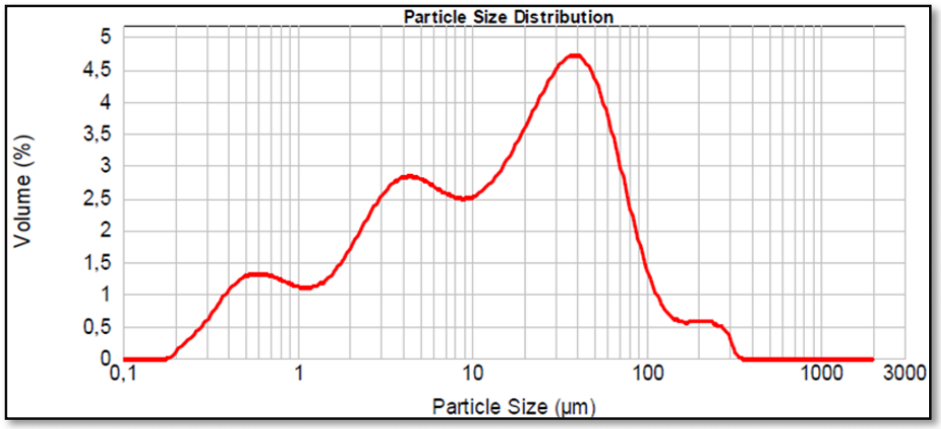

Figure 4: Particle size analysis of cement.

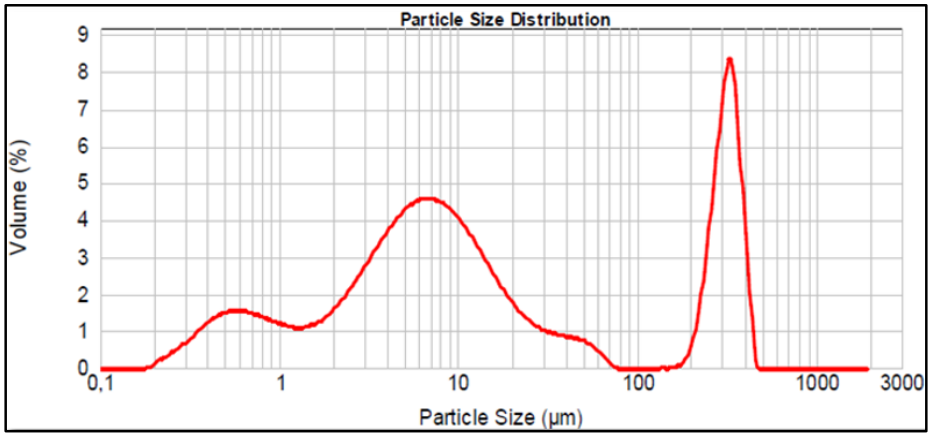

Figure 5: Particle size analysis of lime.

1.2 Experimental methods

1.2.1 Preparation of specimens

The preparation of specimens accordance with NF P94-093 standard [9]; and local recommendations[10]. The compaction of the blocks stabilize with the cement and the lime were achieved by using a hydraulic semi-automatic press with of length is 295 mm, the width is 140 mm and 90 mm of height. The different treatments were carried out according to the different contents and variants:

1. Blocks with: 6%; 8%; 10% and 15% cement
2. Blocks with: 5%; 8% and 10% lime.

The stabilized blocks have undergone various laboratory tests such as flexural strength; wetting and drying test; durability tests.

A. Flexural strength

Flexural strength test is carried out in accordance with NF P18-407[6] (fig .6), with a semi-hydraulic pressure and a compaction of 7MPa.

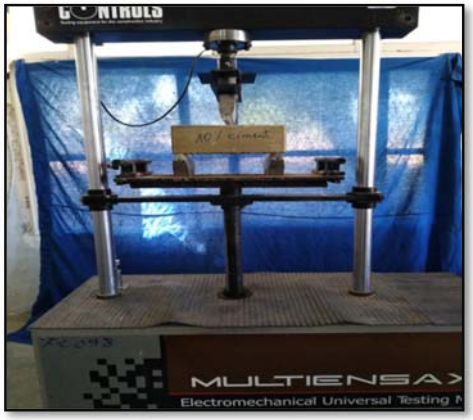

Figure 6: flexural strength test.

B. Shrinkage

The drying shrinkage (fig.7) test of the blocks [11], according to the following procedure:

- Weigh the blocks sealed on each block with an epoxy resin two measuring pads L_1.
- Place the blocks in the oven at a temperature of not less than 33 °C and not more than 45 °C).

- Dry the blocks to constant mass, the mass is considered constant when two successive weighing carried out at 24 h intervals show a decrease in mass < 0.1percentage of the initial mass.
- After drying, remove the blocks from the oven and place them in the laboratory;
- After 6 hours of stabilization, measure the distance between blocks: L_2.
- The shrinkage is calculated according to the following formula (1):

$$R = \frac{L1-L2}{L2} X\ 100 \qquad (1).$$

Figure 7: Shrinkage test.

C. Wetting and drying test

This test is carried out according to the ASTM D 559-57 [12]; it consists of immersing the blocs stabilize of cement end the lime in water for a period of 5 hours and then removed to be dried in an oven at 71 °C for a period of 42 h. This operation is repeated six times[13].

D. Durability test

For the realization of the test, we used only stabilized blocks with a dosage of 8% cement and blocks with a dosage of 10% lime.

For this, we proceeded to the exposure of two walls in real climatic conditions for 22 months (fig .8).The area of exposure is in the southwest of Algiers (Algeria). The average humidity is about 70%. During the exhibition, the extreme temperatures vary between 38.6 °C and 6.3 °C, recorded respectively in July and January. The built walls are visited periodically and visual inspections have been scheduled every 3 months.

Figure 8: Walls built and exposed - February 2019.

2 Results and discussion

2.1 Flexural strength

From figure 9, it can be seen that the flexural strength increases with increasing binder dosage (cement and lime). This increase is mainly due to the good resistance offered by the binder. Blocks stabilized with cement showed higher strengths than those stabilized with lime.

Overall, it can be observed that the values of the mechanical tensile strength of the blocks are greater than 1MPa. However, it can be seen that the value of the mechanical tensile strength of blocks with 15% cement at 2.80MPa is the highest compared to other formulations. Although the value of mechanical tensile strength with 5% lime at 1.25MPa is the lowest.

We can note an improvement of the mechanical resistance to traction respectively of 1.40, 1.75, 2.50 and 2.80MPa for dosages of cement of 6, 8, 10 and 15% compared to the studies of Ngouama[14] and Barro[15], and significantly in conformity with the standard decreed by CRA-terre[16].

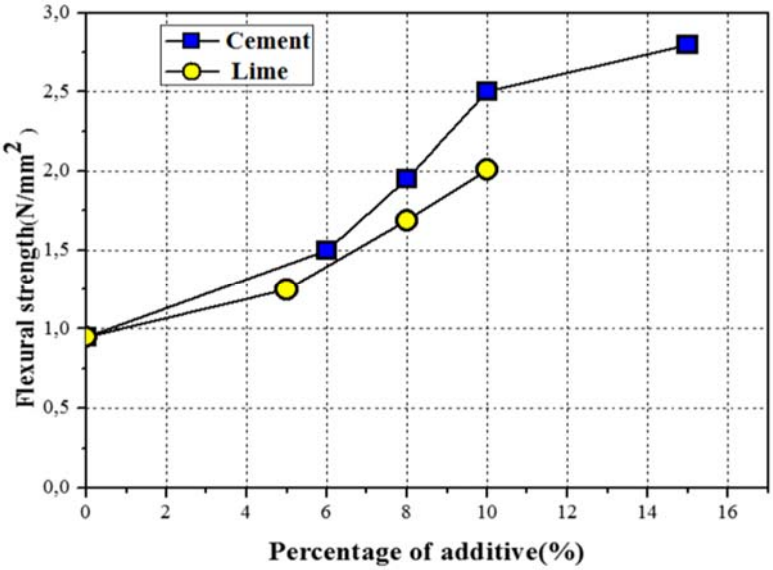

Figure 9: Flexural strength of elaborated blocks.

The strength increases significantly for 5% to 10% of lime with 1.25 MPa and 1.89 MPa respectively, this growth in strength is due to the increase in the potential of exchangeable calcium cations provided by the lime, there is an improvement of up to 10% compared to O.Izemmouren [17], which found 1.39 MPa of mechanical strength to the traction for a dosage of 10% lime.

2.2 Shrinkage

The results of block shrinkage versus additive content are shown in figure 10. The results show that the shrinkage decreases with the increase of the percentage of additives.

The blocks stabilized by cement show less shrinkage compared to the blocks stabilized by lime, because of the hydration phase of cement.

We can note an improvement of shrinkage with values of 0.71, 0.59, 0.42, and 0.33 mm/m for cement dosages 6, 8, 10 and 15% and 0.81, 0.75 and 0.61 mm/m for lime dosages. According to the technical performances of earth blocks stabilized in CRATERRE-EAG[16], the results are acceptable.

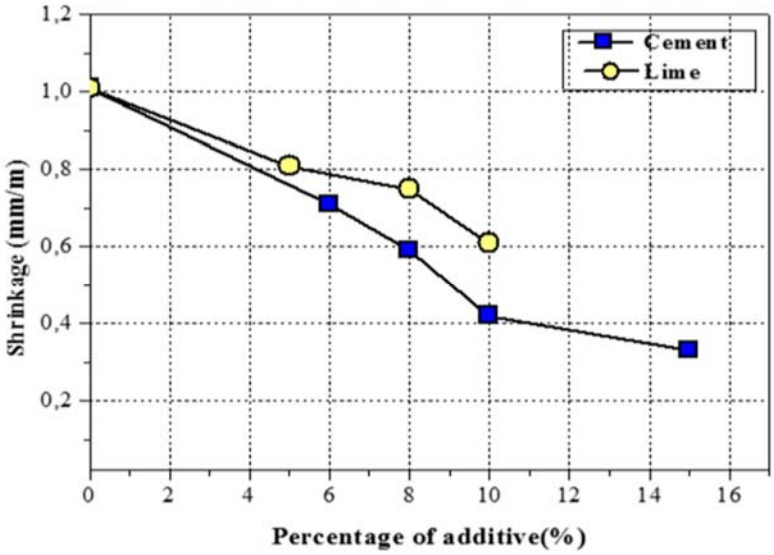

Figure 10: Shrinkage of elaborated blocks.

2.3 Wetting and drying test

Figure 11 shows the state of block stabilized with 10% cement and 5% lime after 6 cycles. The wetting/drying test appears to be very severe. The corners of the blocs are the main defects, for the bloc reinforce with 10% cement the surface weathering, including pitting and chipped edges for the bloc reinforce with 5% lime. This test could be adapted to estimate the water resistance of stabilized blocks by reducing the number of cycles.

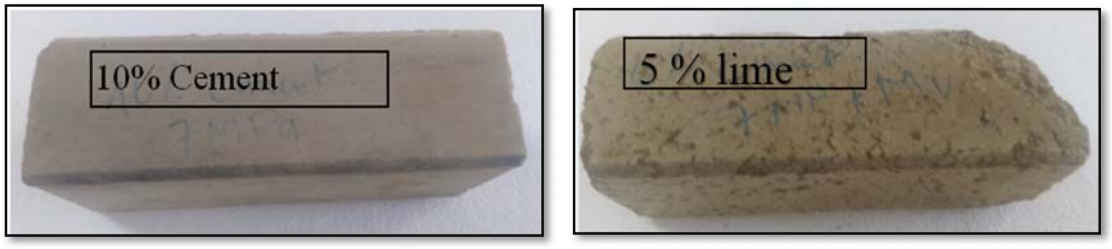

Figure 11: Wetting and drying test.

Figures 12 and 13 show that the weight losses after six wet-dry cycles do not exceed 5%.The weight loss decreases when increasing the dosage of bender.

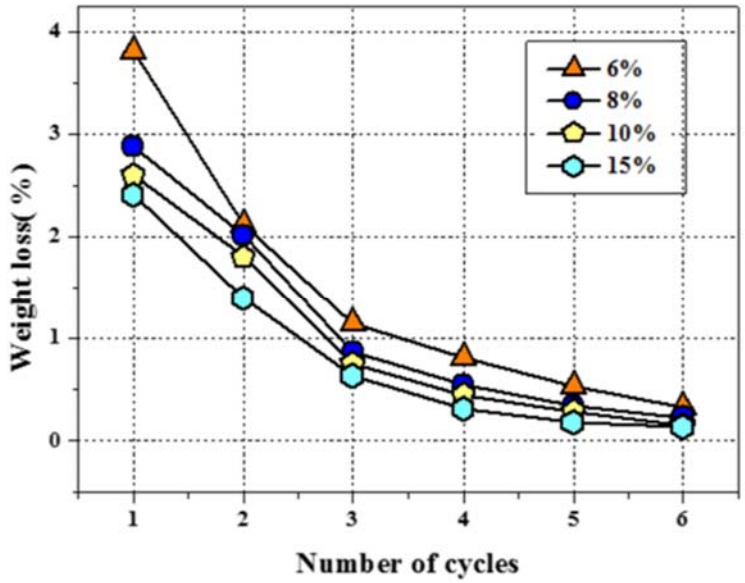

Figure 12: The weight loss for blocks stabilized by cement.

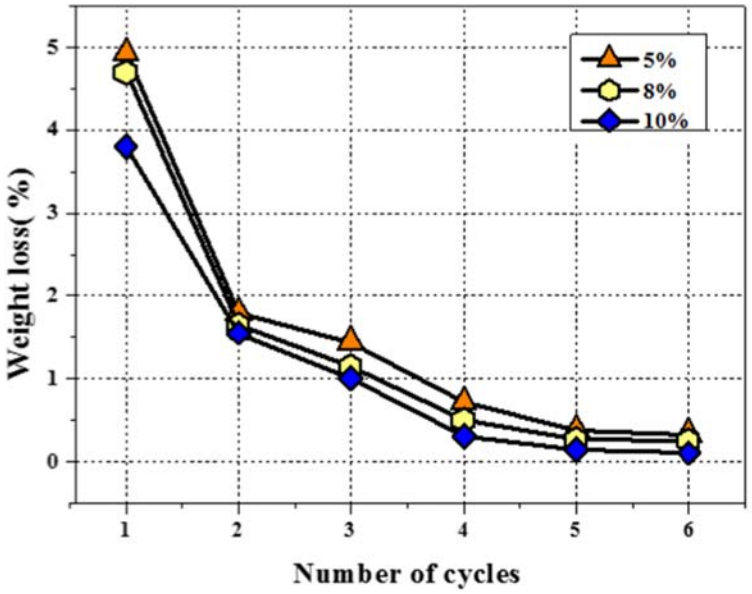

Figure 13: The weight loss for blocks stabilized by lime.

Lime stabilization only interacts with the clay phases. The proportion of minerals representing the clay phases (Kaolinite + Illite) is lower than 15%. Blocks treated with 15%, cement and 10% lime are also affected by an irrecoverable loss of mass, with

respectively a maximum cumulative weight loss of 2.41% and 3.8%. This finding confirms the conclusions of Guettala [9].

2.4 Durability test

The changes included surface roughness, surface pitting, cracking and loss of mass. The survey of the wall shows about that the defects included surface wearing away and cracking (fig.14). The location of the cracking is mostly in the middle parts of amounts of the blocks and the wearing away mostly involves the corners. Differential wearing away appears at the front of these walls; this points that the change does not continue at the same rate from one area of the block to another. Guettela [13] confirmed this after exposing walls with blocks with 10% lime for 48 months..

Figure 14: Wall condition stabilized by 10% lime (November 2020).

Figure 15: Wall condition stabilized with 8% cement (November 2020).

After 22 months, the wall built with blocks stabilize with 8% cement shows no signs of wearing away, but a small piece of block disappears from the first line (fig.15). On the other hand, the earth blocks with 10% lime showed an indication of group of flowers was noted. The upper surface of the wall built with blocks containing 8% cement shows no signs of worsening or rusting and crumbling, but a small surface roughness.

He also stated the importance of the hit/effect of limits, guidelines such as drop size, drop size distribution [18].

3 Conclusion

The present work deals with the valorization and recycling of sediments of the Koudiat Acerdoune dam in the field of construction. The experimental campaign was undertaken to evaluate the mechanical strength, water resistance and durability of cement and lime blocks.

However many conclusions can be drawn:

- The strength increases significantly as the cement content increases.
- An increase in the strength is recorded for the stabilized blocks compacted with an effort of 7MPa. This improvement up to 2.80MPa and 1.89MPa for the blocks stabilized with 15% cement and 10% lime, respectively, compared to the reference blocks.
- The stabilization of the blocks made by sediment improves considerably the durability of the walls.
- The results of durability test show that walls built by blocks stabilized with cement and lime blocks show negligible degradation after exposure to real climatic conditions for several months.

Through this experimental study and according to the geotechnical, chemical descriptions, the recycling of the sediment from dams can reduce can reduce the environmental impact.

4 References

1. Bahar and al, *Performance of compacted cement-stabilised soil,Cement concrete composites vol 26(7) pp 811-820,.* Cement concrete composite 2004.
2. Benazzoug M .Bahar. R, D.d.m.t.s., Séminaire internationale, Innovation et Valorisation en Génie Civil INVACO2. Rabat, Maroc. Novembre 2011. .
3. P. Walker. Bond characteristic of earth block masonry. Materials and Civil Enginnering, p.-., 1999.
4. P. Walker and T. Stace. Properties of some cement stabilised compressed earth blocks and mortars. Materials and Structures, p.-.
5. AFNOR, *Association Française de Normalisation, Analyse granulométrique des sols, Méthode par sédimentation 1992,NF P94-057,.*
6. AFNOR, *Association Française de Normalisation, Analyse granulométrique des sols, Méthode par tamisage 1996, NF P94-056,.*
7. AFNOR *Association Française de Normalisation, détermination des limites d'Atterberg 1993, NF P94-051,.*
8. *GTR. Guide technique pour la réalisation des remblais et des couches de forme. Editions du SETRA-LCPC, Fascicules I & II, 2000, 98. .*
9. AFNOR, S.r.e.e.-D.d.r.d.c.d.u.m.-E.P.N.-E.p.M., NF P 94-093.
10. CNERIB, R.p.l.p.e.m.e.œ.d.b.d.t.s., CNERIB, Algiers,Algeria (1993), 33.
11. AFNOR, *Compressed earth blocks for walls and partitions: definitions - specifications - test methods - delivery acceptance conditions, Saint-Denis La Plaine Cedex:Association française de Normalisation, (2001),XP P13-901,.*
12. American Society for Testing and Materials, A.B.o.A.S., vol. 04.01, Philadelphia, 1993.
13. Guettala, *Durability study of stabilized earth concrete under both laboratory and climatic conditions exposure.* Construction and Building Materials, (2006). **20**(3): p. 119-127.
14. *Ngouama. « Contribution à l'optimisation des briques en terre stabilisées au gel de farine de manioc ». Mémoire d'ingénieur génie civil, Université Marien N'Gouabi, Congo (Brazzaville), 2008.*
15. *Barro. « Étude de l'influence de l'introduction des fibres, graines de coton et résidus dans la stabilisation des sols ». 2iE-2008/2009, Burkina Faso, 2009. documentation.2ieedu.org, consulté le 27/04/2015.*
16. *CRAterre, Guide sur les blocs de terre comprimée : Normes, série N°11. 1998.*
17. IZEMMOUREN and al, *Effet des conditions de cure sur les propriétés physiques et mécaniques des blocs de terre comprimée.* 21ème Congrès Français de Mécanique, 26 au 30 août 2013, Bordeaux, France (FR), 2013.
18. *Kerali AG. Durability of Compressed and Cement-Stabilised Building Blocks. Ph.D. Thesis, Development Technology Unit, Warwick University, 2001.*

The impact of shallow geothermal HVAC systems with heat pump units on the ground and ground water

Impactul sistemelor HVAC geotermale de mică adâncime cu pompe de căldură asupra apei subterane și solului

Răzvan –Silviu Ștefan[1], Daniel Cornea[2]

[1]Engineer- Technical Facility Coordinator ELI-NP, Bucharest, Romania
razvan.stefan@eli-np.ro

[2] Technical University from Bucharest, Romania
danielcornea@hidraulica.utcb.ro

DOI: 10.37789/rjce.2024.15.3.10

ABSTRACT. The paper presents the study conducted to determine the impact of HVAC geothermal systems with heat pumps units on the ground and groundwater. Due its very complexity the HVAC geothermal system with heat pumps units that equips the ELI-NP research infrastructure could be a suitable tool to determining the long-term impact of shallow geothermal systems on the environment. The system has been continuously operating and monitored for 5 years.

Key words: HVAC, heat pumps

Current state of knowledge of the soil and groundwater impact of surface geothermal IVC systems

Geothermal HVAC systems with heat pumps units are now being widely utilized.

Advantages such as very low energy consumption and CO_2 emissions, low maintenance requirements make their use very attractive.

Since the large-scale use of geothermal HVAC systems, especially the high-capacity ones, is of recent date, not many studies and simulations have been carried out regarding their operation.

The thermal transfer between the HVAC System could have an impact on the ground and groundwater in the long run.

In the long run, both the ground and groundwater could be affected by the thermal transfer between the HVAC system and the ground.

Simulations and studies both regarding the evaluation of the thermal loads introduced by the HVAC systems and the long-term response of the ground to the action of these loads, are of particular importance for the determination and evaluation of the possible consequences on the ground and groundwater.

The geothermal HVAC system that equips the ELI-NP research infrastructure has a thermal capacity of 6.2 MW and is made of 1070 geothermal boreholes, each having depth of 120 m. It covers an area of 27,000 m2, the boreholes being grouped within 18 plots (60 boreholes on each plot).

The geothermal HVAC system currently operating at ELI-NP research infrastructure is a suitable tool for determining long-term environmental impacts as well as performing other operational simulations, given its complexity.

The system allows to working out of physical and mathematical models and various simulations with results that contribute to the development of the field.

Hydrogeological monitoring of the geothermal HVAC system built and in operation at ELI-NP

As far as concerning the geothermal HVAC operating at the ELI-NP research infrastructure, monitoring the impact on ground and groundwater is a requirement imposed by the authorities, through the water rights permit.

An important consequence of this fact is that it will be possible to carry out studies and simulations useful for making predictions and forecasts for the behavior of similar systems, in order to evaluate the impact of the systems on the environment, their continuous innovation and optimization.

In order to monitor the hydrogeological geothermal HVAC system in operation at ELI-NP, a hydrogeological monitoring solution was designed and built, as a first step. The monitoring station consists of 8 monitoring boreholes (4 new boreholes and 4 existing boreholes part of a pilot station installed during the execution of the HVAC system).

The design process of the hydrogeological monitoring station was based on the following considerations, models and methods:

- The hydrogeological monitoring station has to capture the impact of the HVAC system on the aquifers in the studied area in terms of quality and quantity.
- The hydrogeological monitoring station has to respond to the need for time tracking of the impact of the HVAC system on the aquifers observed for the entire period of its operation.
- The hydrogeological monitoring station has to be operational at the commissioning of the HVAC system.
- The hydrogeological monitoring station has to comply with the existing regulations and framework (national or European). Currently, the only comparable category that frames the geothermal HVAC system is the waste pits.
- The hydrogeological monitoring station has to take into account the flow directions for each of the previously mentioned aquifers, positioning the boreholes along the main flow direction.
- The hydrogeological monitoring station has to take into account the most unfavorable situation of the thermal impact on the aquifers and be able, in case of hydro-geo-chemical changes, to respond in a timely manner.
- The location of the boreholes within the hydrogeological monitoring station takes into account the direction of groundwater flow for the four aquifers and the possible impact of heat transfer over time.
- Placement of at least two monitoring boreholes, one borehole located upstream of the HVAC system and one borehole downstream of the HVAC system, in the direction of flow.

As a second step, after the construction of the monitoring station, hydrogeological parameters have been permanently recorded aiming the quantitative and qualitative identification of the impact on the ground and groundwater.

Description of the hydrogeological monitoring station that was carried out at ELI-NP

The monitored aquifers are Colentina, Mostiștea and Frătești (A and B). The location of the boreholes within the station related to each of the aquifers (see figure 1) is specified in the project (Stereographic 70).

The monitoring station consists of 8 monitoring boreholes (4 new boreholes and 4 existing boreholes part of a pilot station installed during the execution of the HVAC system).

There are two types of boreholes:

- Monitoring boreholes located upstream in the direction of groundwater flow, which are not influenced by the thermal impact of the IVC system (F0C1, F0M1, F0A1, F0B1)
- Monitoring boreholes located downstream in the direction of groundwater flow, which aim to capture the thermal impact due to the operation of the IVC system (F1C, F1M, F1A, F1B)

The placement of boreholes took into account considerations such as those briefly listed above, criteria listed in Table 2.

Table 1 Depth of installed boreholes

No.	BOREHOLE CODE	Aquifer	Design Depth (m)	Data aquisition system position/ depth (m)
1	F0C1	Colentina	18	10
2	F1C1	Colentina	20	10
3	F01M	Mostistea	50	35
4	F1M	Mostistea	50	35
5	F0A1	Fratesti A	90	75
6	F1A	Fratesti A	90	75
7	F0B1	Fratesti B	125	105
8	F1B1	Fratesti B	125	105

Table 2 Criteria. Basis of the hydrogeological monitoring station design

CRITERIA	RESULT
Geological and hydrological model	Aquifers monitoring: Colentina, Mostiștea, Frătești A, Frătești B
Water flow model	The flow directions for each of the aquifers, positioning the boreholes along the main flow direction.
Legislation criterium	Placement of at least two monitoring boreholes, one borehole located upstream of the HVAC system and one borehole downstream of the HVAC system, in the direction of flow.
Thermal transfer model	The position of the boreholes towards the HVAC System

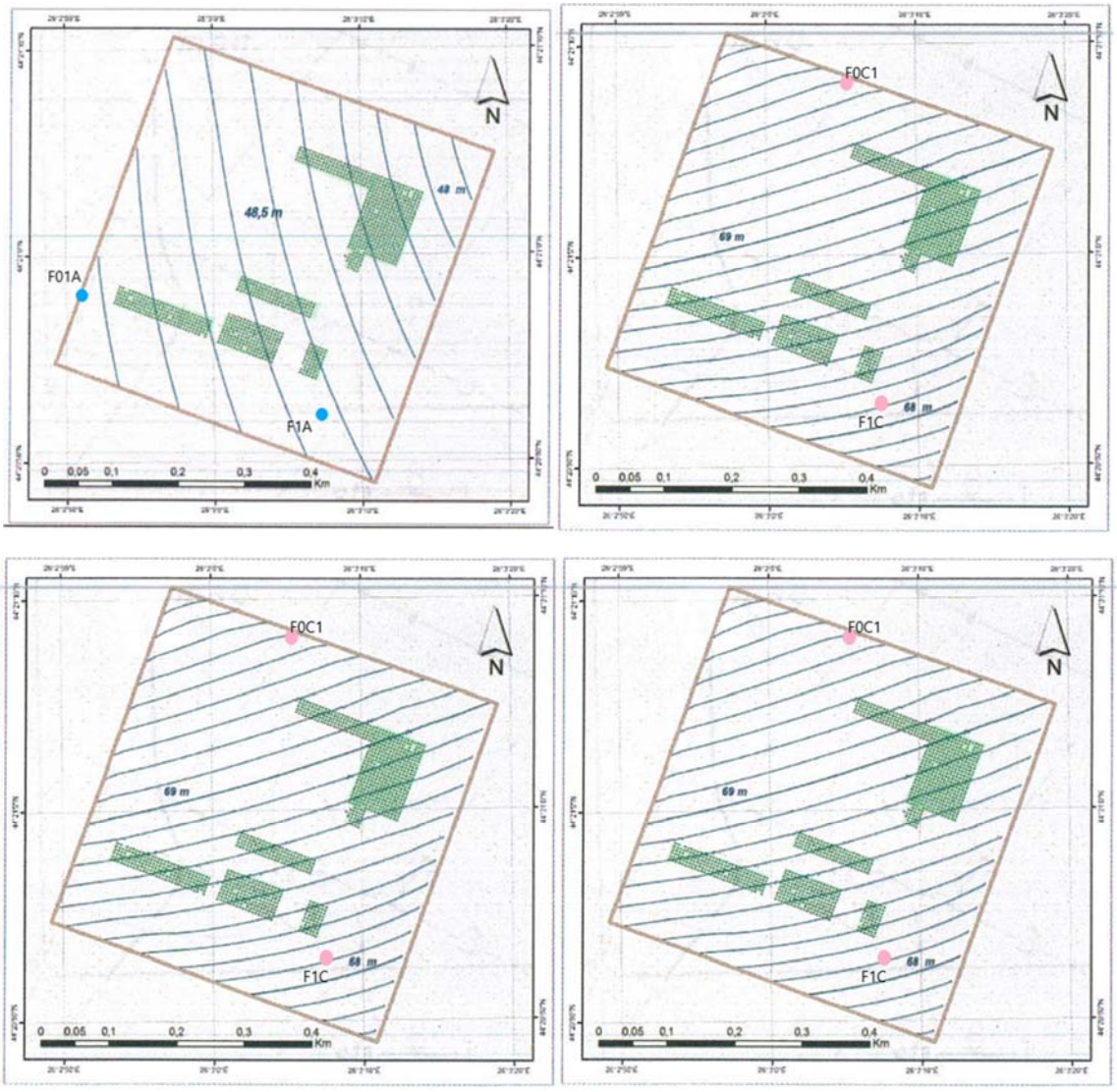

Monitored hydrogeological parameters

The design criteria of the monitoring solution are based on the created models. Thus, through the classic numerical modeling procedure of heat transfer or the transport of miscible compounds, in an aquifer layer, a conceptual model has been created in a first stage. Based on the created conceptula model the numerical hydrodynamic model and thermal transfer model have been developed. The hydrodinamic model considers a rectangular shape of 12 km x 12 km that includes the Colentina, Mostiștea, Frătești A and Frătești B aquifers.

Then the thermal modeling of the behavior of the HVAC system has been performed. A geological model of the area has been also created, as the basis for defining the geometry of the hydrodynamic model.

The thermal transfer model was made for the four aquifers, the estimated effect being for 200, 400, 600, 800, 1600 and 4000 days. One-way operation was considered (heat loss from the HVAC system to the environment), this scenario representing the worst situation for the aquifer environment.

Within the monitoring station, two sets of hydrogeological parameters were measured and collected to monitor the impact of the geothermal HVAC system:

- physical parameters - piezometric levels, temperature
- hydro-geo-chemical and microbiological parameters

The frequency of parameter monitoring, the water sampling program and their analysis are presented in table 3.

The reference values, of the quality indicators of the groundwater was set before the commissioning of the facility, through determinations made by approved laboratories on the samples taken from the monitoring boreholes located upstream in the direction of the flow of the underground water in relation to the objective. The monitoring of physical parameters is performed automatically through the data acquisition units, programmed to ensure the consistency of the recorded data (Table 4).

Tabel 1 Hydrogeological parameters monitoring program

		Physical parameters	**Bio-chemical parameters**
AQUIFER	**Colentina**	Y	Y
	Mostiștea	Y	Y
	Frătești A	Y	Y
	Frătești B	Y	Y
Frequency		Performed automaticaly on daily basis	Water samples to be taken on semester basis In spring (april-may) In autumn (september, october))

Tabel 2 Data aquisition units specifications

		preasure			**temperature**		
		Range	**Accuracy**	**Resolution**	**Range**	**Accuracy**	**Resolution**
AQUIFER	**Colentina**	0 – 10 mH_20	±1.0 cmH_20	0.2 cmH_20	0 - 50 °C	±0.1 °C	0.01 °C
	Mostiștea	0 – 20 mH_20	±2.0 cmH_20	0.4 cmH_20			
	Frătești A	0 – 100 mH_20	±5.0 cmH_20	2.0 cmH_20			
	Frătești B	0 – 100 mH_20	±5.0 cmH_20	2.0 cmH_20			

Results obtained from hydrogeological monitoring

The heat transfer models will be refined and calibrated based on real data and considering the operation in both directions (yielding or receiving heat from the HVAC system in the environment). The literature it specifies that the alternation of the two operation regimes will lead to a cancellation of the thermal effects, as well as to a reduction of their impact on the aquifer environment.

The HVAC system and the hydrogeological monitoring station are in their 5th year of operation. By means of the statistics and monitoring, data are available to highlight the real behavior of the system by comparison with the predictions made based on the physical model. Data acquired from hydrogeological monitoring for each of the aquifers are summarized in the graphs and tables below.

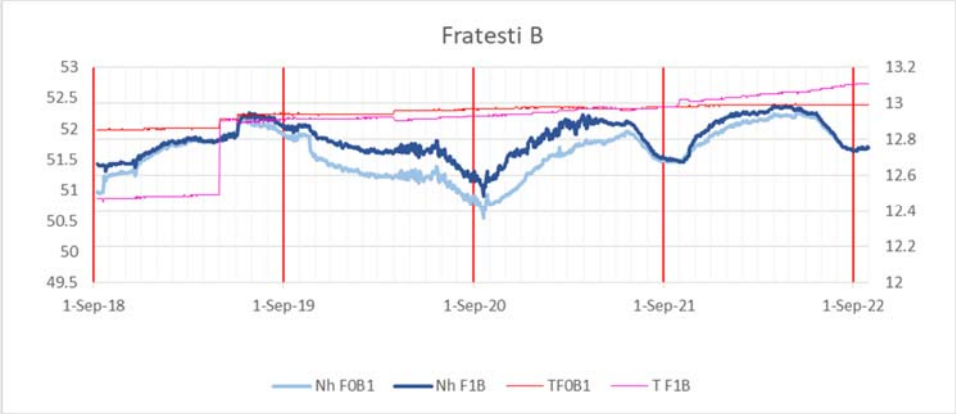

Aquifer Fratesti B				
Borehole	F0B1		F1B	
Date	*Nh*	*T*	*Nh*	*T*
	(mdMN)	*(Celsius)*	*(mdMN)*	*(Celsius)*
62Xju26=	:6	673=:	:639;	6739<
1-Sep-19	51.93	12.94	52.05	12.91
1-Sep-20	50.91	12.97	51.31	12.93
1-Sep-21	51.5	12.98	51.54	12.98
1-Sep-22	51.64	12.99	51.64	13.1

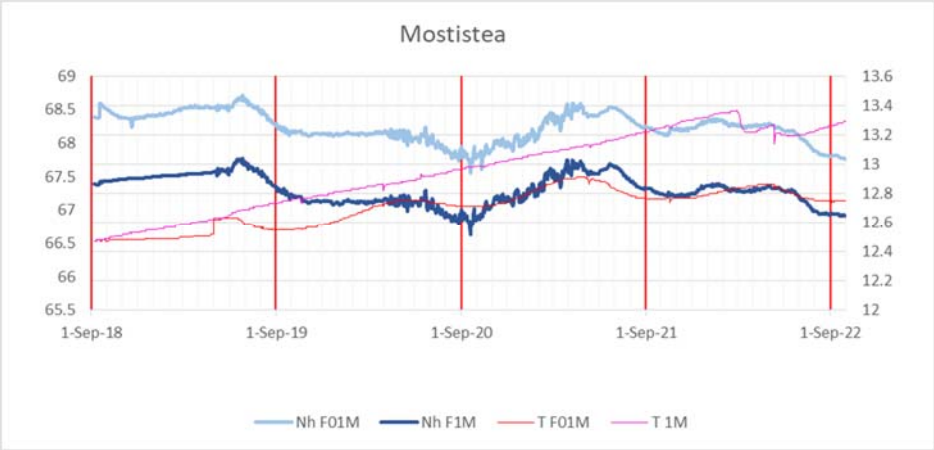

Aquifer Mostistea				
Borehole	F0M1		FM1	
Date	*Nh*	*T*	*Nh*	*T*
	(mdMN)	*(Celsius)*	*(mdMN)*	*(Celsius)*
62Xju26=	;=399	6739<	;<398	6739<
1-Sep-19	68.29	12.55	67.35	12.73
1-Sep-20	67.93	12.71	67	12.97
1-Sep-21	68.25	12.76	67.34	13.22
1-Sep-22	67.8	12.75	66.94	13.26

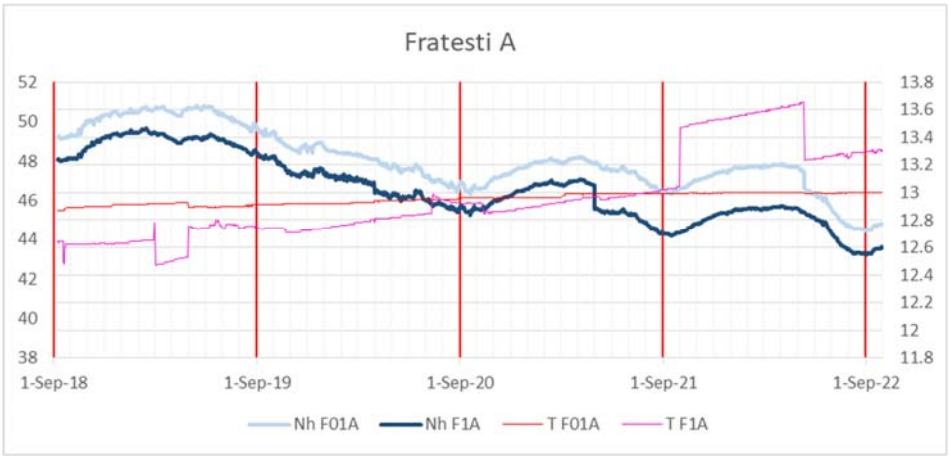

Acquifer Fratesti A				
Borehole	F0A1		F1A	
Date	*Nh*	*T*	*Nh*	*T*
	(mdMN)	*(Celsius)*	*(mdMN)*	*(Celsius)*
62Xju26=	9>36>	673=<	9=35:	673;9
1-Sep-19	49.64	12.91	48.4	12.74
1-Sep-20	46.94	12.96	45.73	12.92
1-Sep-21	46.49	12.99	44.34	13.02
1-Sep-22	44.49	13	43.25	13.3

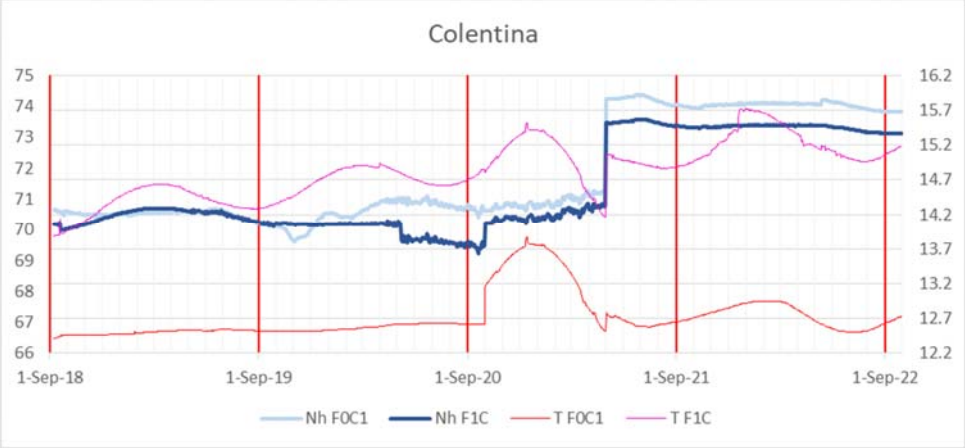

Aquifer Colentina				
Borehole	F0C1		F1C	
Date	*Nh*	*T*	*Nh*	*T*
	(mdMN)	*(Celsius)*	*(mdMN)*	*(Celsius)*
62Xju26=	<53;:	6739	<5377	683==
1-Sep-19	70.24	12.52	70.25	14.29
1-Sep-20	70.82	12.62	69.61	14.73
1-Sep-21	74.05	12.65	73.38	14.89
1-Sep-22	73.83	12.63	73.12	15.05

Solutions for the energy efficiency of buildings located near watercourses through SRE integration. Case Study

Soluții pentru eficiența energetică a clădirilor situate în apropierea cursurilor de apă prin integrarea SRE. Studiu de caz

Daniel Muntean[1], Dănuț Tokar[1], Adriana Tokar[1], Daniel Bisorca[1], Alexandru Dorca[1]

[1]Universitatea Politehnica Timișoara,
Victoriei Square, Nr.2, Timisoara, Romania
E-mail: daniel-beniamin.muntean@upt.ro, danut.tokar@upt.ro, adriana.tokar@upt.ro, daniel.bisorca@upt.ro, alexandru.dorca@upt.ro

DOI: 10.37789/rjce.2024.15.3.11

Abstract. *Currently, approximately 40% of the energy demand in the European Union (EU) is used in buildings and the energy demand for cooling and heating is increasing every year, so the energy efficiency of buildings represents a problem of increased interest and of extreme relevance. The article proposes, through the case study, the installation of a photovoltaic system for the production of electricity on the roofs of the buildings and the cooling and heating of the building using a water-to-water heat pump. Having the advantage of the location of the studied buildings on the banks of the river Bega in the town of Timisoara, the case study proposes the cooling of the spaces in the buildings in two variants, namely in the spring and autumn when the outside temperature is not very high using the river water directly ("free cooling"), and in the summer for the hot months, a water-to-water heat pump to cool the cooling agent to the parameters necessary to achieve a proper air conditioning.*

Key words: *free cooling, water-water heat pump, photovoltaic system, SRE*

1. Introduction

Currently, approximately 40% of the energy demand in the European Union (EU) is used in buildings, of which 80% is the energy required for thermal needs (heating and water preparation in the building), and the energy demand for cooling is increasing every year. Regardless of its form, energy is an indispensable resource for contemporary life. Considering the increase in the requirements related to the energy economy through the sustainable use of human resources, the energy efficiency of buildings represents a problem of increased interest and of extreme relevance [1].

Of the total electricity consumed by a building, in 2018, 18.5% was used to ensure the cooling of the interior spaces, and it is expected that by 2050 this

consumption will triple, due to the increase in the number of air conditioning devices used. Consequently, an efficiency of the air conditioning systems is required in order to reduce the energy consumption and still maintain the cooling parameters required to achieve the comfort of the occupants [2,3].

The integration of renewable energy sources (RES) is no longer a fad but a necessity to reduce the carbon footprint and energy consumption. A safe and sustainable source of energy is the solar one, which together with the modernization of the installations inside the buildings, can contribute both to the implementation of the measures taken by the EU and to the reduction of greenhouse gas emissions and to the prevention of dangerous climate changes [4].

Free cooling is an economic and ecological alternative to the production of cold, successfully used in many countries around the world for cooling data centers. Considering that less mechanical energy is used, the use of harmful refrigerants and fossil fuels that are responsible for keeping the systems in operation is reduced. In order to create a free water cooling system, we have as the first condition to have a water source near the objective, such as sea, river or fountain water [5].

In spring and autumn, when the temperatures inside the buildings are not very high, the cooling requirement being low compared to the summer months, in the situation where there is a cold source of water nearby, this potential can be used directly without involving a other equipment to achieve cooling using electricity. In the functional diagram from Fig. 1 presents the technical solution of free cooling by bypassing the Chiller. The production of electricity often involves air pollution, so the realization of this bypass leads to the reduction of electricity consumption and implicitly to the reduction of greenhouse gases [5].

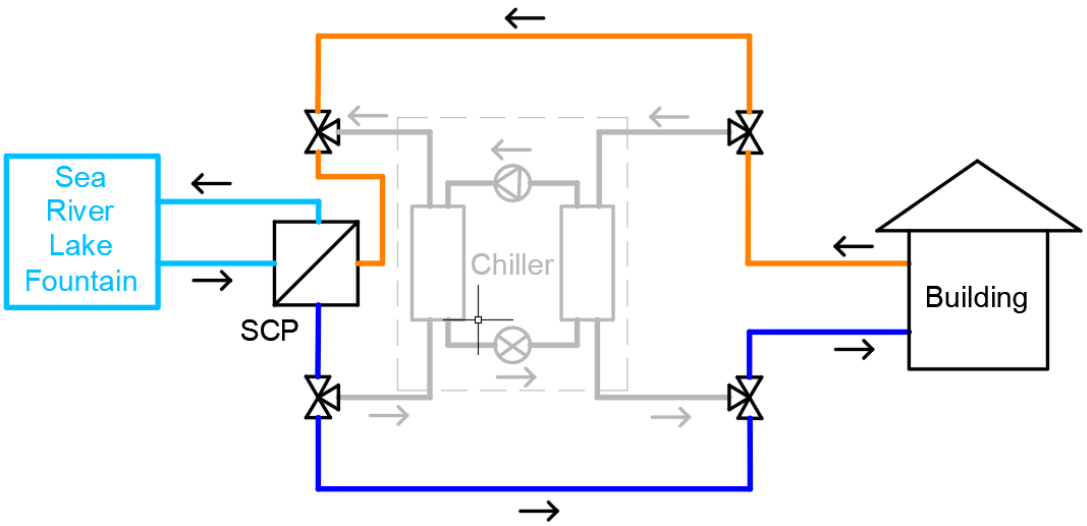

Fig. 1. Operation of the cooling system during spring and autumn

During the summer, when the air temperature in the buildings increases considerably, simultaneously with the increase in the water temperature from the available source, the proper air conditioning in the building spaces can no longer be

achieved by the "free cooling" method, so the installation is switched to version with Chiller (Fig. 2) [5].

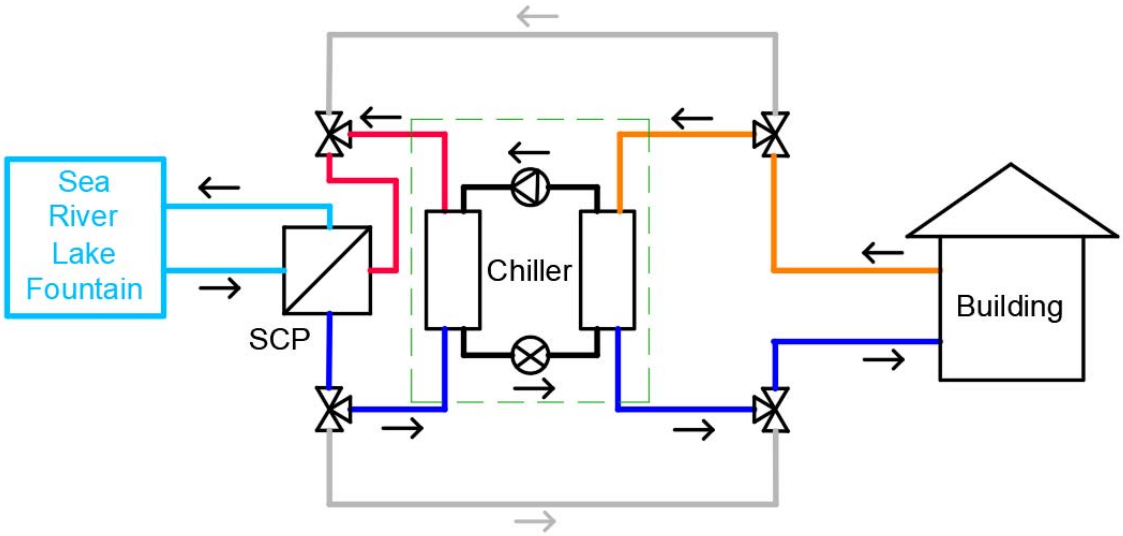

Fig. 1. Operation of the cooling system during the summer

2. Case Study

To carry out the simulations, the simulation programs Polysun SPTX Constructor [6] were used, a comparative study was carried out regarding the performance of the building's heating system, between the current situation and the proposed modernization solution.

The study was carried out on 3 buildings located on the banks of the Bega river that crosses the town of Timisoara (Fig. 3). Building 1 has a maximum height of 5 m, terrace-type roof with a covering made of sandwich panels, Building 2 has a maximum height of 11.5 m, a roof made in 4 pitches with a galvanized sheet covering, and Building 3 has a maximum height of 15 m with a cover made of tiles.

At the moment, the studied buildings are not provided with a centralized air conditioning system that ensures a comfortable temperature in all occupied spaces, but local air conditioning devices are used. This solution has several disadvantages, including the existence of a large number of equipment, most of the time from different manufacturers, which leads to a high cost of use and maintenance. Another aspect would be the fact that in the existing situation the cold source for the air conditioning devices is the air which, compared to the water from the river, reaches a much higher temperature, which determines a much lower COP compared to the solution of using a heat pump the water.

Fig. 3. Situation plan for the studied buildings

The study proposes the implementation of a hybrid system of air conditioning, free cooling and cooling with the help of a heat pump, simultaneously with the production of electricity using photovoltaic solar panels. The electrical energy produced will be able to be used both in the existing internal installation and for powering the heat pump, and the surplus energy produced can be delivered to the NES. The functional scheme of the proposed installation is presented in Fig. 4.

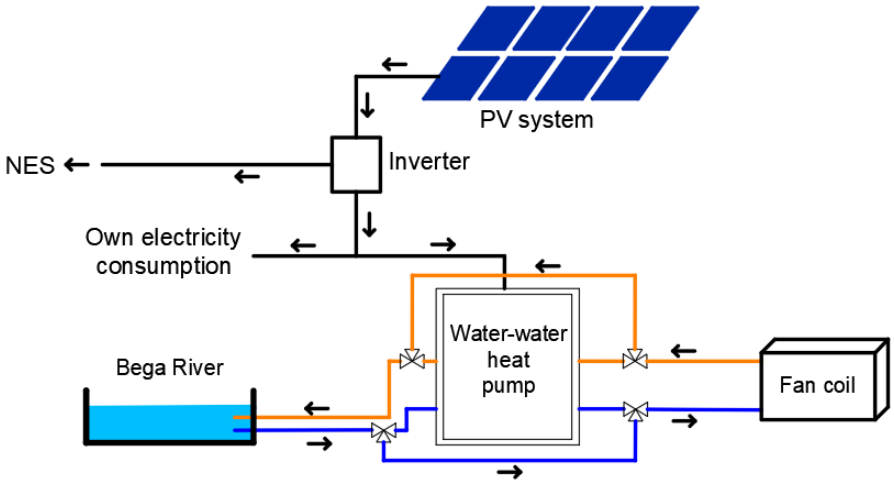

Fig. 4. Functional scheme of the proposed installation

The PV system is composed of 672 EvoCells 400 MIB modules with a maximum production power of 400 Wp, with a total installed power of 268.8 kWp. The positioning of the photovoltaic panels on the studied buildings is shown in Fig. 5.

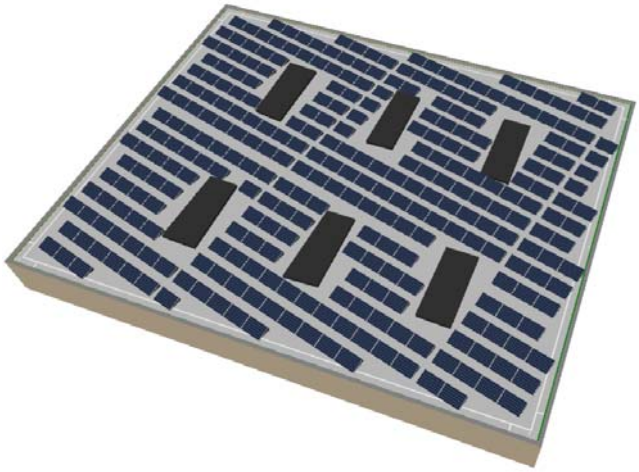

a)

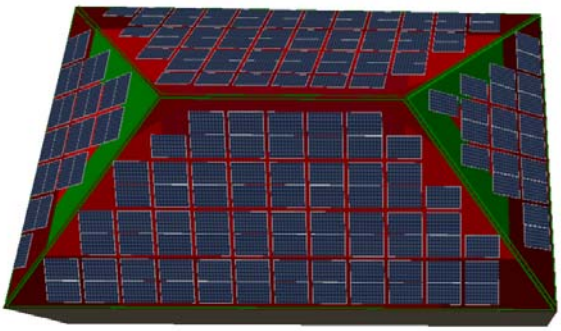

b)

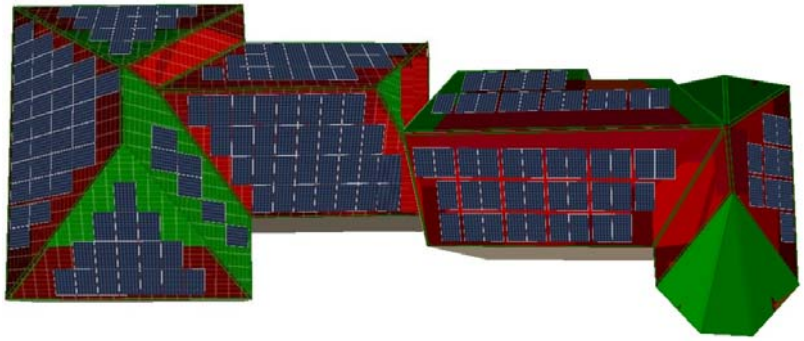

c)

Fig. 5. Placement of PV modules on the studied buildings [6]
a) Building 1, b) Building 2, c) Building 3

An important aspect that must be taken into account in the design phase of the photovoltaic panel system is that of their shading by nearby construction elements (parapet, skylight). By shading the panels, the amount of sunlight reaching their surface is reduced, thus affecting the output power. Photovoltaic cells are each like a link in a chain, the shaded cell being the "weakest link" that determines the reduction of the power availability of all the other links, a principle that also applies to the

photovoltaic modules connected to each other. Finally, the shading of a module in a string can significantly reduce the output power of that string, but not of a parallel string [7]. Through the simulation it can be seen in Fig. 6 which are the panels on Building 1 shaded and to what extent, so that their tying in strings is done according to this aspect or possibly to eliminate the panels that are not efficient or negatively affect the operation of the photovoltaic system.

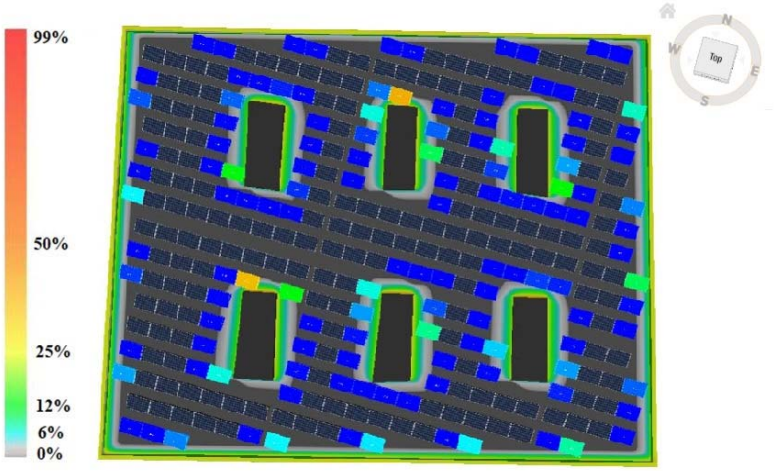

Fig. 6. Umbrirea panourilor fotovoltaice [6]

Following the simulation of the proposed photovoltaic system, a total annual energy produced of 110.84 MWh resulted, the monthly production can be seen in the graph in Fig. 7.

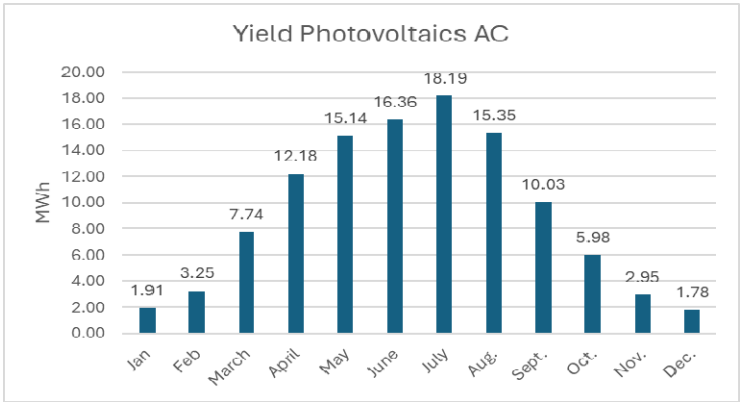

Fig. 7. The monthly alternating current production of the photovoltaic system [6]

An important aspect that must be taken into account is the fact that energy produced with the help of photovoltaic panels has the great advantage of reducing the amount of CO2 compared to the production of electricity using classic fuels. In Fig. 8 shows the amount of CO2 saved using this method of electricity production.

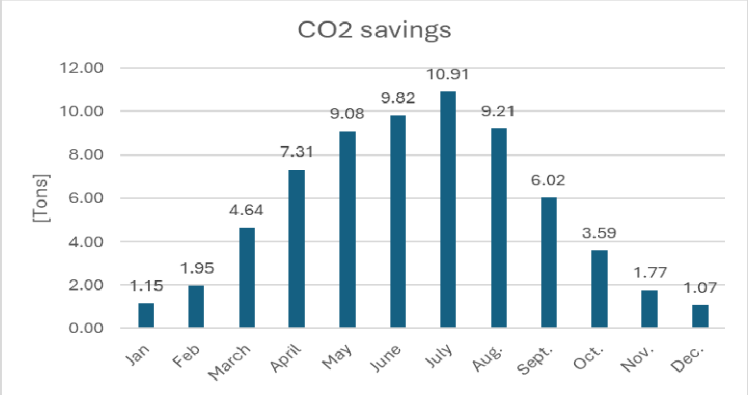

Fig. 8. CO_2 savings [6]

4. Conclusions

The modernization of buildings and installations is an essential step that must be carried out to obtain a reduction in energy consumption to ensure the comfort of the occupants. The heating and cooling of the spaces where we carry out our activities have become more and more problems that must be treated together to find the most sustainable solutions with low energy consumption. Regarding the case study carried out, the heating of the studied buildings can be achieved by reversing the cycle of the heat pump and introducing the hot water produced by it into the interior installation. Referring concretely to the buildings located near water sources (sea, lake, river course), for cooling in particular there is the advantage of using the "free cooling" option in the months that are not very warm and the water temperature is quite cold so that the water heat pump is bypassed and it is introduced directly into the air conditioning system.

References

[1] I. Sarbu, M. Mirza and D. Muntean, "Integration of Renewable Energy Sources into Low-Temperature District Heating Systems: A Review", Energies 15, no. 18, article ID: 6523, 2022.

[2] Maria Jangsten, Peter Filipsson , Torbjorn Lindholm , Jan-Olof Dalenback, "High Temperature District Cooling: Challenges and Possibilities Based on an Existing District Cooling System and its Connected Buildings", Energy 199, 2020.

[3] IEA. The Future of Cooling: opportunities for energy-efficient air conditioning. https://doi.org/10.1787/9789264301993-en. Paris. 2018, accessed in 25.03.2024.

[4] D. Muntean, A. Tokar, D. Tokar, Energy efficiency of educational buildings using photovoltaic panels and heat pumps. Case Study, Revista Română de Inginerie Civilă, Vol. 14, Nr.3, 2023.

[5] *** "Free cooling with water", Available at: https://www.alfalaval.com/industries/hvac/data-center-cooling/free-cooling-water/, Accessed in: 25.03.2024.

[6] ***, Polysun SPTX Constructor software from Vela Solaris.

[7] D. Tokar, D. Muntean, A. Tokar, "Aspecte privind influența umbririi panourilor fotovoltaice asupra producției de energie electrică. Studiu de caz", in Revista Ingineria Instalatiilor, nr.2, 2023.

Considerations regarding the recovery of residual energy for the heating/cooling of buildings and the preparation of domestic hot water

Considerații privind valorificarea energiei reziduale pentru încălzirea/răcirea clădirilor și prepararea apei calde de consum menajer.

Adriana Tokar[1], Daniel Bisorca[1], Daniel Muntean[1], Danut Tokar[1], Marius Adam[1], Cristian Păcurar[1], Alexandru Dorca[1], Andreea-Nicoleta Căinicianu[2]

[1]University Politehnica Timisoara
Victoriei Square, no.2, Timisoara, Romania
E-mail: adriana.tokar@upt.ro, daniel.bisorca@upt.ro, daniel-beniamin.muntean@upt.ro, danut.tokar@upt.ro, marius.adam@upt.ro, cristian.pacurar@upt.ro, alexandru.dorca@upt.ro

[2] RENEWABLES CONSULTING S.R.L.
Victor Hugo Street, no. 44 C, Timisoara, Romania
E-mail: andreea@renewables-invest.com

DOI: 10.37789/rjce.2024.15.3.12

Abstract. *Currently, many opportunities for real energy and cost savings are missed, primarily due to the perception of quantitative heat recovery. However, in the context of the need for the energy efficiency of buildings and technological processes, the recovery and valorisation of residual energy will be a key element. For this reason, the article analyses the recoverable potential from residual energy from various sources and proposes a way to capitalize on it for heating/cooling buildings and preparing domestic hot water.*

Key words: residual energy, recovery, heating/cooling, domestic hot water

1. Introduction

In order to achieve the EU's energy and climate goals, it is necessary that the existing building stock (75% have poor energy performance [1]), in EU member countries, become decarbonized by 2050. As the high share of energy consumption records for the heating and cooling of buildings, it is obvious that energy efficiency measures are needed in the construction sector, to reduce consumption for these services, but also CO_2 emissions. [2], [3], [4].

In addition, the current, rather outdated technologies equipping buildings with low energy efficiency still rely on conventional fuels generating considerable energy

waste. For this reason, in order to participate in the decarbonization of buildings, energy efficiency measures must integrate renewable energy sources (RES) and residual energy recovery methods, both at the local level (micro scale) and at the level of district heating networks (macro scale).

Basically, the waste heat recovery process involves the reuse of thermal energy that would otherwise simply be released into the atmosphere, with negative implications on energy consumption and cost and implicitly on emissions CO_2.

Waste energy recovery systems are designed to capture, store and reuse recovered energy. At the building level, to reduce the total energy demand, in general, the recovery of the exhausted heat through ventilation and air conditioning (HVAC) systems is approached. Energy efficiency directives [1], [4], [5] and specialized literature show that the combination of thermal rehabilitation of buildings (sealing of envelope elements) and the use of ventilation with heat recovery leads to considerable reductions in total energy consumption for space heating/cooling, but also greenhouse gas emissions [6], [7], [8], [9].

Most studies, present in specialized literature, regarding the recovery of residual heat refer to industrial processes, processes that can indeed provide valuable energy sources that contribute substantially to the reduction of total energy consumption. In this regard, studies generally refer to the operation and performance of commonly used technologies, such as [10], [11], [12], [13], [14], [15], [16], [17], [18], [19]: recuperators [14], [15], regenerative and plate heat exchangers [16], [17], furnace regenerators [18], [19], rotary regenerators (rotary air pre-heaters and heat wheels) [11], regenerative and recuperative burners [12], economizers and waste heat boilers and run around coil [13].

A classification of residual energy potential as a function of temperature can be done as follows [10], [20]:

- high temperature - greater than 400 °C - from combustion processes;
- medium temperature - 100–400 °C – combustion gas exhaust;
- low temperature - below 100 °C – hot air discharged from buildings with various destinations (data centers, production spaces, etc.) or wastewater (domestic and industrial sewage installations).

In this context, the article proposes a model of low-temperature waste heat recovery and thermal potential utilization for heating/cooling of buildings. The efficiency of the proposed model is achieved by integrating renewable energy sources (RES) using a photovoltaic system to power the heat pump, the chiller and for own consumption.

3. Low temperature waste heat recovery and utilization system model

The model proposes the valorisation of residual energy from sources that discharge residual energy into the atmosphere. Heat sources whose temperature falls into the low temperature category were considered for the model:

- Data centers (DC);

In Data Center and Server Room spaces the most important parameters that must be controlled and ensured to avoid server failure are temperature and humidity [21], [22], [23]. Inside the rooms, the temperature varies in the range of 35-70°C depending on the number of these equipment's and the height at which they are positioned in the racks (the temperature increases with height) [22], [21], [24]. The usual technologies for recovering energy from hot exhaust air are air-to-water heat recuperators and air-to-water heat pumps.

- Household wastewater sewage systems (SWH);

The temperature of the water discharged through the sewage pipes varies between 37-39°C [25] The heat absorbed by the wastewater is transferred to the cold water through heat exchangers at a temperature of approximately 25-30°C, depending on the material of the pipe SEWAGE.

- Low temperature technological processes (LTTP).

The productive industrial sector has a considerable residual heat potential, and for its valorisation a diversity of technologically mature technologies is available, technologies that are presented in Fig.2.

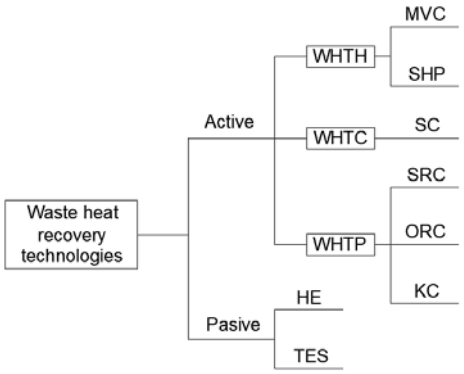

Fig. 2 Types of waste heat recovery technologies
WHTH-Waste heat to heat, WHTC-Waste heat to cold, WHTP-Waste heat to power, MVC-Mechanical vapour compressor, SHP-Sorption heat pump, SC-Sorption chiller, SRC-Steam Rankine Cycle, ORC- Organic Rankine Cycle, KC- Kalina Cycle, HE- Heat exchangers, TES-Thermal Energy

Research attention in the field of heat recovery has been drawn to the high or medium temperature recoverable potential (contained in flue gases), while the low temperature recoverable potential is often neglected. Even though it is possible that the residual potential of the processes that exhaust air or water of lower temperature does not constitute a significant source of residual heat that can be used directly, nevertheless by means of some equipment this potential can be harnessed.

Also, the residual low temperature potential is present in many sectors of activity, such as flat glass melting, food and beverages, chemical, textile, pulp and paper industry, non-metallic mineral processes, wood, other (metal cleaning, painting drying). The low-temperature residual potential is found in considerable quantities, as can be seen in Fig. 3 [20].

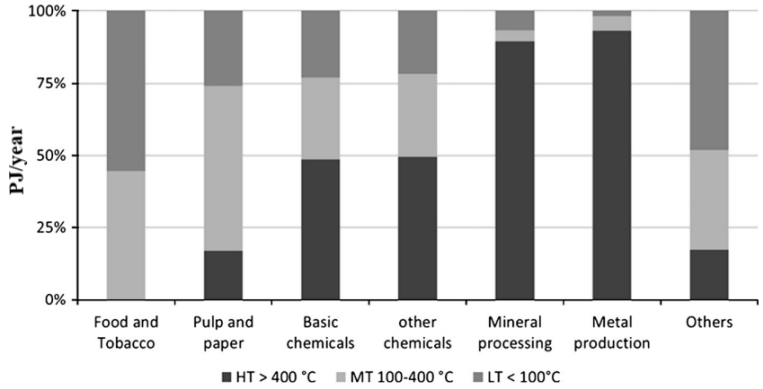

Fig. 3. The temperatures of processes from industry [20]

Thus, in the first stage, by implementing the proposed system model (Fig. 4), the residual potential is recovered from data centers/server room (CD), domestic sewage systems (SWH) and low-temperature technological processes (LTTP), the recovered heat being stored in thermal energy storage tanks (TES 1).

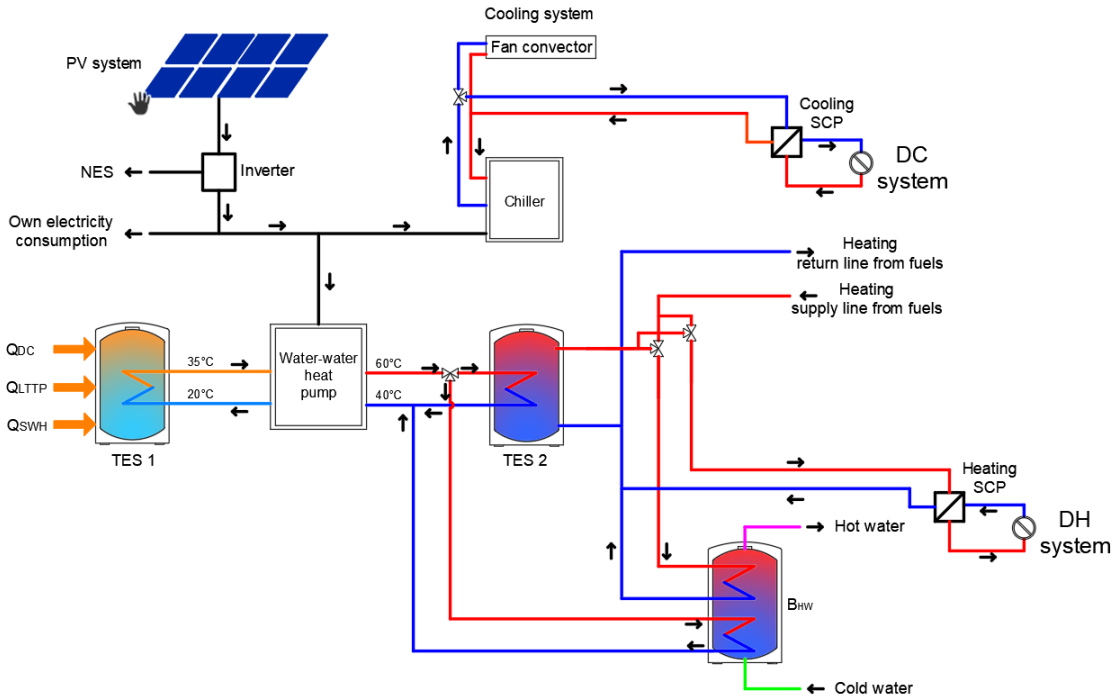

Fig. 4. The proposed model for heating/cooling buildings

In the second stage, by means of water-to-water heat pumps, supplied at a temperature of 35°C, the temperature of the water is raised to a temperature of 60°C and stored in thermal energy storage tanks (TES 2).

The thermal agent produced by the water-to-water heat pumps is transferred either to the boiler related to the internal sanitary installation for the preparation of domestic hot water (B_{DHW}), or to the thermal energy storage tank (TES 2) so that it can

be used again for the preparation of hot water later domestic or to feed the central heating system by means of plate heat exchangers (SCP).

For the efficiency of the proposed model, for the electricity supply of the heat pump, the chiller and the system's own consumption, a photovoltaic system is provided.

The photovoltaic system will be dimensioned in such a way as to ensure during the hot season the electricity needed to power the chiller from the cooling system component and the heat pump from the residual thermal energy recovery system component for the preparation of domestic hot water.

During the cold season, the photovoltaic system will feed the heat pump from the residual thermal energy recovery system component to prepare domestic hot water and to provide renewable energy in the centralized heating system.

The thermal energy surplus of the recovery system can be delivered to the centralized thermal energy supply system of the locality and during the warm season, the possible surplus of electricity from the photovoltaic panels can be delivered to the National Energy System (NES).

Therefore, compared to classical heating/cooling systems that usually have a single heat source providing heat/cooling in heating/cooling installations or heat in district heating systems, the proposed system model is a multi-source system of heat that could effectively solve the problem of heating systems.

3. Conclusions

Heating/cooling of buildings with multiple heat sources enables the large-scale use of waste energy from various applications as well as photovoltaic energy. The proposed system model addresses the integration of several heat sources that together can constitute the main source to feed either directly buildings or a centralized heating/cooling system or can constitute auxiliary heat sources in a system that includes a main source of heat which throughout the heating period maintains the operation at full load, while the auxiliary heat sources are adjusted to meet the different thermal load requirements of the users. These types of systems will improve the average efficiency of all heat sources.

Another advantage of this system model, compared to classic heating systems, is the fact that when a failure occurs in the main heat source, the auxiliary sources remain in operation, thus increasing the reliability of the system. This aspect is also an advantage for the stages of modernization or expansion of the system capacity.

An effective method of capitalizing on the high and medium temperature residual potential, already applicable, is the transfer of residual thermal energy in heating systems, in an energy-efficient manner, by using heat exchangers or heat pumps that prepare thermal agent for heating buildings.

The proposed heating/cooling model can integrate into the concept of smart thermal grids, a concept that can be seen as parallel to smart electrical grids and which focuses on the integration and efficient use of potential energy resources (renewable

and waste), as well as the operation of a structural network that enables distributed generation that may involve interaction with consumers. Through the information network, different parts (heat source, pipeline network, substations, heat/cold user) are connected with each other and integrated into a controlled and intelligent long-distance management system, namely intelligent heating system.

References

[1] European Commission, Energy Performance of Buildings Directive - Aiming to achieve a fully decarbonised building stock by 2050, the Energy Performance of Buildings Directive contributes directly to the EU's energy and climate goals, Available at: https://energy.ec.europa.eu/topics/energy-efficiency/energy-efficient-buildings/energy-performance-buildings-directive_en, Accessed: 14.03.2024

[2] G. Cavazzinia, A. Benato, „Residential Buildings Heating and Cooling Systems: The Key Role of Monitoring Systems and Real-Time Analysis in the Detection of Failures and Management Strategy Optimization", in Processes, vol. 11, no. 5, No. Article ID: 1365, 2023.

[3] [***, „Strategia UE pentru încălzire și răcire - Rezoluţia Parlamentului European din 13 septembrie 2016 referitoare la o strategie a UE pentru încălzire și răcire 2016/2058 (INI)", Available at: https://www.europarl.europa.eu/doceo/document/TA-8-2016-0334_RO.html, Accessed: 14.03.2024

[4] European Parliament, "Directive (EU) 2023/1791 of the European Parliament and of the Council of 13 September 2023 on energy efficiency and amending Regulation (EU) 2023/955", Available at: https://eur-lex.europa.eu/legal-content/EN/TXT/?uri=OJ%3AJOL_2023_231_R_0001&qid=1695186598766, Accessed: 29.03.2024.

[5] European Parliament, „Fit for 55 Package", Available at: https://eur-lex.europa.eu/legal-content/RO/TXT/?uri=CELEX%3A52021DC0550, Accessed: 15.03.2024.

[6] E. Zender–Świercz, "A Review of Heat Recovery in Ventilation", in Energies, Vol. 14, Article ID:1759, 2021.

[7] R.W. Besant, C.J Simonson, "Air-to-air energy recovery" ASHRAE Journal, pp. 31–52, 2000.

[8] J. Dieckmann, K.W.Roth, J. Brodrick, "Air-to-air energy recovery heat exchangers", ASHRAE Journal, pp. 57–58, 2003.

[9] M. Carlsson, M. Touchie, R. Richman, "Investigating the potential impact of a compartmentalization and ventilation system retrofit strategy on energy use in high-rise residential buildings", in Energy and Buildings, Vol. 199, pp. 20–28, 2019.

[10] H. Jouhara, N. Khordehgah, S. Almahmoud, B. Delpech, A. Chauhan, S. A. Tassou, "Waste heat recovery technologies and applications", in Thermal Science and Engineering Progress, Vol. 6, pp. 268–289, 2018.

[11] J. Malinauskaite, H. Jouhara, "Sustainable Energy Technology, Business Models, and Policies: Theoretical Peripheries and Practical Implications", Chapter: A theoretical analysis of waste heat recovery technologies, Imprint Elsevier, 2023.

[12] S. Tangjitsitcharoen, S. Ratanakuakangwan, M. Khonmeak N. Fuangworawong, "Investigation of Regenerative and Recuperative Burners for Different Sizes of Reheating Furnaces", in World Academy of Science, Engineering and Technology International Journal of Mechanical and Mechatronics Engineering, Vol:7, No:10, 2013.

[13] TLV Co. Ltd., Waste Heat Recovery, Available: https://www.tlv.com/steam-info/steam-theory/energy-saving/waste-heat-recovery, Accessed at: March 28, 2024.

[14] M. Adam, A. Tokar, S. Popa-Albu, C. Păcurar, Heat recuperators with plates, Conference with international participation, Buildings Services and Ambiental comfort, Edition a 24-a, pp 248-257, Timisoara, 2015.

[15] A. Petrosyan, “Energy economic suitability of the use of “air-air” recuperators in the climatic conditions of the republic of Armenia”, E3S Web of Conferences, Vol. 97, Article ID: 01014, 2019.
[16] K.M. Smith, S. Svendsen, “The effect of a rotary heat exchanger in room-based ventilation on indoor humidity in existing apart- ments in temperate climates”, in Energy and Buildings, Vol. 116, pp. 349–361, 2016.
[17] A. Negoițescu, A. Tokar, “Theoretical Aproach of Novel Technologies in the Plate Heat Exchangers Field”, in Transactions of Mecanics, Scientific Bulletin of the Politehnica University Timisoara, Romania, Vol. 60 (74), Fasc.1, pp 77-80, 2016.
[18] M. S. El-Behery, A.A. Hussien, H. Kotb, M. El-Shafie, Performance evaluation of industrial glass furnace regenerator, in Energy, Vol. 119, pp. 1119-1130, 2017.
[19] Rafidi Nabil, ”Thermodynamic aspects and heat transfer characteristics of HiTAC furnaces with regenerators”, Royal Institute of Technology, School of Industrial Engineering and Management, 2005.
[20] S. Bruckner, S. Liu, L.a Miro, M. Radspieler, L. F. Cabeza, E. Lävemann, ”Industrial waste heat recovery technologies: an economic analysis of heat transformation technologies”, Applied Energy, vol. 151 (1), pp. 157–167, 2015.
[21] ASHRAE, ”Thermal Guidelines for Data Processing Environments – Expanded Data Center Classes and Usage Guidance”,Whitepaper prepared by ASHRAE Technical Committee (TC) 9.9, 2011.
[22] A. Tokar, D. Muntean, D. Tokar, D. Bisorca, M. Cinca, “Considerations regarding the Recovery and Utilization of Residual Heat from Data Centers”, in Hidraulica- Magazine of Hydraulics, Pneumatics, Tribology, Ecology, Sensorics, Mechatronic, No. 1, 2024.
[23] ASHRAE, Environmental guidelines for datacom equipment, Atlanta, 2008.
[24] S. A. Nada, K. E. Elfeky, Ali M. A. Attia, W. G. Alshaer, “Experimental parametric study of servers cooling management in data centers buildings”, in Heat Mass Transfer, Vol. 53, pp. 2083–2097, 2017.
[25] C. Zaloum, J. Gusdorf, A. Parekh, “Final Report Performance Evaluation of Drain Water Heat Recovery Technology at the Canadian Centre for Housing Technology”, Sustainable Buildings and Communities Natural Resources, Canada Ottawa, 31 2007.

Optimization of wind energy conversion systems

Optimizarea sistemelor de conversie a energiei eoliene

Danut Tokar [1], Adriana Tokar [1], Daniel Muntean [1], Daniel Bisorca [1], Alexandru Dorca[1], Marius Adam[1]

[1] University Politehnica Timisoara
Vctoriei Sq., No.2, 300006 Timisoara, România
E-mail: danut.tokar@upt.ro, adriana.tokar@upt.ro, daniel-beniamin.muntean@upt.ro, daniel.bisorca@upt.ro, alexandru.dorca@upt.ro, marius.adam@upt.ro

DOI: 10.37789/rjce.2024.15.3.13

Abstract. *In close connection with the issue of global security, the issue of ensuring energy resources has been put on the table of consumers and producers of various forms of energy, researchers, but especially politicians and social planners. Ensuring energy independence was put into question after the onset of the oil crisis in 1973, thus the various energy sources and their associated technologies are gradually being replaced by new technologies that integrate renewable energy sources, capable of taking over at an increased level of efficiency the energy requirement.*

Key words: optimization, storage, energy, wind, RES,

1. Introduction

Even if the world's energy resources are enormous, capital resources are limited, which makes the exploitation of these energy resources not accessible even to developed countries, even more so to developing or underdeveloped countries. The solution to the world energy problem depends on political, cultural, economic, geographical, and technical circumstances. The formulated energy programs are shown to be the result of scenarios regarding primary resource provision options and appear to be a response to the current crisis. In reality, the energy scenario for the 2030s is based on the penetration models of new energy technologies [1]. The success of new energy technologies depends on how and in what time they will prove their technical-economic feasibility. The global dimension of the energy problem is obvious, the 1970s led to an increase in the price of oil (Fig. 1), putting in the background the fact that the energy problem must be approached starting from themes such as: resource conservation, the development of new technologies, reducing the impact on the environment, in other words the chance of a future depends on the range of actions taken today.

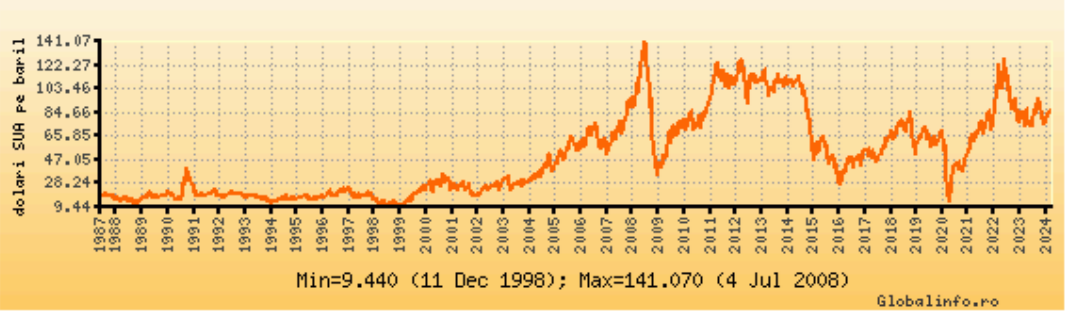

Fig. 1. The history and graphs of the international spot quotations of the barrel of oil [2].

The energy problem between demand and conservation it isdiscussed, also considering population growth, Fig. 2.

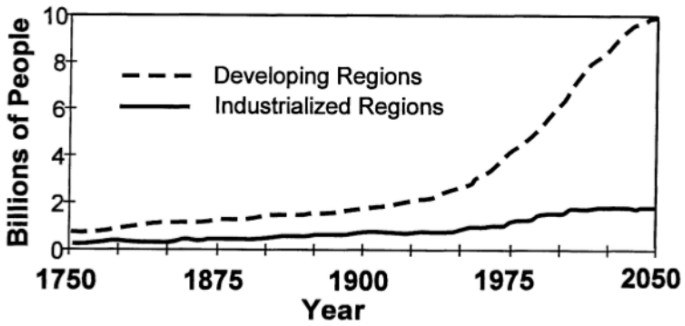

Fig. 2. World population. Projections until the year 2050 [3]

The provision of energy resources to meet energy needs as a result of population growth and technological progress (progress considered energophagous), must be subject to constraints regarding: the time in which a new technology can replace an existing technology, climate change risks, risks regarding the construction of energy capacities, but also risks of a political nature and, more recently, risks of a military nature.

Meeting the demand for energy as a result of the growth of the world population can be achieved either by developing nuclear capacities, or by adopting a nuclear moratorium, and certainly by reducing consumption, in which case is mandatory the development of SRE conversion and storage systems.

Romania was not indifferent to the effects of the oil crisis of the 70s, it can be considered that it understood that the energy future is represented by a mix in which RES must also be part. In this sense, at the beginning of the 80s, important research centers in Romania under the coordination of the Research Center of the Traian Vuia Polytechnic Institute in Timisoara started an extensive project to exploit the wind potential on Mount Semenic [4], and before 1989, Timișoara had the first neighborhood that was supplied with domestic water prepared with the help of solar energy. [5].

Analyzing the renewable energy potential of Romania, it can be found the existence of 5 areas with a photovoltaic potential between 1000 and 1400 kWh/kWp

[6] and also an important wind potential with average wind speeds at heights of 10m, 50m and 100m, between 4.09-7m/s [7].

The multidisciplinary nature of the energy issue, the transition to new technologies for the use of RES, the reduction of energy consumption in production processes and in residential buildings through energy efficiency [1], leads to the promotion of a vigorous energy mix program.

2. Analysis of the optimization possibilities of the wind power plant from Oravița, Caraș Severin county

Analyzing the state of the national energy system (NES) in the period 01.01.2023-31.01.2023, it can be seen that a negative balance is recorded through the contribution of hydropower (Fig. 3)

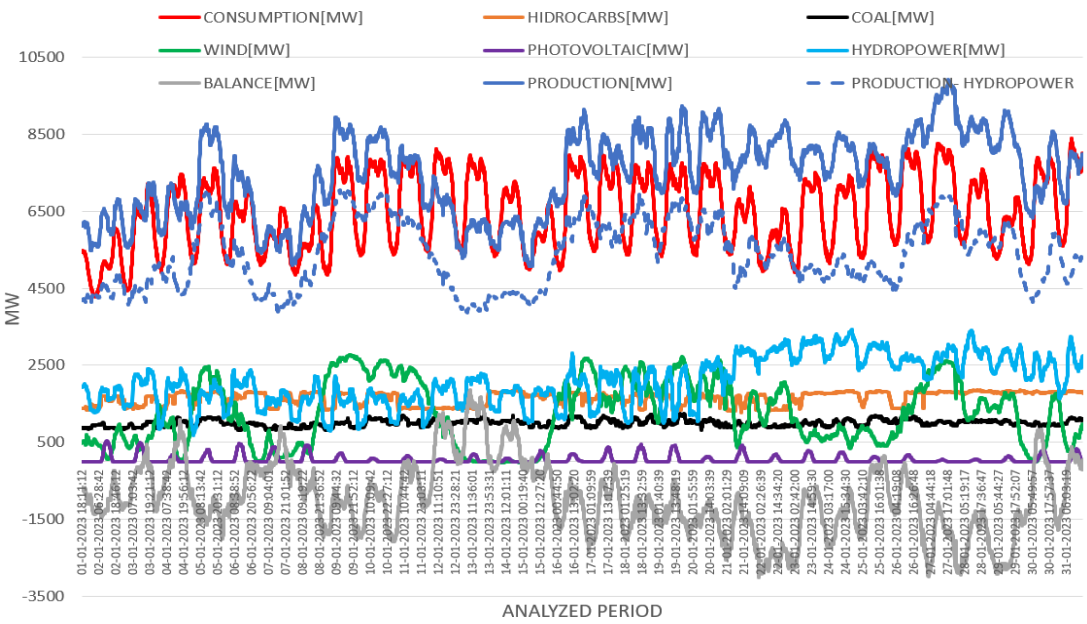

Fig. 3. State of the NES [8]

The share of the types of sources that make up the energy mix (Fig.4. a) indicates that most of the electricity production capacities are below the value of the installed power (Fig.4. b).

As expected, the predictable nature of the areas of the production curve where the sun is not in the sky (between sunset and sunrise) and the unpredictable nature of wind systems (Fig. 3), which still had a contribution of 16.53% in the energy mix in the analyzed period.

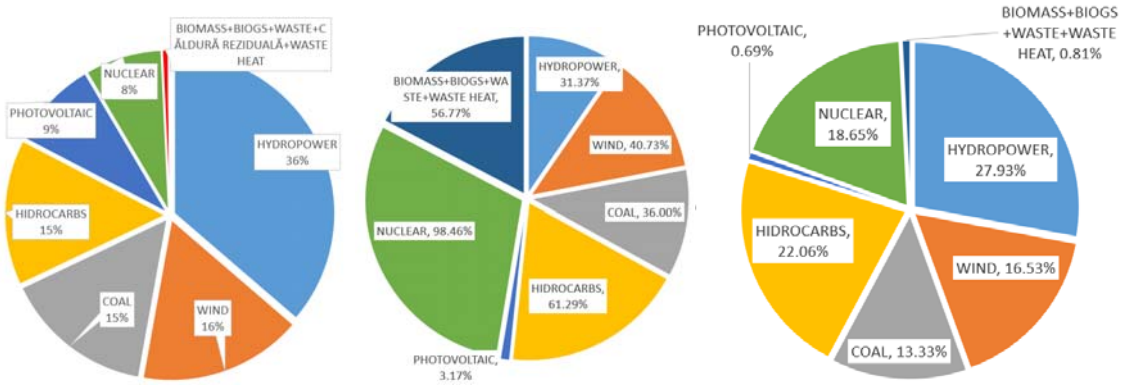

a) b) c)

Fig. 4. The share of the types of sources in the energy mix
a) Installed power [9], b) System status in the period 01.01.2023-.31.01.2023

Without knowing the reasons, we consider it inadmissible not to cover the power gap in the interval in which a positive balance is registered (Fig. 3).

The unpredictability of RES is accepted, it is also known that energy transactions on the stock market are dictated by the mechanisms of the imperfect economy, but we consider inadmissible the dispatching of NES by which hydropower is not properly exploited given that it represented 27.93% of the total energy produced in the analyzed period. In other words, it did not fulfill the role of regulating the load curve in its entirety, thus contributing to maintaining a high price of electricity.

It is also known that the non-functioning of hydropower production capacities depends on maintaining the level in the reservoirs and may be dictated by objective factors (lack of precipitation, scheduled overhauls) but especially by subjective factors (price of electricity, breakdowns because of maintenance inadequate, much too long times for repairs). The first objective cause must be eliminated if we follow Fig. 5

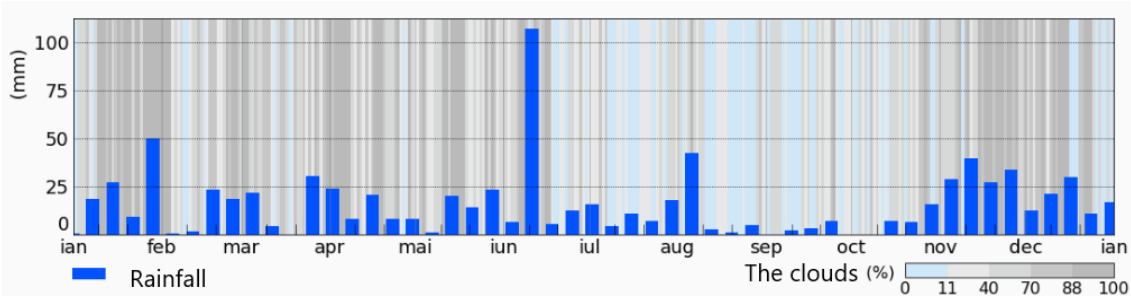

Fig. 5. Amount of precipitation in 2023 [10]

Analyzing the curve of production, consumption, and the balance in Fig. 6, it is found that hydropower covers the power gap until sunrise, without being able to explain why it does not cover this gap after dark.

The fact that the renewable energy potential of Romania is insufficiently exploited is illustrated in Fig. 4.a). It is also known that the renewable potential cannot be exploited in a large percentage if there are no means to cover the power gaps, in other words, without storage capacities.

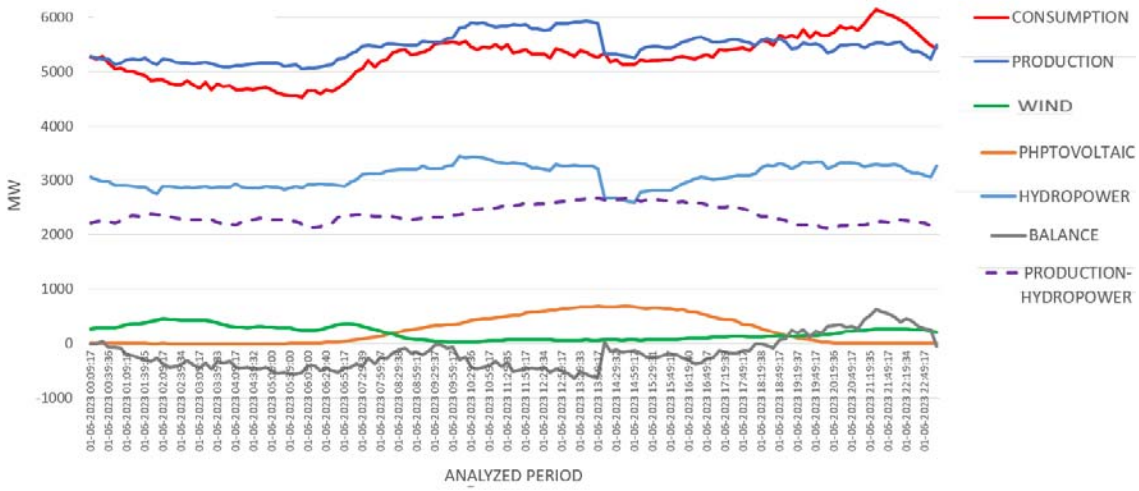

Fig. 6. State of the NES 01.06.2023- 30.06.2023 [8]

It is also known that the renewable potential cannot be exploited in a large percentage if there are no means of covering power gaps, in other words, in the absence of storage capacities.

The specialized bibliography, including [11], proposes a multitude of electrical energy storage procedures, while the optimal solution must be chosen according to the size and specificity of the production, transport/distribution, and use of electrical energy systems.

The article proposes a point of view on the optimization of wind power plants (WPPs) by storing surplus energy in hydraulic energy.

The WPPs hybrid system combined with pumped hydroelectric power plants (PHPPs), presents the advantage of storing amounts of energy of the order of GWh, at a circulation of powers up to 1GW and with storage periods of hours, days or even seasonal storage [11], [12]. These storage systems can successfully supply the power gaps and can also be frequency regulation systems of the power system.

Even if the storage technology is known, the capital problems, the geographical ones, which overlap with the actions of environmental activists, the costs related to the transport of electricity and the efficiency of pumping slow down for the moment the realization of SHPs coupled to SRE.

The specialized literature deals in numerous reviews from simple solutions for storing the electrical energy produced/that can be produced, in the potential energy of water to be used in periods of power gap [13, 14], to systems bolder underground pumped storage where hydraulic energy is stored in a cavity (obtained from impermeable materials) placed underground by raising the soil covering this cavity [15].

Particular attention is paid to low head storage systems as a result of research in the field of high head storage and tide conversion technologies [16], of cascaded storage systems which have the advantage of reduced evaporation and therefore an

increase in efficiency of approx. 15% compared to classic systems with lower tank and upper tank [17].

The dynamic regime in which the wind turbines operate poses problems regarding the full exploitation of the wind energy, since the maximum conversion of the wind energy can be done according to Eq (1).

$$MPPT=f(\omega_{opt}) \quad ...(1)$$

The generator load regulation algorithm at variable wind speeds is based on the regulation algorithms based on the turbine rotor kinetic energy in which the dual-fed induction rotor regulation system of the asynchronous generator performs the regulation load of the pumping system which is driven with using a synchronous machine with permanent magnets [18].

The article proposes an optimization solution for the WPPS Oravița, Caraș Severin county, starting from the renewable potential of the area, the power installed in SRE and the possibilities of electricity storage.

In the area there is a WPPS with a total installed power of 9MW, composed of 6 wind turbines with 3 blades (LCB1…LCB6) with a hub height of 110m, with an installed power of 1.5MW/turbine (Fig.7).

Fig. 7. Location of the Oravita wind power plant [19]

WPPS is installed in an agricultural area (low roughness), the prevailing wind direction is SE, the wind speed varies between 3.65 m/s to 6.36 m/s (the minimum speed of 3.65 m/s is slightly more higher than the typical speeds of low-speed wind turbines), Table 1.

Table 1

Wind speed [19]

Height (m)	Mean wind speed (m/s)	Maximum mean wind speed (m/s)	Maximum wind speed (m/s)
51.5	4.64	27.09	35.45
49	4.6	27.1	35.85
40	4.447	26.49	36.21
10	3.4	20.94	31.74

According to equation (2) the power of a wind turbine is profoundly influenced by the wind speed.

$$P=\frac{1}{2}\cdot\rho\cdot C_{\rho}\cdot A\cdot v^{3} \qquad (2)$$

Where, wind turbine power (P) in W, air density (ρ) in kg/m^3, gravitational acceleration (g) in m/s^2, area swept by wind turbine blades (A) in m^2, turbine power coefficient (Cp) , wind speed (v) in m/s.

From the analysis of Table 1 and Fig. 8, it is observed that in the absence of storage when the optimal angular speed is exceeded, when the price of electricity is low, or when the demand for electricity is low, the wind turbine / WPPS is stopped, potentially causing significant financial losses.

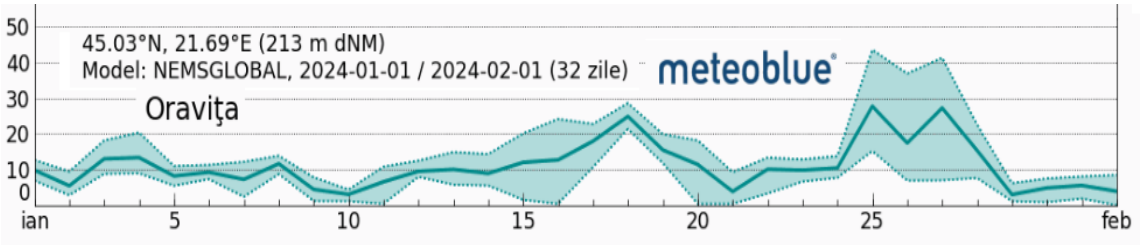

Fig. 8. Wind speed in Oravita, January 2024 [10]

A maximum capture of wind energy can only be achieved on the basis of a mathematical model that takes into account the variation of wind speed, the inertia of the turbine rotor, the mechanical stresses and even the geometry of the turbine that changes over time. This is practically impossible without storage.

Capturing the energy of the maximum wind energy (at any value of the wind speed) is only possible if the electricity is charged in two directions: in the network at the value of the forecasted electric power and in a storage system capable of taking over the surplus energy produced regardless of the variations in wind speed over time.

The wind turbine will operate at the maximum power point (MPP), capturing maximum wind energy, regardless of the restrictions imposed by the National Energy Dispatcher.

The city of Oravița has two artificial lakes built between the years 1700 and 1750 for the purpose of providing drinking water and water for industry, regularizing floods, supplying water to a thermal power plant and for leisure (Fig. 9). The "Big" lake, with an area of 1.4 ha located at an altitude of 315 m, has a length of 230 m and a width of 120 m, a reception area of 9 km^2 and a volume of 133300 m^3. The dam has a height of 13.4 m, but currently has a high degree of silting. About 800m downstream, at an altitude of 285m, there is the "Small" Lake with a surface area of 0.2ha, a reception area of 10 km^2 and a volume of 43,000 m^3. The dam of approx. 9.6 m is in an advanced state of degradation with significant seepage.

Fig. 9. Oravița Valley [20]

Analyzing the variation of the wind speed and the existence of the two storage lakes at a distance of 5.1km from the WPPS, the optimization of the operation of the WPPS can be achieved through the construction of a hydroelectric power plant HPP for which different scenarios can be made.

Taking into account the storage capacity of the "Small" lake of 43000m^3, the energy accumulated in hydraulic energy can provide according to (Eq.3) a power equal to the installed power of the wind turbines for 1740s.

$$P=\rho \cdot g \cdot Q \cdot H \cdot \eta \qquad (3)$$

Where, electrical power (P) in W, water density (ρ) in kg/m^3, water flow in m^3/s, turbine head (H) in m, the conversion yield (η).

3. Conclusions

The wind system works optimally in terms of energy if it captures the maximum wind energy.

The stochastic character of SRE due to meteorological factors makes it impossible to fully exploit the renewable potential. If for solar systems the time interval in which these systems are not functional is known and measures can be taken to ensure the load curve by classic systems (coal, hydrocarbons), the grid coupling of WPPS registers great frequency assurance problems due to variable wind speed.

Expansion of the WPPS, including the exploitation of the offshore wind potential of the Black Sea is not possible without storage.

Although hydroelectricity storage has reached maturity, the implementation of storage capabilities is dependent on geographic conditions, capital resources, pumping costs, community acceptance, politic assumption, and regional instability.

References

[1] W. Hafele, „Energia într-o lume finită. Căi spre un viitor viabil", Editura Politică, Bucureşti, 1983.
[2] https://www.globalinfo.ro/z/pretul_petrolului_titeiului_brent_europa_cotatia_internationala. Accesat 05.02.2024, 15:13
[3] C. Coeteze, M. Murpheree, D.V. Niekerk, C. Brecker, Feasibility study on the decentralisation and institutional capacity development for the Directorate Agricultural Disaster Risk Management, 2013
[4] Zaharia C., Cum s-a asezat rugina peste proiectul de eoliene in communism, Green Report, 2011, disponibil online: https://www.green-report.ro/cum-s-asezat-rugina-peste-eolienele-bdquoepocii-de-aurrdquo/, accesat: 07.02.2024.
[5] Timisoara was one step away from becoming the city of the sun, available at: https://www. banatulazi.ro, accesed 07.02.2024
[6] ***, Solargis, Solar resource maps of Romania, available at: https://solargis.com/maps-and-gis-data/ download/ romania, accesed 07.02.2019
[7] ***, Wind maps, available at: https://globalwindatlas.info, accesed: 07.02.2019
[8] ***, Energy sistem operation, available at: , https://www.transelectrica.ro/, accesed:01.03.2024
[9] ***, ANRE, Power installed, available at: https://anre.ro/puteri-instalate/, accesed:01.03.2024
[10] ***, Amount of precipitation in 2023, available at: https://www.google.com/ search? q= meteoblue, accesed: 5.03.2024
[11] Tokar D., Stroita C., Tokar A., Rusen A., Hybrid System that Integrates the Lost Energy Recovery on the WaterWater Heat Pump Exhaust Circuit, 4th International Conference World Multidisciplinary Civil Engineering-Architecture-Urban Planning Symposium (WMCAUS), IOP Conf. Series: Materials Science and Engineering 603 (2019) 042002 IOP Publishing, Prague, Czech Republic, 17- 21 June, 2019.
[12] J.A. J. Capilla, J. A. Carrion, E. Alameda-Hernandez, Optimal site selection for upper reservoirs in pump-back systems, using geographical information systems and multicriteria analysis, Renewable Energy, Vol.86, pp.429- 440, 2016
[13] Van Vliet M.T.H., Wiberg D., Leduc S., Riahi K., Power-generation system vulnerability and adaptation to changes in climate and water resources, Nature Climate Change, Vol. 6, No. 4, pp. 375-380, 2016.
[14] Rehman, L. M. Al-Hadhrami, Md. M. Alam, Pumped hydro energy storage system: A technological review, Renewable and Sustainable Energy reviews, Vol. 44, pp. 586- 598, 2015
[15] J. Olsen, K. Paasch, B. Lassen, C. T. Veje, A new principle for underground pumped hydroelectric storage, Journal of Energy Storage, Vol.2, pp. 54- 63, 2015
[16] R. Ansorena Ruiz, L.H. de Vilder, E. B. Prasasti, M. Aouad, A. De Luca, B. Geisseler, K.Terheiden, S. Scanu, A. Miccoli, V. Roeber, M. Marence, R. Moll, J.D. Bricker, N. Goseberg, Low-head pumped hydro storage: A review on civil structure designs, legal and environmental aspects to make its realization feasible in seawater, Renewable and Sustainable Energy Review, Vol. 160, No. 112281, 2022
[17] J. D. Hunt,M. A. Vasconcelos de Freitas, A. O. Pereira Jr., A review of seasonal pumped-storage combined with dams incascade in Brazil, Renewable and Sustainable Energy Reviews, Volume 70, pp. 385-398, 2017
[18] M. Han, G. T. Bitew , S. A. Mekonnen, W. Yan, Wind Power Fluctuation Compensation by Variable Speed Pumped Storage Plants in Grid Integrated System: Frequency Spectrum Analysis, CSEE Journal of Power and Energy Systems, Vol. 7, No. 2, pp.381- 395, 2021
[19] S.C. Topside Services S.R.L., Location of the Oravița wind power plant , Wind Park Assessment – "POENI" Oravita – Romania, rev.1, pp.1 -38, 2012
[20] D. Tokar, D. Foris, A. Tokar, T. Foris, Sustainable development of disadvantaged regions by renewable energy sources integration, Proceedings of the 2019 International Conference Economic Science for Rural Development, Issue 51, pp. 237-244, Jelgava, LLU ESAF, 9-10 May 2019

Dynamic Simulation Modeling. (DSM) for Building Energy Performance and HVAC Equipment Selection. A Case Study

Modelare prin simulare dinamică (DSM) pentru performanța energetică a clădirilor și selecția echipamentelor HVAC. Studiu de caz.

Andrei Dună[1]

[1]Politehnica University Timișoara

Victoriei Square, Nr.2, Timisoara, Romania
E-mail: andrei.duna@student.upt.ro

Coordinator: Ștefan Dună

E-mail: stefan.duna@upt.ro

DOI: 10.37789/rjce.2024.15.3.14

Abstract. *The paper presents a case study in which a dynamic simulation modeling (DSM) calculation was carried out to assess the energy performance of a building in Giroc, a locality adjacent to the city of Timișoara, using the VABI Elements software. The characteristics were determined based on which the HVAC equipment was selected.*

Key words: *VABI Elements, dynamic simulation, DSM, envelope, parameters, buildings, cooling demand, heating demand*

1. General information

1.1. Objectives of the approach

What kind of house do we want?"

Most often, in the endeavor to build a building intended for residential use, a family desires certain functionalities to ensure:

a. *Optimal Comfort achieved through*:

- Thermal Comfort: Ensuring a pleasant temperature in all seasons, through efficient heating and cooling systems, as well as quality insulation.

- Acoustic Comfort: Sound insulation to reduce noise from outside and other parts of the house.
- Air Quality: Ventilation and air purification systems to maintain a healthy and fresh indoor environment.
- Lighting: Maximizing natural lighting and ensuring well-designed artificial lighting for visual comfort.
- Ergonomics: Interior design that facilitates movement and reduces discomfort, with furniture and equipment adapted to the needs of the residents.

b. *Enhanced Safety achieved through***:**

- Structural Security: The construction must comply with building safety standards, be resistant to natural factors (earthquakes, floods) and use high-quality materials.
- Security against Intrusions: Security systems such as alarms, surveillance cameras, motion sensors, and sturdy locks. An alarm system, surveillance cameras, and high-security locks can provide peace of mind and protection.
- Fire Prevention: Smoke detectors, fire extinguishers, and a clear evacuation plan in case of fire.
- Health Safety: Non-toxic materials, prevention of mold, and ensuring proper hygiene.

c.*Energy Efficiency* achieved by providing quality Insulation, double-glazed windows, and energy-efficient heating and cooling systems which can reduce costs and environmental impact.

d. *Green Spaces and Sustainability*: Gardens, outdoor recreation areas, and possibly solar panels or rainwater collection systems for sustainability and savings.

e. *Smart Home Technology*: Automated control systems for lighting, temperature, security, and other aspects of the home for comfort and efficiency.

f. *Ergonomic Design*: Ergonomically designed living spaces to maximize comfort and functionality - for example, kitchens with well-thought-out workspaces, spacious bathrooms, etc.

g. *Intelligent Zoning*: Creating separate areas for different activities (work, relaxation, sleep) can help maintain a healthy balance in the home.

h. *Air Guality*: Ventilation, treatment, and air purification systems to ensure a healthy and fresh indoor environment.

i. *Accessibility*: Design that allows access and comfort for people of all ages and abilities.

j. *Natural and Artificial Lighting*: Maximizing natural light and providing adequate artificial lighting for visual comfort.

k**.** *Durable and Quality Materials*: Using durable and high-quality materials that ensure a longer lifespan of the building and reduce the need for frequent maintenance.

To address the functionalities mentioned above in a unified manner, the current specialized literature recommends the use of Dynamic Simulation Modeling.

2. Dynamic Simulation Modeling

2.1. (DSM) - a tool in the design and construction of a residential building.

Dynamic Simulation Modeling is a powerful tool in the architect's and engineer's toolkit, enabling data-driven decisions to create buildings that are comfortable, energy-efficient, and sustainable.[3]. To facilitate this resolution, recent literature [1] and practice resort to dynamic simulation modeling (DSM), which can be an extremely valuable tool in designing and constructing a residential building that meets the above requirements through the following:

1. *Energy efficiency optimization*: DSM can simulate the thermal performance of the building, aiding in optimizing insulation, building
orientation, windows, and heating/cooling systems for maximum energy efficiency.

2. *Thermal and acoustic comfort analysis*: Through DSM, various space usage scenarios and their impact on thermal and acoustic comfort can be assessed, allowing adjustments in the design phase.

3. *Study of natural and artificial lighting*: Simulations can help optimize the use of natural light and design artificial lighting systems to maximize visual comfort and energy efficiency.

4. *Indoor air quality assessment*: DSM allows for the simulation of ventilation and air circulation, important for maintaining good indoor air quality.

5. *Structural safety analysis*: Simulations can test the structural strength of the building in different conditions, such as earthquakes or strong winds.

6. *Security systems evaluation*: Simulations can assist in the optimal placement of surveillance cameras, motion sensors, and other
security elements.

7. *Sustainability and environmental impact*: DSM can assess the building's impact on the environment, aiding in the design of a sustainable building.

8. *Flexibility and adaptability*: DSM can anticipate the future needs of occupants, allowing the design of a flexible and adaptable space.

Dynamic Simulation Modeling (DSM) is a sophisticated computational technique used in the field of building design and energy analysis. It involves creating a detailed computer model of a building that simulates its performance under various conditions over time.

2.2. Followed procedure

Given the specialization, among all the above dynamic simulations and considering there are multiple mathematical relationships and basic concepts to be taken into account, in the analyzed case, we chose to use Dynamic Simulation Modeling (DSM) with the objective of evaluating the energy performance of a building with a parallelepiped configuration and the thermal comfort inside, and later having the possibility to choose equipment for HVAC. The mathematical relationships

and models that form the basis for a DSM simulation must be optimized, adjusted, and calibrated for the considered building, so as to encompass all its unique features, such as geometry, orientation, type and characteristics of construction materials, desired or existing HVAC systems, and the functions of the spaces in the building. To perform a simulation of the energy performance and thermal comfort of a building in the design stage located in Timișoara, Romania, using the information and mathematical relationships we have, the following input data about the building are necessary:

a. *Building Dimensions and Configuration*: Building plans including length, width, height, and number of floors. Also, the internal configuration (e.g., position and size of partition walls, position of windows and doors).

b. *Building Material Properties*: Information about materials used for walls, windows, roof, and floors, including their thermal transfer coefficients (U-value) and thermal capacity.

c. *Building Orientation and Positioning*: The direction the building faces, as this affects sun exposure and prevailing wind directions.

d. *Building Insulation*: Details regarding thermal insulation of walls, roof, windows, and floors.

e. *Heating, Cooling, and Ventilation Systems*: Type and efficiency of heating, cooling, and ventilation systems, including any heat recovery systems.

f. *Building Usage*: Information on how the building is used, including the number of occupants, types of electrical and electronic equipment, lighting, and any processes or activities generating heat.

g. *Local Climate Conditions*: Meteorological data for Timișoara, such as average monthly temperatures, humidity, wind speed, and solar radiation intensity.

h. *Operational Time Schedule*: The building's usage schedule, including variations throughout the day or year.

i. *Thermal Comfort Objectives*: Desired parameters for thermal comfort, such as specific indoor temperatures.

3. The mathematical relationships and models that form the basis for a DSM

Dynamic Simulation Modeling (DSM) for building energy performance and HVAC (Heating, Ventilation, and Air Conditioning) equipment selection involves a complex process that uses mathematical models and simulation software to assess a building's energy performance and to optimize the selection and sizing of HVAC equipment[8]. Below are some of the relevant equations and principles used in this context:

3.1 Thermal Balance for a Room or Building

The thermal balance is fundamental in modeling the energy performance of buildings and can be expressed as:

$$Q_{total}=Q_{internal}+Q_{solar}+Q_{transmission}+Q_{infiltration}-Q_{ventilation}-QHVA_{CQtotal} \quad (1)$$
$$Q_{total}=Q_{internal}+Q_{solar}+Q_{transmission}+Q_{infiltration}-Q_{ventilation}-Q_{HVAC}$$

where:

- Q_{total} is the net thermal load on the space (positive for heating, negative for cooling);
- $Q_{internal}$ is the heat generated internally by occupants, equipment, etc;
- Q_{solar} is the heat gain through windows from solar radiation;
- $Q_{transmission}$ is the heat transferred through walls, roofs, and other elements of the building envelope;
- $Q_{infiltration}$ is the heat lost or gained through uncontrolled air leakage;
- $Q_{ventilation}$ is the heat lost or gained through controlled ventilation;
- Q_{HVAC} is the thermal load removed or added by the HVAC system.

3.2 Calculation of the Heat Transfer Coefficient (U-ValConvective and radiative heat transfer equation):

$$Q^{\cdot}=U\cdot A\cdot(T_{int}-T_{ext})Q^{\cdot}=U\cdot A\cdot(T_{int}-Text) \quad (2)$$

where:

- $Q^{\cdot}$ represents the rate of heat transfer;
- U is the overall heat transfer coefficient;
- A is the heat transfer area;
- T_{int} and T_{ext} are the indoor and outdoor temperatures, respectively.

$$U=11hext+\sum(diki)+1hintU=hext1+\sum(kidi)+hint11 \quad (3)$$

where:

- U is the heat transfer coefficient of a building element (W/m^2K);
- h_{ext} and h_{int} are the external and internal heat transfer coefficients, respectively (W/m^2K);
- di and ki are the thickness and thermal conductivity of each layer of the building element.

4. Simulation of HVAC System Performance

Simulating HVAC systems involves calculating thermal loads and the response of the HVAC system to these loads. A simplified model for an HVAC system can be expressed through its efficiency and response capacity:

$$QHVAC=COP\times E_{input}QHVAC=COP\times E_{input} \quad (4)$$

where:

- QHVAC is the heat removed or added by the HVAC system (W).
- COPCOP is the Coefficient of Performance of the system (a measure of system efficiency).
- E_{input} is the electrical or thermal energy consumed by the system (W).

4. Dynamic Modeling

Dynamic modeling involves using differential equations to represent the temporal variations of temperature and other relevant variables within the building. A simplified example could be:

$$CdTdt=Q_{total}−QHVACCdtdT=Qtotal−QHVAC \quad (5)$$

where:

- CC is the thermal capacity of the space (J/K).
- dTdtdtdT is the rate of change of temperature over time.
- TT is the temperature inside the space.

These equations are just a starting point. Detailed DSM models for buildings will include many other aspects, such as detailed modeling of airflows, complex interactions between different spaces and systems in the building, as well as integration with renewable energy sources and energy storage systems. Specialized software, such as EnergyPlus, TRNSYS, or IESVE and VABI are often used to perform such detailed simulations.With this information, mathematical relationships can be used to dynamically model heat transfer, energy consumption, the impact of insulation, and the efficiency of HVAC systems. Also, estimates can be made for heat gains and losses, as well as for thermal comfort inside the building. In the case study, the VABI ELEMENTS SOFTWARE was used[8]. There are also other simulation software such as EnergyPlus or DesignBuilder that can be used to perform these types of complex simulations.

4. Information about vabi elements software

With the help of VABI Elements software, a fairly accurate 3D model of a building can be quickly created for dynamic simulation modeling (DSM) to evaluate a building's energy performance and indoor thermal comfort. This calculation takes into account detailed information about the building's structure and installations, as well as specific details regarding occupancy levels and schedules.

The software provides a simulated environment which, for the buildings to be analyzed, can be calibrated based on available measured and recorded consumption data. It can then be used to test various scenarios either at the whole building level or at the level of a zone or a room, to identify potential energy consumption issues and improvements that can be made to both the building and its installations.

For the building analyzed in our study, to simulate the building's performance over a flexible time period, the calculation uses hourly climate data files corresponding to the Timișoara area. It analyzes periods from the warm season, with peak maximum temperatures, and the cold season, with peak low temperatures.

Dynamic simulation modeling helped us understand how the chosen building for the study works from the perspective of consumption, energy management, and comfort, relative to its potential. Usually, residential buildings, institutions, cultural and sports buildings can have poor energy and comfort performance if there is no active management of the building and its related installations, including their regular maintenance. Significant energy savings can be achieved through modeling existing equipment, their control settings or from BMS - Building Management System, and by assessing the effect of changes on possible control methods. Also, many buildings have reference values for their heating and cooling that lead to waste both for energy used in heating and that used in cooling under conditions of simultaneity.

The VABI model allows an assessment of the impact of changes through simulation before the beneficiary commits to investments for improving efficiency as well as for determining the characteristics of HVAC equipment. The effects of changes in building use (such as a reorganization of internal occupancy patterns) can also be evaluated before implementation.Starting in 2008, the issue of potential health risks due to Bisphenol A (BPA) - a chemical found in plastic materials, was raised. BPA is a chemical that has been used to harden plastics over the last 40 years in the production of medical devices, CDs, water bottles, food and beverage packaging, and many other products found in building materials.VABI Elements can also take into account BPA in the evaluation of building performance. BPA can be incorporated into the ESOS - Energy Savings Opportunity Scheme process and offers possibilities for analysis and classification of the building within the provisions of ISO 50001 - Energy Management Standard.

5.Case study

5.1. Information about the analyzed building and the chosen solutions

The study conducted was used for the 'design' phase of the heating and internal sanitary installations, titled 'Construction of a ground-floor house, car and pedestrian access, carport', located in Giroc, Timis County.

The project was designed to comply with the requirements of Romanian or European standards, and where different regulations exist, the most stringent ones will be followed in principle. The design of the indoor sanitary installations is based on the architectural plans of the building, with the positioning of the sanitary groups and sanitary objects. The preparation of hot water is achieved with the help of a vertical boiler with a volume of 300 liters, equipped with two coils and an electric resistance of 3 kW. The primary coil is supplied with heat using an air-to-water heat pump with a power of 14 kW. The secondary coil is supplied with thermal agent from completely automated vacuum tube solar panels. Energy consumption for hot water preparation is

reduced by setting economical delivery temperatures for the consumable water. The prescribed value for locally or centrally prepared hot water using conventional sources is 60 ºC. The temperature of the water in the boiler can be automatically raised to 60 ºC once every 2 days for 2 hours during the night to eliminate the possibility of Legionella contamination; otherwise, the temperature can be maintained at 50 ºC. Hot water for the pool is prepared through a tubular heat exchanger made of titanium, supplied with thermal agent from a fully automated solar panel kit.

Parameters considered for winter calculation: Exterior • Design exterior temperature: Te = -15°C • Relative humidity: φ= 90% Interior • Design interior temperature: Bedroom: Ti =20°C, Bathroom: Ti =24°C, Living room: Ti =20°C, Kitchen: Ti =20°C • Relative humidity: φ= 35 - 60%.

The calculation of the heat demand of the rooms was carried out according to the Romanian standard SR-1907/1,2-2014. All the installed power of the circuits was distributed from the heat pump located in the technical space on the ground floor.

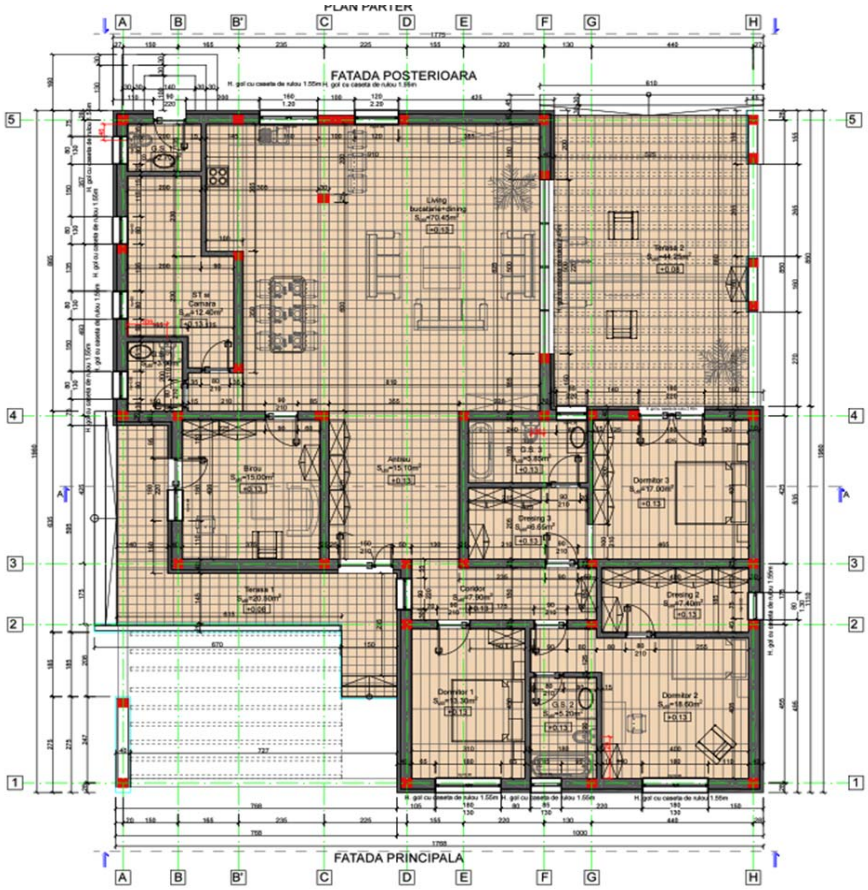

Fig. 1. The interior characteristics of the rooms in the studied building

The installed system is intended to compensate for heat losses through the external construction elements until achieving the calculated interior temperatures,

both during cold months and seasonally. The technical room is equipped with an air-to-water heat pump with a power of 14 kW. Additionally, the heat pump will produce domestic hot water through the boiler with two coils and a single-phase electric resistance of 3 kW. For the optimal operation of the system, a variable temperature automation has been proposed for the underfloor heating circuit, with adjustment possible through the local thermomechanical automation system of the underfloor heating. For cooling purposes, a ceiling cooling system of Uponor Renovis type has been provided, following the calculations obtained according to SR 6648-1:2014 " Ventilation and air conditioning installations. Calculation of heat inputs from the outside and of the (sensible) cooling thermal load for the calculation of the rooms of an air-conditioned building. Basic prescriptions" and SR 6648-2:2014 " Ventilation and air conditioning installations. External climatic parameters" . The Uponor Renovis system for the ceiling consists of a 15 mm gypsum board panel in which the high-quality Uponor PE-Xa pipe is already factory-integrated. The elements can be installed as dry-mounted panels on almost any type of ceiling using a 27/60 CD profile substructure available on the market. After filling and sanding the joints, the Uponor Renovis system elements can be immediately installed. For building ventilation, i.e., the supply of fresh air and heat recovery, circular heat recovery units mounted in the wall have been provided, with 3 speed stages and a copper heat exchanger. A minimum of 50 m^3/h of fresh air flow is ensured. The energy efficiency of the recovery is 95%.

The characteristics of the building envelope elements were also defined based on the details from the architectural project, resulting in the thermal transfer resistances presented in Table 1. The exterior walls of the building are made of brick masonry with cavities and thermal insulation with a thickness of 10 cm. For the terrace-type roof, the use of a 20 cm thick layer of mineral wool insulation was proposed. The ground floor slab was also thermally insulated with a 5 cm thick layer of extruded polystyrene placed beneath the reinforced concrete slab.

The calculation was performed at the level of each room, according to the thermal zoning presented in Figure 1. Thus, for each room, parameters such as: winter design indoor temperature, summer design indoor temperature, air changes per hour, installed lighting power were defined. The aforementioned parameters are presented in Table 1. As the number of building occupants, 4 permanent occupants were considered.

Table 1

Thermal resistances of the building envelope elements

Designation of Envelope Element	Thermal Resistance R [m^2K/W]
Exterior Walls	3.05
Flat Roof	5.58
Slab in Contact with the Ground	4.66
Exterior Joinery	0.77

The calculation was performed at the level of each room, according to the thermal zoning presented in Figure 2. Thus, for each room, parameters such as: winter

design indoor temperature, summer design indoor temperature, air changes per hour, installed lighting power were defined. The aforementioned parameters are presented in Table 1. As the number of building occupants, 4 permanent occupants were considered. Upon running the analysis in the calculation program, several useful data have been obtained. Figure 3 shows the heat losses through transmission corresponding to each envelope element of the building. The most significant heat losses occur at the level of the exterior walls and the terrace-type roof.

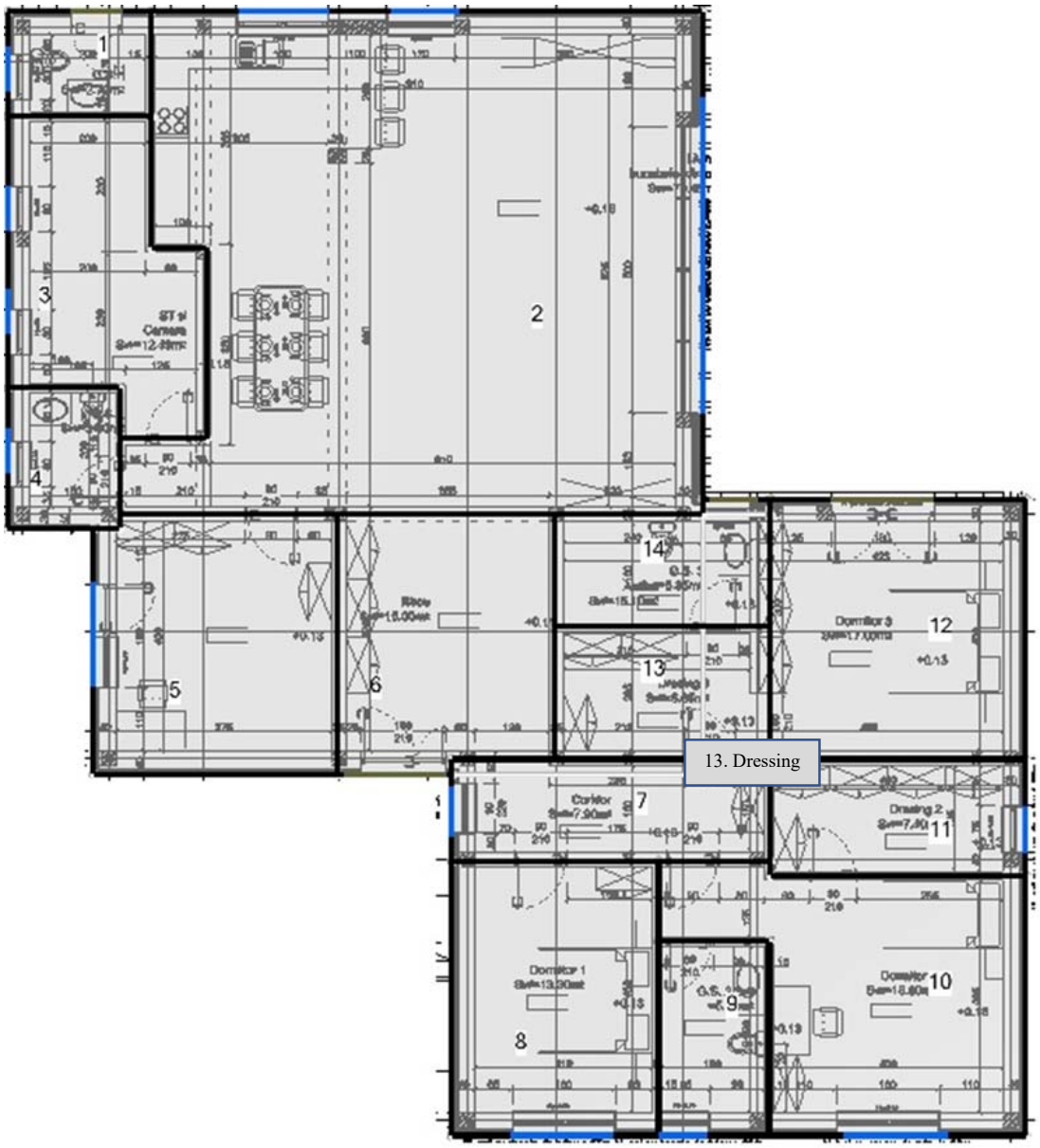

Fig. 2. The thermal zoning of the building

Table 2

Parameters related to the rooms in the building

No.	Denumire incapere/Room name	Temperatura interioara de calcul iarna/Interior deisgn temperature for winter [°C]	Temperatura interioara de calcul vara/Interior deisgn temperature for summer [°C]	Putere instalata iluminat/ Installed lighting power [W/m^2]	Numarul de schimburi orare de aer/Number of air changes per hour [h^{-1}]
1	G.S	24	-	10	10
2	Bucatarie si dining/kitchen and dining	22	26		
3	ST-tehnical space/pantry	22	-		
4	G.S	24	-		
5	Birou/Office	22	26		
6	Antreu/Hallway	22	26		
7	Corridor	22	26		
8	Dormitor/Bedroom1	22	26		
9	G.S 2	24	-		
10	Dormitor/bedroom2	22	26		
11	Dressing 2	22	-		
12	Dormitor/bedroom3	22	26		
13	Dressing 3	22	-		
14	G.S 3	24	-		

Additionally, as a result of the simulation, the values of the cooling and heating requirements for each room were obtained, as centralized in Table 2. The total heating requirement of the building is 11.40 kW, and the total cooling requirement is 10.56 kW. These values were the starting point for sizing the equipment at the level of each room and the heat pump.

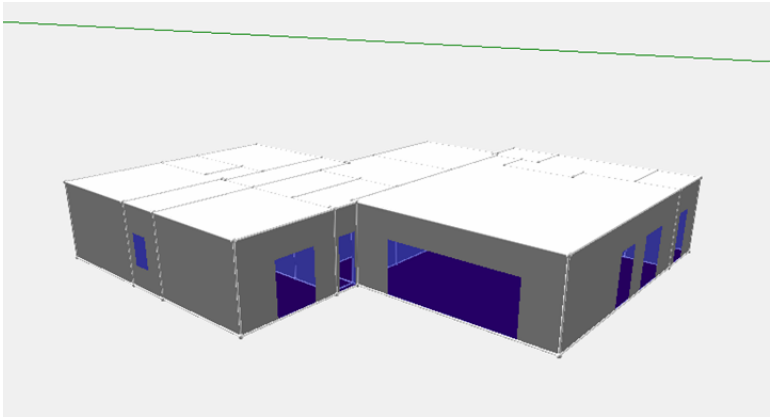

Fig. 3. D calculation model in VABI software

5.2. Calculations performed with VABI software

Table 3

Maximum cooling load per room

No. Room	Room type	Temp [°C]	Sensible cooling load [W]	Latent cooling load[W]	Total cooling load[W]	[W/m^2]	[W/m^2]	Month max	Time max
Living-Kitchen and dining	VG	26	3400	183	3583	49	17	August	11
St-tehnical space/pantry	TR	26	484	0	484	41	15	June	20
Office	VG	26	978	14	992	63	22	June	19
Antreu/hallway	VKR	26	172	0	172	13	5	July	20
Corridor	VKR	26	420	0	420	59	22	June	19
Dormitor/bedroom 1	VG	26	756	14	770	56	20	August	19
Dormitor/bedroom 2	VG	26	743	14	757	41	15	August	19
Dressing2	VG	26	408	20	428	67	24	August	10
Dormitor/bedroom 3	VG	26	305	20	325	20	7	July	8
Dressing3	VG	26	201	20	221	34	12	Ju;y	8

Table 4

Monthly cooling load for building

Time Period	May	June	July	August	September	Max
8	4872	5142	5284	4887	3311	July
9	5020	5344	5439	5337	3849	July
10	5483	5771	5904	5834	4678	July
11	5155	5441	5547	5478	4477	July
12	5328	5505	5606	5626	4857	August
13	5475	5596	5699	5765	5104	August
14	5536	5634	5763	5828	5150	August
15	5399	5536	5656	5709	5009	August
16	4945	5203	5297	5227	4425	July
17	4927	5214	5328	5179	4303	July

Table 5

Daily output Month July

Temp Outside[°C]	Max temp inside cooling [°C]	Internal cooling load [W]	External cooling load [W]	Building Temp variation[W]	Total sensible cooling load[W]	Total latent cooling load[W]	Total cooling load[W]
21.5	26	2141	2845	0	4986	297	5284
23.4	26	1687	3456	0	5142	297	5439
25.7	26	1663	3944	0	5607	297	5904
27.1	26	1024	4226	0	5250	297	5547
28.1	26	1000	4308	0	5309	297	5606
28.9	26	995	4407	0	5402	297	5699
29.6	26	976	4490	0	5466	297	5763
30.4	26	949	4410	0	5359	297	5656
31.0	26	1104	3996	0	5100	197	5297
31.5	26	1148	3983	0	5131	197	5328
31.4	26	1164	4095	0	5260	197	5457
31.0	26	1888	4140	0	6027	267	6295
30.3	26	1922	3932	0	5854	267	6121

Table 6

The maximum cooling load occurs in July at 19

No.Room	Sensible[W]	Latent[W]	Cooling load [W]
Living-bucatarie and dining	1927	183	2110
St-tehnical space and pantry	471	0	471
Office	965	14	979
Antreu/hallway	172	0	172
Corridor	411	0	411
Dormitor/bedroom1	722	14	736
Dormitor/bedroom2	712	14	726
Dressing 2	238	14	252
Dormitor/bedroom3	241	14	255
Dressing 3	168	14	182
Total	6027	14	6295

Table 7

Calculation heat loss residential building ground floor

No.	Room Name	ISSO	Temp [°C]	Transm-ission [W]	Venti-altion [W]	Reheat [W]	Total[2] [W]	Total [W/m^2]	Total [W/m^3]
1	G.S	51	24	370	63	0	433	150	53
2	Living-Bucatatarie /kitchen	51	22	2245	1471	0	3716	51	18
3	ST pantry /hallway	51	22	423	237	0	660	56	20
4	G.S	51	22	361	67	0	428	139	50
5	Birou/ office	51	22	677	313	0	991	63	22
6	Antreu/ hallway	51	22	254	266	0	520	39	14
7	Corridor	51	22	236	137	0	373	53	19
8	Dormitor/ bedroom1	51	22	583	277	0	860	62	22
9	G.S2	51	22	378	97	0	475	108	18
10	Dormitor/ bedroom2	51	22	664	368	0	1033	56	20
11	Dressing 2	51	22	215	128	0	343	53	19
12	Dormitor/ bedroom3	51	22	556	331	0	886	54	19
13	Dressing3	51	22	82	126	0	208	32	12
14	G.S 3	51	24	357	117	0	473	83	32
Total				7400	3999	0	11399	57	20

5.3. Selection of equipment for installations following calculations with VABI software

Equipment selected following the calculations of dynamic simulation modeling (Dynamic Simulation Modeling - DSM) with VABI Elements software for the studied house:

- Vitosol 200-TM vacuum tube collector. TheVitosol 200-TM vacuum tube collector was specially designed for horizontal installation in large systems on flat roofs and for apartment buildings. The absorbers can be rotated at 45 degrees to best reflect the sun's trajectory without increasing shading.
- Mitsubishi Electric PUHZ-SHW140YHA heat pump This outdoor heat pump unit features Zubadan technology, which allows it to maintain its nominal heating power down to -15°C and continue operating down to -28°C.
- Coated domestic hot water calorifier with 2 fixed heat exchangers.

Data have been calculated on following basis: primary circuit at T1 and proper energy source; production of DHW in continue way from 10 °C at t2, DHW that can

be taken in the first 10’ and in the first hour from storage at 60°C, input 10°C and output 45°C, sanitary water according to UNI CTI 8065.

6. Conclusions

This paper presents the method of determining theheating and cooling requirements for a residential building, using the VABI Elements automatic calculation program. For the case study building, the heating and cooling needs were determined, for each room and for the building as a whole. Modeling the building in the VABI program allowed for quick and organized results, even in the case of minor architectural changes that occurred during the project development.[5]#The use of the VABI calculation program represents a useful tool in the calculations of heating and cooling needs, as it offers an optimal perspective through the 3D visualization of the analyzed building and the possibility of analyzing multiple scenarios [8].

References

[1] Eicker, U. (2014). "Energy Efficient Buildings with Solar and Geothermal Resources".Publisher: Wiley. This book provides a detailed look at the use of renewable sources in combination with DSM modeling for energy efficiency in buildings.

[2] Crawley, D. B., Hand, J. W., Kummert, M., & Griffith, B. T. (2008). "Contrasting the capabilities of building energy performance simulation programs". Journal: Building and Environment, vol. 43, no. 4. Publisher: Elsevier. A detailed comparison of various building energy performance simulation programs, including aspects related to DSM.

[3] Strachan, P., Svehla, K., & Heusler, I. (2018). "Building Performance Simulation for Design and Operation". Publisher: Routledge. A comprehensive resource for understanding how simulations can influence the design and operation of buildings.

[4] Hensen, J. L. M., & Lamberts, R. (Eds.). (2011). "Building Performance Simulation for Design and Operation". Publisher: Spon Press. This book explores various methods and applications of building performance simulation, including DSM.

[5] Capozzoli, A., & Serale, G. (2017). "Dynamic simulation models for the evaluation of buildings' energy performance: A review". Journal: Journal of Building Performance Simulation. Publisher: Taylor & Francis. A paper that provides foundational information on energy consumption in buildings and the role of simulation modeling.

[6] Pérez-Lombard, L., Ortiz, J., & Pout, C. (2008). "A review on buildings energy consumption information". Journal: Energy and Buildings, vol. 40, no. 3. Publisher: Elsevier. A paper that provides foundational information on energy consumption in buildings and the role of simulation modeling.

[7] Clarke, J. A. (2001). "Energy Simulation in Building Design". Publisher: Butterworth-Heinemann. This book is a classic and detailed guide for energy simulation in building design, providing the necessary foundations for understanding DSM.

[8] ***, VABI Elements software.

Analysis of engineering solutions implemented for a hotel

Analiza soluţiilor inginereşti implementate pentru un hotel

Vera Danici-Guțul[1], Vladimir Grebinicenco[1], Vera Guțul[1]

[1]Technical University of Moldova
The municipality. Chisinau, str. Ștefan cel Mare 168, Republic of Moldova
E-mail: vera.gutul@acagpm.utm.md, veravutcariov@yahoo.com

DOI: 10.37789/rjce.2024.15.3.15

Abstract. *The purpose of this paper is to analyses the solutions for the heating and domestic hot water supply system for a modernized hotel in the city of Chisinau for the climatic conditions of the Republic of Moldova. In the paper, the implemented solutions were analyses, the investment recovery term was determined. The Republic of Moldova does not have its own energy sources, and the need to implement alternative sources is obvious. In this sense, the use of heat pumps, photovoltaic panels form an energy efficient, economical and more ecological system than any thermal energy generating installation.*

Key words: heating, domestic hot water, heat demand, heat pumps, photovoltaic panels

1. Introduction

The construction sector is one of the largest energy consumers in the Republic of Moldova. The objectives of the state policy in the field of energy are established in the Energy Strategy of Moldova until the year 2030 [1]. The document provides for the increase of security in the energy field, because the Republic of Moldova is affected by such factors as: the politicization of trade in energy resources, the increase in electricity and natural gas prices.

Lower energy consumption and a higher degree of energy and ecological efficiency [2] can be advanced by introducing new technologies (more efficient engineering installations and equipment, buildings with reduced energy consumption, buildings with intelligent heating/cooling systems ...).

Features of heating of hotels, hotels or guest houses up to 500 m^2 are determined by the nature of their operation. As a commercial enterprise, a mini-hotel must bring profit to its owners without compromising the comfort and satisfaction of hotel guests.

- Residential and non-residential premises will have to be heated;
- Warming up should be as fast as possible (the room was empty - you did not heat it, the guest checked in - the room was immediately warmed up);
- Washing dishes in hotels with their own restaurants requires a lot of hot water;

- The maximum consumption of hot liquid will be in the evening and morning, when the majority of guests take a shower; The standard for calculating the rate of hot water consumption among guests is 50 liters per person;
- Room occupancy usually has seasonal fluctuations. In winter you will need a lot of heat, and in summer you will need hot water. Also, in summer it is mandatory to use the air conditioning system.

Operating costs directly affect financial results. Therefore, reducing heating and hot water supply costs in the hotel business is of significant importance. Heat pumps are the optimal heat generators for mini-hotels.

2. Requirements for engineering installations in hotels of engineering installations in hotels and the analysis of the solutions implemented in a Hotel in Chisinau

Heating, ventilation, air conditioning should be designed in accordance with [3, 4, 10]. In hotels of categories “four stars” and above, it is necessary to ensure the operation of engineering systems from at least two separate sources. All heat exchangers and pumping equipment must have a reserve of at least 100%. For hotel premises, a ventilation system with natural and (or) mechanical impulse should be provided. For hotels of categories “four stars” and above, mechanical ventilation should be provided in additional service areas.

Ventilation systems for conference rooms, catering establishments, halls for physical education and recreation, swimming pools, cinema rooms, battery rooms located in hotels must be separate from the ventilation systems of other rooms in these buildings. Air conditioning of hotel rooms should be equipped with local control devices or with programming of heat and humidity parameters. Heating for hotels involves supplying coolants heated to 60 degrees to radiators. For water floors, use liquid up to 35 degrees. Hot water is heated up to 50 degrees. The total liquid consumption will depend on the size of the restaurant and kitchen. Usually this is at least 3000 litters daily. Air heating of a hotel involves a complete refusal of gas or the use of a boiler as a backup energy source. Air-to-water heat pumps operate in frosts down to -15 degrees and are used as primary or additional heating equipment. The system can cool buildings in the summer, that is, it is multifunctional. Hot water supply is available. The heated air is distributed throughout the rooms in the building through ventilation ducts.

In order to analyses the efficiency of the implemented engineering solutions, a hotel located on Ciuflea street, Chisinau municipality was examined. The recently modernized building, in 2020, has: 16 hotel rooms, restaurant for 80 people, breakfast room, bar, offices, dental office, conference room for 150 people, technical and storage spaces in the basement. Height regime: S + P + 2E + M, with the surface - 700 m^2.

During the modernization of the building, the following measures were implemented: thermal insulation of the external wall, of the ceiling of the building and the windows were changed. The calculation of the heat requirement for the building

was made for two boundary conditions of outdoor air temperature -16°C and 0.6°C at a constant indoor air temperature of 20°C. The -16°C/20°C module was selected to determine the required power of the thermal plant; and the 0.6°C/20°C mode was selected to estimate the amount of heat needed throughout the entire heating season to maintain the set indoor temperature. The outside air temperature of -16°C is the temperature of the coldest 5 days, and 0.6°C corresponds to the average temperature of the heating season for Chisinau, the duration of the heating period being 166 days. The heat requirement for the entire building surface during the cold period of the year is 42 kW for the -16°C/20°C module, and 22.5 kW for the 0.6°C/20°C module, respectively. The heat requirement for the heating season, according to calculations, is: 89640 kW.

Until the modernization works are carried out, there was a problem with achieving and maintaining comfortable temperature in the offices and living spaces in the building. The thermal plant could not cope, and the gas consumption was very high. In 2021, two Split type heat pumps, manufacturer NIBE, model AMS 10-16 + HBS 05-16, each of 16 kW - were connected to the existing heating plant, equipped with a 49 kW gas boiler, which is used only for the winter season, for heating (Fig. 1). An amount of 157 thousand lei was invested for a set, including installation and accessories. The pumps worked very economically, quietly. Invoice amounts have decreased considerably compared to previous years. The owners made the decision, in 2023, to install the third heat pump in the existing system, fully providing the heat required.

The heat pumps are connected in cascade/parallel and controlled by NIBE KVR 10-30 control panels.

a) b)

Fig. 1. a) NIBE heat pumps connected to the existing heating plant;
b) External blocks of the NIBE heat pump

Fig. 2 shows the dependence of the heating power and COP of these pump models according to the outside air temperature for different temperatures of the heating agent.

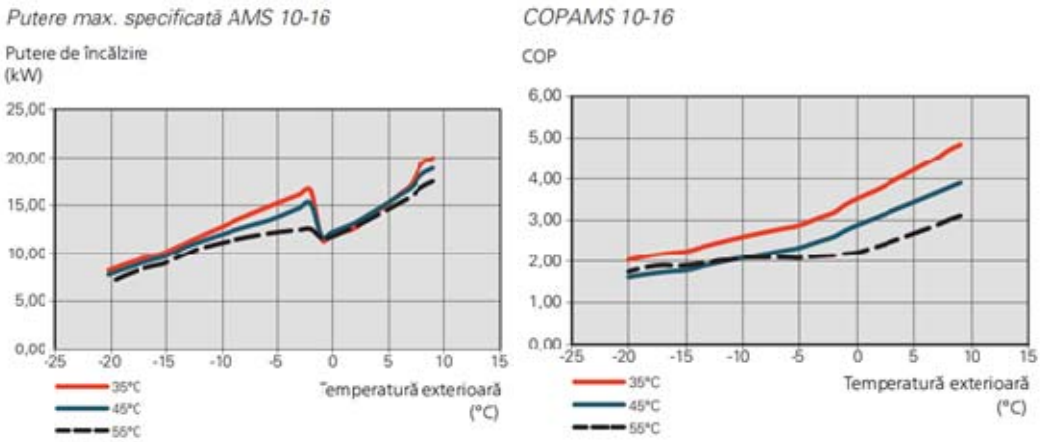

Fig. 2. Dependence of the heating power and COP depending on the outside air temperature for different temperatures of the heating agent [5]

From Fig. 2, it can be seen that with the decrease in the temperature of the outside air, the thermal power of the heat pump also decreases. At the same time, the electricity consumption increases, respectively the COP decreases. At temperatures lower than - 5 ℃, the COP coefficient decreases.

Panel-type steel radiators are used as heating elements. The pipes are made of polypropylene insulated pipe.

a) b)

Fig. 3**.** a) Solar panels with vacuum tubes for the preparation of DHW
b) Boilers with 2 coils for DHW preparation

When modernizing the building, it was invested in solar panels for the preparation of domestic hot water (DHW), 3 solar panels of 15 vacuum tubes, which prepare DHW in 3 boilers of 200 liters with 2 coils (Fig. 3 b). The amount of the investment reached 140 thousand lei. Showing a good result on the electricity consumption bill for the preparation of domestic hot water, in 2023, another solar

panel of 30 vacuum tubes with a 300-liter boiler was invested and mounted for 60 thousand lei (Fig. 3. a).

Taking into account the high consumption of electricity, approximately 95% compared to gas consumption, for heating and other needs, in the year 2023, the owner invested in the photovoltaic panel system which includes: 40 panels x 415 W, Inverter 25 kW, accessories for installation, design, installation and commissioning services, in the amount of 190 thousand lei. The installed panels have a total power of 16.6 kW of the 30 kW allowed by the Inverter. Since the electricity consumption is not fully covered by the photovoltaic system, the owner plans to add 30 more solar panels to the system [9].

3. Calculation of the recovery period of implemented solutions

Considering that a heat pump can be used both for heating the building and for cooling it, in the given paper a comparative analysis of the efficiency of heat pumps for heating systems only was made. To perform the calculations, the following initial data are required: initial investments and operating expenses.

When comparing the heating system between the heat pumps and the gas boiler, the prices set by the National Agency for Energy Regulation of the Republic of Moldova for the 2023-2024 heating season were used.

In the calculations, the following parameters were used:

- Calorific value of natural gas: 33.5 MJ/m^3 (9.3 kWh/m^3);
- The price for 1 m^3 of gas is 18.07 lei [6];
- The price for 1 kWh of electricity: 2.39 lei [7].

As an initial investment, the cost of the entire system was taken into account, which includes:

- 3 heat pumps, auxiliary equipment, accessories for heat pump connection, installation and commissioning;
- gas condensing boiler.

Knowing the required heat produced by the thermal power plant for a year and the capacity of the heat pump given by the manufacturer [5] will determine the amount of electricity required by the heat pump to produce the same amount of heat. Natural gas consumption will be determined based on the condition that 1 m^3 of natural gas produces 9.3 kWh/m^3 of heat.

The results of the calculations are presented in Tables 1 and 2.

Exchange rate: 1 Euro=19.30 lei, according to the National Bank of Moldova data on the day of the calculation [8].

Table 1

Electricity consumption emerging from the data producers and heat demand

The analyzed object	The heat requirement for the cold period (0.6°C/20°C), kWh	COP heat pump to t_e =0,6 °C	Electricity consumption in the cold period for heating, kWh
hotel	89640	2,95	30386

Tablel 2

The investment recovery period for the heat pump

Expenses for the heating system	Air-water heat pump	Thermal power plant 49 kW
1.Initial investments, lei	A=471000	B=0, existence
The amount of thermal energy required for the cold period of the year, kWh	89640	89640
The amount of electricity/gas required for the cold period of the year	30386 kWh electricity	10953 m^3 natural gas
2. Operating expenses, lei	X=72622	Y=197920
Investment recovery period, years T=(A-B)/(Y-X)	The investment recovery period for the heat pump is 3 years 274 days	

From Table 2 it can be seen that the recovery period is very small. This is due to high natural gas prices. Until the price increase in 2021, this investment would recover in 7-8 years, which is still a good result.

Part of the electricity consumed would be recovered with the help of the purchased photovoltaic system. The authors made a simulation of the production of electric current by the photovoltaic system for the examined hotel with the help of software ver.5.2, PVGIS [9], the results are presented in Fig. 4.

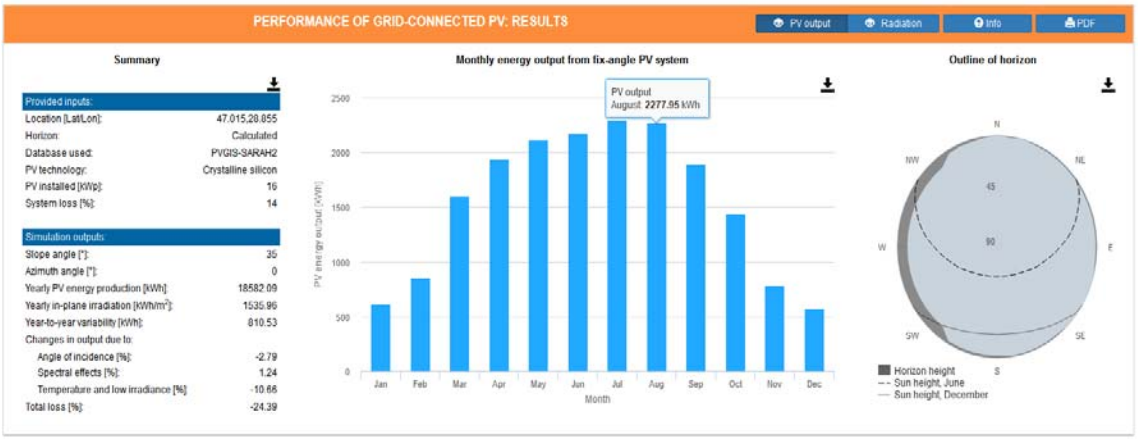

Fig. 4. Simulation of the production of electric current of the photovoltaic system for the hotel [9]

From the results obtained in Fig. 4 it can be seen that with the photovoltaic system it would produce approx. 5 thousand kWh of electricity consumed in the heating season, which is 12.7 thousand lei at current prices, the recovery period being - approx. 15 years. But which is not correct, because in the cold season, photovoltaics has a low production, and in the warm season, the production increases considerably. During the warm period of the year, electricity is consumed for air conditioning, ventilation, lighting, office equipment, etc. Based on the knowledge and experience gained, an investment for such a photovoltaic panel system is recouped in 7-8 years.

4. Conclusions

Following the study, the following conclusions can be made:

- heat pumps are good solutions for hotels, only on the condition that these buildings are new and were built according to the norms in force, or energy efficiency works are planned for the building;
- if the heat pump is used only for heating a building, the investment recovery period is 3-4 years. Considering the unstable gas prices, the increasingly warm climate during the cold period of the year, the choice in favor of heat pumps is obvious;
- air-water heat pumps are able to provide heating/cooling of buildings ensuring comfortable conditions throughout the year, have a long lifespan and require minimal maintenance;
- it is beneficial to use heat pumps connected to photovoltaic panels, especially for the summer period when operating in cooling mode.

References

[1] HG Nr. 102 din 05-02-2013. Cu privire la Strategia energetică a Republicii Moldova până în anul 2030. https://www.legis.md/cautare/getResults?doc_id=68103&lang=ro.
[2] European Climate Pact, 2023. https://climate-pact.europa.eu/about/climate-change_ro.
[3] GOST 30494 "Здания жилые и общественные. Параметры микроклимата в помещениях. 2011.
[4] NCM E.04.01:2017 „Protecția termică a clădirilor", 2017.
[5] NIBE ENERGY SYSTEMS. Air/Water Heat Pump NIBE AMS 10-16. Installer Manual. 2018. HB EN 1826-3331942. https://nibe.ru.
[6] Prețurile reglementate pentru furnizarea gazelor naturale. https://anre.md
[7] Tarifele/prețurile reglementate ale titularilor de licență din sectorul electroenergetic. https://anre.md
[8] Ratele de schimb (curs valutar). https://www.bnm.md/
[9] Photovoltaic geographical information system. PVGIS ver.5.2, software. https://re.jrc.ec.europa.eu.
[10] NCM C.01.12:2018. Clădiri şi construcții publice. Общественные здания и сооружения; Public buildings. Informații generale.

Strategies for Achieving a Net-Zero Carbon Footprint in Wastewater Systems

Strategii pentru atingerea unei amprente de carbon net-zero în sistemele de canalizare și epurarea apelor uzate

Cristina Iacob[1], Anagabriela Deac [1], Dan Mureșan[1], Andrei Bolboacă[1], Teodor Chira[1]

[1] Technical University of Cluj-Napoca
St. Memorandumului 28, Cluj-Napoca, Romania
E-mail: cristina.iacob@insta.utcluj.ro, anagabriela.deac@insta.utcluj.ro, muresan.dan@insta.utcluj.ro, andrei.bolboaca@insta.utcluj.ro, teodor.chira@insta.utcluj.ro

DOI: 10.37789/rjce.2024.15.3.16

Abstract. *The world is currently undergoing a transition from a linear economy to a circular one, with the wastewater sector offering numerous opportunities for decarbonization and mitigating the impacts of climate change. Urban wastewater systems are significant sources of greenhouse gas emissions, highlighting the need for a shift towards net-zero carbon states. This paper aims to provide insights into minimizing carbon footprints and achieving net-zero carbon conditions in wastewater systems by examining sources of GHG emissions and exploring effective mitigation strategies. Strategies for decarbonization include operational optimization, energy and resource recovery, source separation systems, and decentralization. Implementing these strategies is crucial for reducing the impacts of climate change and achieving sustainability goals in wastewater systems.*

Key words: wastewater systems, wastewater treatment, GHG emissions, mitigation, strategies, carbon footprint, climate change

1. Introduction

Currently, the world is undergoing a transition from a linear economy to a circular one. In the wastewater sector, numerous opportunities and strategies exist for decarbonization and mitigating the impact of climate change. Human activities have driven approximately 1.0°C of global warming above pre-industrial levels. If current trends persist, global warming is expected to reach 1.5°C between 2030 and 2052 [1]. Warming from anthropogenic emissions will persist in the long term, causing climate changes such as sea level rise, extreme weather, ecological imbalance, economic and political insecurities. These risks are influenced by various factors including the

magnitude and rate of warming, geographic location, levels of development and vulnerability, and the choices made regarding adaptation and mitigation strategies.

Greenhouse gases (GHGs) contribute to global warming by absorbing energy and limiting the escape of this energy into space. They act like a blanket, insulating the Earth and retaining heat within the atmosphere [2]. Urban wastewater systems, which include sewer networks, wastewater treatment facilities and receiving water bodies, are sources of GHG emissions that contribute to climate change. Removing organic contaminants and nutrients has been the traditional focus of biological wastewater treatment, but nowadays there is a shift toward integrated operations that prioritize resource recovery and reaching a net-zero carbon state.

Wastewater holds significant energy and resource potential, with biogas and nutrient recovery opportunities. Efforts to integrate water, energy, sanitation, and carbon management are crucial, especially in the face of climate change. In wastewater systems, net-zero transitions requirements include energy balance, greenhouse gas emissions, chemical use, and sludge disposal. Reducing chemical and transportation impacts, streamlining processes, and optimizing energy use are all necessary to achieve net-zero carbon emissions.

2. GHG emissions in the wastewater systems

According to international protocols and standards [3], GHG emissions can be categorized in:

- Scope 1 emissions, which are direct GHG emissions arising from sources controlled or managed by the reporting entity.
- Scope 2 emissions, which are indirect GHG emissions associated with production of energy that has been purchased by the reporting entity (e.g. electricity, steam, heat, or cooling).
- Scope 3 emissions represent all other indirect emissions, which may involve emissions linked with material production, including extraction of raw materials and the production processes of purchased materials, fuels, or services.

Figure 1 illustrates the classification presented above.

The greenhouse gas emissions linked to the water supply and wastewater cycle must take into consideration all emissions occurring throughout the process. This includes water withdrawal, treatment, and transportation, as well as consumer use, disposal, emissions from sewer networks, wastewater treatment, and final discharge. The waste industry, which includes wastewater systems and landfills, is responsible for around 3% of all anthropogenic greenhouse gas emissions worldwide [5].

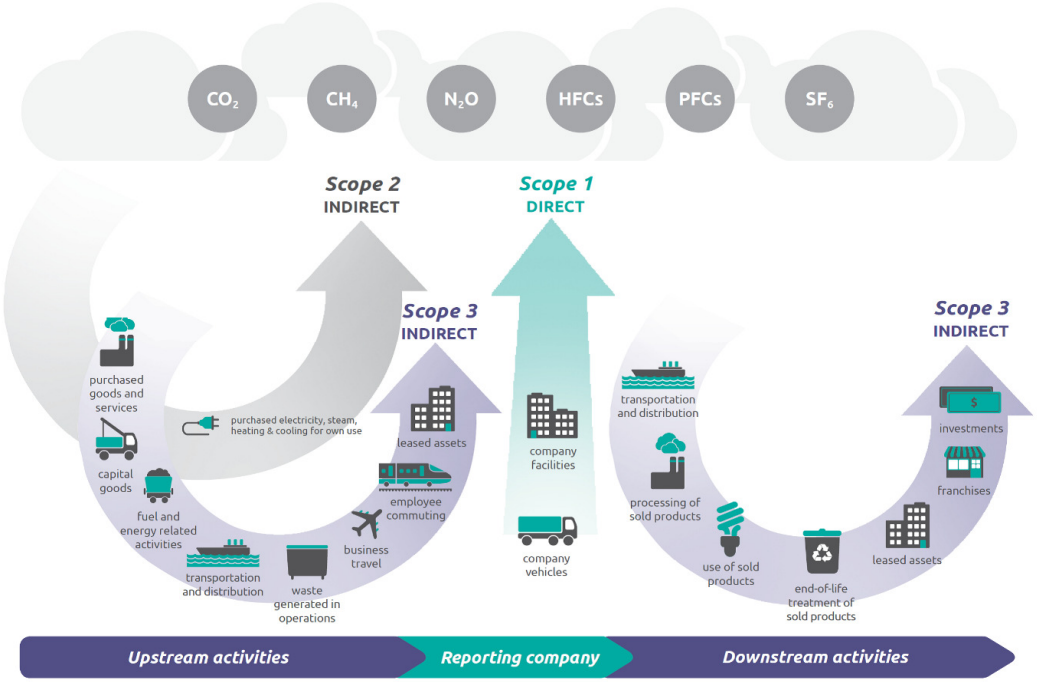

Fig. 1. Overview of GHG Protocol scopes and emissions [4]

2.1. Scope 1

Scope 1 emissions in the wastewater sector include both wastewater collection and treatment. The collection segment involves direct gas emissions - CH4, N2O, and H2S, that are released in sewers in the absence of oxygen.

The emission of gases originates from biological processes happening inside sewer pipes, prompted by the presence of organic matter, nutrients, and microorganisms. These processes occur in anaerobic, anoxic, or aerobic environments and emanate from sewer sediments (which might accumulate at the base of sewer pipes due to variations in flow), from the water volume, and from biofilms forming on pipe walls.

Scope 1 emissions from the wastewater treatment plants (WWTPs) involve the production of carbon dioxide (CO_2), methane (CH_4), and nitrous oxide (N_2O) arising from the biological wastewater treatment process. These GHG emissions should be controlled and reduced due to their high global warming potential [6].

The Global Warming Potential (GWP) is used to facilitate comparisons of the global warming impacts of various gases. Essentially, it measures how much energy the emissions of one ton of a gas will absorb over a specified period, typically 100 years, relative to the emissions of one ton of carbon dioxide (CO_2). A higher GWP indicates that a given gas has a greater warming effect on Earth compared to CO_2 over that time frame [2]. A carbon dioxide equivalent or CO_2 equivalent, abbreviated as CO_2-eq is a metric measure used to compare the emissions from various greenhouse gases on the basis of their global-warming potential (GWP), by converting amounts of

other gases to the equivalent amount of carbon dioxide with the same global warming potential [7].

CO_2 emissions arise from both the biological treatment process and on-site electricity consumption. In the biological treatment process, organic carbon from wastewater is either incorporated into biomass or oxidized to CO_2.

Promoting energy efficiency in the operation of treatment facilities will help decrease CO_2 emissions from the site, leading to a reduction in treatment costs by boosting energy savings. This approach not only enhances cost-effectiveness but also minimizes the environmental footprint of operational activities.

Nitrous oxide (N_2O) and methane (CH_4) are both potent GHG gases. When emitted to the atmosphere, they significantly contribute to climate change. According to Eurostat, the GWP for methane is 25 and for nitrous oxide 298 [7].

These emissions are sometimes omitted from carbon footprint assessments in the wastewater sector, emphasizing the necessity for a more thorough consideration to truly attain zero emissions.

Globally, wastewater treatment is the fourth largest sector responsible for N_2O emissions and accounts for around 3–10% of all atmospheric N_2O emissions [8].

The nitrification and denitrification processes employed for removing nitrogenous compounds from wastewater lead to the emission of N_2O. The primary source of these emissions is the activated sludge process, where nitrifying bacteria produce N_2O under aerobic or anoxic conditions. While N_2O production in aerobic conditions is solely attributed to ammonia-oxidizing bacteria, both nitrite-oxidizing and ammonia-oxidizing bacteria contribute to its generation under anoxic conditions. Additionally, a small amount of N_2O is produced by the grit and sludge storage tanks onsite.

The primary sources of CH_4 emissions in wastewater treatment facilities are the anaerobic digestion process and its component units, such as the centrifuge, buffer tank for digested sludge, storage tank for dewatered sludge, and exhaust gas from the cogeneration plant.

The sludge processing units contribute to 72% of methane emissions from the wastewater treatment plant, and approximately 1% of the COD (chemical oxygen demand) entering the plant is emitted as methane [5].

Globally, the wastewater sector contributes to roughly 5–7% of anthropogenic CH4 emissions, ranking fifth among major sources, following livestock (32%), oil and gas (25%), landfills (13%), and coal mining (11%) [8].

2.2. Scope 2 – GHGs from energy use

Energy is the main operating cost of wastewater treatment. The North American WWTPs consume approximately 1–4% of the total energy production, and in Europe, the consumption is approximately 1% [9].

Electricity is needed throughout the wastewater system for different operations, which include sewage collection and wastewater treatment and sometimes water reuse. WWTPs are often designed to operate using gravity flow whenever possible, thus

ensuring enhanced process security. The wastewater is collected from consumers through the sewer network. Depending on the local ground profile and the position of the wastewater treatment plant, pumping might be necessary for the water to reach the treatment facility. Here, the water quality is corrected in accordance with the prevailing regulations. The treated wastewater is then discharged into a local receiving water body, usually by gravitation. Hence, energy use in wastewater systems is determined by the treated flow, pollutant load, final effluent quality, the types of treatment process employed, level of monitoring and automation and experience of the operations staff.
The processes that consume the greatest amount of energy in the wastewater treatment plant are:

- biological treatment, conventional or advanced, especially aeration and sludge recirculation.
- the sludge line, where conventional or advanced anaerobic digestion is implied, sludge pumping, sludge drying and dewatering.

Scope 2 GHG emissions also include energy generation in the wastewater treatment plant. Biomethane, sometimes called *green gas,* is an effective and environmentally beneficial substitute for natural gas. Biomethane is an enhanced form of biogas, obtained by the removal of water vapor, hydrogen sulfide, and carbon dioxide. Because it offers the possibility to manage organic waste, provide clean energy, and find novel applications in both urban and rural locations, biomethane is increasingly being used as a carbon-neutral fuel. Nowadays, a lot of large capacity WWTPs collect biogas resulting from the anaerobic digestion of sludges. After that, the biogas can be gathered and utilized to run a combined heat and power (CHP) plant, which can produce steam or hot water as well as electricity that can be used internally at the facility or exported to the power grid.
Even though more complex processes are needed, that demand more energy to run, the extra energy that is created as heat and power from the extra biogas produced, results in a net reduction in greenhouse gas emissions.

2.3. Scope 3 – GHGs from energy use

Scope 3 emissions arise from activities both upstream and downstream of the wastewater system value chain. The categories typically encompassed by scope 3 emissions include:

- purchased goods and services;
- activities related to fuel and energy;
- transportation and distribution, including both upstream and downstream processes;
- waste treatment;
- employee business travel and commuting;
- lease or hire of equipment;
- use of sold products;

- end-of-life treatment of sold products;

As the focus now shifts to net zero emissions and complete responsibility, more organizations are examining their entire value chain to determine the operation's total greenhouse gas effect. Water and wastewater organizations could reduce overall GHG emissions by influencing their suppliers and working with vendors who fully account for their GHG emissions.

3. Strategies and opportunities for decarbonization

Collecting, transporting, and especially treating wastewater to meet the quality standards set by environmental regulations constitute the most energy-intensive aspect of the water infrastructure sector. However, it also represents the sector with the greatest potential for decarbonization or achieving carbon neutrality. There are numerous key opportunities for decarbonization through optimization in wastewater systems. A few of these are briefly described below.

3.1. Operational optimization and control strategies

The opportunities for decarbonization within wastewater systems include various levels of operation, from pumping to sludge treatment [5]. These are shortly presented below.

Wastewater Pumping: Pumping operations, from collecting to effluent, represent a significant portion of energy use. Strategies for reducing energy consumption include using variable frequency drives (VFDs) and smaller pumps to adapt to changing flow rates, conducting pump maintenance to optimize performance, implementing pumping controls such as flow management, and utilizing data-driven strategies for economic and energy benefits.

Secondary Treatment: Secondary treatment consumes substantial energy, particularly for aeration and ammonia oxidation. To reduce the carbon footprint, feasible strategies involve exploring alternative carbon capture methods, maintaining aeration systems for peak performance, monitoring dissolved oxygen and nitrogen species in real-time, and controlling emissions like N_2O.

Sludge Treatment: Decarbonization opportunities in sludge treatment focus on generating more biogas for energy recovery through improved operations, minimizing fugitive methane emissions, reducing flaring of unused biogas, and decreasing chemical usage in sludge concentration processes.

At whole facility level operational strategies include optimizing peak flow and load management and considering the use or reduction of chemicals and additives in plant operations.

Overall, decarbonization involves implementing a combination of strategies across various operational levels to achieve significant reductions in energy use and carbon emissions.

3.2. Energy and resource recovery

Various energy extraction technologies can be used to fit existing WWTPs. These include options like anaerobic digesters or membrane reactors, as well as processes for recovering energy from salinity gradients or osmosis, along with the utilization of fuel cells. These adaptations aim to achieve net-zero carbon emissions. Below are some methods for enhancing operation in anaerobic digestion (AD) technologies and optimizing sludge management, along with a renewable hybrid process for recovering energy from highly saline brine and treated wastewater effluents.

In recent decades, **anaerobic digestion** (AD) has been employed in WWTPs to stabilize sludge while generating biogas. This approach aims to attain energy and carbon neutrality in medium and large capacity municipal WWTPs. AD offers multiple advantages, including the use of energy from produced biogas - as heat or electric power, the potential to recover valuable nutrients from the liquid stream in the form of struvite or other fertilizer products, a decrease in the amount of sludge requiring disposal, and an improvement in the quality of biosolids for land application. On the other hand, AD use in municipal wastewater facilities presents a few challenges such as the possibility of process instability and failure, the need for personnel with training to optimize the process, odor problems, and the limited financial returns from biogas or biosolids.

There are several methods to improve anaerobic digestion (AD) systems in municipal wastewater facilities. Some of these methods include:

- sludge pretreatment for enhancing the overall rate of anaerobic energy conversion by increasing the surface area of solid particles, improving biogas production, and reducing volatile solids.
- providing optimal conditions for microbial activity and biogas production by adjusting parameters including temperature, pH, and hydraulic retention time, resulting in higher energy conversion efficiency.
- use of anaerobic co-digestion by adding co-substrates such as food waste, fats, oils, and grease (FOG), or agricultural residues to increase organic loading and improve biogas yield.
- utilizing biogas effectively for obtaining heat or electricity minimizes the need for using fossil fuels, which lowers carbon emissions from the production of energy.
- employment of nutrient recovery technologies like struvite recovery from centrate might reduce the demand for synthetic fertilizers and reduce the carbon emissions associated with their manufacturing.
- installing methane capture systems to prevent the release of methane into the atmosphere; the captured methane also represents a sustainable energy source, which allows an additional reduction of the carbon footprint.
- a better management of digestate, which is the material left over after anaerobic digestion. Reducing methane emissions during storage and application of digestate can also help reduce the overall carbon footprint.

Pretreatment of sludge before anaerobic digestion is needed to enhance the efficiency of energy conversion. There are various existing pretreatment technologies, such as thermal, chemical, mechanical, and electrical methods, that aim to increase the surface area of solid particles, improve biogas production, and reduce volatile solids. Thermal pretreatment processes like CAMBI™ and EXELYS™ have shown promise in improving anaerobic digestion performance, but their widespread adoption faces challenges such as uncertain net benefits and operational issues related to toxicity, odors, and maintenance [5].

Unintended negative effects also need to be carefully evaluated, such as how thermal pretreatment affects dissolved organic nitrogen and if pretreatment techniques are feasible for mixed waste streams.

Further optimization, economic analysis, and mitigation of operational challenges are necessary to promote the widespread implementation of sludge pretreatment technologies in anaerobic digestion processes.

Salinity gradient energy (SGE) recovery processes

The integration of SGE recovery techniques into WWTPs offers an opportunity to reduce the carbon footprint by producing renewable energy from resources that would otherwise be wasted and reducing dependency on fossil fuel-based energy sources.

SGE recovery processes, also known as osmotic power or blue energy, harness the energy created from the difference in salt concentration between two fluids. It is the thermodynamic reverse of using energy to desalinate saline water [5].

The energy generated when the low-concentration stream, treated wastewater, and the pre-treated high-concentration stream are brought into contact in the reverse electrodialysis membrane module is used to self-power the reclamation treatment performed in the treatment facility (see fig.2).

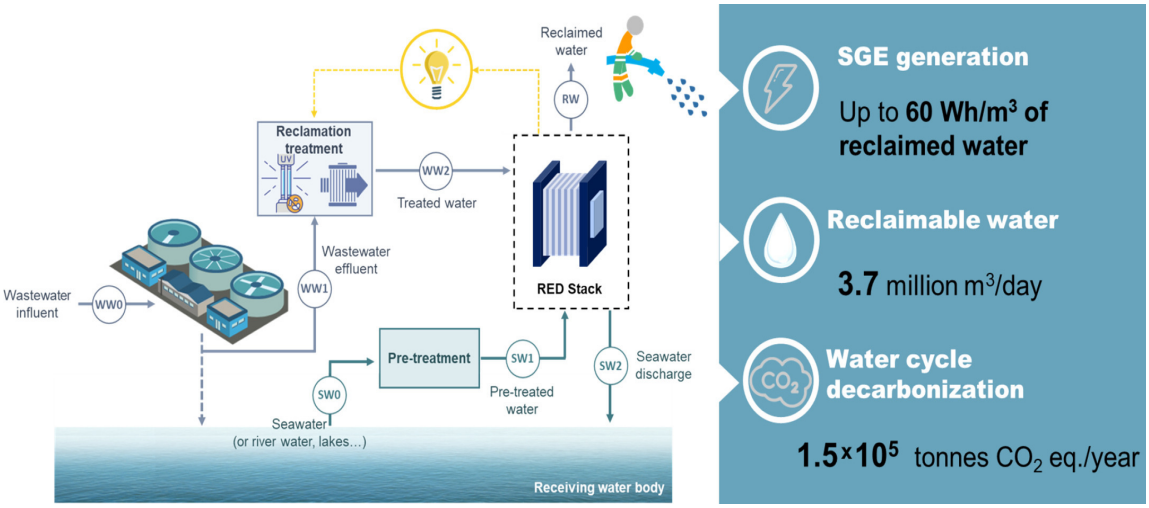

Fig. 2. Salinity gradient energy (SGE) recovery processes flow diagram [10]

3.3. Thermal energy from wastewater

The integration of thermal energy recovery from wastewater with modern district energy systems is a key aspect of sustainable urban heating solutions. Traditional district heating systems, dating back to the 19th century, relied on high-temperature steam or hot water produced through combustion of primary energy sources like coal or natural gas. However, advancements in district heating technology have enabled the utilization of low-grade thermal energy sources, including wastewater, for heating purposes.

These modern district heating systems operate at lower temperatures than their predecessors, allowing for the integration of heat recovery from municipal wastewater. Using heat pumps, thermal energy is extracted from passing sewage and transferred to a secondary hot water loop within the district heating system. This recovered heat is then circulated to end-use systems, contributing to the overall heating needs of connected buildings (see fig.3).

Modern district energy systems may significantly reduce greenhouse gas emissions while offering effective and sustainable heating solutions for urban areas by using wastewater as a thermal energy source.

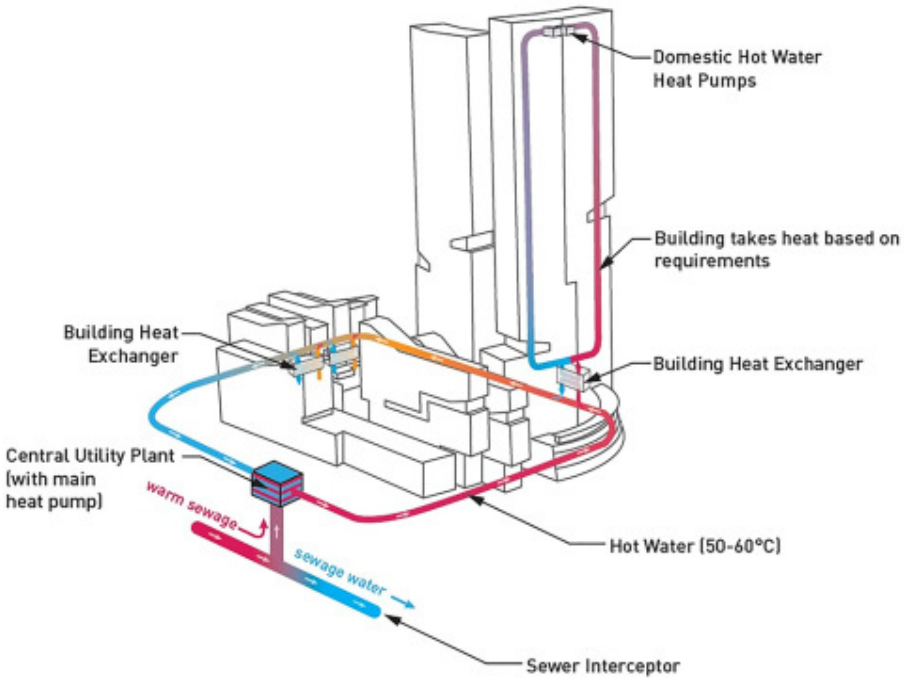

Fig. 3. Schematic of a district heating system sourced to a wastewater interceptor and serving district buildings with building heat and hot water. [5]

3.4. Source separation systems and decentralization.

Source separation systems involve segregating urine and black water (BW) from wastewater, allowing for more efficient nutrient recovery and reducing greenhouse gas (GHG) emissions (see fig.4).

Source separation systems have the potential to enhance the efficiency of wastewater treatment processes, reduce GHG emissions, and improve nutrient recovery, contributing to environmental sustainability.

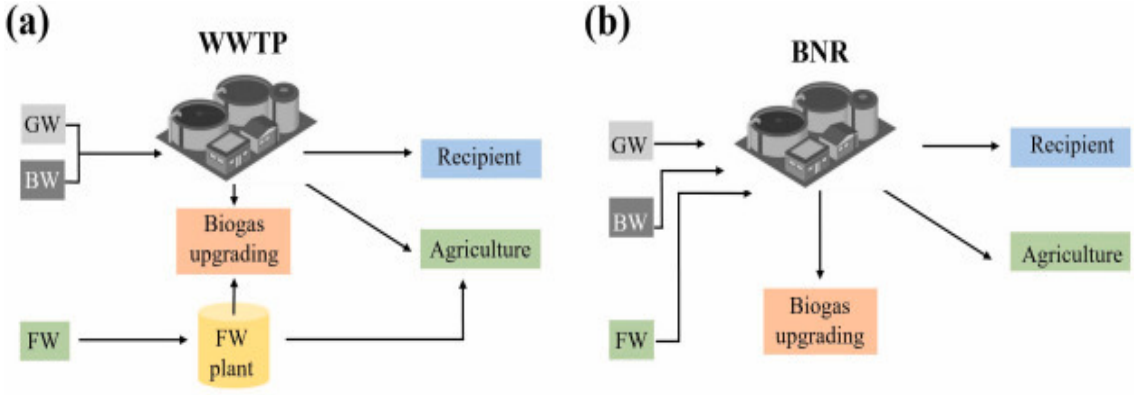

Fig. 4. (a) Conventional systems vs (b) source separation system of wastewater treatment. GW- greywater; BW- blackwater; FW- food waste; BNR- biological nutrient removal [8].

Decentralized wastewater systems have several benefits, including reducing the significant initial investment and operation costs, encouraging the reuse of wastewater, generating employment, and making better use of available space and energy.

These units, which are positioned close to the source of wastewater generation and adapted to specific site conditions, can operate independently or in conjunction with centralized wastewater systems.

Studies suggest that decentralized systems can significantly decrease energy and capital invested in sewage collection and transportation. Natural treatment technologies can be applied, simplifying operations, and reducing costs, particularly beneficial for middle- and lower-income countries. Initiatives like DEWATS aim to implement decentralized treatment and sanitation in developing countries, providing reliable operation and stable effluent quality without technical energy inputs.

4. Conclusions

The transition from a linear to a circular economy presents significant opportunities for decarbonization and mitigating climate change impacts in the wastewater sector.

Understanding and addressing greenhouse gas (GHG) emissions in wastewater systems is essential for reducing climate change and achieving sustainability goals.

By dividing emissions into three categories—Scope 1, Scope 2, and Scope 3—we can identify their sources and develop strategies for reduction.

This paper has explored various aspects of GHG emissions in wastewater systems, including sources, classifications, and impacts, while also presenting mitigation strategies and opportunities for decarbonization.

Strategies towards carbon neutrality include optimizing operations, recovering energy and resources, and integrating cutting-edge technology like thermal energy from wastewater and salinity gradient energy recovery.

By implementing these strategies, wastewater facilities can significantly reduce the carbon footprint of wastewater systems, mitigate climate change impacts, and move towards a more sustainable and resilient future.

References

[1] IPCC – „Global Warming of 1.5°C. An IPCC Special Report on the impacts of global warming of 1.5°C above pre-industrial levels and related global greenhouse gas emission pathways... „ Cambridge University Press, Cambridge and New York, 2018
[2] https://www.epa.gov/ghgemissions/understanding-global-warming-potentials
[3] https://ghgprotocol.org/
[4] Greenhouse Gas Protocol (WRI, WBSCD) - „Corporate Value Chain (Scope 3) Accounting and Reporting Standard"
[5] Zhiyong Jason Ren, Krishna Pagilla – „Pathways to Water Sector Decarbonization, Carbon Capture and Utilization", IWA Publishing, June 2023
[6] Giorgio Mannina et al. - „Greenhouse gas emissions from integrated urban drainage systems: Where do we stand?", Journal of Hydrology, Volume 559, 2018.
[7]***, Glossary:Carbon dioxide equivalent - Statistics Explained (europa.eu), Available at: https://ec.europa.eu/eurostat/statistics-explained/index.php?title=Glossary:Carbon_dioxide_ equivalent
[8] Mojtaba Maktabifard et al. – „Net-zero carbon condition in wastewater treatment plants: A systematic review of mitigation strategies and challenges", Renewable and Sustainable Energy Reviews, Volume 185, 2023.
[9] Santos, E.,Albuquerque, A., Lisboa, I., Murray, P., Ermis, H. – „Economic Assessment of Energy Consumption in Wastewater Treatment Plants: Applicability of Alternative Nature-Based Technologies in Portugal", Water, Volume 14, 2022.
[10] T. Sampedro, L. Gómez-Coma, I. Ortiz, R. Ibañez - „Unlocking energy potential: Decarbonizing water reclamation plants with salinity gradient energy recovery", Science of The Total Environment, Volume 906, 2024
[11] Rani, A., Snyder, S.W., Kim, H. et al.– "„Pathways to a net-zero-carbon water sector through energy- extracting wastewater technologies", npj Clean Water 5, 49, 2022.
[12] Rissman J., Bataille C., Masanet E., Aden N., Morrow W. R., Zhou N. and Williams E. D. (2020). Technologies and policies to decarbonize global industry: review and assessment of mitigation drivers through 2070. Applied Energy, Volume 266
[13] European Environment Agency - Annual European Union greenhouse gas inventory 1990–2021 and inventory report 2023
[14] Sudeep Nair, Biju George, Hector M. Malano, Meenakshi Arora, Bandara Nawarathna – „Water–energy–greenhouse gas nexus of urban water systems: Review of concepts, state-of-art and methods", Resources, Conservation and Recycling, Volume 89, 2014.
[14] Elena C. Blanco, Mariano Martín, Pastora Vega –"Achieving energy self-sufficiency in wastewater treatment plants by integrating municipal solid waste treatment: A process design study in Spain", Journal of Environmental Chemical Engineering, Volume 11, Issue 5, 2023
[15] M. P. Wilson ,F. Worrall – "The heat recovery potential of 'wastewater': a national analysis of sewage effluent discharge temperatures", Environmental Science: Water Research & Technology, Issue 10, 2021

Shifting to low GWP alternatives in commercial refrigeration

Trecerea la alternative cu GWP scăzut în refrigerarea comercială

Adrian Mihai[1]

[1]University Politehnica Timisoara
Victoriei Square, no.2, Timisoara, Romania
E-mail: adrian.mihai@student.upt.ro

Coordinator: Adriana Tokar, Daniel Muntean

E-mail: adriana.tokar@upt.ro, daniel-beniamin.muntean@upt.ro

DOI: 10.37789/rjce.2024.15.3.17

Abstract
Adoption of the new regulation 2024/573 of the European Parliament and of the Council, due to the increase in global warming, commercial refrigeration adapts, together with the reduction of the possibility of using refrigerants with a GWP greater than 150 units starting from 2025. In this way, the transition to refrigerants with GWP less than 150 units becomes mandatory for manufacturers of stationary refrigeration equipment. Refrigerants with GWP below 150 units are from category A2L (slightly flammable refrigerants) and A3L (flammable refrigerants) and this implies greater safety measures in installation and service than in the case of refrigerants from category A1L (non-flammable refrigerants).

Key words: *commercial refrigeration, low GWP, A2L refrigerants, A3L refrigerants.*

1. Introduction

The refrigerants with GWP greater than 150 units that we know now are towards the end of their service life according to regulation 573/2024 of the European Parliament and the Council [1], but also the beginning of a new stage in the development of refrigerants and the equipment that uses them. At the same time, the technological advance allows us to use refrigerants with low GWP such as CO2 for a long time from now, but from an economic point of view it is known that it is not sustainable in all economies, so refrigerants in the A2L category (only slightly flammable) with GWP below 150 units represents a viable solution with immediate application in commercial refrigeration (Fig. 1) [2].

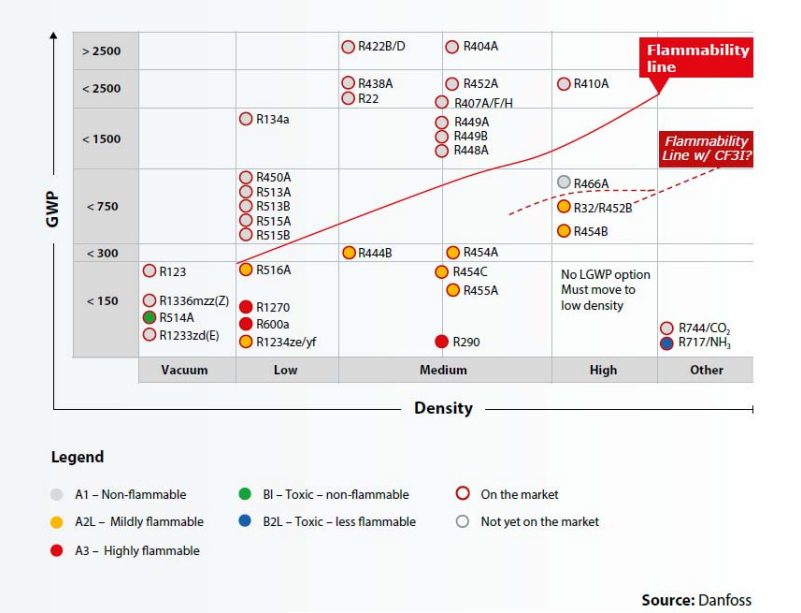

Fig.1. Main refrigerants in the market [2]

2. Case study

This study shows the differences between an installation using refrigerant R404A – A1L with GWP -AR4, 3922 units and an installation using refrigerant R455A -A2L with GWP -AR4, 148 units. Both of them are installed on the same type of cold room Fig.2 [3].

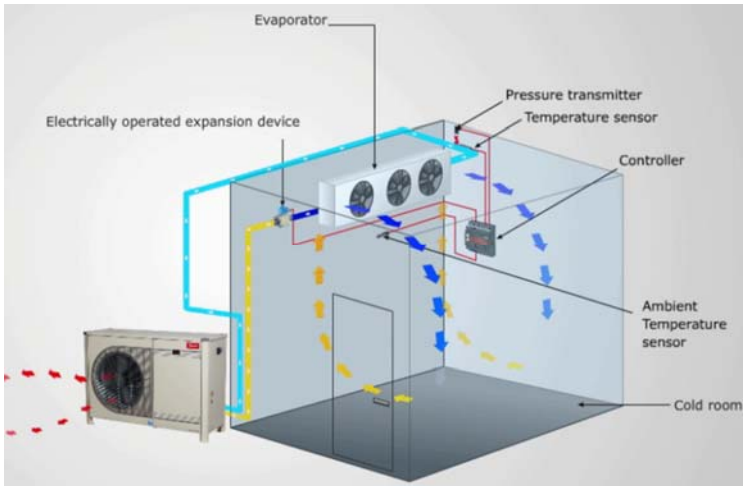

Fig.2. Cold storage room [3]

The cold room cooling capacity requirement calculation (Table 1) is done with Scelte Selection Software by ECO Modine [4]:

Table 1

Calculating cold requirements [4]

Scelte SELECTION SOFTWARE
Adrian Mihai

ECO heat transfer coolers
MODINE
Cold Room
3/24/2024

Internal length	m	5.000	Internal volume	m³	60.000
Internal width	m	4.000	Cold room position	Internal	
Internal height	m	3.000	Traffic	Medium	
	Insulation		**Thickness mm**	**Conductivity W/(m*°C)**	**Ext. T. wall? W/(m*°C)**
Wall A	Polyurethane foam 40 kg/ m3		100	0.020	30.0
Wall B	Polyurethane foam 40 kg/ m3		100	0.020	30.0
Wall C	Polyurethane foam 40 kg/ m3		100	0.020	30.0
Wall D	Polyurethane foam 40 kg/ m3		100	0.020	30.0
Ceiling	Polyurethane foam 40 kg/ m3		100	0.020	30.0
Floor	Concrete		200	1.512	16.0
Mean value					
Freezing point			°C	-1.2	
Water content			%	81	
Specific heat BEFORE freezing			kJ/(kg*°C)	3.54	
Latent heat for freezing			kJ/kg	258.20	
Specific heat ABOVE freezing			kJ/(kg*°C)	1.79	
Respiration heat			W/kg-24h	1.07	
Cold room : Preservation of fresh products					
Max room capacity by load 120 kg/ m³			kg	5040.000	
Products introduced daily			kg	504.000	
Temperatura aria esterna / Relative humidity			°C / %	30.0 / 80	
Room temperature / Relative humidity			°C / %	2.0 / 80	
Load temperature			°C	15.0	
Cooling time			h	18.0	
Number of personnel in room / Occupancy				1	
Hours of stay in room			h	1.0	
Lighting			W/m²	10.0	
Wall dispersion		24.00 h	kW	34.651	
Air changes		24.00 h	kW	13.243	
Ventilation		24.00 h	kW	3.346	
Product cooling		24.00 h	kW	8.589	
Respiration		24.00 h	kW	5.393	
Packaging		24.00 h	kW	0.000	
Personnel		24.00 h	kW	0.266	
Lighting		24.00 h	kW	0.200	
Other		24.00 h	kW	0.000	
TOTAL		**24.00 h**	**kW**	**65.687**	
Compressor running hours		24.00 h	h	12.00	
Hourly Plant Load		**24.00 h**	**kW**	**5.474**	

This old cold room is coolled by one condensig unit Tecumseh with piston compressor, model SILFH 4544 ZTX (Fig.3), which works with refrigerant R404A and having an evaporation temperature of -8°C and GWP = 3992. The performances of the SILFH4544-ZTX at the point of operation are presented in Table 2, and the mechanical and physical characteristics in Table 3 [5].

Fig. 3. Data sheet SILFH4544-ZTZ [5]

Table 2

Performance at specified operating point SILFH4544-ZTX data al 50 Hz [5]

Characteristics	Notation	U.M.	Value
Cooling Capacity	Q_C	kW	5.49
Total Power Input	P	kW	3.10
Coeficient de performanță	COP	W/W	1.77
Current at 400 V	I	A	6.16
Condensing Temperature	T_c	ºC	45.00
Subcooling	T_{SC}	K	4.67

Table 3

The characteristics for condensing unit Type SILFH4544-ZTX [5]

Characteristics	U.M.	Value
Mechanical and physical		
Diameter condenser fan/Speed	mm/rpm	450 / 830
Number of fans	pcs	1
Total Fan Power Input	W	95
Height	mm	837
Depth / Width	mm	654/1174
Suction Diameter	inch	7/8
Liquid Line	inch	½
Suction Type		Cu Type
Net Weight	kg	90.0
Sound		
Dew temp. for refrigeration applications (MT)	°C	-8.0

The second instalation according to the new regulation is condensig unit Tecumseh with piston compressor, model SILFH 4544P-TX (Fig.4), which works with refrigerant R455A and having an evaporation temperature of -8°C and GWP =148.

Fig. 4. Data sheet SILFH4544P-TX [5]

The performances of the SILFH4544P-TX at the point of operation are presented in Table 4, and the mechanical and physical characteristics in Table 5 [6].

Table 4

Performance at specified operating point SILFH4544P-TX data al 50 Hz [6]

Characteristics	Notation	U.M.	Value
Cooling Capacity	Q_C	kW	5.49
Total Power Input	P	kW	2.73
Coeficient de performanță	COP	W/W	2.01
Current at 400 V	I	A	5.73
Condensing Temperature	T_c	ºC	45.00
Subcooling	T_{SC}	K	4.67

Table 5

The characteristics for condensing unit Type SILFH4544P-TX [6]

Characteristics	U.M.	Value
Mechanical and physical		
Diameter condenser fan/Speed	mm/rpm	450 / 1100
Number of fans	pcs	1
Total Fan Power Input	W	185.0
Height	mm	710
Depth / Width	mm	652/1169
Suction Diameter	inch	7/8
Liquid Line	inch	½
Suction Type		Cu Type
Net Weight	kg	92.0
Sound		
Dew temp. for refrigeration applications (MT)	°C	-8.0

3. Comparative analysis

The investments costs presented in Fig 5. a), shows the differences betwen instalation with R404Aand instalation with R455A, this is showing that the new technology is more expensive than the old one.
When we talk about annual exploitation costs, the performances of the new equipments conparative with old one is better and the cost are much lower (Fig. 5 b).
Evaluating the GWP performances (Fig 5 c) the new instalation with R455A is much more safe from environment point of view .

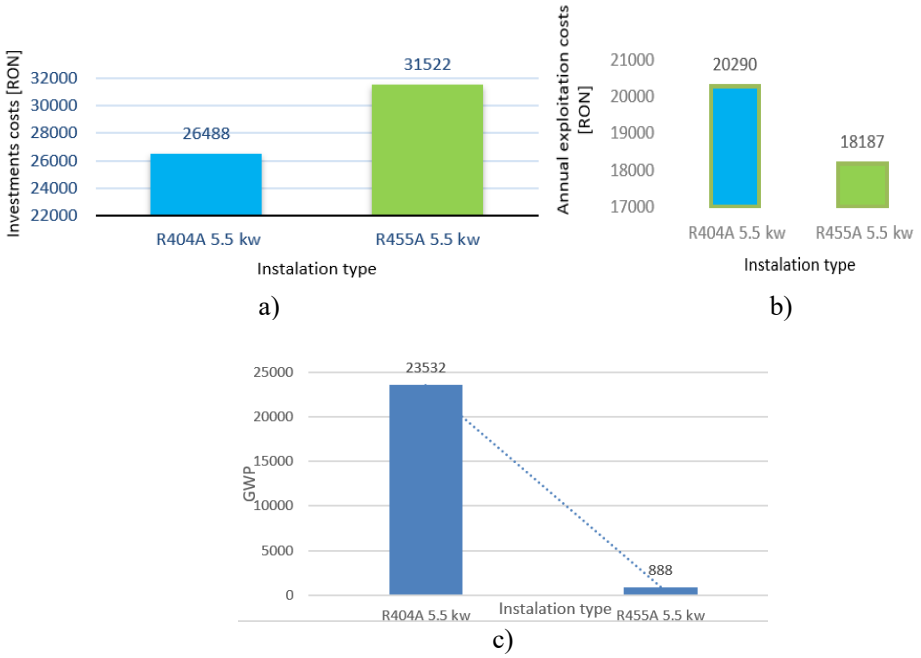

Fig 5. The investment and explitation costs exprimate in RON, respectively the GWP
a) Investments costs; b) Operating costs; c) GWP

6. Conclusions

Using R455A freon, we notice that from the point of view of the investment cost it is slightly higher, but at the same time the difference between the two technologies is relatively small compared to the total investment.

Being very similar technologies, the technicians do not require a high degree of technical training, only increased attention to the safety measures in assembly and service due to the A2L class of the refrigerant.

Analyzing from the point of view of the operating cost, it can be seen that thanks to the improved COP, we have a technology with lower energy consumption, which contributes a lot to the recovery of the investment.

At the same time, from the point of view of the environment, a drastic decrease in GWP is observed, so we can say that this refrigerant significantly helps to reduce the contamination of the atmosphere with greenhouse gases.

In accordance with the new European rules F-Gas 573/2024, manufacturers of refrigeration equipment are prepared to offer technical-economic solutions with low GWP, viable at affordable prices compared to those of the old solution with high GWP**.**

References

[1] ***, Regulation (EU) 2024/573 of the European Parliament and of the Council of 7 February 2024 on fluorinated greenhouse gases, amending Directive (EU) 2019/1937 and repealing Regulation (EU) No 517/2014.

[2] Danfoss, Accelerate refrigerant transition and turn down climate impact, Available: https://assets.danfoss. com/ documents/209637/AD135486444159en-001202.pdf, Accessed at: March 24, 2024.

[3] Danfoss, Cold storage room "what you need to know about refrigeration" – part 2, Available: https://www.danfoss.com/en/service-and-support/case-stories/dcs/cold-storage-room-what-you-need-to-know-about-refrigeration-part-2/, Accessed at: March 24, 2024.

[4] ECO Modine, Software Selection Software, 2024.

[5] Tecumseh, Tecumseh data sheet generator - Product Specification SILFH4544P-TX, Available at: https://www.tecumseh.com/Product/SILFH4544P-TX?option=SK43130202, Accessed in: March 24, 2024.

About the evaluation of the coefficient of performance for a heat pump

Despre evaluarea coeficientului de performanță al unei pompe de căldură

Florin Iordache[1], Florin Băltărețu[1], Alexandru Drăghici[1]

[1]Technical University of Cvil Engineering Bucharest
Bd. Lacul Tei nr. 122 - 124, cod 020396, Sector 2, Bucharest, Romania
E-mail: fliord@yahoo.com, florin.baltaretu@utcb.ro

Abstract. *The present work represents a continuation of our research in the field of evaluating the thermal efficiency (coefficient of performance) of a heat pump, research started and published in 2019 [1]. In the previous work it was considered the refrigerating machine, this time we will refer exclusively to the mechanical vapor compression heat pump. The evaluation of the COP for a heat pump is absolutely mandatory in the calculation procedure of contribution of the renewable resources of energy, offered by the implementation of a heat pump in the thermal utility supply systems in buildings (space heating and/or hot water preparation).*

Key words: *heat pump, efficiency*

DOI: 10.37789/rjce.2024.15.3.18

1. Introduction

The efficiency of a heat pump is defined as the ratio between the thermal power delivered by the heat pump condenser and the mechanical power supplied by the heat pump compressor. Taking into account this definition and the theoretical graphical representations of the heat pump's operating cycle, the expressions of the two types of powers mentioned and finally the expression of the heat pump's performance coefficient were established, as will be presented below.

2. Description of the evaluation procedure

The thermodynamic cycle of the refrigerant in the pressure-specific enthalpy diagram (log)*p-h* [2] it is schematically shown in Fig. 1. The actual adiabatic compression process follows the line 1-2, the line 1-2' being the ideal situation in which the adiabatic compression process would take place at constant specific entropy.

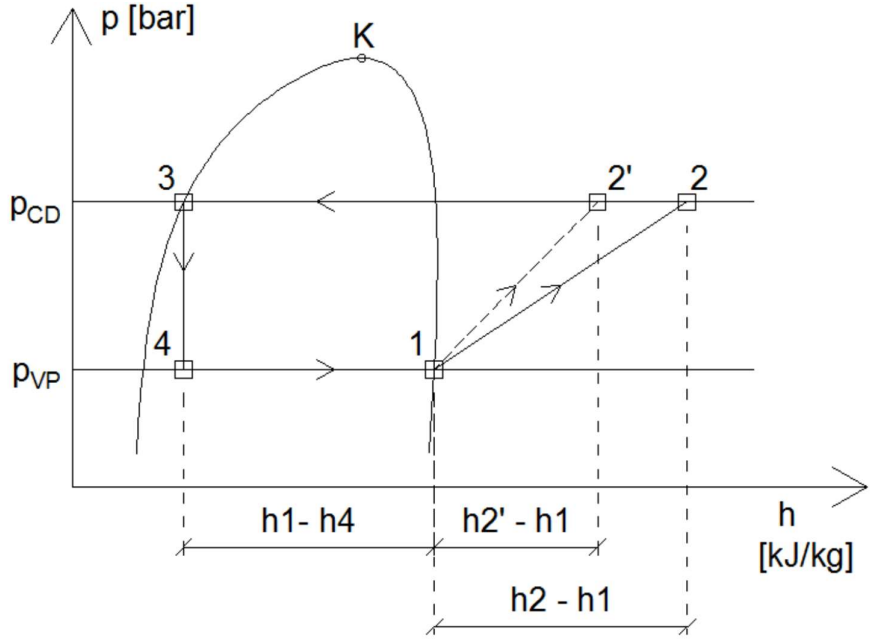

Fig. 1. The characteristic points in the log *p-h* diagram

The isentropic efficiency of the compressor [3] is defined as:

$$\eta_{iz} = \frac{h_{2'1}}{h_{21}} = \frac{h_{2'} - h_1}{h_2 - h_1} \tag{1}$$

The efficiency of the heat pump is defined as:

$$\begin{aligned} \varepsilon_{PC} &= \frac{h_{23}}{h_{21}} = \frac{h_{2'3} + h_{22'}}{h_{21}} = \frac{h_{2'3}}{h_{21}} + \frac{h_{22'}}{h_{21}} = \frac{h_{2'3}}{h_{2'1}} \cdot \frac{h_{2'1}}{h_{21}} + \frac{h_{21} - h_{2'1}}{h_{21}} = \\ &= \varepsilon_{PC}^{IZ} \cdot \eta_{iz} + 1 - \eta_{iz} = 1 + \eta_{iz} \cdot \left(\varepsilon_{PC}^{IZ} - 1 \right) \end{aligned} \tag{2}$$

where;

$$\varepsilon_{PC}^{IZ} = \frac{h_{2'3}}{h_{2'1}} \tag{3}$$

The following notations were used:

$$\begin{aligned} &h_{23} = h_2 - h_3;\ h_{21} = h_2 - h_1;\ h_{2'3} = h_{2'} - h_3; \\ &h_{2'1} = h_{2'} - h_1;\ h_{22'} = h_2 - h_{2'}; \end{aligned} \tag{4}$$

As can be seen, apart from the efficiency of the heat pump, ε_{PC}, an isentropic efficiency of the heat pump, ε^{IZ}_{PC}, was defined. Relation (2) allows the determination of the energy efficiency of the heat pump, ε_{PC}, depending on the isentropic efficiency, ε^{IZ}_{PC}:

$$\varepsilon_{PC} = 1 + \eta_{iz} \cdot \left(\varepsilon_{PC}^{IZ} - 1 \right) \tag{5}$$

We define the overall coefficient of performance (COP) of the heat pump taking into account the efficiency of the electric motor, η_{el}, which feeds the pump compressor:

$$COP_{PC} = \eta_{el} \cdot \varepsilon_{PC} \tag{6}$$

The efficiency of the heat pump used as a refrigerator in the same temperature limits is:

$$\varepsilon_{MF} = \varepsilon_{PC} - 1 \tag{7}$$

In this case, the corresponding Energy Efficiency Ratio (EER) is:

$$EER_{MF} = \eta_{el} \cdot \varepsilon_{MF} \tag{8}$$

We obtain the final expressions for EER and COP:

$$\begin{aligned} &EER = \eta_{el} \cdot \varepsilon_{MF} = \eta_{el} \cdot \eta_{iz} \cdot \left(\varepsilon_{PC}^{IZ} - 1 \right) \\ &and \\ &COP = \eta_{el} \cdot \varepsilon_{PC} = \eta_{el} \cdot \left[1 + \eta_{iz} \cdot \left(\varepsilon_{PC}^{IZ} - 1 \right) \right] \end{aligned} \tag{9}$$

As it turns out quite clearly, the central core of the energy efficiency of the heat pump is represented by the isentropic efficiency of the heat pump. To determine the isentropic efficiency of the heat pump, an analysis was undertaken between the energy efficiency and thermal parameters of 6 refrigerants (R410A, R134a, R407C, R507, R32, R152a) using the CoolPack and CoolTools software [2]. The range of temperatures investigated was between –15°C and 20°C for the cold environment and 35°C and 75°C for the warm environment.

The procedure for the use of the software was as follows:

- setting the refrigerant;
- setting the couple of temperatures of the cold and warm environments (θ_{VP} and θ_{CD});
- setting the compressor efficiency to the value 1;
- tracing the cycle and establishing the energy efficiency as a heat pump.

In addition, the energy efficiency of the cycle was also determined. In this way, 4 important parameters of the cycle could be determined, namely: vaporization and condensation temperatures of the refrigerant, Carnot energy efficiency and isentropic energy efficiency of the cycle.

Two types of correlations were made:

- the correlation between the isentropic energy efficiency, ε^{lZ}_{pc} and the Carnot energy efficiency, ε^{C}_{pc}
- the correlation between the isentropic energy efficiency, ε^{lZ}_{pc} and the difference between the condensation and vaporization temperatures of the heating agent, $\Delta t = t_{cd} - t_{vp}$.

We present below the 2 types of correlations obtained for each of the 4 refrigerants mentioned.

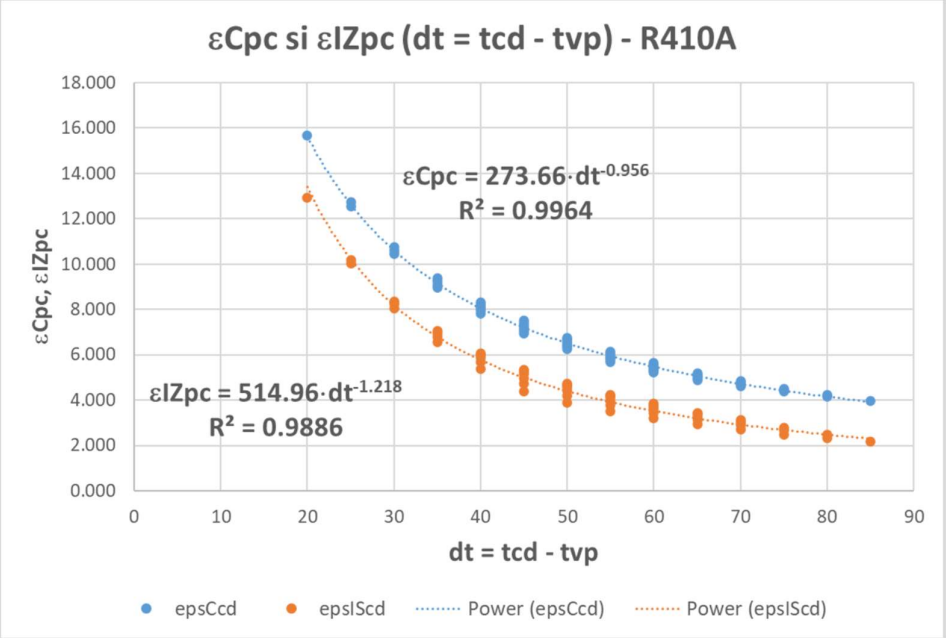

Fig. 2. The correlations for R410A

Figure 2 shows the correlations resulting from processing the data obtained using the CoolPack software, for the refrigerant R410A. We refer to the correlation between the Carnot energy efficiency of the heat pump, ε^{C}_{pc}, and the temperature difference dt, between the condensation temperature, t_{cd}, of the refrigerant and the vaporization temperature, t_{vp}. Figure 2 also shows the correlation obtained between the isentropic energy efficiency of the heat pump, ε^{lZ}_{pc}, and the temperature difference dt.

Figure 3 shows the same type of correlations, but related to the refrigerant R134a.

The mentioned temperature difference dt can be determined depending on the temperature difference between the warm environment, θ_{cd}, and the cold environment, θ_{vp}, due to the relationships:

$$\begin{aligned} &t_{cd} = \theta_{cd} + \Delta t;\ t_{vp} = \theta_{vp} - \Delta t \\ &dt = t_{cd} - t_{vp};\ d\theta = \theta_{cd} - \theta_{vp} \\ &dt = d\theta + 2 \cdot \Delta t \end{aligned} \tag{10}$$

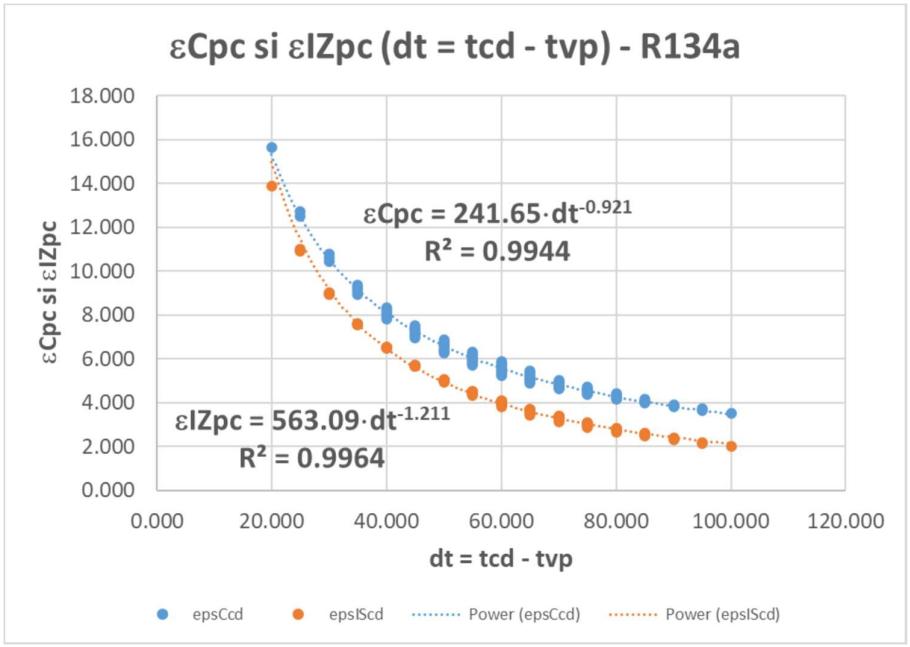

Fig. 3. The correlations for R134a

A second category of attempted correlations was made between isentropic energy efficiency and Carnot energy efficiency and the results were linear correlations, as one can see in figures 4 and 5.

Figure 4 shows, for the refrigerant R410A, the correlation between the isentropic energy efficiency of the heat pump, ε^{IZ}_{pc}, and the Carnot energy efficiency of the heat pump, ε^{C}_{pc}. Similar results are presented in Figure 5 for the refrigerant R134a.

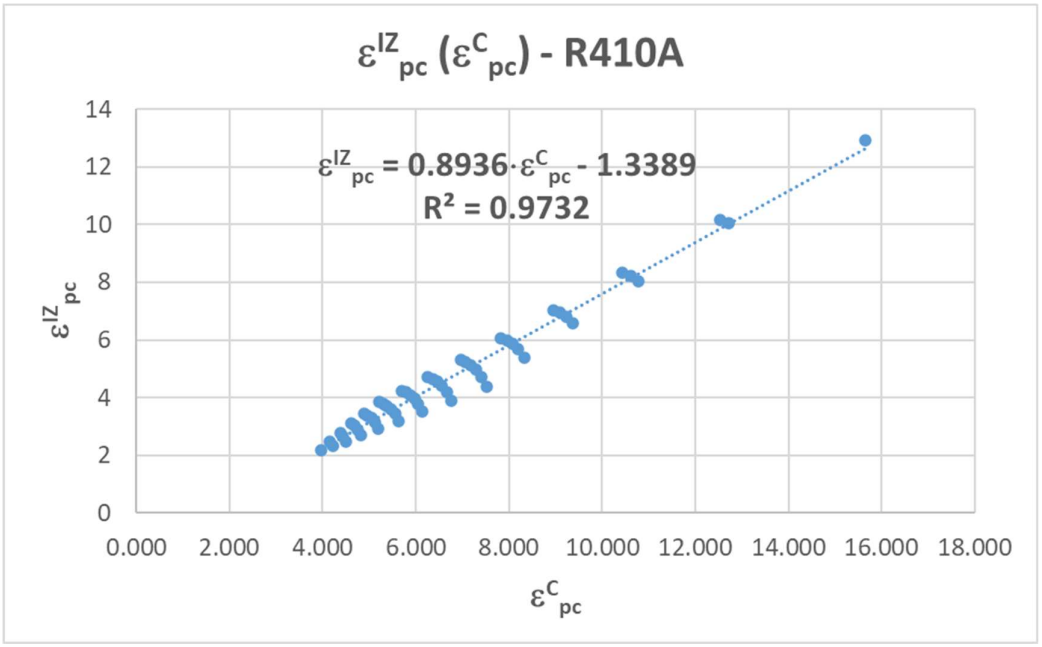

Fig. 4. The correlation between efficiencies for R410A

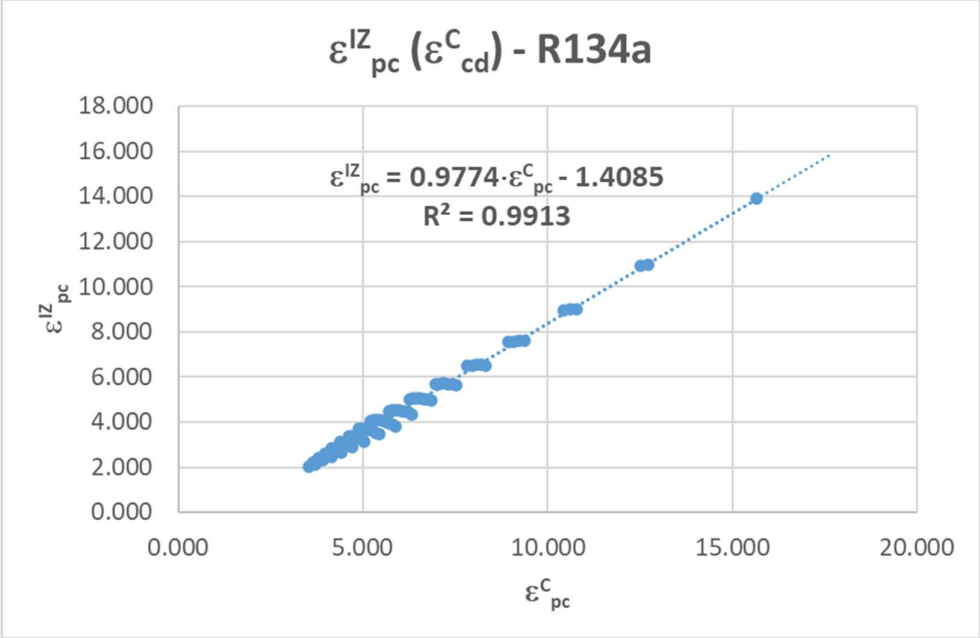

Fig. 5. The correlation between efficiencies for R134a

For the rest of the refrigerants analyzed, only the final results obtained are presented in Tables 1 and 2. As it was mentioned before and it results from relations (9), the central core is the isentropic energy efficiency of the heat pump, ε^{IZ}_{pc}, which makes the correlations shown in figures 2 and 3 preferable from an operative point of view.

For the 4 refrigerants the results are presented in Tables 1 and 2, containing the correlations regarding the isentropic energy efficiency of the heat pump.

Table 1

Correlation ε^{IZ}_{pc} = ·f(dt) for various refrigerants

Refrigerant	Correlation
R410A	$\varepsilon^{IZ}_{pc} = 514.96 \cdot dt^{-1.218}$
R134a	$\varepsilon^{IZ}_{pc} = 563.09 \cdot dt^{-1.211}$
R407C	$\varepsilon^{IZ}_{pc} = 705.53 \cdot dt^{-1.284}$
R507	$\varepsilon^{IZ}_{pc} = 938.59 \cdot dt^{-1.385}$
R32	$\varepsilon^{IZ}_{pc} = 418.76 \cdot dt^{-1.145}$
R152a	$\varepsilon^{IZ}_{pc} = 378.87 \cdot dt^{-1.093}$

Table 2

Correlation $\varepsilon^{IZ}_{pc} = \cdot f(\varepsilon^{C}_{pc})$ for various refrigerants

Refrigerant	Correlation
R410A	$\varepsilon^{IZ}_{pc} = 0.8936 \cdot \varepsilon^{C}_{pc} - 1.3389$
R134a	$\varepsilon^{IZ}_{pc} = 0.9774 \cdot \varepsilon^{C}_{pc} - 1.4085$
R407C	$\varepsilon^{IZ}_{pc} = 0.9676 \cdot \varepsilon^{C}_{pc} - 1.6081$
R507	$\varepsilon^{IZ}_{pc} = 0.9454 \cdot \varepsilon^{C}_{pc} - 1.8408$
R32	$\varepsilon^{IZ}_{pc} = 0.9387 \cdot \varepsilon^{C}_{pc} - 1.3431$
R152a	$\varepsilon^{IZ}_{pc} = 0.9773 \cdot \varepsilon^{C}_{pc} - 1.0909$

Also of interest was the graphical representation as a whole of the 2 types of graphs that allow the visualization of the isentropic energy efficiency of the 4 refrigerants analyzed.

Figure 6 shows the graphs of the correlations between the isentropic energy efficiency, ε^{IZ}_{pc}, and the difference between the condensation and vaporization temperatures of the thermal agents. It is observed that for the 4 refrigerants analyzed, the group of corresponding curves is quite compact and it could be represented by the correlation corresponding to the refrigerant R407C (as a mean).

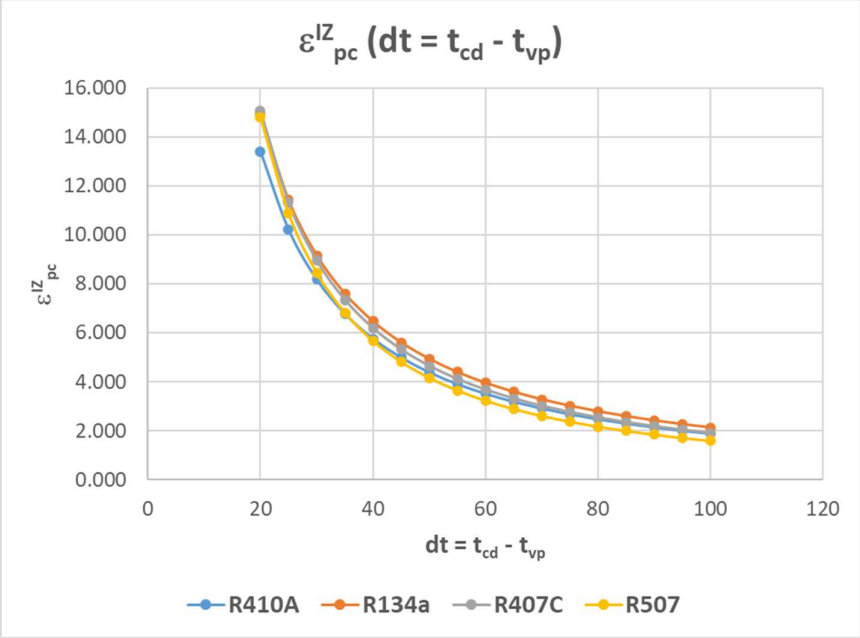

Fig. 6. The correlation $\varepsilon^{IZ}_{pc} = \cdot f(dt)$ for various refrigerants

Figure 7 shows the graphs of the correlations between the isentropic energy efficiency, ε^{IZ}_{pc}, and the Carnot energy efficiency, ε^{C}_{pc}. It is observed that for the 4 refrigerants analyzed, the group of corresponding lines is quite compact and could possibly be also represented by the corresponding correlation of the R407C refrigerant.

If it will be proven for a larger number of refrigerants that the same correlation stands, it would be preferable to retain this correlation in the useful procedure of identification of the isentropic energy efficiency, ε^{IZ}_{pc}.

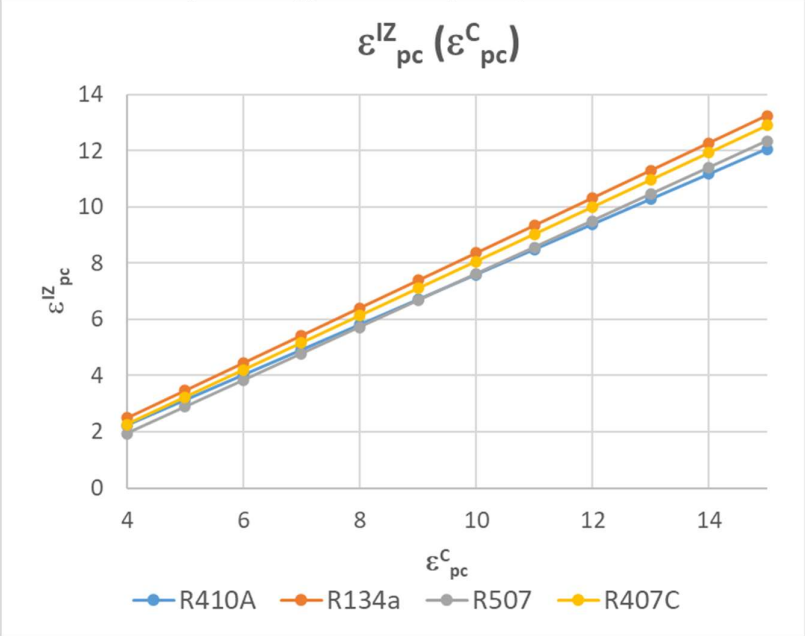

Fig. 6. The correlation $\varepsilon^{IZ}_{pc} = \cdot f(\varepsilon^{C}_{pc})$ for various refrigerants

Conclusions

As can be seen from the equation (9), that allow the evaluation of useful performance coefficients for heat pumps, they depend on the isentropic energy efficiency, ε^{IZ}_{pc}, on the isentropic efficiency of the compressor, η_{iz}, and on the efficiency of the electric motor which drives the heat pump compressor, η_{el}. The current work mainly refers to the isentropic energy efficiency of the heat pump, ε^{IZ}_{pc}, which can be determined by the correlations established and presented, depending on the temperatures of the ambient environments of the evaporator and the condenser of the heat pump.

The correlation based on the Carnot energy efficiency is simple and easy to use, being a linear correlation, but it requires the prior determination of the Carnot energy efficiency according to the temperatures of the ambient media, θ_{cd} and θ_{vp}.

The correlation between the isentropic energy efficiency and the temperatures of the ambient media, θ_{cd} and θ_{vp}, through relations (10) and those in lines 2, 3, 4 and 5 of table 1, allows the operational determination of the isentropic energy efficiency.

It is worth remembering the verification of the degree of uniqueness of the linear correlation between the isentropic energy efficiency and the Carnot energy efficiency of the heat pump.

Notations

t_{vp} – vaporization temperature of the refrigerant, °C;
t_{cd} – condensation temperature of the refrigerant, °C;
θ_{vp} – cold environment temperature, °C;
θ_{cd} – warm environment temperature, °C;
Δt – average temperature difference at the evaporator and at the condenser, °C;
h_1, h_2, h_3, h_4 – specific enthalpy for nodes 1, 2, 3 and 4 of the refrigeration cycle, kJ/kg;
$h_{2'}$ – specific enthalpy of node 2' of the refrigeration cycle, kJ/kg;
η_{iz} – isentropic efficiency of the compressor, -;
η_{el} – efficiency of the electric motor that drives the compressor, -;
ε_{pc} – energy efficiency of the machine as a heat pump, -;
ε_{mf} – energy efficiency of the machine as a refrigerator, -;
ε^{C}_{pc} – Carnot energy efficiency of the heat pump, -;
ε^{IZ}_{pc} – isentropic energy efficiency of the heat pump, -;
COP – coefficient of performance for the heat pump, -;
EER – energy efficiency ratio as a refrigerator; -.

References

[1] F. Iordache, A. Drăghici. Procedure for evaluating performance indicators for refrigeration machines or heat pumps, *Revista Română de Inginerie Civilă*, Volumul 10 (2019), nr. 4, pp. 396-406.
[2] ***, CoolPack 1.50, CoolTools v1.1.1 (A Collection of Simulation Tools for Refrigeration), https://www.ipu.dk/products/coolpack/ . https://www.ipu.dk/products/cooltools/ .
[3] F. Iordache, M. Tălpigă. Simplified procedure for evaluating energy performance of heat pumps. Energy and economic analysis, *Revista Română de Inginerie Civilă*, Volumul 13 (2022), nr. 4. doi: 10.37789/rjce.2022.13.4.3
[4] R. Tillner-Roth. A. Yokozeki. An international standard equation of state for difluoromethane (R-32) for temperatures from the triple point at 136.34 K to 435 K and pressures up to 70 MPa. *J. Phys. Chem. Ref. Data*, 26 (6):1273–1328, 1997. doi:10.1063/1.556002.
[5] R. Tillner-Roth, H.D. Baehr. A International Standard Formulation for the Thermodynamic Properties of 1,1,1,2-Tetrafluoroethane (HFC-134a) for Temperatures from 170 K to 455 K and Pressures up to 70 MPa. *J. Phys. Chem. Ref. Data*, 23:657–729, 1994. doi:10.1063/1.555958.
[6] E.W. Lemmon. Pseudo-Pure Fluid Equations of State for the Refrigerant Blends R-410A, R-404A, R-507A, and R-407C. *Int. J. Thermophys.*, 24 (4):991–1006, 2003. doi:10.1023/A:1025048800563.
[7] S.L. Outcalt, M.O. McLinden. A Modified Benedict-Webb-Rubin Equation of State for the Thermodynamic Properties of R152a (1,1-difluoroethane). *J. Phys. Chem. Ref. Data*, 25 (2):605–636, 1996. doi:10.1063/1.555979.
[8] L. Neumaier, D. Roskosch, J. Schilling, G. Bauer, J. Gross, A. Bardow. Refrigerant Selection for Heat Pumps: The Compressor Makes the Difference. *Energy Technol*., 11 (2023): 2201403. https://doi.org/10.1002/ente.202201403.